

IMPROVEMENT OF CO<sub>2</sub> FLOOD PERFORMANCE

Third Annual Report  
October 1, 1986--September 30, 1987

By  
J.P. Heller  
F.S. Kovarik  
J.J. Taber

January 1989

Performed Under Contract No. FC21-84MC21136

New Mexico Institute of Mining and Technology  
New Mexico Petroleum Recovery Research Center  
Socorro, New Mexico



Bartlesville Project Office  
U. S. DEPARTMENT OF ENERGY  
Bartlesville, Oklahoma

## DISCLAIMER

This report was prepared as an account of work sponsored by an agency of the United States Government. Neither the United States Government nor any agency thereof, nor any of their employees, makes any warranty, express or implied, or assumes any legal liability or responsibility for the accuracy, completeness, or usefulness of any information, apparatus, product, or process disclosed, or represents that its use would not infringe privately owned rights. Reference herein to any specific commercial product, process, or service by trade name, trademark, manufacturer, or otherwise, does not necessarily constitute or imply its endorsement, recommendation, or favoring by the United States Government or any agency thereof. The views and opinions of authors expressed herein do not necessarily state or reflect those of the United States Government or any agency thereof.

Printed in the United States of America. Available from:

National Technical Information Service  
U.S. Department of Commerce  
5285 Port Royal Road  
Springfield, VA 22161

NTIS price codes

Paper copy: **A11**

Microfiche copy: **A01**

DOE/MC/21136-17  
Distribution Category UC-122

IMPROVEMENT OF CO<sub>2</sub> FLOOD PERFORMANCE

THIRD ANNUAL REPORT  
October 1, 1986--September 30, 1987

By  
J.P. Heller  
F.S. Kovarik  
J.J. Taber

January 1989

Work Performed Under Contract No. FC21-84MC21136

Prepared for  
U.S. Department of Energy  
Assistant Secretary for Fossil Energy

Royal J. Watts, Project Manager  
Morgantown Energy Technology Center  
P.O. Box 880  
Morgantown, WV 26505

Prepared by  
New Mexico Institute of Mining and Technology  
New Mexico Petroleum Recovery Research Center  
Socorro, New Mexico



## ABSTRACT

This report provides results obtained for the third year of a three-year, comprehensive, cost-shared, applied research program designed to improve oil recovery through carbon dioxide (CO<sub>2</sub>) flooding. The program was composed of three areas: Task 1--Phase Behavior and Fluid Property Measurements, Task 2--Mixing of CO<sub>2</sub> and Oil During Flow in Reservoir Rocks, and Task 3--Mobility Control in CO<sub>2</sub> Floods.

In Task 1, the continuous phase equilibrium apparatus was used to measure simultaneously the viscosity, density, and composition of CO<sub>2</sub>-hydrocarbon systems at high pressure. These data were compared to a well-known correlation used in predicting viscosities in reservoir simulation studies. Other work in this area consisted of slim-tube tests using CO<sub>2</sub> and both a synthetic and a crude oil in order to study the effects of methane on optimum oil recovery with CO<sub>2</sub>.

In Task 2, the performances of secondary and tertiary displacements of crude oil by CO<sub>2</sub> in cores were measured and compared to predictions made with a multi-component, one-dimensional simulator. Results from the core tests suggest that it may be possible to achieve optimum oil recovery with CO<sub>2</sub> at pressures which are lower than the conventionally obtained optimum pressure estimated from a slim-tube test. In the final part of this task, flow visualization experiments were conducted in glass micromodels to study the effect of micro-heterogeneity on the flow of CO<sub>2</sub> and surfactant-generated foam.

In Task 3, procedures and equipment were developed to measure the steady-state mobility of foam-like dispersions of dense CO<sub>2</sub> in surfactant solutions. A number of surfactants were tested, and effects such as surfactant concentration, flowing CO<sub>2</sub> fraction or quality, and permeability of rock samples were studied. Additionally, direct thickeners (either novel polymers or associative compounds) were synthesized and tested with the goal of increasing the viscosity of dense CO<sub>2</sub>. Finally, the engineering aspects of applying mobility control agents are discussed.



## TABLE OF CONTENTS

TITLE PAGE . . . . .	i
ABSTRACT . . . . .	ii
TABLE OF CONTENTS . . . . .	iii
LIST OF FIGURES . . . . .	vi
LIST OF TABLES . . . . .	xii
GENERAL INTRODUCTION . . . . .	1
PROJECT SUMMARY . . . . .	2
DISCUSSION OF RESULTS . . . . .	9
1. AREA I - PHASE BEHAVIOR & FLUID PROPERTIES OF CO <sub>2</sub> /HYDROCARBON MIXTURES (F.S. Kovarik). . . . .	9
1.1 New Generation Continuous Phase Equilibrium (CPE) Experiment . . . . .	9
1.1.1 General Procedure Used for the Four-Component Synthetic Oil System . . . . .	9
1.1.2 Discussion of Results . . . . .	10
1.1.3 C <sub>5</sub> -C <sub>10</sub> -C <sub>16</sub> C <sub>30</sub> Systems . . . . .	10
1.1.4 Comparison of Experiments at 100°F, CPE 207, 216 and 212 . . . . .	13
1.1.5 Comparison of Viscosity Data to the Lohrenz, Bray and Clark Correlation . . . . .	26
1.1.5.1 The Correlation . . . . .	26
1.1.5.2 Results of Calculations . . . . .	31
1.2 Effect of Solution Gas on the Development of Miscibility . . . . .	42
1.2.1 Introduction . . . . .	42
1.2.2 Literature Review . . . . .	42
1.2.3 Experimental Program . . . . .	44
1.2.4 Results and Discussion . . . . .	46
1.2.4.1 Synthetic Oil System . . . . .	46
1.2.4.2 Crude Oil System . . . . .	54
1.2.5 Conclusions . . . . .	66
1.2.6 Future Work . . . . .	66
2. AREA II - MIXING OF CO <sub>2</sub> AND OIL DURING FLOW IN RESERVOIR ROCK (F.S. Kovarik)68	68
2.1 Secondary and Tertiary CO <sub>2</sub> /Oil Coreflood Data: Experimental vs. Simulation . . . . .	68
2.1.1 Introduction . . . . .	68
2.1.2 Experimental Aspects . . . . .	68
2.1.3 Experimental/Simulation Results . . . . .	69
2.1.4 Mixing Parameters Sensitivity Analysis . . . . .	89
2.1.5 Conclusions . . . . .	94
2.1.6 Future Work . . . . .	100
2.2 Flow Visualization Experiments . . . . .	100
2.2.1 Introduction . . . . .	100
2.2.2 Generating In-situ Foam in the Presence of Oil . . . . .	101
2.2.3 Generating In-situ Foam in the Absence of Oil . . . . .	105

2.2.4	Effect of Microscopic Heterogeneity on Displacements . . . . .	110
2.2.5	Surfactant Solution Tests . . . . .	116
2.2.6	Stable Foam Displacements . . . . .	116
2.2.6.1	Results Common to Displacements 5-1 Through 5-5 . . . . .	119
2.2.6.2	Results Common to Maljamar Oil Displacements . . . . .	119
2.2.6.3	Results from High Pressure Maljamar Displacement . . . . .	121
2.2.6.4	Results from Soltrol® Displacement . . . . .	121
2.2.7	Conclusions . . . . .	122
2.2.8	Future Experiments . . . . .	122
3.	<b>SUPPLEMENTARY RESEARCH IN AREA II--TRANSITION ZONE LENGTH (J.P. Heller)</b> 23	
3.1	Introduction . . . . .	123
3.2	The Minimum Length of Transition Zone, Due to Longitudinal Dispersion Alone, in a Uniform Pack . . . . .	124
3.3	Stratified Packing . . . . .	124
3.4	Non-uniform Flow Resulting From Frontal Instability . . . . .	125
3.5	Dispersive Stabilization of Anomalous Transition Zones . . . . .	126
3.6	The Onset of Fingering From a Graded Concentration Front . . . . .	127
3.7	Conclusions . . . . .	128
4.	<b>AREA III - MOBILITY CONTROL IN CO<sub>2</sub> FLOODS (J.P. Heller)</b> . . . . .	128
4.1	Introduction . . . . .	128
4.2	Background . . . . .	129
4.3	CO <sub>2</sub> -Foams . . . . .	131
4.3.1	Overview . . . . .	131
4.3.2	Past Work . . . . .	132
4.3.3	Description of the Foam Mobility Measurement Apparatus . . . . .	132
4.3.4	Interpretation of the Experimental Data . . . . .	136
4.3.5	CO <sub>2</sub> -Mobility Measurements . . . . .	136
4.3.5.1	The Effect of Surfactant Concentration . . . . .	136
4.3.5.2	The Effect of Flowing CO <sub>2</sub> Fraction (Foam Quality) . . . . .	142
4.3.5.3	The Effect of Rock Sample Permeability . . . . .	142
4.3.5.4	Conclusions . . . . .	149
4.3.6	Surfactant Screening . . . . .	157
4.3.6.1	Review of Surface Chemistry and Surfactant for Foams . . . . .	157
4.3.6.2	Surfactant Screening Results . . . . .	157
4.3.6.3	Measurements of Surface and Interfacial Tensions . . . . .	158
4.3.6.4	Measurements of Foam Height . . . . .	168
4.3.6.5	Measurements of pH after Thermal Aging . . . . .	168
4.3.7	Dynamic Adsorption Experiment . . . . .	170
4.3.7.1	Description of the Experiment and Apparatus . . . . .	170
4.3.7.2	Past and Current Results . . . . .	173
4.4	Future Foam Studies . . . . .	175
4.5	Direct Thickeners . . . . .	175
4.5.1	Method I . . . . .	176
4.5.2	Method II . . . . .	179
4.5.3	Method III . . . . .	179
4.5.4	Conclusions . . . . .	186
4.6	Laboratory Procedures for the Assessment of Mobility Control Additives in CO <sub>2</sub> Floods . . . . .	186
4.6.1	Introduction and Background . . . . .	186
4.6.2	Considerations of Model Design (for Assessment of CO <sub>2</sub> Mobility Control) . . . . .	189

4.6.3	Test System for Evaluation of Mobility Control . . . . .	190
4.6.4	Flooding Experiments . . . . .	191
4.7	Mobility Control of Actual CO <sub>2</sub> Floods . . . . .	194
4.7.1	Field Application of CO <sub>2</sub> Mobility Control . . . . .	194
4.7.2	Reservoir Use of CO <sub>2</sub> -Foam . . . . .	195
4.7.3	Prospective Field Use of Direct Thickeners . . . . .	197
4.7.4	Conclusions About Field Use of Mobility Control . . . . .	199

REFERENCES . . . . .	200
----------------------	-----

APPENDICES

APPENDIX A - Sample Calculation for Critical CO <sub>2</sub> Flow Rate . . . . .	205
APPENDIX B - Experimental Data for the CO <sub>2</sub> +n-C <sub>10</sub> +n-C <sub>16</sub> Displacement Runs . . . . .	207
APPENDIX C - CO <sub>2</sub> Density Prediction . . . . .	225



## LIST OF FIGURES

Figure 1.1	Diagram of CPE apparatus. . . . .	11
Figure 1.2	Initial oil viscosity and saturation oil viscosity for the synthetic oil/CO <sub>2</sub> system.. . . .	14
Figure 1.3	Viscosity/density/time plot for synthetic oil at 100°F and 1300 psia (CPE 207).. . . .	15
Figure 1.4	Viscosity/density/time plot for synthetic oil at 100°F and 1500 psia (CPE 216).. . . .	16
Figure 1.5	Viscosity/density/time plot for synthetic oil at 100°F and 2000 psia (CPE 212).. . . .	17
Figure 1.6	Top 50% ternary with viscosity for synthetic oil at 100°F and 1300 psia (CPE 207). . . . .	18
Figure 1.7	Top 50% ternary with viscosity for synthetic oil at 100°F and 1500 psia (CPE 216). . . . .	19
Figure 1.8	Top 50% viscosity ternary for synthetic oil at 190°F and 2000 psia (CPE 214).. . . .	20
Figure 1.9	Complete viscosity ternary for synthetic oil at 190°F and 2000 psia (CPE 214).. . . .	21
Figure 1.10	Viscosity/density/time plot for synthetic oil at 150°F and 1500 psia, lower phase (CPE 215). . . . .	22
Figure 1.11	Viscosity/density/time plot for synthetic oil at 150°F and 1500 psia, upper phase (CPE 215). . . . .	23
Figure 1.12	Viscosity/density/time plot for synthetic oil at 190°F and 2000 psia, lower phase (CPE 214). . . . .	24
Figure 1.13	Viscosity/density/time plot for synthetic oil at 190°F and 2000 psia, upper phase (CPE 214). . . . .	25
Figure 1.14	Complete viscosity ternary for Maljamar separator oil at 90°F and 1200 psia (CPE 210). . . . .	27
Figure 1.15	Viscosity/density/time plot for Maljamar separator oil at 90°F and 1200 psia (upper and lower phase).. . . .	28
Figure 1.16	Viscosity/density/time plot for Maljamar separator oil at 90°F and 1200 psia (upper phase).. . . .	29
Figure 1.17	Viscosity/density/time plot for Maljamar separator oil at 90°F and 1200 psia (lower phase).. . . .	30

Figure 1.18	Comparison of calculated and experimental viscosities for the system CO <sub>2</sub> +nC <sub>5</sub> +nC <sub>10</sub> +nC <sub>16</sub> +nC <sub>30</sub> (P= 2000 psia, T = 190°F)..	37
Figure 1.19	Comparison of calculated and experimental viscosities for the system CO <sub>2</sub> +nC <sub>5</sub> +nC <sub>10</sub> +nC <sub>16</sub> +nC <sub>30</sub> (P= 2000 psia, T = 100°F)..	38
Figure 1.20	Comparison of calculated and experimental viscosities for the system nC <sub>6</sub> +nC <sub>16</sub> ..	39
Figure 1.21	Comparison of calculated and experimental viscosities for Maljamar separator oil + CO <sub>2</sub> (P= 1200 psia, T = 90°F)..	40
Figure 1.22	Comparison of calculated and experimental viscosities for several crude oils..	41
Figure 1.23	Influence of composition of crude oil on calculated viscosity error for the system Maljamar separator oil + CO <sub>2</sub> ..	43
Figure 1.24	Schematic of experimental apparatus..	45
Figure 1.25	Phase equilibria of CO <sub>2</sub> and nC <sub>6</sub> (T = 100°F)..	47
Figure 1.26	Minimum miscibility pressure of CO <sub>2</sub> and nC <sub>6</sub> (T = 100°F)..	48
Figure 1.27	Slim tube recovery curves for Oil B..	50
Figure 1.28	Slim tube recovery curves for Oil C..	51
Figure 1.29	Minimum miscibility pressure of synthetic oil system (C <sub>1</sub> -C <sub>4</sub> -C <sub>10</sub> )..	52
Figure 1.30	CO <sub>2</sub> -nC <sub>4</sub> -C <sub>10</sub> calculated ternary diagram (P = 1650 psia)..	53
Figure 1.31	Ternary faces of quaternary system, Run B-1 (P = 1406.7 psia, T = 160°F)..	55
Figure 1.32	Composition route of Run B-1 (P = 1406.7 psia, T = 160°F)..	56
Figure 1.33	Concentration history of C <sub>1</sub> , Oil B (T = 160°F)..	58
Figure 1.34	Concentration history of C <sub>4</sub> , Oil B (T = 160°F)..	59
Figure 1.35	Concentration history of C <sub>10</sub> , Oil B (T = 160°F)..	60
Figure 1.36	Concentration history of C <sub>1</sub> , Oil C (T = 160°F)..	61
Figure 1.37	Concentration history of C <sub>4</sub> , Oil C (T = 160°F)..	62
Figure 1.38	Concentration history of C <sub>10</sub> , Oil C (T = 160°F)..	63
Figure 1.39	Minimum miscibility pressure of Maljamar crude oil system (T = 90°F)..	65
Figure 1.40	Concentration history of C <sub>1</sub> , crude oil (T = 90°F)..	67

Figure 2.1	Schematic of the CO <sub>2</sub> /crude oil displacement apparatus. . . . .	70
Figure 2.2	Schematic of the back pressure regulator system. . . . .	71
Figure 2.3	Experimental oil recovery curves - Run 1 and Run 2; 1014 psia, Q/Qc = 0.387 and 1160 psia, Q/Qc = 13.4. . . . .	77
Figure 2.4	Ternary phase diagram of CO <sub>2</sub> +nC <sub>10</sub> +nC <sub>16</sub> at 1600 psia and 93°F. . . . .	80
Figure 2.5	Ternary phase diagrams of CO <sub>2</sub> +nC <sub>10</sub> +nC <sub>16</sub> at 1200 psia and 93°F. . . . .	81
Figure 2.6	Ternary phase diagrams of CO <sub>2</sub> +nC <sub>10</sub> +nC <sub>16</sub> at 1100 psia and 93°F. . . . .	82
Figure 2.7	Experimental and simulated oil recovery and gas production - Run 4, 1634 psia, Q/Qc = 23.4. . . . .	83
Figure 2.8	Experimental and simulated oil recovery and gas production - Run 5, 1656 psia, Q/Qc = 8.54. . . . .	83
Figure 2.9	Experimental and simulated oil recovery and gas production - Run 6, 1202 psia, Q/Qc = 2.28. . . . .	84
Figure 2.10	Experimental and simulated oil recovery and gas production - Run 9, 1206 psia, Q/Qc = 2.58. . . . .	84
Figure 2.11	Experimental and simulated oil recovery and gas production - Run 10, 1212 psia, Q/Qc = 1.46. . . . .	85
Figure 2.12	Experimental and simulated oil recovery and gas production - Run 7, 1096 psia, Q/Qc = 1.95. . . . .	87
Figure 2.13	Experimental and simulated oil recovery and gas production - Run 8, 1100 psia, Q/Qc = 1.31. . . . .	88
Figure 2.14	Experimental and simulated oil recovery and gas production - Run 11, 1100 psia, Q/Qc = 1.16. . . . .	88
Figure 2.15	Experimental and simulated oil recovery of the tertiary CO <sub>2</sub> displacement. . . . .	90
Figure 2.16	Effects of changes in flowing fraction on oil recovery during single-contact miscible displacements - 1600 psia, 93°F. . . . .	92
Figure 2.17	Effects of changes in mass transfer rate on oil recovery during single-contact miscible displacements - 1600 psia, 93°F. . . . .	92
Figure 2.18	Effects of changes in longitudinal dispersion rate on oil recovery during single-contact miscible displacements - 1600 psia, 93°F. . . . .	93
Figure 2.19	Effects of changes in flowing fraction on oil recovery during immiscible displacements - 1200 psia, 93°F. . . . .	95

Figure 2.20	Effects of changes in mass transfer rate on oil recovery during immiscible displacements - 1200 psia, 93°F. . . . .	96
Figure 2.21	Effects of changes in longitudinal dispersion on oil recovery during immiscible displacements - 1200 psia, 93°F. . . . .	96
Figure 2.22	Effects of flowing fraction on saturation distribution for displacements at the $L_1$ - $L_2$ separation pressure at 0.5 PV injected. . . . .	97
Figure 2.23	Effects of mass transfer rate on saturation distribution for displacements at the $L_1$ - $L_2$ separation pressure at 0.5 PV injected. . . . .	98
Figure 2.24	Effects of longitudinal dispersion on saturation distribution for displacements at the $L_1$ - $L_2$ separation pressure at 0.5 PV injected. . . . .	99
Figure 2.25	Micromodel apparatus. . . . .	102
Figure 2.26	Heterogeneous pore network MM-II. . . . .	103
Figure 2.27	Micromodel experiment with $CO_2$ -foam displacing Maljamar crude ( $T = 90^\circ F$ , $P = 1320$ psia, surfactant concentration 0.38 wt. %). Dark lines indicate initial $CO_2$ flow paths through high permeability streaks. . . . .	106
Figure 2.28	Micromodel experiment with $CO_2$ -foam displacing Maljamar crude. Same conditions as Fig. 2.27. Initial surfactant solution flow paths following the $CO_2$ slug indicated. . . . .	106
Figure 2.29	Micromodel experiment with $CO_2$ -foam displacing Maljamar crude. Same conditions as Fig. 2.27. Foam generation sites indicated by the X's. . . . .	107
Figure 2.30	Micromodel experiment with $CO_2$ -foam displacing Maljamar crude. Same conditions as Fig. 2.27. Secondary $CO_2$ flow paths indicated. . . . .	107
Figure 2.31	Micromodel experiment with $CO_2$ -foam displacing Maljamar crude. Same conditions as 2.27. Final $CO_2$ flow paths. There is general penetration of the matrix, with oil recovery estimated at 95% OOIP. . . . .	108
Figure 2.32	Heterogeneous pore network MM-II. . . . .	108
Figure 2.33	Homogeneous pore network MM-H. . . . .	112
Figure 2.34	Heterogeneous pore network MM-I. . . . .	112
Figure 2.35	Flow paths of surfactant solution through middle and lower portion of MM-H. . . . .	113
Figure 2.36	Residual oil in the upper and lower portions of MM-H concentrated toward the outlet. . . . .	113
Figure 2.37	Plot of surface tension vs. surfactant concentration of Alipal CD-128 sample. . . . .	118
Figure 4.1	Compressibility of $CO_2$ at $20^\circ C$ . . . . .	133

Figure 4.2	Calibration of capillary tube flowmeter. . . . .	134
Figure 4.3	Schematic of the CO <sub>2</sub> -foam mobility measurement apparatus.. . . .	135
Figure 4.4	Measurements of surface and interfacial tensions, Alipal CD-128 (A).. . . . .	138
Figure 4.5	Measurements of surface and interfacial tensions, Chembetaine BC-50 (Z). . . . .	138
Figure 4.6	Measurements of surface and interfacial tensions, Varion CAS (Z). . . . .	139
Figure 4.7	Measurements of surface and interfacial tensions, Enordet X2001 (A).. . . . .	139
Figure 4.8	Effect of surfactant concentrations. . . . .	140
Figure 4.9	Effect of CO <sub>2</sub> fraction.. . . .	143
Figure 4.10	Pure dense CO <sub>2</sub> flow.. . . .	145
Figure 4.11	Immiscible simultaneous flow of brine and dense CO <sub>2</sub> .. . . .	145
Figure 4.12	Effect of rock sample permeability. . . . .	147
Figure 4.13	Relative mobility of CO <sub>2</sub> -foam at high velocity range. . . . .	150
Figure 4.14	Measurements of anionic surface and interfacial tensions, Foamer NES 25(A).. . . . .	159
Figure 4.15	Measurements of anionic surface and interfacial tensions, Alipal CO-436 (A).. . . . .	159
Figure 4.16	Measurements of anionic surface and interfacial tensions, Synperonic 91/2.5S (A). . . . .	160
Figure 4.17	Measurements of anionic surface and interfacial tensions, Witcolate 1276 (A). . . . .	160
Figure 4.18	Measurements of amphoteric surface and interfacial tensions, Aromox T/12 (Amph). . . . .	161
Figure 4.19	Measurements of amphoteric surface and interfacial tensions, Aromox C/12 (Amph). . . . .	161
Figure 4.20	Measurements of amphoteric surface and interfacial tensions, Aromox DM16 (Amph).. . . . .	162
Figure 4.21	Measurements of amphoteric surface and interfacial tensions, Aromox DMC (Amph). . . . .	162

Figure 4.22	Measurements of cationic surface and interfacial tensions, Aerosol C61 (C). . . . .	163
Figure 4.23	Measurements of cationic surface and interfacial tensions, Arfoam 2386(C). . . . .	163
Figure 4.24	Measurements of nonionic surface and interfacial tensions, Emulphogene BC-720 (N). . . . .	164
Figure 4.25	Measurements of nonionic surface and interfacial tensions, Neodol 91-2.5S/32 (N). . . . .	164
Figure 4.26	Measurements of nonionic surface and interfacial tensions, Makon 14 (N). . . . .	165
Figure 4.27	Measurements of nonionic surface and interfacial tensions, Biosoft EA 10 (N). . . . .	165
Figure 4.28	Measurements of zwitterionic surface and interfacial tensions, Deriphath BAW (Z). . . . .	166
Figure 4.29	Measurements of zwitterionic surface and interfacial tensions, Deriphath 160C (Z). . . . .	166
Figure 4.30	Measurements of zwitterionic surface and interfacial tensions, Monateric B203 (Z). . . . .	167
Figure 4.31	Measurements of zwitterionic surface and interfacial tensions, Varion CADG-LS (Z). . . . .	167
Figure 4.32	Sample shaking machine. . . . .	169
Figure 4.33	Dynamic adsorption apparatus. . . . .	171
Figure 4.34	Steps involved in the synthesis of unsymmetrical trialkyltin fluorides.. . . .	182
Figure 4.35	Viscosity of Hex <sub>2</sub> BuSnF in various hydrocarbons. . . . .	183
Figure 4.36	Viscosity vs. concentration curves for tris (trimethylsilylpropyl)tin fluoride in various solvents at 25°C. . . . .	185
Figure 4.37	Viscosity of tris (trimethylsilylpropyl)tin fluoride at high concentrations; solvent n-hexane; temp. 25°C.. . . .	185
Figure 4.38	Waterflood of Baker Dolomite core. . . . .	192
Figure 4.39	Unthickened propane flood of Baker Dolomite core. . . . .	193

## LIST OF TABLES

Table 1.1	Equilibrium Bubble Point CO <sub>2</sub> Composition: Comparing the CPE and Static PVT Cell Experiments with a Four Component Synthetic Oil . . . . .	12
Table 1.2	Comparison of Calculated and Experimental Viscosity for the CO <sub>2</sub> -C <sub>5</sub> -C <sub>10</sub> -C <sub>16</sub> -C <sub>30</sub> System at 190°F and 2000 psia (CPE 214). . . . .	32
Table 1.3	Comparison of Calculated and Experimental Viscosity for the CO <sub>2</sub> -C <sub>5</sub> -C <sub>10</sub> -C <sub>16</sub> -C <sub>30</sub> System at 100°F and 2000 psia (CPE 212). . . . .	33
Table 1.4	Comparison of Calculated and Experimental Viscosity for the System nC <sub>6</sub> -nC <sub>16</sub> . . . . .	34
Table 1.5	Comparison of Calculated and Experimental Viscosity for the System Maljamar Separator Oil + CO <sub>2</sub> at 90°F and 1200 psia (CPE 210). . . . .	35
Table 1.6	Comparison of Calculated and Experimental Data for Several Crude Oil Systems . . . . .	36
Table 1.7	Summary of Synthetic Oil Runs . . . . .	49
Table 1.8	Effluent Concentration History for Oil B-1 Used to Determine Composition Path in Figure 1.32. . . . .	57
Table 1.9	Preliminary Results of Maljamar Crude Oil Runs . . . . .	64
Table 2.1	Properties of Core B7 . . . . .	72
Table 2.2	Summary of Hydrocarbon Fluid Properties . . . . .	73
Table 2.3	Summary of CO <sub>2</sub> Properties . . . . .	74
Table 2.4	Summary of Vertical CO <sub>2</sub> -Synthetic Oil Displacements . . . . .	75
Table 2.5	Summary of CO <sub>2</sub> +nC <sub>10</sub> +nC <sub>16</sub> Phase Behavior at 93°F . . . . .	78
Table 2.6	Displacements in the Presence of Oil . . . . .	104
Table 2.7	Displacements in the Absence of Oil . . . . .	109
Table 2.8	Displacements in Different Micromodels . . . . .	111
Table 2.9	Foamability Test of Alipal CD-128. . . . .	117
Table 2.10	Displacements with Higher Surfactant Concentration. . . . .	120
Table 4.1	CO <sub>2</sub> -Foam Mobility Measurements - Effect of Surfactant Concentrations. . . . .	141
Table 4.2	CO <sub>2</sub> -Foam Mobility Measurements - Effect of CO <sub>2</sub> Foam Fraction . . . . .	144
Table 4.3	Pure Dense CO <sub>2</sub> Flow . . . . .	146
Table 4.4	Immiscible Simultaneous Flow of CO <sub>2</sub> and 1% Brine. . . . .	146

Table 4.5	CO <sub>2</sub> -Foam Mobility Measurements - Effect of Rock Sample Permeability . . . . .	148
Table 4.6	Results of Surfactant Screening. . . . .	152
Table 4.7	Preliminary Results of Dynamic Adsorption Experiment. . . . .	174
Table 4.8	Calibration Results with Modified Set-Up. . . . .	174
Table 4.9	Viscosities of Poly $\alpha$ -Olefins in Dense Hydrocarbon Gases. . . . .	178
Table 4.10	Synthesis of Low Molecular Weight Poly-1-olefins . . . . .	180
Table 4.11	Synthesis of Diene-Containing Terpolymers. . . . .	180
Table 4.12	Viscosity of Various Trialkyltin Fluorides in Propane at a Concentration of Approximately 0.35%. . . . .	183

## GENERAL INTRODUCTION

This is the Third Annual Report on the PRRC research project, "Improvement of CO<sub>2</sub> Flood Performance," and it describes work that has been done during the past year in three task areas: Phase Behavior and Fluid Property Measurements, Mixing of CO<sub>2</sub> and Oil During Flow in Reservoir Rocks, and Mobility Control for CO<sub>2</sub> Floods. Each of these topics is the subject of a major section of this report.

This report also summarizes research accomplished during the first two years of the project, and thus can be considered a three-year final report. The reader is referred to the annual reports covering the first two years of the project and to the technical literature for additional details.

In each of the task areas, there are references to work yet to be done. Such topics represent not only extensions of current research, but also new directions, the need for which has become apparent during the course of the past three years. A new three-year research program continuing our work on the "Improvement of CO<sub>2</sub> Flood Performance" has recently commenced (October, 1987).

## PROJECT SUMMARY

All three-year tasks have been addressed and the results are summarized here. Details on several of the project areas are presented in the first two annual reports of this project; task numbers refer to the original proposal.

### Task 1 - Phase Behavior and Fluid Property Measurements (F.S. Kovarik)

- 1.1 Test the operation of low volume, high pressure crystal holder and associated instrumentation with which the viscosity of CO<sub>2</sub>-hydrocarbon mixtures can be measured using an oscillating quartz crystal.

A new quartz crystal viscometer has been developed, validated, and installed in the new continuous phase equilibrium (CPE) apparatus. Other CPE modifications have been completed and the system now has a temperature and pressure operating range of  $T < 250 \pm 0.1^\circ\text{F}$  and  $P < 5000$  psi. The CPE experiment has been designed to give rapid, simultaneous measurements of viscosity, density, and composition of flowing equilibrium phases.

- 1.2 Perform viscosity measurements along with phase composition and density measurements for mixtures of CO<sub>2</sub> with several synthetic oils at temperatures and pressures which produce liquid-vapor (L-V), liquid-liquid (L<sub>1</sub>-L<sub>2</sub>) and liquid-dense phase (L-F) equilibria.
- 1.3 Perform viscosity, phase composition and density measurements for CO<sub>2</sub>-crude oil systems in the L-V, L<sub>1</sub>-L<sub>2</sub> and L-F regions.

(1.2 and 1.3) Simultaneous viscosity/density/composition measurements have been performed on several CO<sub>2</sub>/synthetic oil and CO<sub>2</sub>/crude oil systems. These data are being used to develop viscosity/density/composition correlations with CO<sub>2</sub>/hydrocarbon mixtures. These correlations are expected to have broad-ranged applications in reservoir simulation studies. These studies assess the effect of viscosity and density ratios on local mixing and displacement behavior at reservoir conditions. Further details are presented by Kovarik and Taylor in the paper entitled "Viscosity Measurements of High Pressure CO<sub>2</sub>/Hydrocarbon Mixtures," presented at the 1987 AIChE Annual Meeting, New York City, November 15-20. The development of these new correlations is part of the newly approved three-year continuation research program (1987-1990) on CO<sub>2</sub> flood performance.

- 1.4 Evaluate performance of viscosity correlations for CO<sub>2</sub>-hydrocarbon mixtures.

The new CPE viscosity data were compared to the well-known Lohrenz-Bray-Clark correlation which is commonly used for predicting CO<sub>2</sub>/oil mixture viscosities in reservoir simulation studies. The need for a new correlation for CO<sub>2</sub>/oil systems was demonstrated. Viscosity dependency on density, composition and temperature was also examined.

- 1.5 Extend Helfferich's analysis of composition paths to analyze displacement behavior of the CO<sub>2</sub>-C<sub>1</sub>-C<sub>4</sub>-C<sub>10</sub> system.

In order to study the effect of solution gas on miscibility, MMP's (minimum miscibility pressures) of several synthetic oil and real oil mixtures with different methane compositions were measured. For the C<sub>1</sub>-C<sub>4</sub>-C<sub>10</sub> synthetic oil system, a 6.25% increase in MMP was observed when the methane composition was increased from 10% to 30% while a constant C<sub>4</sub>-C<sub>10</sub> ratio was maintained. Initial results did not show a significant increase in MMP with the addition of up to 30 mole % methane in the crude oil system. However, a second order effect is still being investigated.

If we choose the MMP above the pressure at which no methane bank is observed, the MMP may be too conservative. Observation of the composition route indicates that operation below the original bubble point pressure could result in high recovery even though this is an immiscible process.

- 1.6 Develop an improved correlation for minimum miscibility pressure which accounts more accurately for the distribution of hydrocarbon components present in the C<sub>5</sub>-C<sub>30</sub> fraction of the crude oil, and for the effects of the presence of contaminants in the CO<sub>2</sub>.

An improved correlation for MMP was developed which accounts more accurately for the distribution of hydrocarbon components present in the C<sub>5</sub>-C<sub>30</sub> fraction of the crude and for the effects of contaminants in the CO<sub>2</sub>. Details are presented in the first annual report as well as in SPE 14149 and SPE 14150.

#### Task 2 - Mixing of CO<sub>2</sub> and Oil During Flow in Reservoir Rocks (F.S. Kovarik)

- 2.1 Perform single phase miscible displacements with fluids having matched density and viscosity at three flow rates in sandstone and carbonate reservoir core samples. Obtain Coats-Smith parameters for the rock by history matching effluent composition data.

Core properties, effluent composition data, and Coats-Smith parameters for single phase miscible displacements in reservoir cores were obtained. Details are presented in the first two annual reports and in SPE 14147, SPE 14898, and SPE 15017.

- 2.2 Predict performance of gravity stable CO<sub>2</sub> floods (no water present) based on single phase Coats-Smith parameters and independent measurements of phase behavior and fluid properties using a one-dimensional process simulator.

- 2.3 Perform gravity stable CO<sub>2</sub> flood and compare performance with prediction.

(2.2-2.3) Predicted and measured performances of secondary displacements of oil by CO<sub>2</sub> in core samples were compared. See summary of conclusions for these tasks below.

- 2.4 Perform miscible displacements in both oil and water phases after steady state flow of oil and water is established in the same cores as in 2.1. Obtain Coats-Smith parameters.

Effluent composition data and Coats-Smith parameters for steady-state miscible displacements with oil and water present were obtained. Details were presented in the first two annual reports and in SPE 15389.

- 2.5 Predict performance of gravity stable tertiary CO<sub>2</sub> floods using a one-dimensional simulator.

2.6 Perform gravity stable tertiary CO<sub>2</sub> floods and compare performance with prediction.

(2.5-2.6) Predicted and measured performances of tertiary CO<sub>2</sub> floods in core samples were compared.

Conclusions covering Tasks 2.2-2.3 and 2.5-2.6.

- (a) There is experimental evidence which indicates the possibility of conducting immiscible displacements with recoveries characteristic of multiple-contact miscible displacements at pressures which correspond to the formation of a liquid-liquid type of phase behavior. This phenomenon possibly can be correlated with the very low interfacial tension between the CO<sub>2</sub>-rich and oil-rich liquid phases.
- (b) Experimental and simulation results show that the CO<sub>2</sub>-rich liquid phase can effectively displace and recover residual oil even under high water saturations such as are encountered during CO<sub>2</sub> displacement of a waterflooded porous media.
- (c) An increase in the CO<sub>2</sub> injection pressure was observed during displacements conducted at a pressure where three-phase separation occurs; this finding supports the conjectured improvement of sweep efficiency in a multiphase flow setting.
- (d) The presence of substantial microscopic pore structure heterogeneity, correlated by a flowing fraction less than one in the Coats-Smith model, has a more adverse impact during immiscible CO<sub>2</sub> floods even if that displacement is conducted at the two-liquid phase separation pressure.
- (e) The effect of the changes in mass transfer rate is more severe during miscible displacements than during near-miscible displacements as indicated by a larger relative drop in recovery at 1.2 PV.
- (f) Variations in longitudinal dispersion are almost insignificant in one-dimensional CO<sub>2</sub> floods.

A paper entitled "Efficient Immiscible Laboratory Coreflood Displacements in the Presence of a Condensed CO<sub>2</sub> Phase" is being presented at the 1988 SPE Rocky Mountain Regional Meeting, Casper, Wyoming, May 11-13 by Lansangan and Kovarik.

2.7 Attempt to correlate Coats-Smith parameters with direct observation of rock pore structure observed in thin section.

Coats-Smith parameters were correlated with direct observations of rock pore structure from thin sections. Details are presented in the first year annual report and in SPE 15017.

2.8 Perform flow visualization experiments to examine qualitative effects of microscopic heterogeneity and flow of foam on mixing of CO<sub>2</sub> and crude oil.

Flow visualization experiments were designed to examine the effects of pore structure and flow of foam on mixing of CO<sub>2</sub> and oil. Results of these experiments led to the following conclusions:

- (a) Continuous foaming was obtained in the Soltrol/water system after oil was displaced, as opposed to slug flow and in-situ foam generation for the Maljamar oil-water system.
- (b) Foam bubbles coalesced and foam generation was inhibited when foaming agents flowed into models containing oil. However, if there is a large enough water barrier between the oil and the foam, the oil may not cause coalescence. Thus, in systems where waterflooding is an important mechanism, the deleterious effect that oil has on foam may be reduced.
- (c) Continuous foaming can be inefficient in diverting fluids into unswept pores.
- (d) Cycles of in-situ foaming, followed by a CO<sub>2</sub> sweep of continuous phase paths, were effective in diverting fluids into unswept pores.
- (e) Foam was generated at the front of both CO<sub>2</sub> and surfactant solution slugs.
- (f) Pressure drops across the model were higher when foam was generated, and fluid diversion took place.
- (g) The condition of a small pore throat opening into a larger pore space aided the generation of foam in glass micromodels.
- (h) Higher surfactant concentrations improved foamability over the range of concentrations studied.
- (i) Fluid diversion can be caused not only by foam and lamellae but also by multiple interfaces of oil, CO<sub>2</sub>, and surfactant solution.
- (j) In the absence of a discontinuous CO<sub>2</sub> phase (foam), surfactant solution inhibits oil/CO<sub>2</sub> contact and oil recovery because the CO<sub>2</sub> preferentially flows through the surfactant solution phase.
- (k) At low surfactant concentrations, the presence of a methyl violet dye increased surface tension. This dye also depressed the ability of the surfactant solution to form emulsions with isooctane.

Further details on flow visualization experiments will be presented in SPE paper 17359 entitled: "The Effect of Microscopic Heterogeneity on CO<sub>2</sub>/Foam Mobility: A Mechanistic Study," at the 1988 SPE/DOE Sixth Symposium on Enhanced Oil Recovery, Tulsa, April 17-20 by Huh, Cochrane, and Kovarik.

### Task 3 - Mobility Control in CO<sub>2</sub> Floods

(J.P. Heller)

- 3.1 Improve laboratory procedures and apparatus for measuring the steady state mobility of foam-like dispersions of dense CO<sub>2</sub> in surfactant solutions.

This sub-task was completed in previous years. The apparatus and foam mobility measurement procedures are discussed in section 4.3.3 of this report.

- 3.2 Utilize above apparatus and other available equipment to perform CO<sub>2</sub>-foam mobility measurements for several surfactants and oilfield rock types over broader ranges of flow rates, surfactant concentration and flowing volume ratios. Related measurements will include adsorption and thermal stability tests to evaluate prospective surfactant for such CO<sub>2</sub> foams.

Tests described in Section 4.3.5 of the report include mobility measurements with two types of sandstone. These show that CO<sub>2</sub>-foam is not equally effective in all porous media. The most exciting result is that the relative reduction of mobility caused by foam is apparently much greater in the higher permeability rock. Description of this effect is not completed by these tests alone, but they indicate that even greater uniformity of flow can be achieved with foams than could be expected by the decrease in mobility ratio alone. Further experiments of this type are important to define the numerical bounds of the effect.

This report contains other CO<sub>2</sub>-foam mobility tests to determine the influences of surfactant concentration, and of flowing CO<sub>2</sub> fraction or "quality". A number of screening tests to measure the suitability of surfactants for this use are given. Additional laboratory and analytical work is planned for the further development of this method of mobility reduction in the continuation of this research.

- 3.3 Synthesize and test promising types of dense CO<sub>2</sub>-soluble polymers in search for suitable direct thickeners. Initial polymers to be investigated will be atactic polyalphaolefins.

This sub-task was completed early in the project. Only Ziegler-Natta catalysts could be used for the intended polymerizations. Exploratory syntheses with several members of this class were accordingly performed. A catalog of suitable catalyst combinations, concentrations, times and temperatures for the polymerizations was published in the first and second annual reports of this project.

- 3.4 Extend search for direct thickeners to include more complex co- and ter-polymers with the goal of synthesizing the highest molecular weight polymers that retain appreciable solubility in dense CO<sub>2</sub>.

The more complex hydrocarbon polymers specified in this sub-task were previously synthesized, characterized and tested, and the work reported in the second annual report of this project.

In consequence of those discoveries, the scope of direct thickener research has been considerably expanded. This new work develops a novel class of direct thickeners, the so-called associative polymers. They form polymeric solutions even though at least some of the bonds between the individual monomers are only transient. The research is described under the headings Method II and Method III. The earlier Method I research was useful here as well, because it enabled classification of structural features that enhance solubility for both associative and classical polymers.

The study has already produced (by Method III) a class of materials that can viscosify butane and propane to the extent that would be needed for use as an effective mobility control additive for Liquefied Petroleum Gas (LPG) floods, or for completely water-free "hydraulic" fracturing of the formation (utilizing butane as the frac fluid with ordinary proppants). Conclusions from the earlier work, as well as a more detailed account of the developments in Methods II and III in the continuing search for direct thickeners, is presented in Section 4.5 of the report.

- 3.5 Reconstruct and improve facility for the conduct of high pressure CO<sub>2</sub> secondary and tertiary floods in relatively large laboratory systems, with the design goal of assessing prospective mobility control additives.

Redesign of the "instrumented core" system achieves greater integrity of the lateral confinement of the flow, and consequently greater reliability. The system is described in the second annual report. Construction of a second high-pressure system, utilizing lateral flow confinement by a low-melting alloy encapsulant, is also in process. Section 4.63 of the report discusses this sub-task.

- 3.6 Utilizing the above system, perform a sequence of unprotected and mobility controlled CO<sub>2</sub> floods to test by direct comparison the utility of available mobility control methods.

Additives with which informative test sequences can be performed have recently become available. These core floods measure the displacement efficiency in larger samples, both with and without the additives to be tested. The test results will be useful as semi-quantitative indicators of the effectiveness of these additives in oil reservoirs. Work has been proceeding during the contract period, and is described in Section 4.6.4 of the report. Because the direct thickeners of light hydrocarbons were well developed, the first large core flood experiments utilize thickened and unthickened propane at high pressure as the alternative displacement fluids. (In solvent power, propane is closer than butane to CO<sub>2</sub>.)

Prior to the corefloods with propane, ordinary brine floods were performed to reduce the oil saturation to a tertiary, waterflooded condition. The analysis of these tests is given in the Section 4.6.4, and the tests are proceeding. The direct thickener in use is butyldiamyltin fluoride, one of the more effective of the unsymmetric molecules developed in Method III, described under sub-task 3.4.

As noted, the research on the mobility of CO<sub>2</sub>-foam has also progressed well in this contract period, to the point that large core floods with these mobility control additives can now be performed. When completed, a second large core will be operated in parallel with the first, as pumping equipment becomes available. The first mobility controlled test in it will be with a CO<sub>2</sub>-foam, using one of the surfactants already tested. In these floods, it will be possible to utilize the information about foam behavior that we have obtained only recently and reported here.

- 3.7 Search for other credible but less time-consuming methods to assess the usefulness of particular mobility control methods.

It has been concluded that, as incomplete and time-consuming as are long corefloods for testing the effectiveness of mobility control additives, there is no credible or practical substitute. The technical reasons for this conclusion, based on analysis of displacement mechanisms in reservoir models, are given in Sections 4.6.1 and 4.6.2 of the report.

- 3.8 Investigate reservoir engineering aspects of the application of mobility control methods. This will include studies of optimum levels of thickening, slug design criteria and economic process constraints.

The last major section of the report, 4.7, discusses the topics of this and the next sub-tasks. More general reservoir and operations engineering considerations concerning the

use of mobility control additives are given, in comparison with the water-alternating-with-gas (WAG) procedure currently used in many oilfields. Some of the special problems that might arise during the practice of mobility control with CO<sub>2</sub>-foams and with direct thickeners are discussed.

**3.9 Assist in the definition and solution of various operation engineering problems that will accompany the field use of mobility control additives in CO<sub>2</sub> floods.**

Initial guidelines, for the design of more efficient, mobility controlled CO<sub>2</sub> floods, have been developed in this project. These can be used by an operator's project engineers as starting points in the field situations they face. Special communication efforts to fulfill this sub-task have included conduct of seminars or detailed discussions on the principles and applications of mobility control, with engineers of a number of companies and laboratories.

## DISCUSSION OF RESULTS

### 1. AREA I - PHASE BEHAVIOR & FLUID PROPERTIES OF CO<sub>2</sub>/HYDROCARBON MIXTURES

#### 1.1 New Generation Continuous Phase Equilibrium (CPE) Experiment

During last year, the Continuous Phase Equilibrium (CPE) group posted four major accomplishments toward the goal of establishing the utility of the CPE apparatus. The first of these achievements was to show that crystal viscometers could operate in a CO<sub>2</sub>-crude oil system where composition changes while temperature and pressure remain constant. A CO<sub>2</sub>-crude oil experiment (CPE 210) diminished fears that heavy asphaltenes would precipitate onto the surface of the crystals and render them ineffective.

By the end of November 1986, there had been sufficient testing of the crystal viscometers to establish compliance with the original requirements for these instruments. At that time the four-year research and development stage of the viscometer project was ended, and a report (PRRC 87-2) was written to document the operation procedures and construction of the viscometer and pressure vessel.

Between February and April 1987 the computer programs which manage and process data were rewritten for easier use. Specifically, the programs were made versatile enough to handle most CO<sub>2</sub>-hydrocarbon systems, in contrast to the previous system which required that the programs be written to accommodate each specific system of hydrocarbons. This improvement will save time and relieve the requirement of having personnel intimately familiar with the long and complex process programs.

The latest accomplishment is the completion of six scheduled CPE experiments. These give details of the equilibrium phase behavior of a four-component synthetic oil system with CO<sub>2</sub> at pressures from 1300 psia to 2000 psia and temperatures from 100°F to 190°F. Results from these experiments show continuity and predictability in the data that extends the confidence limits of the CPE apparatus, and provide a data base for the extensive error analysis currently being conducted. After completion of the error analysis, tabular data with error estimates correlating viscosity and density with composition will be published for this system and future hydrocarbon-miscible gas systems.

Viscosity data on the C<sub>5</sub>-C<sub>10</sub>-C<sub>16</sub>-C<sub>30</sub> system presented in the paper, "Viscosity Measurements of High-Pressure CO<sub>2</sub>/Hydrocarbon Mixtures," by Kovarik and Taylor are slightly different (within a few percent) than some of the data presented here because:

- (1) Calculations for the paper were made after extensive system error analysis.
- (2) Data points located two standard deviation points out were removed. The data presented in the paper should be considered slightly more accurate. All conclusions are exactly the same.

##### 1.1.1 General Procedure Used for the Four-Component Synthetic Oil System

Six CPE experiments involving the dilution of a four-component synthetic separator oil with CO<sub>2</sub> have been conducted at six different pressure-temperature combinations in order to document the fluid properties of this system. The oil was composed of approximately 14 mole %-nC<sub>5</sub>, 54%-

nC<sub>10</sub>, 19%-nC<sub>16</sub>, and 13%-C<sub>30</sub> (squalene). Temperatures and pressures in the different experiments ranged from 100°F to 190°F and 1300 psia to 2000 psia, respectively.

In each experiment, the fluid reservoir (see Fig. 1.1), instruments, and tubing were completely filled with oil up to the back pressure regulators (160 cc). Once an experiment was started, fluid was sampled alternately from the top and bottom sample ports at three minute intervals until the experiment was stopped at the phase split. At this time the viscometers were cleaned with tetrahydrofuran, and the vacuum bandwidths were re-checked. The experiment was restarted and continued until the lower phase liquid was depleted.

Throughout the experiment CO<sub>2</sub> was injected at a constant rate that was initially selected according to the miscibility of CO<sub>2</sub> in the oil at the conditions of the experiment (see Table 1.1). Two density and two viscosity measurements were taken every six minutes, one set from the upper sample port and one set from the lower sample port; gases evolved from the oil were analyzed by gas chromatograph once every half hour for each sample stream. Separator fluid was collected in air-tight sample vials that were filled for one hour before switching to the next sample vial. Each sample vial filled represented one data point for correlating viscosity and density to fluid composition. The recombined fluid composition was calculated for each sample from (1) the weight of oil in the sample vial, (2) the volume of gas evolved from the sample vial, (3) two gas composition analyses averaged over the sample period, and (4) the composition of the oil from the liquid chromatograph analysis. For each sample ten viscosity and ten density readings were averaged to produce a representative viscosity and density.

### 1.1.2 Discussion of Results

The table and graphs presented here are used both for the continuing validation of the CPE apparatus and the correlation of viscosity/density/composition. Tabular data presenting information for the latter purpose will appear in a subsequent report following the completion of an error analysis. Since the accuracy of the densitometers and viscometers used in the CPE apparatus have been extensively investigated (Cullick & Mathis, 1984; Orr & Silva, 1983; Taylor et al., 1987) the error analysis will be focused on two other aspects of the system: (1) the instruments and method used to obtain high-pressure fluid compositions from low-pressure data (known as recombination) and (2) the time association of fluid properties to fluid composition. The latter originates from the fact that at any specific time the fluids in the various instruments are not at a constant composition, but form a stream that changes continuously toward higher CO<sub>2</sub> concentration in the upstream direction. Time association is particularly important in the first hours of the experiment when CO<sub>2</sub> concentration is low, and viscosity is changing rapidly with respect to time.

Two CPE experiments are scheduled as a portion of the error analysis routine in part to determine a time association "offset" for each instrument as a function of injection rate. These experiments will be conducted on a binary CO<sub>2</sub>/hydrocarbon system for which viscosity composition data are available from other sources and will serve as a comparative reference that will help determine the reliability of data from the more complex and heretofore unknown systems now being studied.

### 1.1.3 C<sub>5</sub>-C<sub>10</sub>-C<sub>16</sub>-C<sub>30</sub> Systems

A series of PVT (static cell) experiments have been performed on a four-component synthetic oil to determine bubble point pressures over a range of CO<sub>2</sub> concentrations and temperatures. In Table 1.1, bubble point CO<sub>2</sub> concentrations from the static cell are compared phase split CO<sub>2</sub>

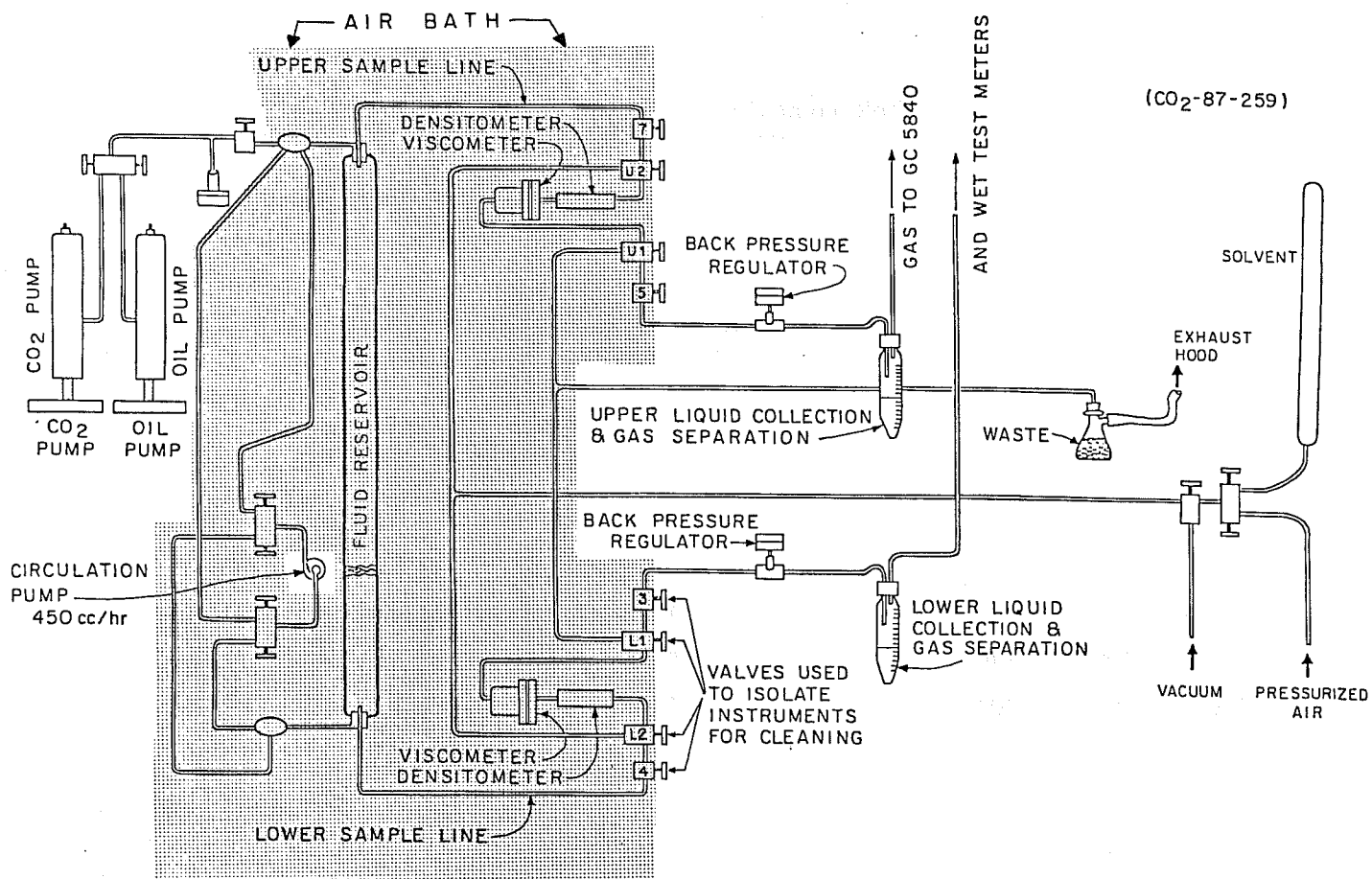


Figure 1.1. Diagram of CPE apparatus.

Table 1.1

Equilibrium Bubble Point CO<sub>2</sub> Composition: Comparing the CPE  
and Static PVT Cell Experiments with a Four Component Synthetic Oil

CO<sub>2</sub> Composition at Phase Split for C<sub>5</sub>-C<sub>10</sub>-C<sub>16</sub>-C<sub>30</sub> System

Run No.	Temp. (°F)	Pressure (psia)	Injection Rate (cc/hour)	Mole % CO <sub>2</sub>		Difference
				at Bubble Point (static cell)	at Phase Split (CPE)	
207	100	1300	16	85 %	84 %	- 1 %
216	100	1500	12	88 %	84 %	- 4 %
212	100	2000	12	94 %	93 %	- 1 %
215	150	1500	8	70 %	67 %	- 3 %
217	190	1300	8	56 %	53 %	- 3 %
214	190	2000	8	70 %	68 %	- 2 %

concentrations from the CPE experiments. If CPE experiments were operating in true phase equilibrium, the two sets of data would agree; the difference gives a measure of how far out of equilibrium the CPE experiments are running. The comparison shows CPE concentrations are lagging equilibrium values by an average of 3.2%.

Fig. 1.2 shows the viscosity of pure oil at the beginning of each run and the viscosity of the CO<sub>2</sub> saturated oil just before phase split. The experimental run numbers have been labeled by each data point for easy reference to other graphs presented here. There is no viscosity information on this system in the literature for comparison; however, the data are consistent in a relative sense. The viscosity at phase split, or saturation viscosity, is significant because it is the lowest viscosity obtained by the oil-rich phase, and it reflects the solubility of CO<sub>2</sub> in the system. For example, at 100°F and 1300 psia the viscosity of the oil is reduced by a factor of 8, but at the same pressure and 190°F, oil viscosity is only reduced by a factor of 1.6. The saturation viscosity is actually lower at 100°F than at 190°F. The explanation for this lies primarily in that CO<sub>2</sub> is more soluble at the lower temperature while the negative sloped saturation viscosity curves in Fig. 1.2 reflect increased CO<sub>2</sub> solubility with pressure. Because the saturation viscosity is a single point boundary condition, characteristic of a CO<sub>2</sub>/oil system at a specific temperature and pressure, a viscosity ratio involving the saturation viscosity could possibly be used as a parameter in future viscosity-composition correlations.

#### 1.1.4 Comparison of Experiments at 100°F, CPE 207, 216 and 212

Figs. 1.3-1.5 show the viscosity/density/time ( $\mu, \rho, t$ ) diagram for CPE experiments at 1300, 1500, and 2000 psia, respectively, all at 100°F. Viscosity and density scales are identical in these plots so they may be compared more easily. Prior to phase split the upper and lower sets of instruments should measure the same fluid, and so upper and lower viscosity lines should coincide as should upper and lower density lines. When these lines fail to coincide, it is partly due to instrument error and partly due to imperfect mixing, which results in one sample port passing fluid richer in CO<sub>2</sub> than the other port. An example of imperfect mixing is illustrated in Fig. 1.3 where differences in measured CO<sub>2</sub> content are labeled on the curve. In Figs. 1.4 and 1.5 upper and lower concentrations are close enough that an average concentration can be displayed at the top of each diagram to represent both sample streams.

The small scatter in viscosity measurements prior to CO<sub>2</sub> injection is a problem still awaiting satisfactory explanation; however, it has been shown in earlier tests that above 0.5 centipoise, measurement errors are almost always above reference values. Usually in repeated measurements of the same fluid, the smallest value will be repeated with more frequency than any of the larger values, and it is the smallest repeated value that is taken to be the most probable viscosity for that sample.

The most noticeable post phase-split trend that comes from comparing these three diagrams is the divergence between upper and lower phase fluid properties which is large at low pressure and small at high pressure. This trend suggests that at some pressure not far above 2000 psia, CO<sub>2</sub> may be miscible in all proportions with the oil.

Pseudo-ternary diagrams in Figs. 1.6-1.9 show composition labeled with viscosity for CPE experiments 207, 216, and 214. The viscosity and composition data shown in these figures may be altered slightly when these data appear in tabular form following the error analysis previously mentioned. Note that Figs. 1.6-1.8 show only the top half of the ternary diagram in order that the details of the two-phase envelope may be seen. Figs. 1.10-1.13 show ( $\mu, \rho, t$ ) plots for the 150°F and 190°F experiments. A separate graph for each phase is used with higher temperature experiments

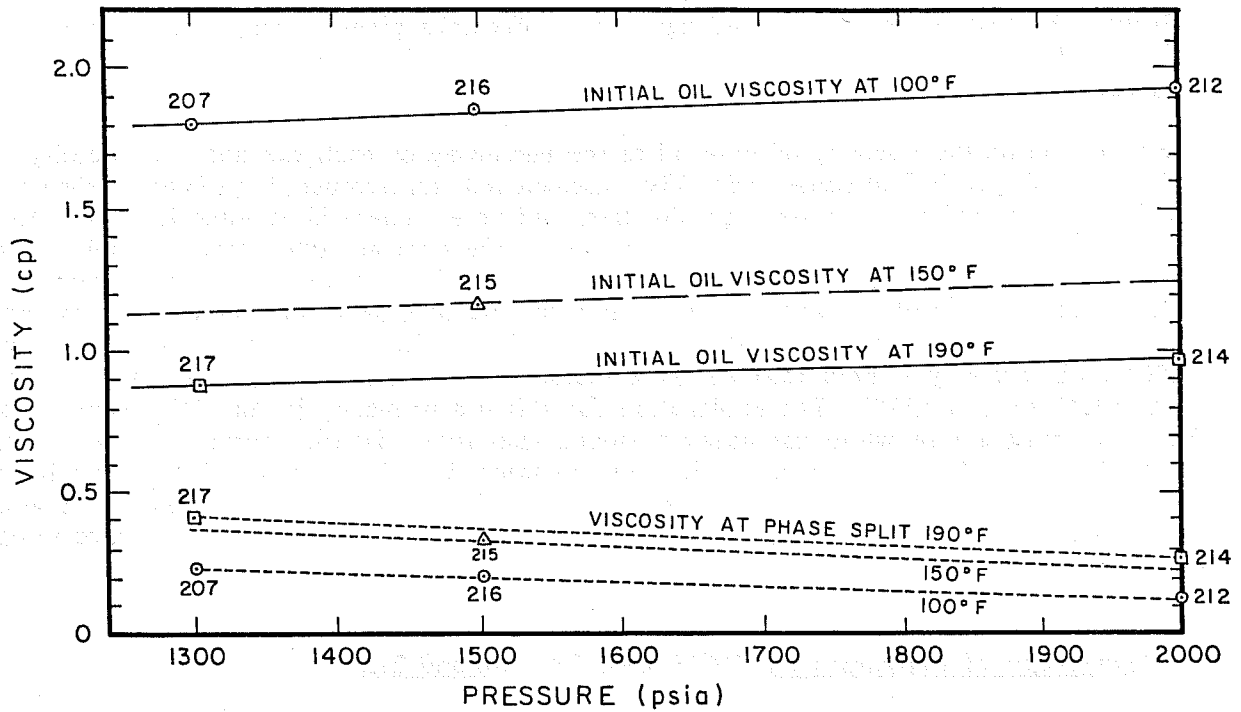


Figure 1.2. Initial oil viscosity and saturation oil viscosity for the synthetic oil/CO<sub>2</sub> system.

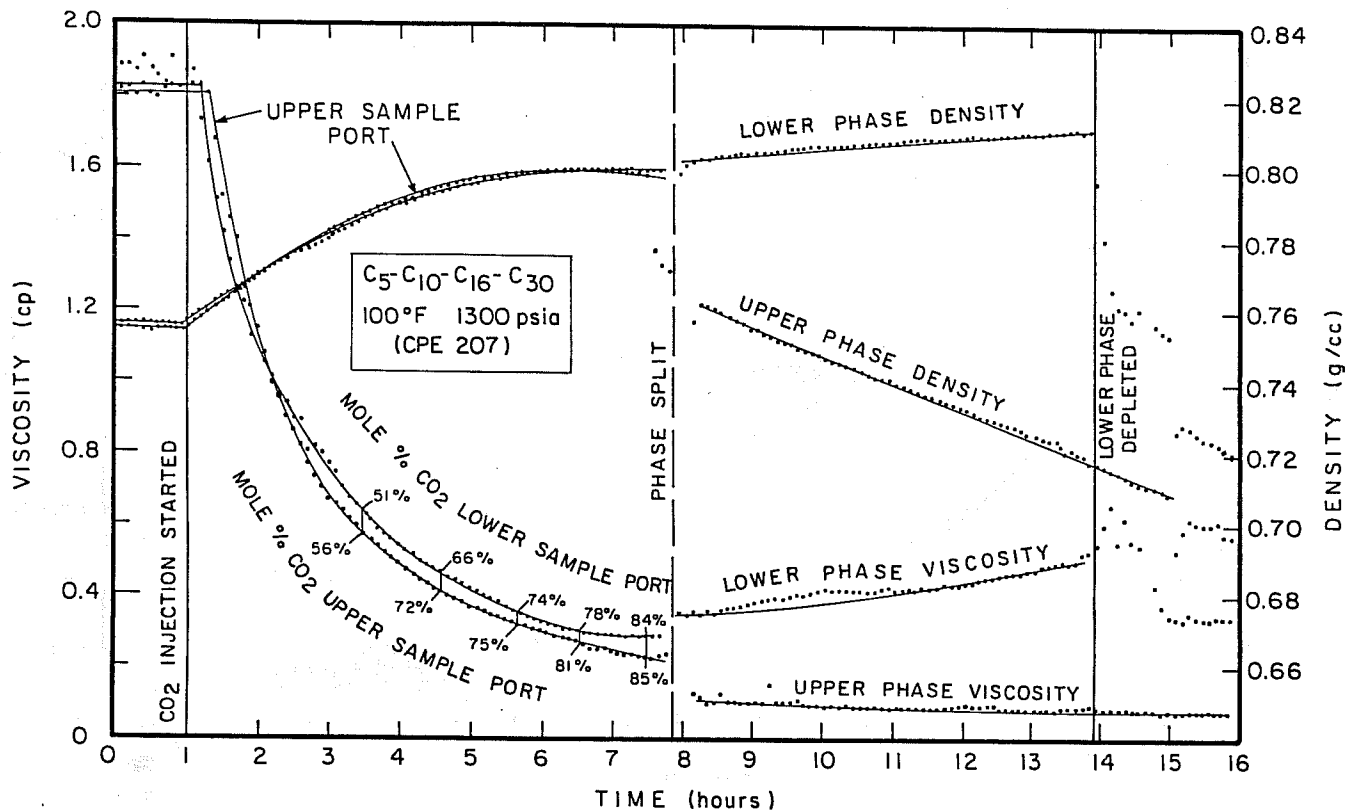


Figure 1.3. Viscosity/density/time plot for synthetic oil at 100°F and 1300 psia (CPE 207).

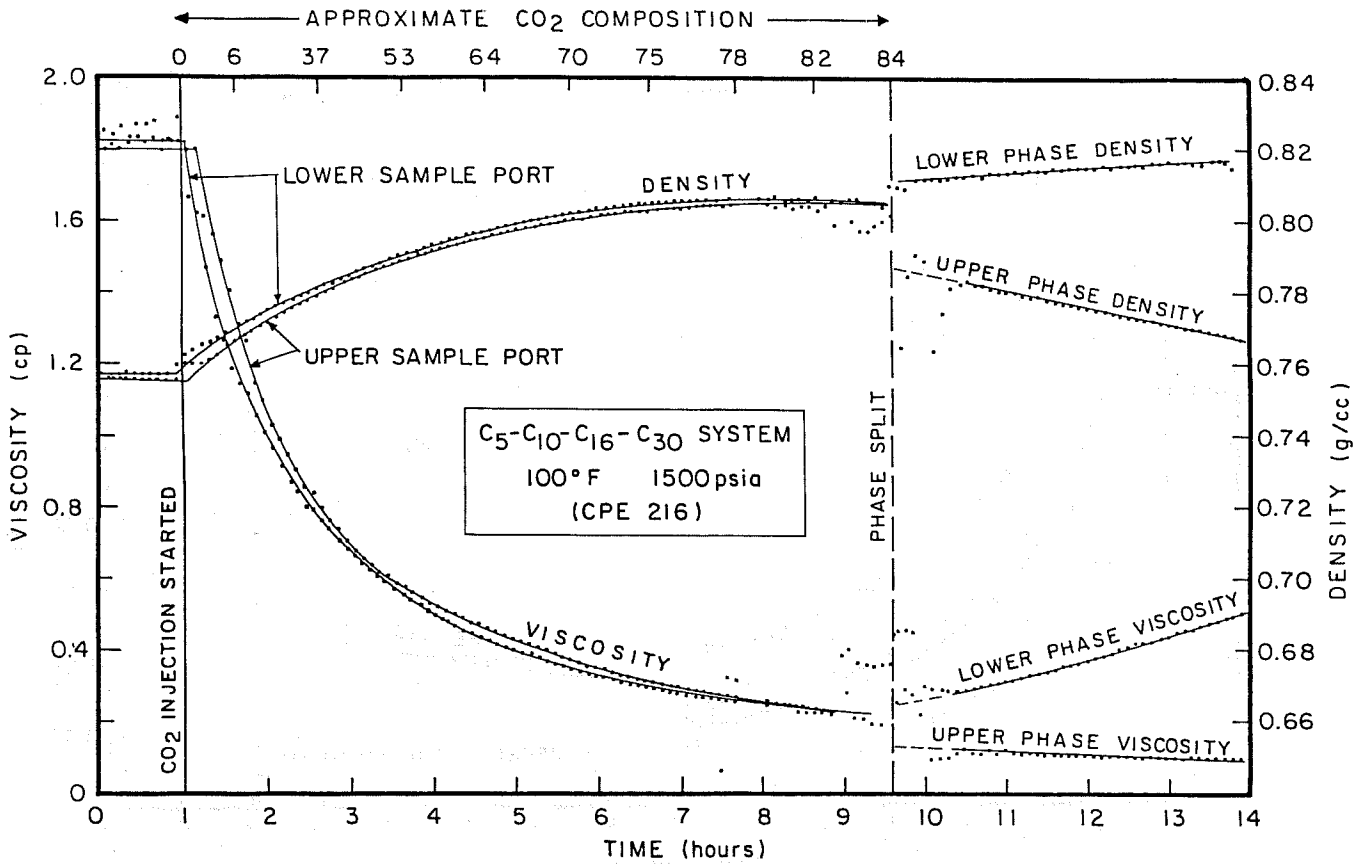


Figure 1.4. Viscosity/density/time plot for synthetic oil at 100°F and 1500 psia (CPE 216).

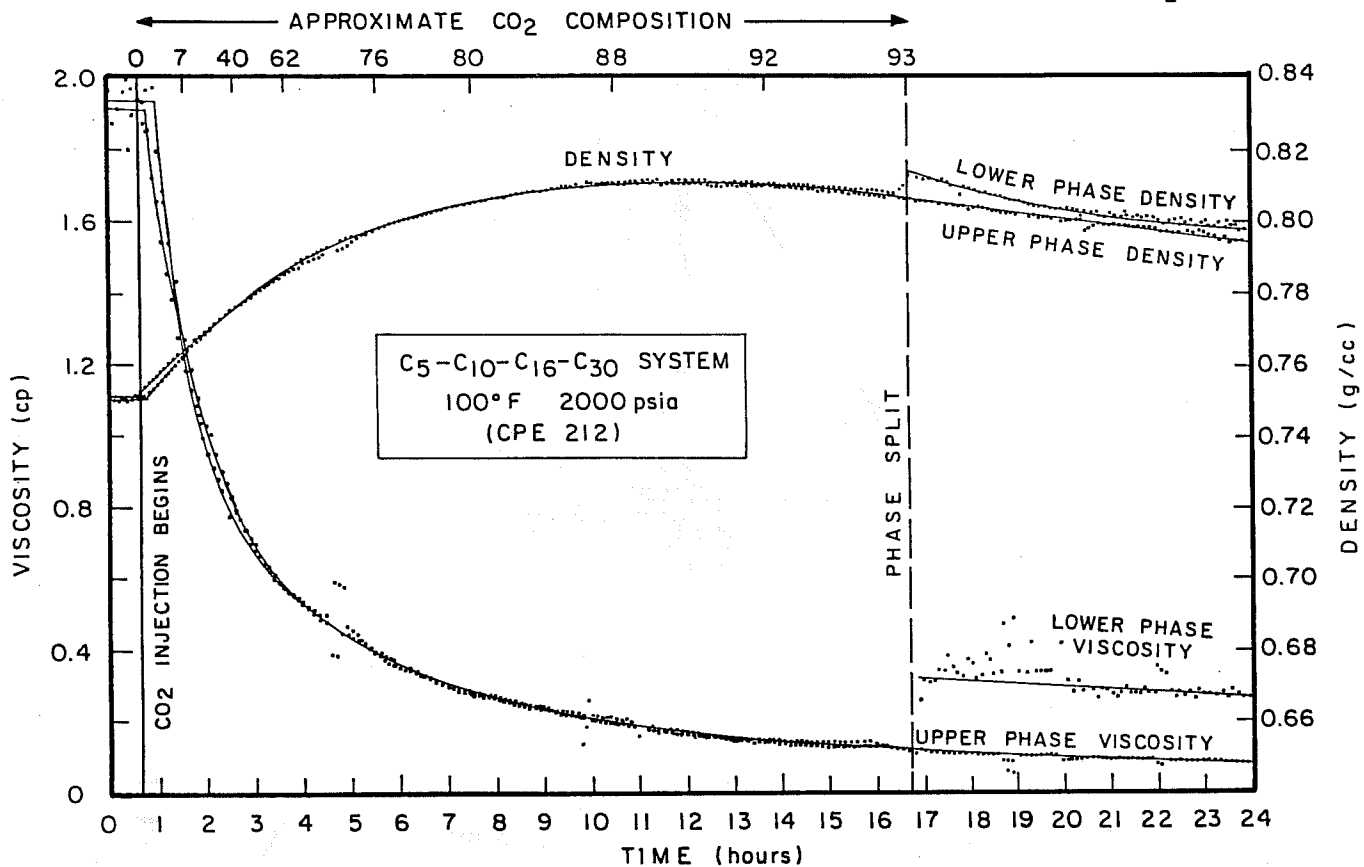


Figure 1.5. Viscosity/density/time plot for synthetic oil at 100°F and 2000 psia (CPE 212).

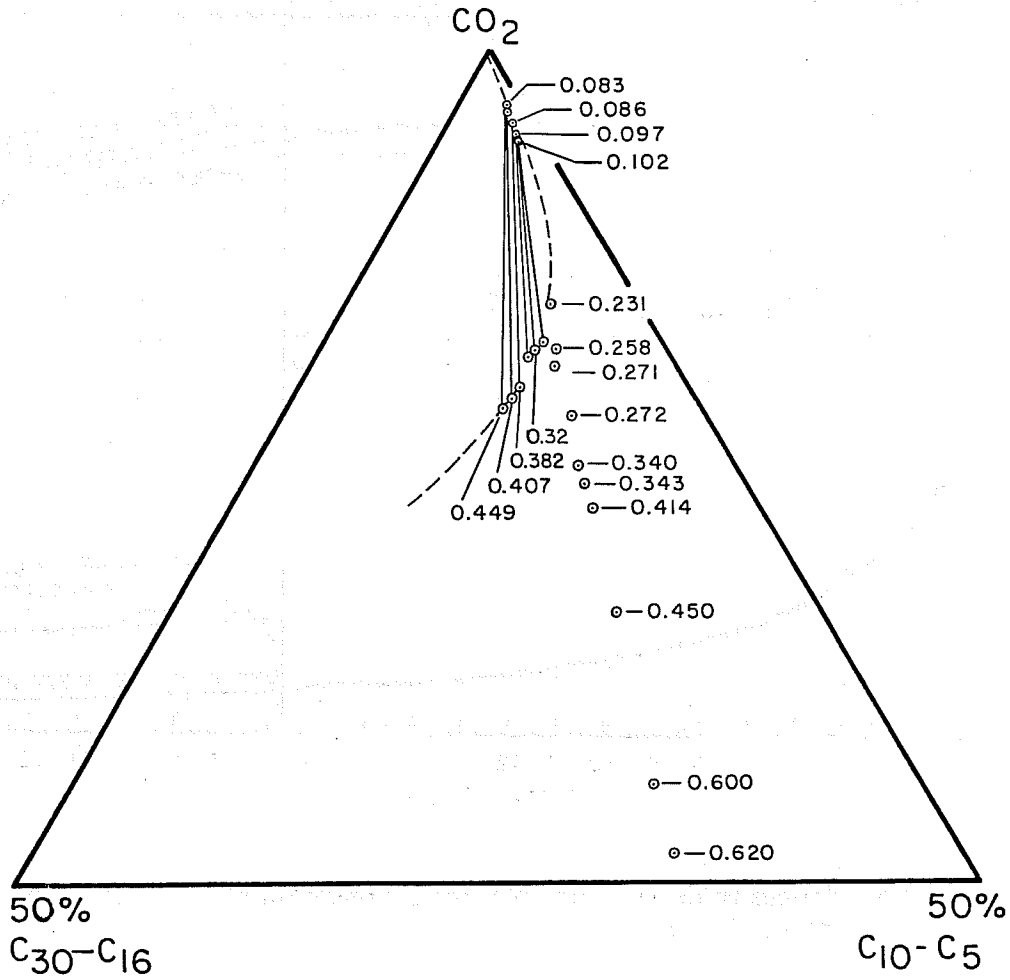


Figure 1.6. Top 50% ternary with viscosity for synthetic oil at 100°F and 1300 psia (CPE 207).

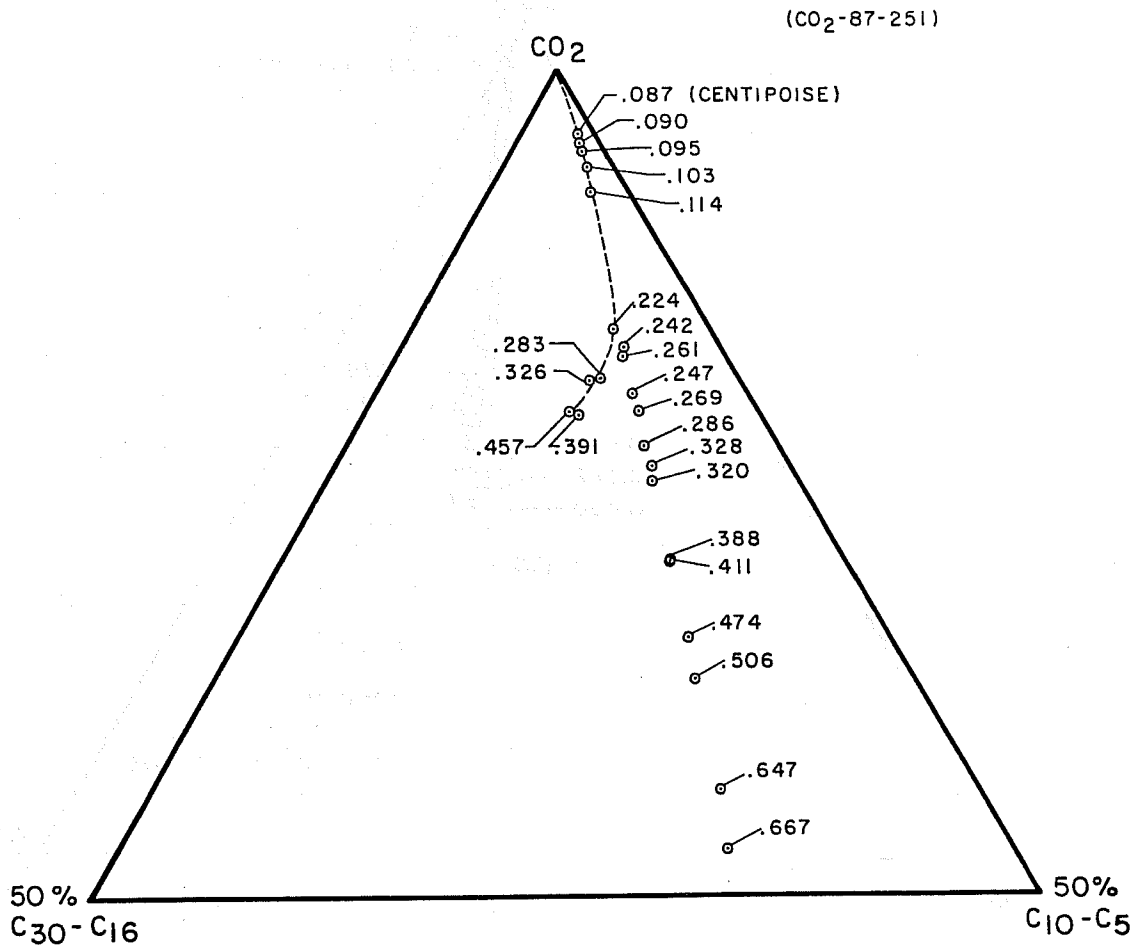


Figure 1.7. Top 50% ternary with viscosity for synthetic oil at 100°F and 1500 psia (CPE 216).

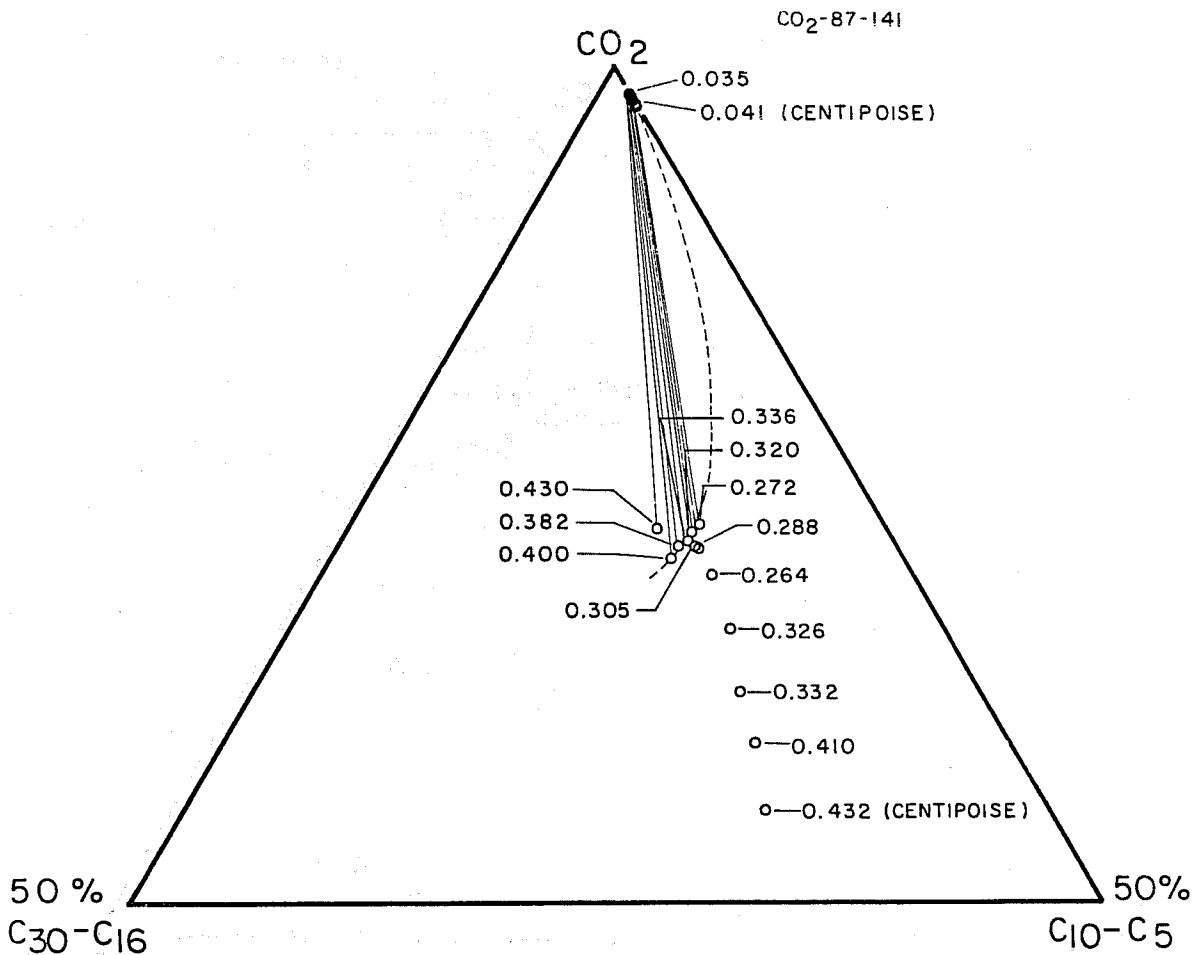


Figure 1.8. Top 50% viscosity ternary for synthetic oil at 190°F and 2000 psia (CPE 214).

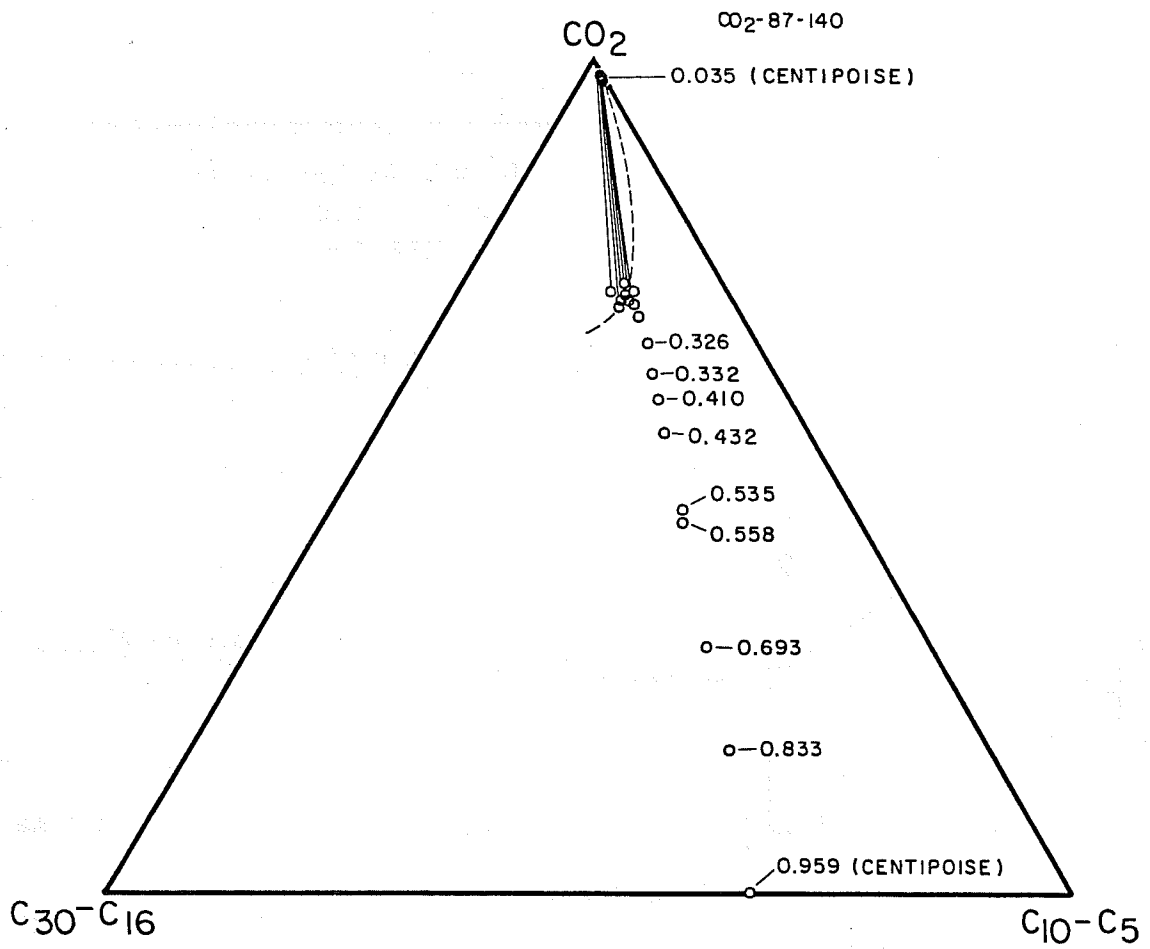


Figure 1.9. Complete viscosity ternary for synthetic oil at 190°F and 2000 psia (CPE 214).

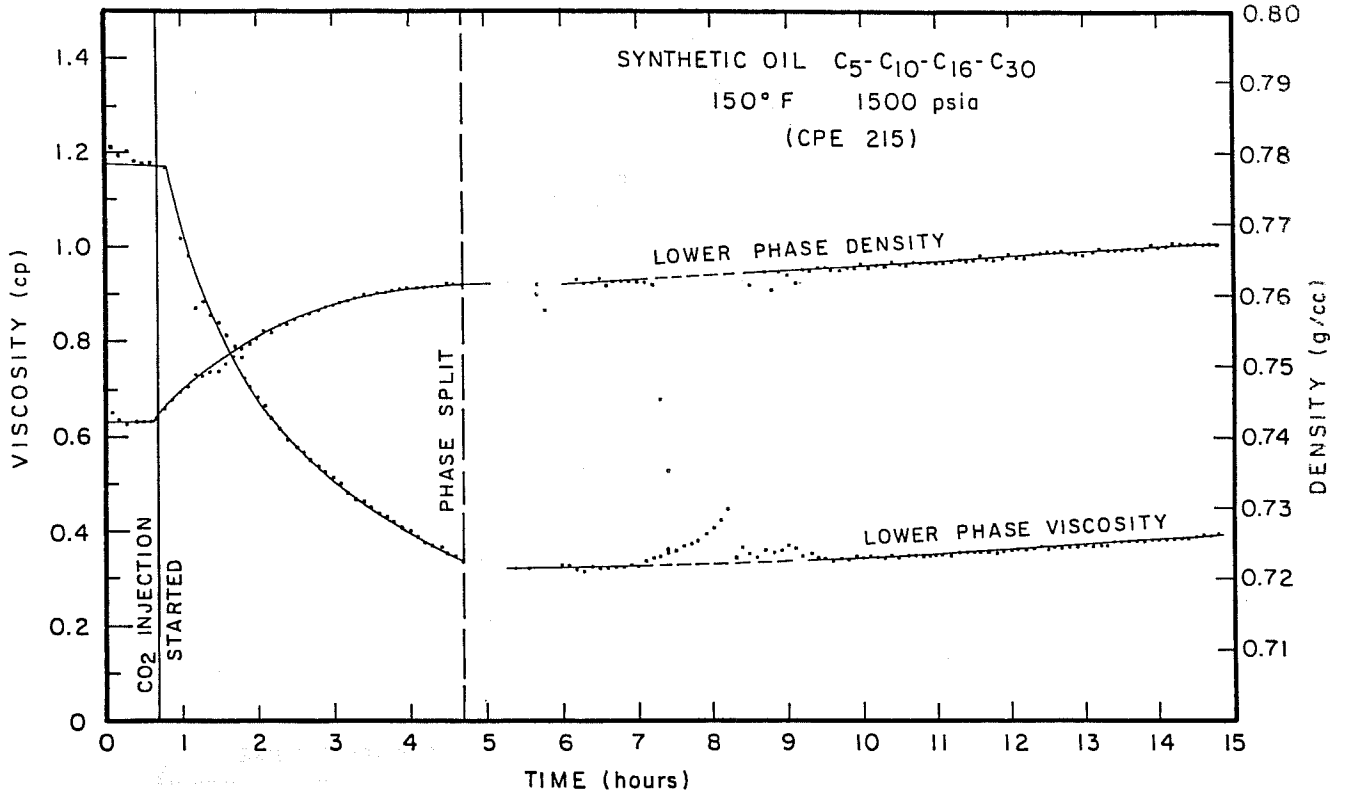


Figure 1.10. Viscosity/density/time plot for synthetic oil at 150°F and 1500 psia, lower phase (CPE 215).

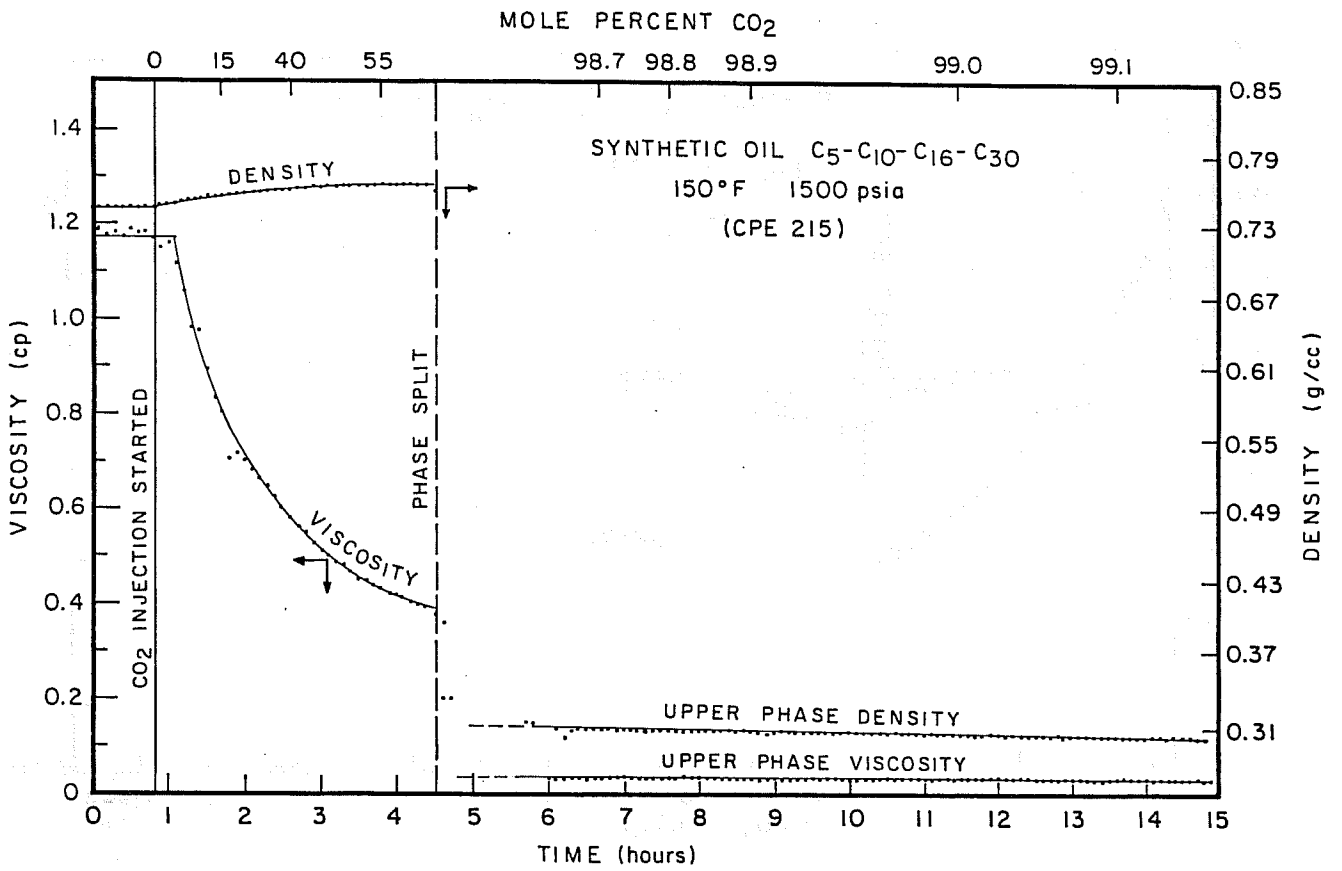


Figure 1.11. Viscosity/density/time plot for synthetic oil at 150°F and 1500 psia, upper phase (CPE 215).

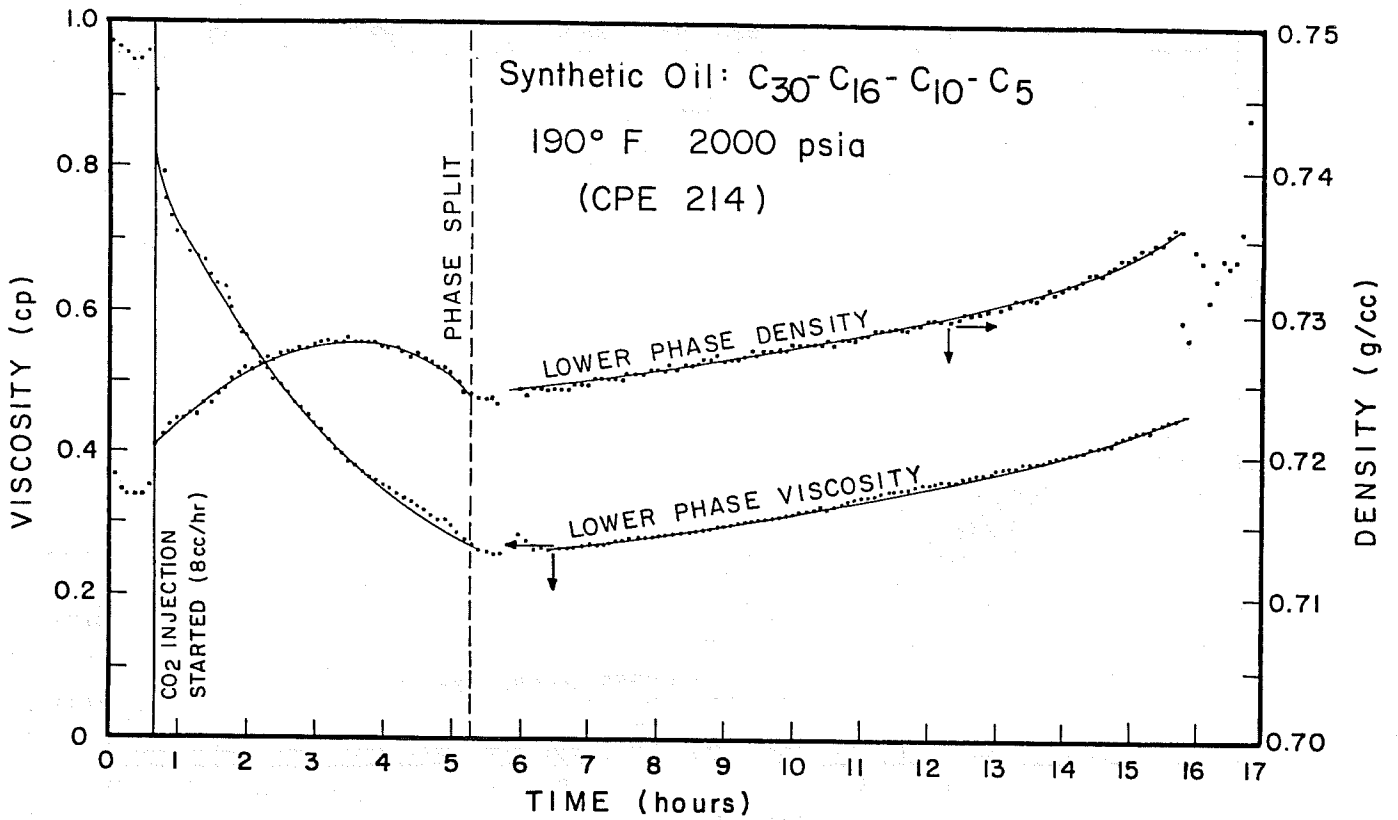


Figure 1.12. Viscosity/density/time plot for synthetic oil at 190°F and 2000 psia, lower phase (CPE 214).

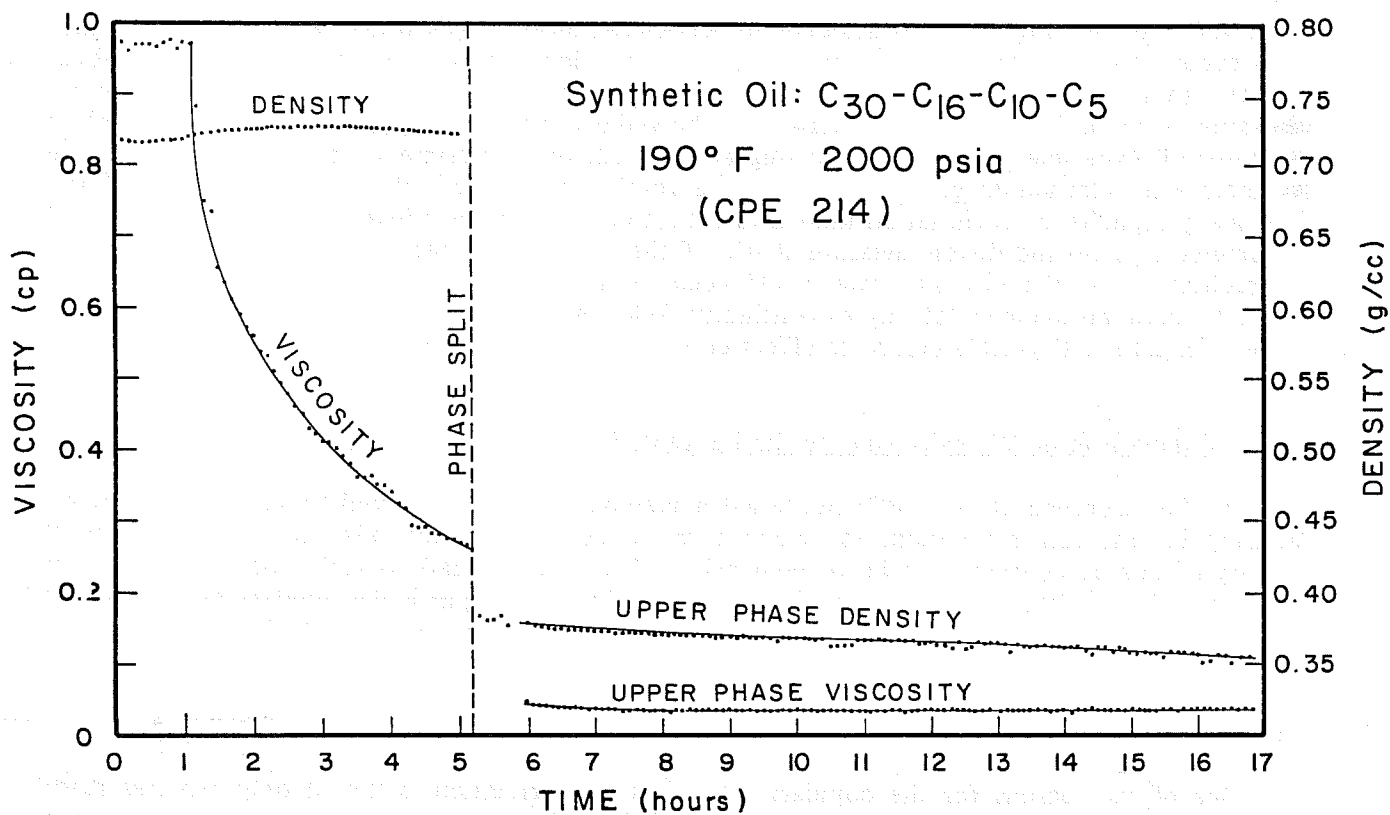


Figure 1.13. Viscosity/density/time plot for synthetic oil at 190°F and 2000 psia, upper phase (CPE 214).

because of large differences between upper and lower phase fluid properties. The lower phase ( $\mu, \rho, t$ ) plot from CPE 215 (Fig. 1.10) shows erroneous data between hours 7 and 9 which happened when valve #4 (see Fig. 1.1) was accidentally left closed after a back pressure regulator adjustment. This caused fluid in the lower instruments to come slowly to atmospheric pressure. The low density readings were used automatically in the viscosity equation to calculate the erroneous viscosities seen in Fig. 1.10. Figs. 1.14-1.17 show the ternary and ( $\mu, \rho, t$ ) plots for the Maljamar separator oil experiment. At the beginning of hour 12, this experiment was stopped, and the viscometers were cleaned to check for asphaltene fouling of the crystals. It was of much concern that heavy asphaltene precipitation known to collect on PVT cell windows would also collect on the viscometer crystals and distort measurements. If the crystals had been fouled in this manner, then a discontinuity of the viscosity data would occur as a result of cleaning. The viscosity plots in Fig. 1.15 show no evidence of any discontinuity following hour 12, which probably means that not enough asphaltene deposit occurred to affect crystal performance.

### 1.1.5 Comparison of Viscosity Data to the Lohrenz, Bray and Clark Correlation

In 1964 Lohrenz et al. (LBC) published a method, which is routinely used in the petroleum industry in reservoir simulation, to calculate the viscosity of crude oils. In order to check the validity of this correlation, a series of comparisons between calculations and experimental data was performed for different systems containing hydrocarbons. Of particular interest are the systems containing CO<sub>2</sub>, given the anomalies this component presents with respect to hydrocarbons.

#### 1.1.5.1 The Correlation

One of the reasons for the popularity of the LBC correlation is that it only requires readily available data; in addition, its computation is simple and easy to include in computer programs. The equations are based on the correlation of Jossi et al. (1962) which are adapted by LBC to crude oil systems. In our comparisons, only the liquid phase was considered.

The viscosity ( $\mu$ ) is calculated in the LBC correlation by

$$[(\mu - \mu^*) \zeta + 10^{-4}]^{\frac{1}{4}} = 0.1023 + 0.023364 \rho_r + 0.058533 \rho_r^2 - 0.040758 \rho_r^3 + 0.0093324 \rho_r^4 \quad (1.1)$$

where

$$\mu^* = \frac{\sum_{j=1}^n (x_j \mu_j^* \sqrt{\mu_j})}{\sum_{j=1}^n (x_j \sqrt{\mu_j})}, \quad (1.2)$$

n = number of components

$$\zeta = \frac{\sum_{j=1}^n (x_j T_{c_j})^{1/6}}{\left( \frac{\sum_{j=1}^n (x_j \mu_j)^{1/2}}{\sum_{j=1}^n (x_j P_{c_j})^{2/3}} \right)} \quad (1.3)$$

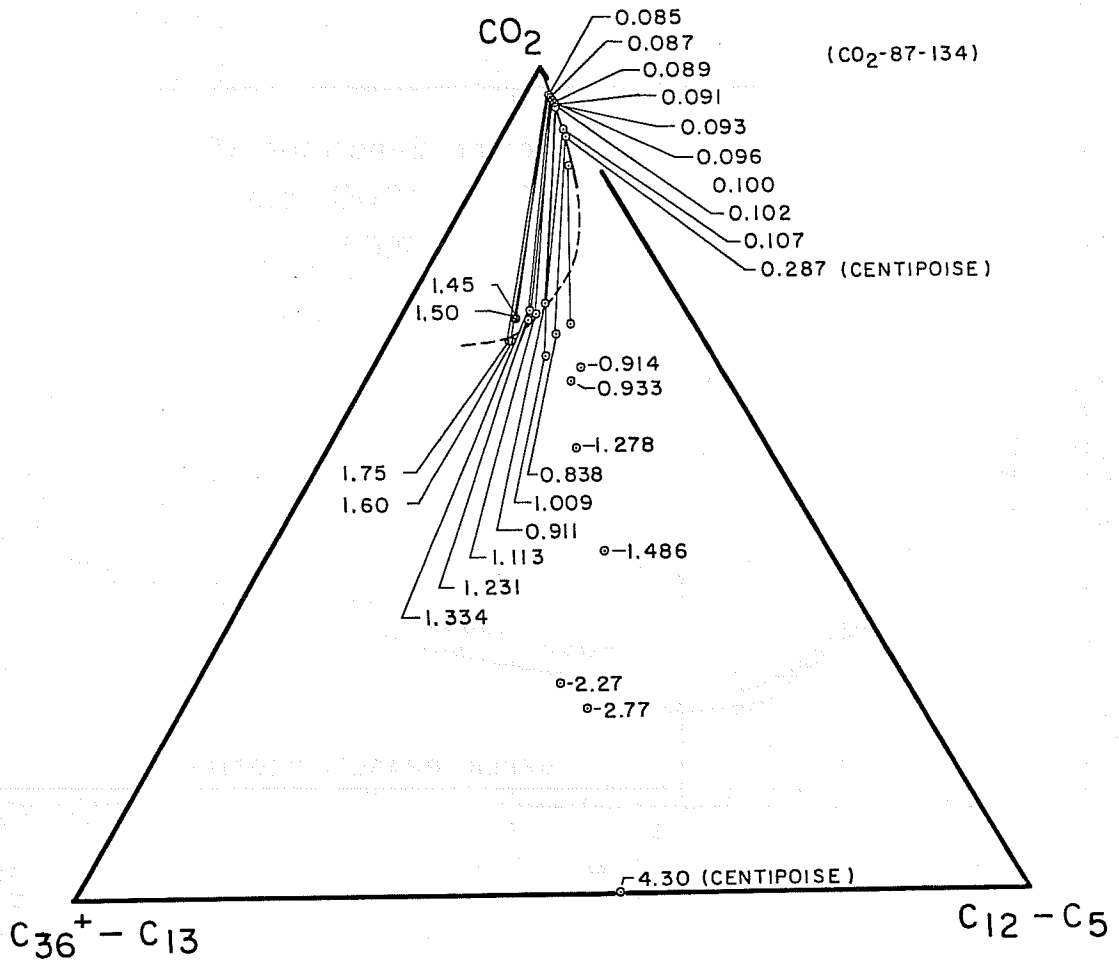


Figure 1.14. Complete viscosity ternary for Maljamar separator oil at 90°F and 1200 psia (CPE 210).

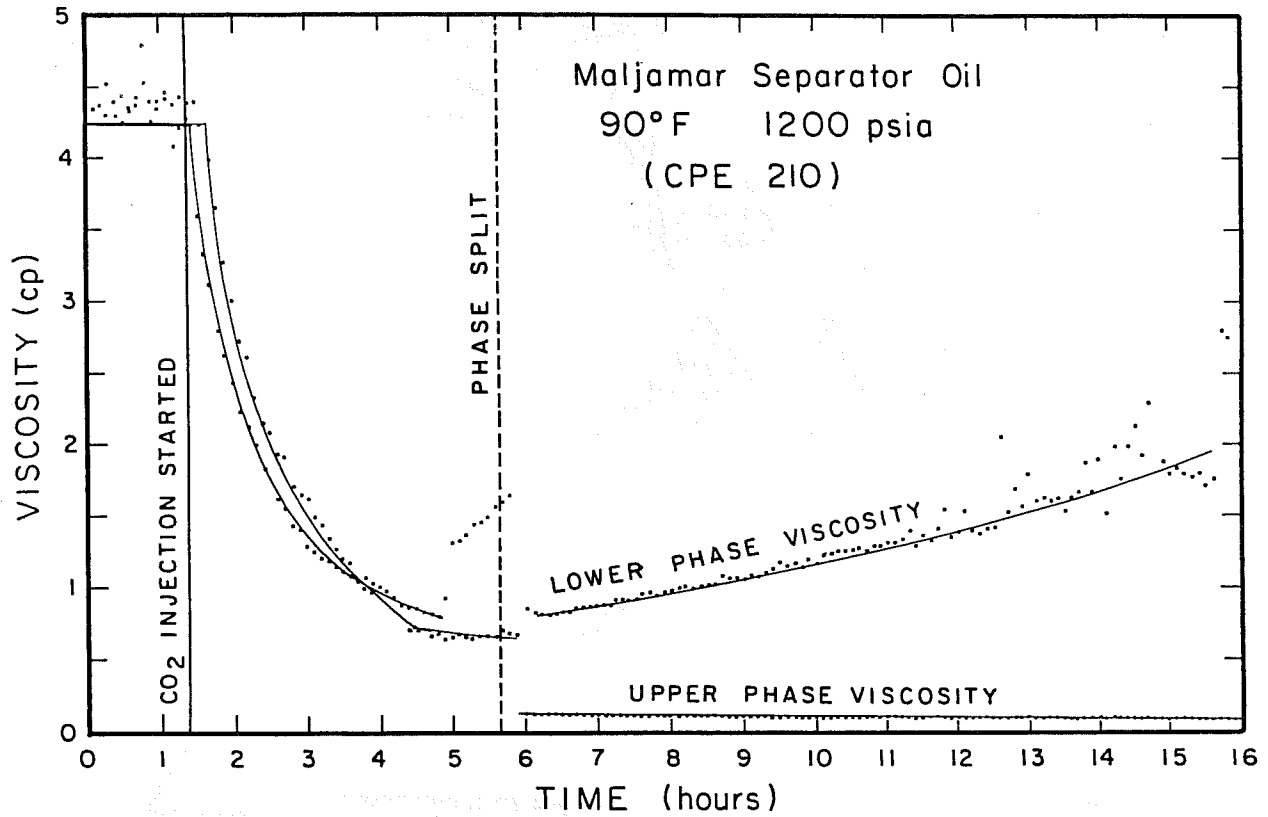


Figure 1.15. Viscosity/density/time plot for Maljamar separator oil at 90°F and 1200 psia (upper and lower phase).

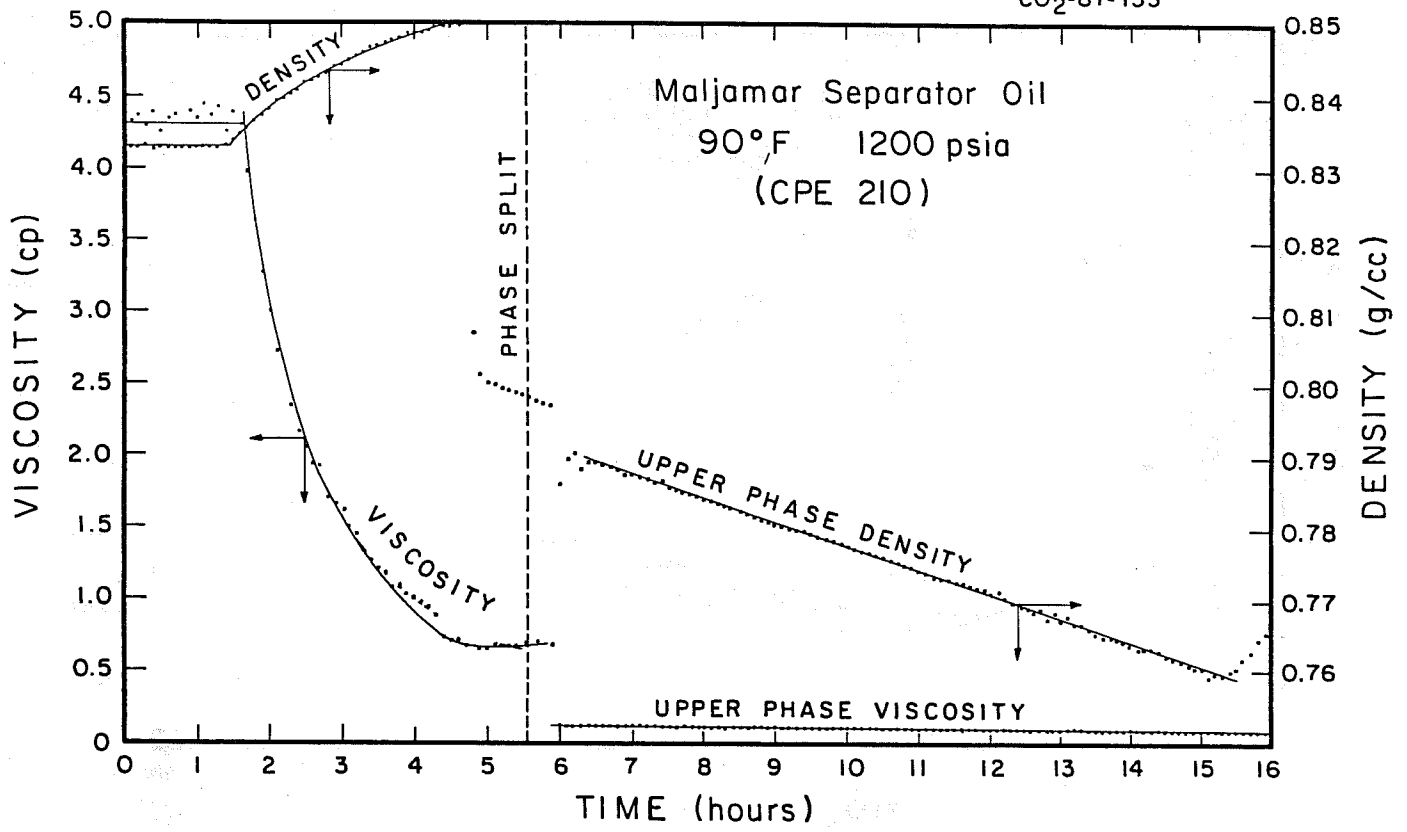


Figure 1.16. Viscosity/density/time plot for Maljamar separator oil at 90°F and 1200 psia (upper phase).

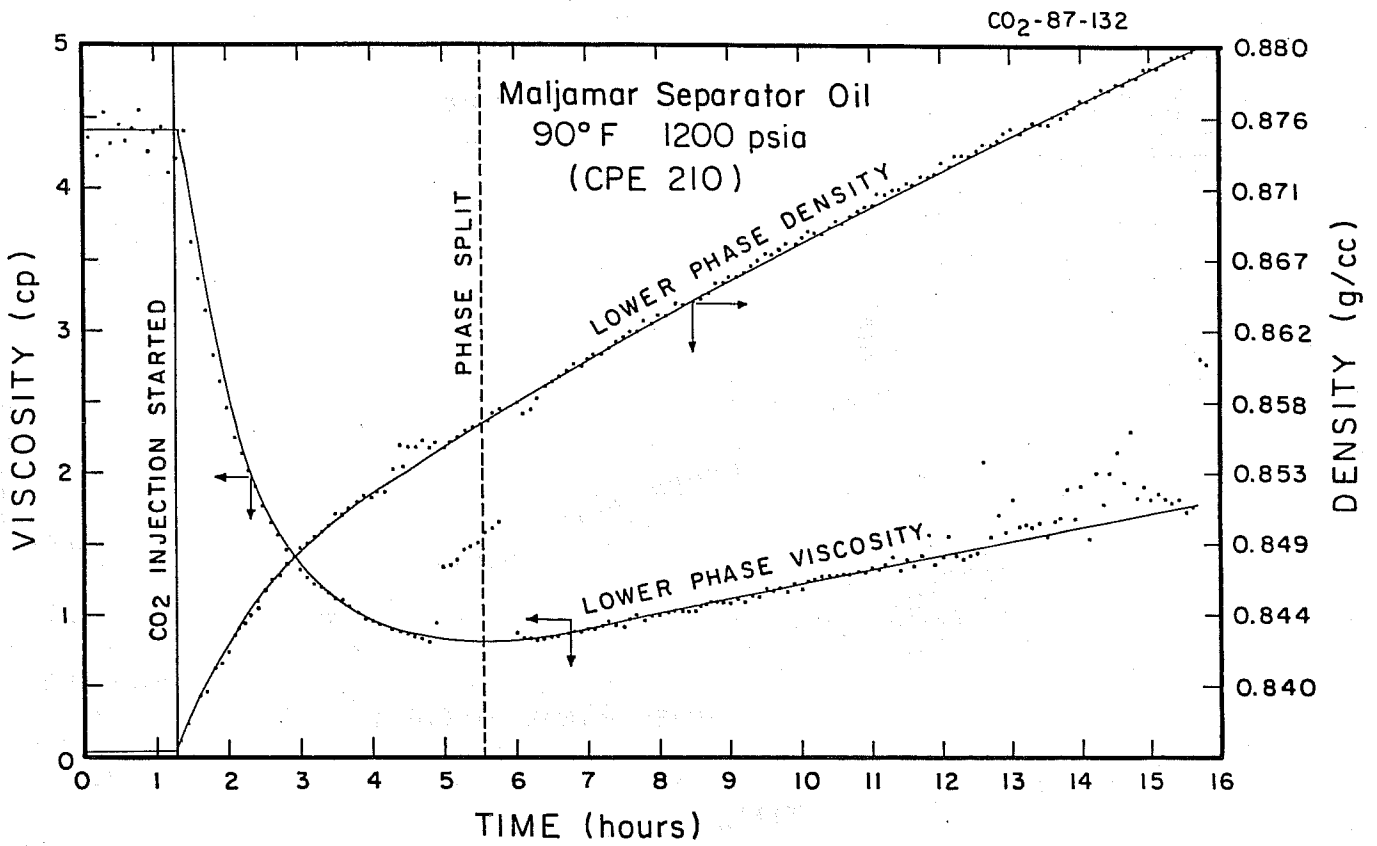


Figure 1.17. Viscosity/density/time plot for Maljamar separator oil at 90°F and 1200 psia (lower phase).

$$\rho_r = \frac{\rho}{\rho_c} \quad (1.4)$$

$$\rho_c = \frac{1}{V_c} = \frac{1}{\sum_{\substack{j=1 \\ j \neq C_{7+}}}^n (x_j V_{cj}) + x_{C_{7+}} V_{cC_{7+}}} \quad (1.5)$$

$$\mu_j^* \zeta_j = 34 \times 10^{-5} T_{rj}^{0.94} \quad (\text{if } T_{rj} < 1.5), \quad (1.6)$$

$$\mu_j^* \zeta_j = 17.78 \times 10^{-5} (4.58 T_{rj} - 1.67)^{5/8} \quad (\text{if } T_{rj} > 1.5) \quad (1.7)$$

$$\zeta_j = \frac{T_{cj}^{1/6}}{M_j^{1/2} P_{cj}^{2/3}} \quad (1.8)$$

$$T_{rj} = \frac{T}{\sum_{j=1}^n (x_j T_{cj})} \quad (1.9)$$

The critical volume of the  $C_{7+}$  fraction is estimated from:

$$V_{cC_{7+}} = 21.573 + 0.015122 M_{C_{7+}} - 27.656 G_{C_{7+}} + 0.070615 M_{C_{7+}} + G_{C_{7+}} \quad (1.10)$$

It was found in our calculations that for heavier pure components the use of Eq. 1.10 for  $V_c$  is preferable to the real critical volume of the component. This equation must be considered part of the correlation in all the cases.

The data required for this set of equations are the critical properties and molecular weight of each component ( $P_{cj}$ ,  $T_{cj}$ ,  $V_{cj}$ ,  $M_j$ ), the composition and density of the system ( $x_j$ ,  $\rho$ ) and the molecular weight and specific gravity of the  $C_{7+}$  fraction ( $M_{C_{7+}}$ ,  $G_{C_{7+}}$ ).

### 1.1.5.2 Results of Calculations

The calculations were performed for several systems of interest to the petroleum industry. The results are summarized in Tables 1.2-1.6 and Figs. 1.18-1.22.

The deviation of the calculated viscosity from the corresponding experimental values can be as high as 60% in some cases. Simple binary hydrocarbon systems like  $C_6 + C_{16}$  still show errors of

Table 1.2

Comparison of Calculated and Experimental Viscosity for the  
CO<sub>2</sub>-C<sub>5</sub>-C<sub>10</sub>-C<sub>16</sub>-C<sub>30</sub> System at 190°F and 2000 psia (CPE 214)

CO <sub>2</sub>	nC <sub>5</sub>	nC <sub>10</sub>	nC <sub>16</sub>	C <sub>30</sub>	$\rho$ (g/cm <sup>3</sup> )	$\mu$ exp (cp)	$\mu$ calc. (cp)	error %
.0000	.1266	.5344	.1935	.1455	.718	.970	.7712	-20.5
.2995	.1015	.3668	.1330	.0992	.723	.689	.6912	0.3
.4509	.0811	.2864	.1035	.0781	.726	.534	.5485	2.8
.5573	.0636	.2322	.0840	.0630	.727	.432	.4246	-1.7
.6283	.0522	.1953	.0711	.0531	.727	.332	.3412	2.8
.6980	.0396	.1589	.0588	.0488	.725	.264	.2737	3.7
.7273	.0351	.1428	.0535	.0413	.725	.272	.2374	-12.7
.7126	.0339	.1516	.0577	.0442	.726	.288	.2563	-11.0
.7143	.0323	.1509	.0580	.0445	.727	.305	.2582	-15.3
.7234	.0302	.1456	.0571	.0437	.728	.320	.2525	-21.1
.7177	.0275	.1492	.0597	.0460	.729	.336	.2645	-21.3
.7333	.0257	.1397	.0571	.0442	.730	.364	.2512	-31.0
.7155	.0236	.1494	.0627	.0489	.731	.382	.2780	-27.2
.7068	.0209	.1527	.0670	.0525	.732	.400	.2964	-25.9
.7257	.0176	.1387	.0653	.0527	.734	.430	.2866	-33.4

Table 1.3

Comparison of Calculated and Experimental Viscosity for the  
CO<sub>2</sub>-C<sub>5</sub>-C<sub>10</sub>-C<sub>16</sub>-C<sub>30</sub> System at 100°F and 2000 psia (CPE 212)

CO <sub>2</sub>	nC <sub>5</sub>	nC <sub>10</sub>	nC <sub>16</sub>	C <sub>30</sub>	$\rho$ (g/cm <sup>3</sup> )	$\mu$ exp (cp)	$\mu$ calc. (cp)	error %
.0000	.1322	.5380	.1924	.1375	.750	1.965	1.2504	-36.4
.0748	.2040	.4469	.1598	.1145	.760	1.604	1.4273	-11.0
.3913	.0770	.3299	.1179	.0839	.774	.986	1.1469	16.3
.6230	.0565	.2002	.0703	.0500	.784	.674	.6044	-10.3
.6933	.0491	.1596	.0577	.0404	.791	.519	.4633	-10.7
.7361	.0430	.1378	.0485	.0346	.797	.424	.3844	-9.3
.7682	.0387	.1208	.0426	.0298	.802	.356	.3290	-7.6
.8051	.0316	.1006	.0366	.0262	.805	.305	.2719	-10.8
.8387	.0270	.0831	.0298	.0215	.808	.272	.2190	-19.5
.8774	.0222	.0617	.0223	.0614	.810	.242	.3356	38.7
.8833	.0189	.0607	.0219	.0153	.811	.219	.1618	-26.1
.8993	.0142	.0536	.0193	.0136	.811	.193	.1461	-24.3
.9173	.0138	.0423	.0153	.0112	.811	.173	.1269	-26.6
.9253	.0130	.0379	.0138	.0100	.810	.159	.1192	-25.0
.9398	.0115	.0298	.0110	.0079	.809	.148	.1066	-28.0
.9349	.0100	.0282	.0105	.0074	.808	.138	.1035	-25.0
.9515	.0087	.0246	.0091	.0062	.807	.127	.0975	-23.2
.9593	.0074	.0208	.0075	.0049	.805	.117	.0913	-21.9
.9635	.0066	.0186	.0068	.0044	.803	.113	.0884	-21.7
.9758	.0058	.0113	.0042	.0028	.805	.110	.0812	-26.2

Table 1.4

Comparison of Calculated and Experimental Viscosity for the System  
nC<sub>6</sub>-nC<sub>16</sub>. (after Dymond et al., 1980)

nC <sub>6</sub>	nC <sub>16</sub>	T (°F)	$\rho$ (g/cm <sup>3</sup> )	$\mu$ exp (cp)	$\mu$ calc. (cp)	error %
.80	.20	77.13	.6989	.584	.5768	-1.2
.80	.20	77.13	.7001	.599	.5865	-2.1
.80	.20	77.13	.7070	.646	.6461	.0
.80	.20	77.13	.7412	1.023	1.0678	4.4
.80	.20	77.13	.7609	1.403	1.4483	3.2
.80	.20	122.07	.6781	.443	.4362	-1.4
.80	.20	122.07	.7202	.701	.7814	11.5
.80	.20	122.07	.7850	1.857	2.1305	14.7
.80	.20	166.86	.7015	.552	.5990	8.5
.80	.20	166.86	.7880	1.736	2.2377	28.9
.80	.20	166.86	.8462	4.399	5.9461	35.2
.80	.20	211.95	.7203	.660	.7835	18.7
.80	.20	211.95	.8148	2.446	3.4884	42.6
.60	.40	256.73	.7409	1.227	1.1941	-2.7
.60	.40	256.73	.7698	1.978	1.8866	-4.6
.60	.40	483.62	.7287	.928	.9933	7.0
.60	.40	483.62	.7778	2.005	2.1510	7.3
.60	.40	167.25	.6964	.581	.6180	6.4
.60	.40	167.25	.8087	3.033	3.5927	18.5
.60	.40	212.16	.6732	.444	.4510	1.5
.60	.40	212.16	.7855	1.797	2.4381	35.7
.60	.40	212.16	.8487	5.225	7.1389	36.6
.40	.60	77.00	.7526	1.737	1.5258	-12.2
.40	.60	77.00	.7705	2.277	2.0380	-10.5
.40	.60	121.96	.7753	2.190	2.2055	.7
.40	.60	121.96	.8049	3.915	3.6210	-7.5
.40	.60	212.05	.7777	1.824	2.2955	25.8
.20	.80	76.89	.7792	3.275	2.4196	-26.1
.20	.80	121.91	.7802	2.690	2.4607	-8.5
.20	.80	121.91	.8183	6.014	4.7037	-21.8
.20	.80	166.89	.8037	3.661	3.6602	.0
.20	.80	166.89	.8490	9.344	8.0370	-14.0
.20	.80	212.04	.8390	6.163	6.7440	9.4

Table 1.5

Comparison of Calculated and Experimental Viscosity for the System  
Maljamar Separator Oil + CO<sub>2</sub> at 90°F and 1200 psia (CPE 210)

CO <sub>2</sub>	C <sub>3</sub>	nC <sub>6</sub>	nC <sub>5</sub>	nC <sub>6</sub>	C <sub>7+</sub> (g/cm <sup>3</sup> )	$\rho$ (cp)	$\mu$ exp (cp)	$\mu$ calc.	error %
.2584	.0258	.0631	.0502	.0416	.5609	.8431	2.270	2.2169	-2.3
.5408	.0017	.0093	.0209	.0349	.3924	.8495	1.278	1.1780	-7.8
.6230	.0012	.0068	.0175	.0306	.3209	.8535	.933	.8761	-6.1
.6791	.0004	.0026	.0087	.0227	.2865	.8592	.838	.7287	-13.0
.7152	.0003	.0021	.0064	.0166	.2594	.8624	.911	.6235	-31.6
.6522	.0002	.0014	.0065	.0178	.3219	.8651	1.009	.9167	-9.2
.7037	.0002	.0012	.0055	.0132	.2762	.8678	1.113	.7166	-35.6
.7050	.0002	.0013	.0051	.0134	.2750	.8702	1.231	.7295	-40.7
.7071	.0002	.0012	.0052	.0142	.2721	.8727	1.334	.7381	-44.7
.6940	.0003	.0020	.0061	.0146	.2830	.8751	1.499	.8152	-45.6
.6997	.0002	.0009	.0043	.0118	.2831	.8771	1.639	.8170	-50.2
.6715	.0001	.0008	.0042	.0131	.3103	.8792	1.846	.9853	-46.6
.6705	.0001	.0007	.0041	.0128	.3118	.8820	1.984	1.0244	-48.4

Table 1.6

Comparison of Calculated and Experimental Data for Several  
Crude Oil Systems--Reported by Turek et al. (1984)

Oil	N <sub>2</sub>	C <sub>1</sub>	CO <sub>2</sub>	SH <sub>2</sub>	C <sub>2</sub>	C <sub>3</sub>	C <sub>4</sub>	nC <sub>5</sub>	nC <sub>6</sub>	C <sub>7+</sub>	T (°F)	$\rho$ (g/cm <sup>3</sup> )	$\mu$ exp (cp)	$\mu$ calc. (cp)	error %
A	.0021	.0347	.6514	.0000	.0229	.0225	.0182	.0172	.0119	.2119	105.	.855	1.07	.7869	-26.5
A	.0005	.0105	.6995	.0000	.0093	.0103	.0096	.0102	.0079	.2422	105.	.907	2.20	1.4317	-34.9
A	.0008	.0019	.7105	.0000	.0015	.0020	.0023	.0032	.0027	.2751	105.	.940	6.10	2.3814	-61.0
A	.0007	.0063	.6443	.0000	.0056	.0060	.0057	.0060	.0047	.3214	105.	.930	4.10	3.0253	-26.2
A	.0000	.0132	.6408	.0000	.0105	.0115	.0101	.0100	.0079	.2953	105.	.903	2.50	1.9737	-21.1
A	.0010	.0209	.6267	.0000	.0154	.0166	.0146	.0142	.0106	.2800	105.	.884	1.50	1.5384	2.6
B1	.0007	.0288	.6512	.0000	.0174	.0161	.0139	.0131	.0121	.2447	106.	.875	.68	.8685	27.7
B1	.0002	.0096	.6562	.0000	.0076	.0077	.0083	.0084	.0086	.2934	106.	.903	2.20	1.3824	-37.2
B1	.0000	.0010	.6572	.0000	.0013	.0016	.0021	.0026	.0031	.3311	106.	.918	7.50	1.8358	-75.5
B1	.0002	.0060	.6831	.0000	.0045	.0044	.0046	.0048	.0050	.2874	106.	.923	5.04	1.5850	-68.6
B2	.0047	.1265	.0042	.0000	.0665	.0691	.0618	.0524	.0292	.5856	106.	.820	1.80	2.2107	22.8
B2	.0000	.0296	.6671	.0000	.0199	.0189	.0162	.0099	.0046	.2338	106.	.866	.82	.7603	-7.3
B2	.0000	.0158	.6769	.0000	.0135	.0124	.0096	.0065	.0046	.2607	106.	.873	1.90	.8740	-54.0
C1	.0000	.1980	.0000	.0000	.0638	.0664	.0474	.0244	.0249	.5751	94.	.767	1.80	1.2458	-30.8
C1	.0002	.0477	.6985	.0000	.0229	.0241	.0213	.0174	.0167	.1512	94.	.846	.56	.4069	-27.3
C1	.0001	.0084	.7747	.0000	.0072	.0072	.0076	.0022	.0045	.1881	94.	.893	6.90	.5871	-91.5
F	.0058	.1557	.0458	.1325	.0032	.0953	.0608	.0426	.0342	.0372	105.	.774	1.10	1.2431	13.0
F	.0007	.0316	.6321	.0340	.0000	.0276	.0255	.0110	.0064	.0113	105.	.858	.85	.8123	-4.4
F	.0020	.0054	.6872	.0096	.0000	.0091	.0105	.0055	.0035	.0061	105.	.918	4.30	1.6618	-61.4

(CO<sub>2</sub>-87-317)

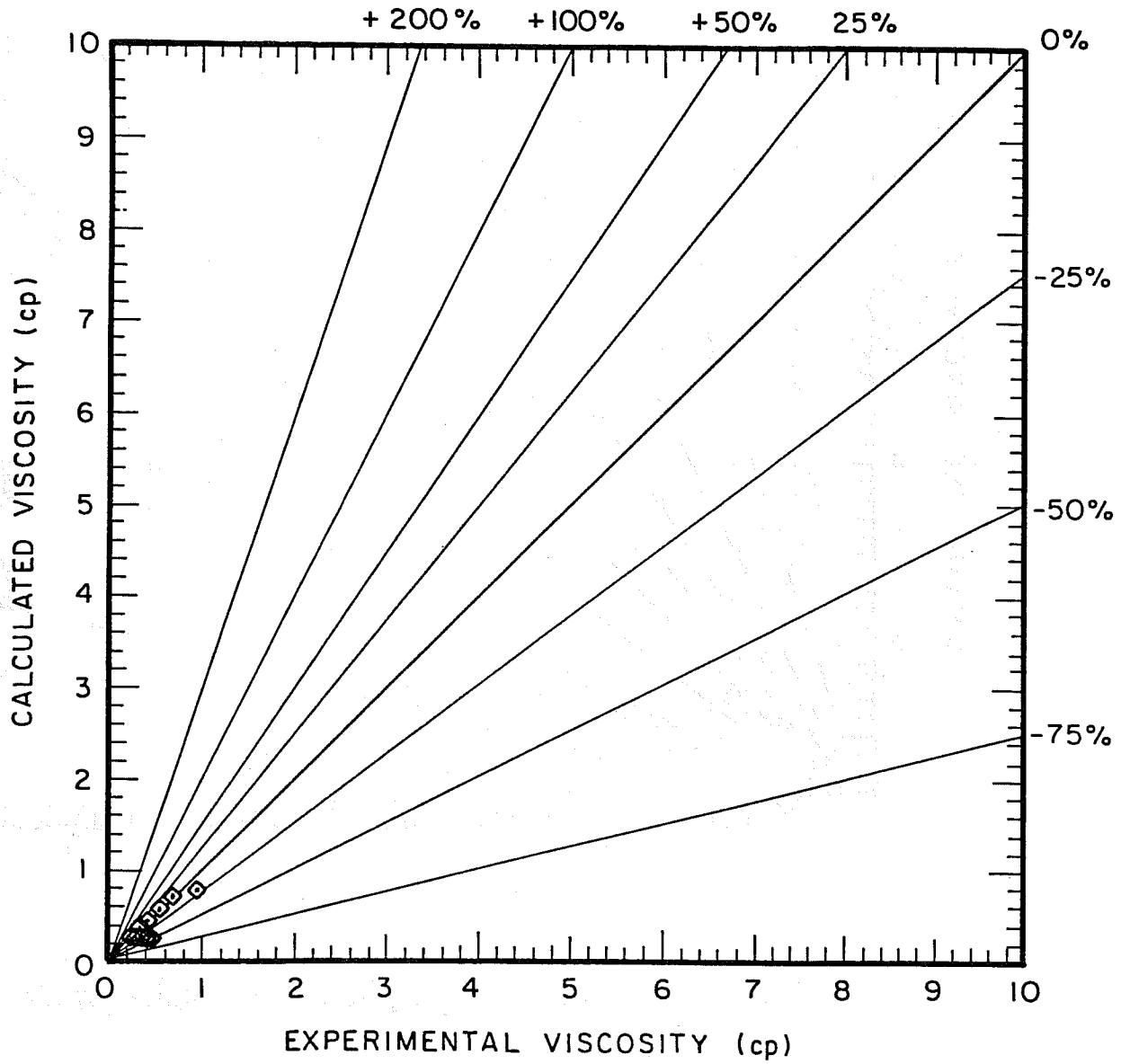


Figure 1.18. Comparison of calculated and experimental viscosities for the system CO<sub>2</sub>+nC<sub>5</sub>+nC<sub>10</sub>+nC<sub>16</sub>+nC<sub>30</sub> (P = 2000 psia, T = 190°F) [See Table 1.2].

(CO<sub>2</sub>-87-316)

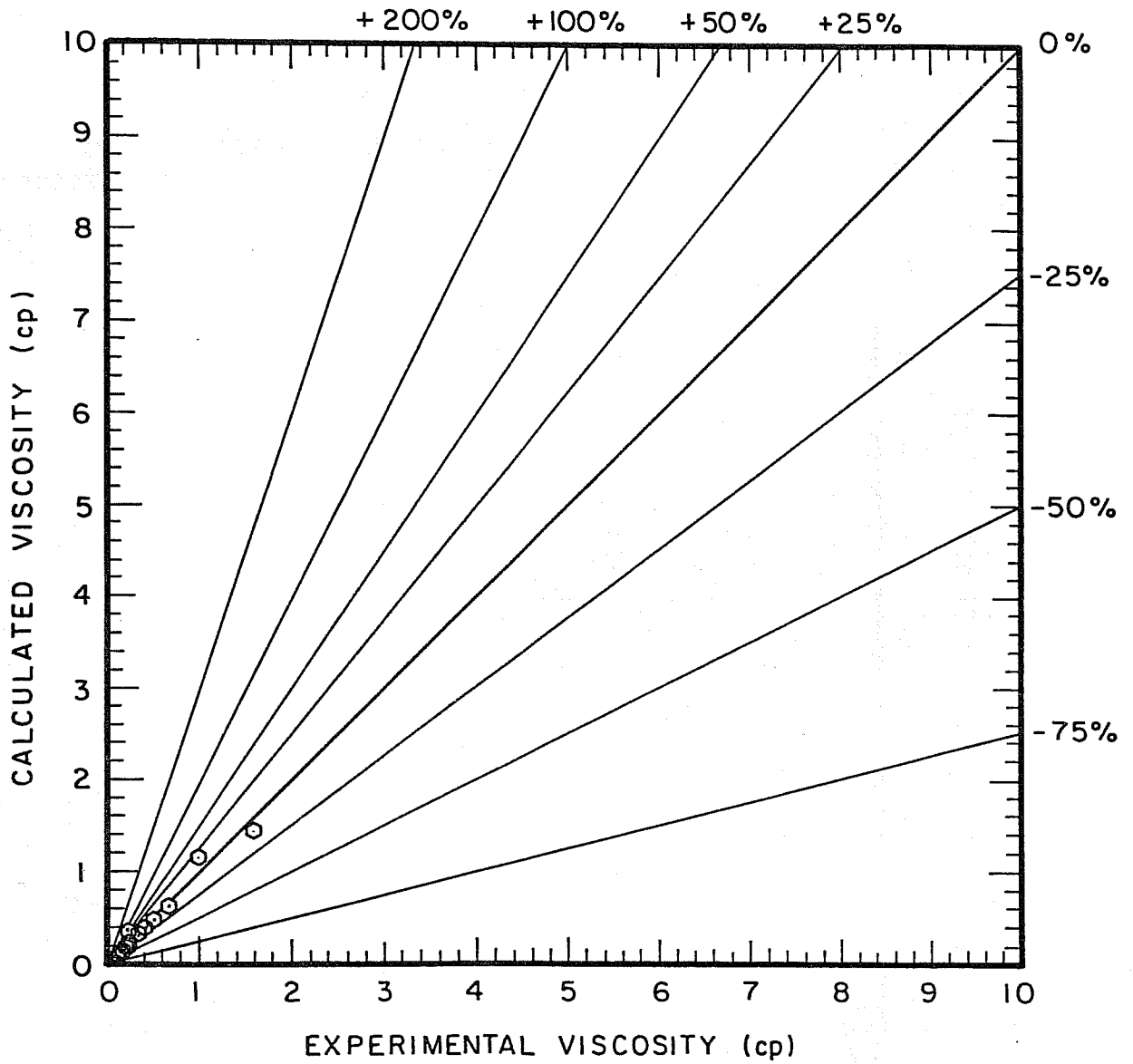


Figure 1.19. Comparison of calculated and experimental viscosities for the system CO<sub>2</sub>+nC<sub>5</sub>+nC<sub>10</sub>+nC<sub>16</sub>+nC<sub>30</sub> (P = 2000 psia, T = 100°F) [See Table 1.3].

(CO<sub>2</sub>-87-314)

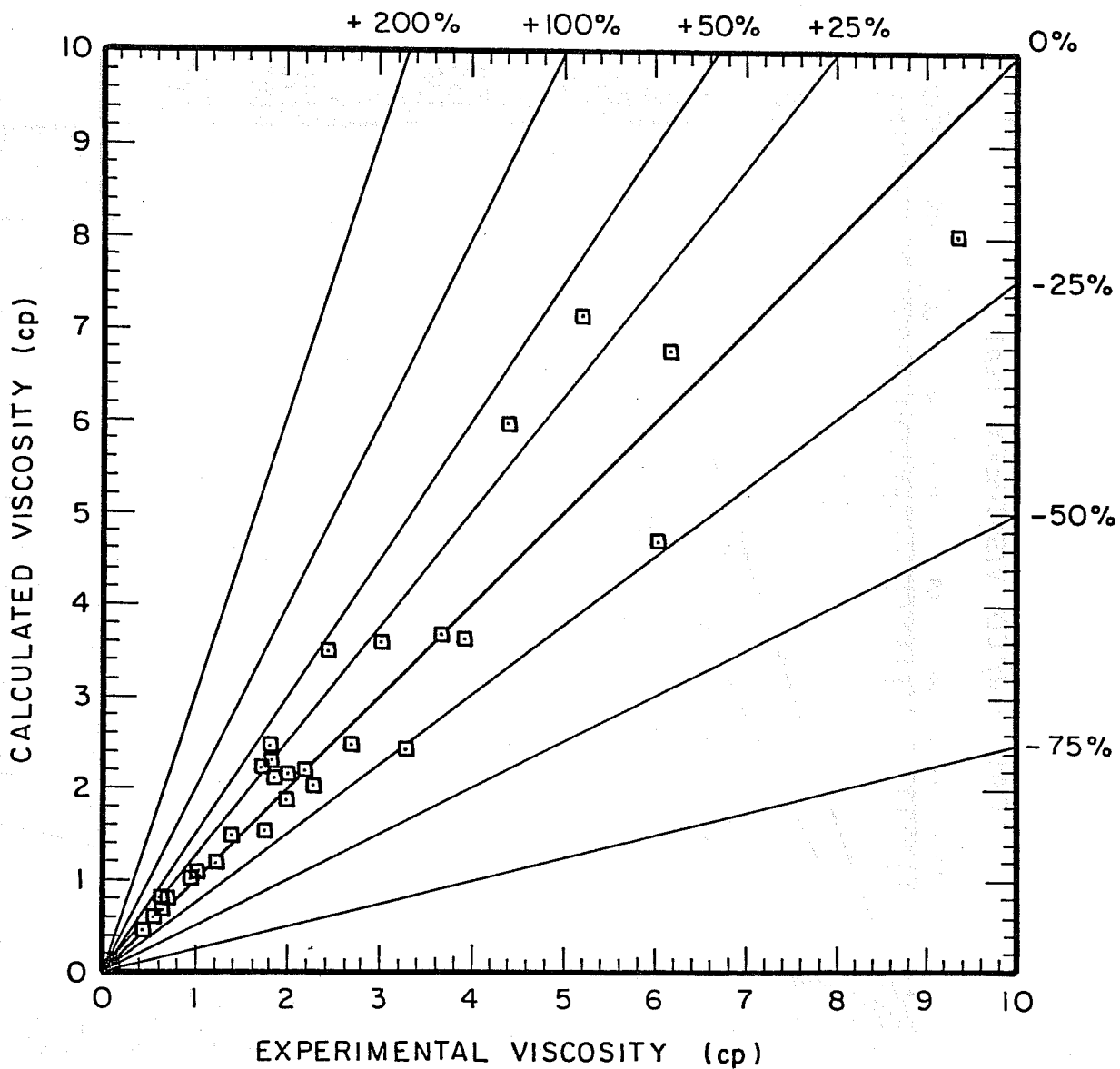


Figure 1.20. Comparison of calculated and experimental viscosities for the system  $nC_6+nC_{16}$  [see Table 1.4].

(CO<sub>2</sub>-87-315)

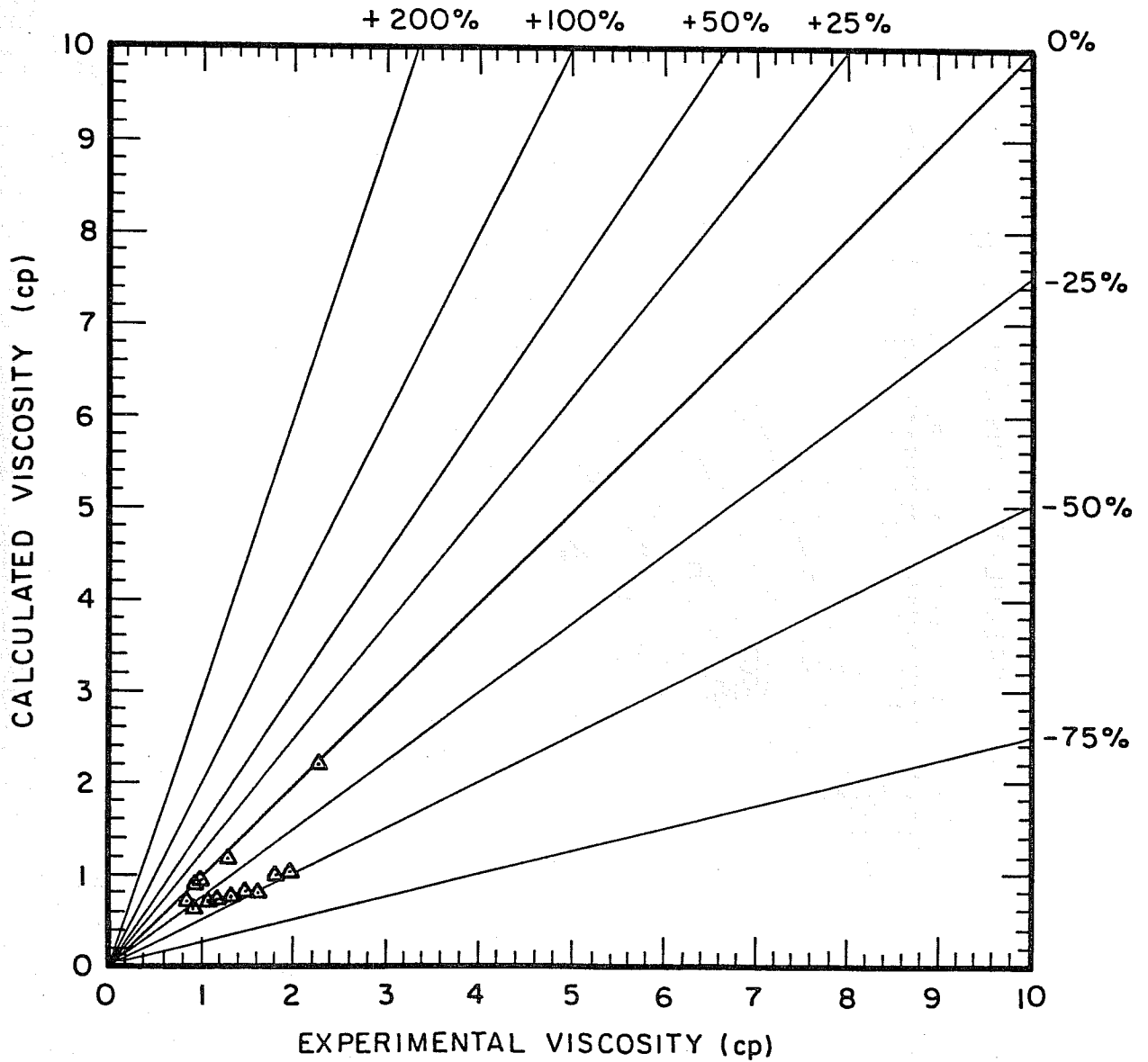


Figure 1.21. Comparison of calculated and experimental viscosities for Maljamar separator oil + CO<sub>2</sub> (P = 1200 psia, T = 90°F) [see Table 1.5].

(CO<sub>2</sub>-87-313)

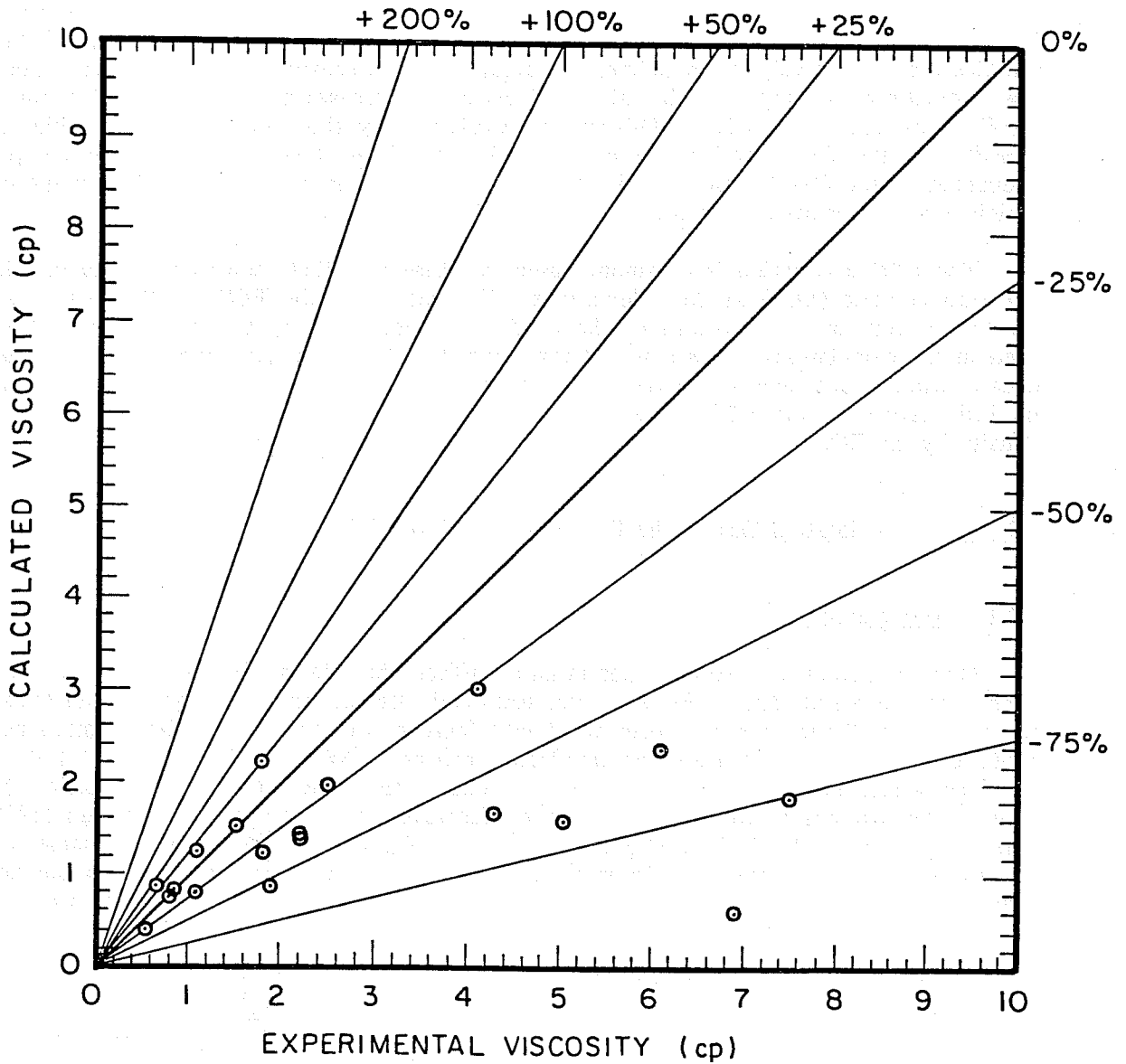


Figure 1.22 Comparison of calculated and experimental viscosities for several crude oils (Turek, et al., 1984) [see Table 1.6].

that order, even if the critical volume of  $C_{16}$  is calculated from Eq. 1.10. Systems containing  $CO_2$  can also show important deviations, and it is worth noting that Lohrenz et al. did not use systems with  $CO_2$  to develop their correlations.

An interesting result appears in the series of calculations using Maljamar separator oil +  $CO_2$ . In the experiments performed for this system, the oil is continuously contacted by the  $CO_2$ , and samples are successively taken to measure composition, viscosity and density. It is apparent from the calculations that the error in calculated viscosity increases as the process of contacting the oil by  $CO_2$  proceeds (Fig. 1.23). This can be explained by the fact that some heavier components constituting the  $C_{7+}$  fraction are extracted by the  $CO_2$ , hence changing the composition and properties of the  $C_{7+}$  fraction. This change of properties is not accounted for in the calculations, which is surely a source of error.

The LBC correlation is commonly used in phase-equilibria computer packages which use an equation of state (EOS) in the calculations. The results of the EOS are then used as input data for this correlation. The results of the LBC correlation are very sensitive to the value of density used in the calculations. It is a well-known fact that cubic EOS produce relatively high errors in density calculations; hence, the results for viscosity of those packages are affected not only by the intrinsic errors of the LBC correlation but also by the errors produced by the calculations of density by the EOS.

## 1.2 Effect of Solution Gas on the Development of Miscibility

### 1.2.1 Introduction

How the presence of solution gas in an oil affects the minimum miscibility pressure (MMP) has been a controversial topic. For example, Rathmell, Stalkup and Hassinger (1971) argued that the addition of methane to a reservoir oil should increase the MMP, and that a methane-rich bank ahead of the  $CO_2$  is evidence of an immiscible process. Holm and Josendal (1974) also stated that the presence of methane in the reservoir oil reduces the efficiency of oil extraction by  $CO_2$  and extends the distance of the immiscible zone. However, Metcalfe and Yarborough (1979) reported that the synthetic oils of  $C_4 + C_{10}$  and  $C_1$  (25%) +  $C_4 + C_{10}$  have almost the same MMP values. The salting out of  $C_1$  does not disappear until the displacement becomes first-contact miscible. In order to answer this contradiction, a detailed experimental study was undertaken using the following oil systems:

synthetic oil ( $C_1 + C_4 + C_{10}$ ), and  
crude oil ( $C_1 +$  Maljamar stock tank oil).

### 1.2.2 Literature Review

A literature survey about the effect of solution gas on MMP was begun by reviewing general MMP correlations for  $CO_2$  flooding. Previous correlations revealed that the two most important parameters are temperature and oil composition. Several MMP correlations of contaminated carbon dioxide were also found. Either pseudocritical temperature or the mole fraction of impurities was used as a parameter. Results from these correlations show that methane and nitrogen in the  $CO_2$  stream increase the MMP, while ethane through pentane and hydrogen sulfide contaminants decrease the MMP. No consensus, however, exists about the effect of solution gas in reservoir oil on MMP. Rathmell, Stalkup, and Hassinger (1971) first reported that the presence of methane in reservoir oil results in the production of a methane bank and increased MMP. Holm and Josendal (1974) also

(CO<sub>2</sub>-87-318)

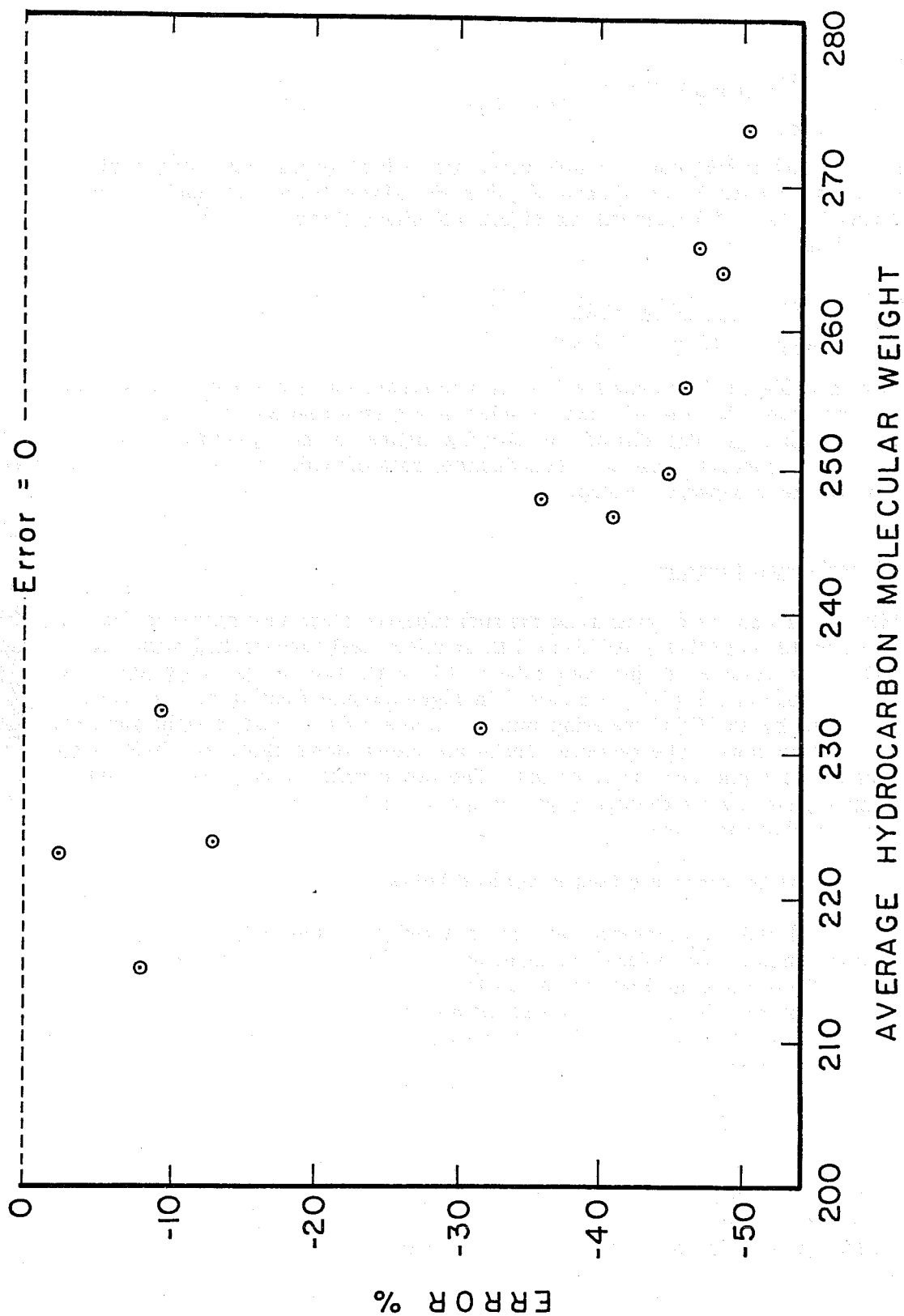


Figure 1.23. Influence of composition of crude oil on calculated viscosity error for the system Maljamar separator oil + CO<sub>2</sub>.

stated that methane has an adverse effect on MMP, although it is not significant (around 10% higher). The first correlation in terms of the mole fraction of methane and nitrogen was proposed by Cronquist (1978):

$$\frac{\text{MMP}_{\text{live oil}}}{\text{MMP}_{\text{dead oil}}} = (\text{temp.})^{0.0015279} \cdot y_{(C_1 + N_2)} \quad (1.11)$$

Yellig and Metcalfe (1980) used a simple correlation which stated that if the bubble point pressure (BPP) is higher than the MMP of dead oil, then the MMP of live oil should be the BPP. Alston, Kokolis, and James (1985) included the effects of ethane through butane and hydrogen sulfide in their correlation:

$$\frac{\text{MMP}_{\text{live oil}}}{\text{MMP}_{\text{dead oil}}} = \frac{y_{(C_1 + N_2)}^{0.136}}{y_{(C_{2-4} + H_2S)}} \quad (1.12)$$

Orr, Jensen, and Silva (1981) compared the pseudoternary phase diagram of separator and reservoir oil. They concluded that the addition of solution gas enlarged the two-phase envelope. But the addition of solution gas also shifted the limiting tieline to the favorable direction and the plait point to the lower concentration of carbon dioxide, both of which compensate for the effect of the enlargement of the two-phase envelope.

### 1.2.3 Experimental Program

MMP studies were performed using the slim tube/coreflood unit shown in Fig. 1.24. The slim tube is a coiled 12.2-m (40-ft), 0.635-cm I.D. stainless steel tube packed with 170-200 mesh glass beads. The pore volume of this slim tube is 147 cm<sup>3</sup>, and the permeability is 5800 md. Oil mixtures and injection gas (CO<sub>2</sub>) are stored in high-pressure floating piston accumulators. These fluids are driven by an HPLC metering pump. At the effluent end, a sight glass was installed to view the transition zone. The produced fluids are blown down through a back-pressure regulator and separated into liquid and vapor phases. The liquid phase is captured in a multiport sampler, and the vapor phase passes through a gas chromatograph and a wet test meter. Both phases are analyzed by gas chromatography.

The experimental procedure used is outlined below:

1. The oil and CO<sub>2</sub> transfer cells are charged after the cells are evacuated. A predetermined number of moles of methane are then added to the oil transfer cell.
2. The fluids are equilibrated to a run temperature and pressure.
3. The slim tube is saturated with an oil mixture.
4. The oil is injected at the CO<sub>2</sub> displacement rate to establish a pressure gradient across the slim tube.
5. 1.2 PV of CO<sub>2</sub> are injected at a constant flow rate.
6. 
 

a) Inlet and outlet pressures	}	vs. PV CO <sub>2</sub> injected
b) Injection flow rate		
c) Production volume of gas and liquid		
d) CO <sub>2</sub> breakthrough point are recorded.		
7. The gas and liquid composition are analyzed.

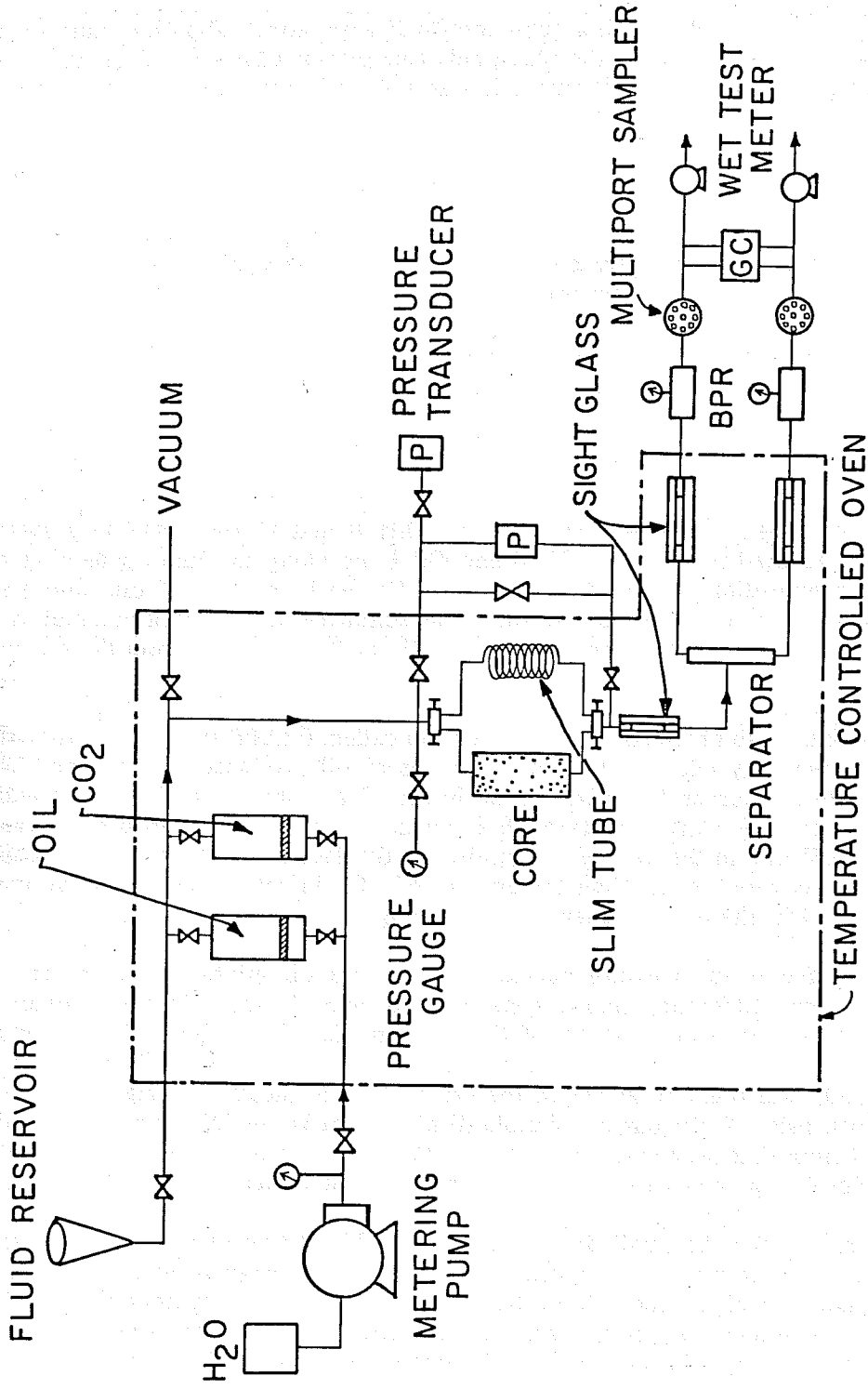


Figure 1.24. Schematic of experimental apparatus.

## 1.2.4 Results and Discussion

After the construction of the slim tube/coreflood apparatus, validation runs were performed with CO<sub>2</sub> and normal hexane. From the phase behavior plot of CO<sub>2</sub> and nC<sub>6</sub> (Fig. 1.25), the MMP was about 1160 psia at 100°F. In this study, it was 1145 psia from the recovery-pressure curve at CO<sub>2</sub> breakthrough (Fig. 1.26).

### 1.2.4.1 Synthetic Oil System

The first displacement runs were conducted with a synthetic oil system (C<sub>1</sub> + nC<sub>4</sub> + C<sub>10</sub>) at 160°F. The composition of this system was:

Mixture	C <sub>1</sub>	nC <sub>4</sub>	C <sub>10</sub>
Oil A	0	40	60
Oil B	10	36	54
Oil C	30	28	42

The Oil A mixture is a ternary system, and Oils B and C are quaternary systems with an increasing amount of methane added. Oil B and Oil C lie along the line connecting the 100% C<sub>1</sub> peak and Oil A composition in a ternary diagram. For each mixture of oil, four slim tube displacements were done at different pressures. The summary of the experimental results can be found in Table 1.7. (The actual oil compositions are 1% or 2% different from the originally planned oil compositions).

The density data were obtained from the program called TRAPP supplied by the Gas Processors Association. The recovery data are the pore volumes of oil produced at the time of CO<sub>2</sub> breakthrough. The recovery curves for mixtures of B and C are shown in Figs. 1.27 and 1.28. The recovery curve before the CO<sub>2</sub> breakthrough is almost a 45° line at pressures above MMP. It deviates from the 45° line in the case of an immiscible displacement. At pressures below the MMP, the amount of oil recovered is less than the amount of CO<sub>2</sub> injected because the volume change of CO<sub>2</sub> upon dissolution in the oil is greater than the change at higher pressures.

The recovery factor vs. pressure curves for all three oil mixtures are shown in Fig. 1.29. There is no significant difference among systems A, B, and C except in the recovery of Oil C at 1700 psia. From these curves, the MMP's of Oil A (no methane) and Oil B (11.92% methane) are at 1600 psia, and the MMP of Oil C (30% methane) is at 1700 psia. From the phase equilibrium data of Oil A (Fig. 1.30), the pressure at which the critical tieline meets the original oil composition is approximately 1650 psia. Multicontact miscible displacement is possible at and above this pressure. The phase equilibrium data were calculated by the Peng-Robinson equation of state (1976). These predictions are closely matched with the experimental data of Metcalfe and Yarborough (1979).

A possible reason for the small discrepancy in the MMP from the experiment and the phase equilibrium calculations is that the composition route from the original oil composition to the CO<sub>2</sub> injection gas is not a straight line. It probably deviates from the straight line to the righthand side on a ternary diagram, then passes around the critical point. Deviation of the composition route was also reported by Metcalfe and Yarborough (1979) as a chromatographic separation of butane and decane in porous media.

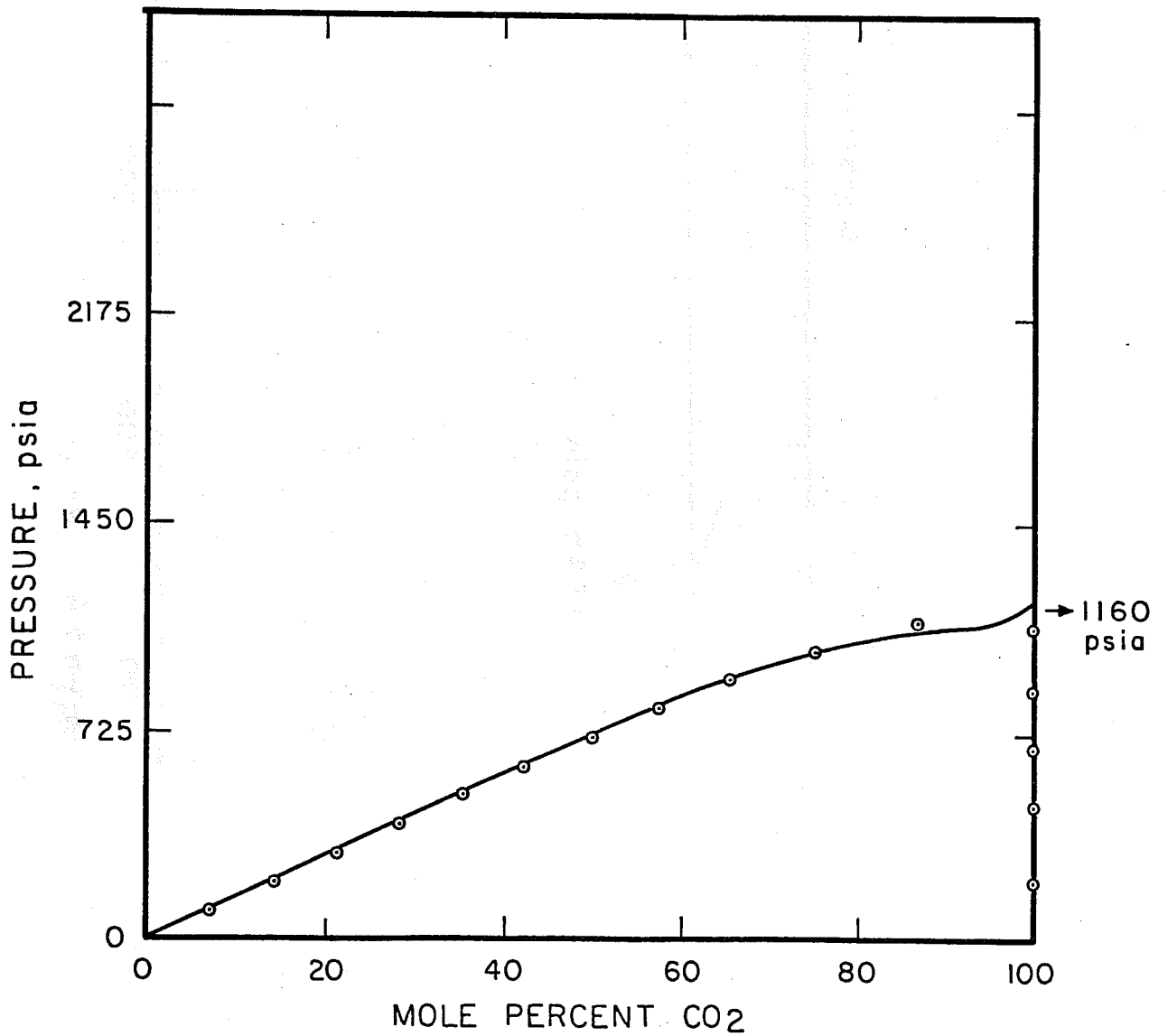


Figure 1.25 Phase equilibria of CO<sub>2</sub> and nC<sub>6</sub> (T = 100°F) [after Turek, et al., 1984].

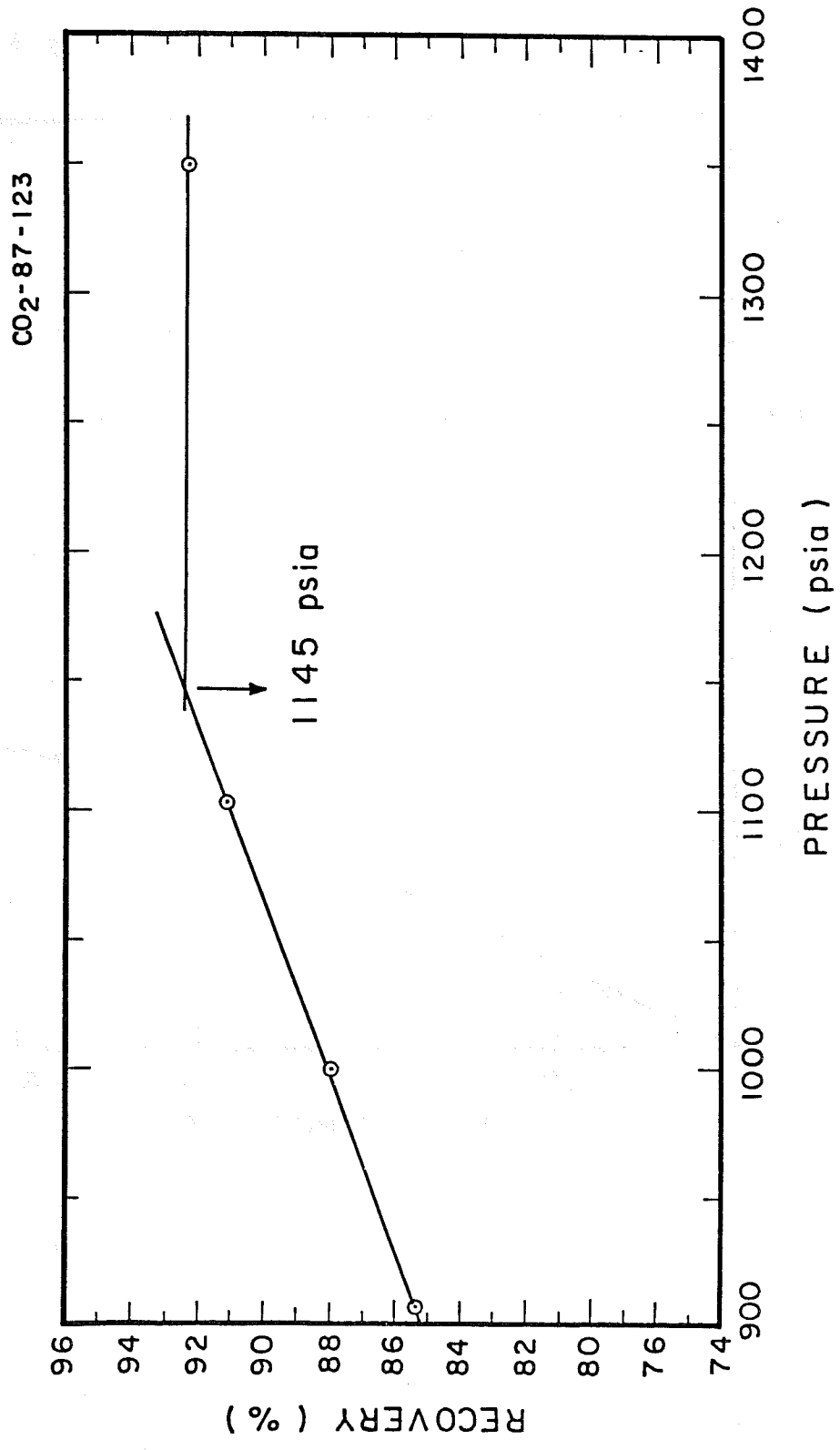


Figure 1.26. Minimum miscibility pressure of CO<sub>2</sub> and nC<sub>6</sub> (T = 100°F).

Table 1.7  
Summary of Synthetic Oil Runs

System	Pressure (psia)	Composition			Density (gm/cc)	Recovery (fraction)	MMP (psia)
		C <sub>1</sub>	C <sub>4</sub>	C <sub>10</sub>			
A-1	1384.7	0	41.34	58.66	.6717	.7341	
A-2	1547.5	0	41.34	58.66	.6730	.8227	1600
A-3	1596.0	0	41.34	58.66	.6735	.8610	
A-4	1707.6	0	41.34	58.66	.6744	.8465	
B-1	1406.7	11.92	37.98	50.10	.6578	.7101	
B-2	1494.2	11.92	37.98	50.10	.6586	.7795	1600
B-3	1591.4	11.92	37.98	50.10	.6595	.8515	
B-4	1701.5	11.92	37.98	50.10	.6606	.8414	
C-1	1415.6	29.93	31.79	38.29	.6277	.7401	
C-2	1511.4	29.93	31.79	38.29	.6239	.7776	1700
C-3	1600.0	29.93	31.79	38.29	.6249	.8636	
C-4	1706.4	29.93	31.79	38.29	.6262	.8893	

(CO<sub>2</sub>-87-312)

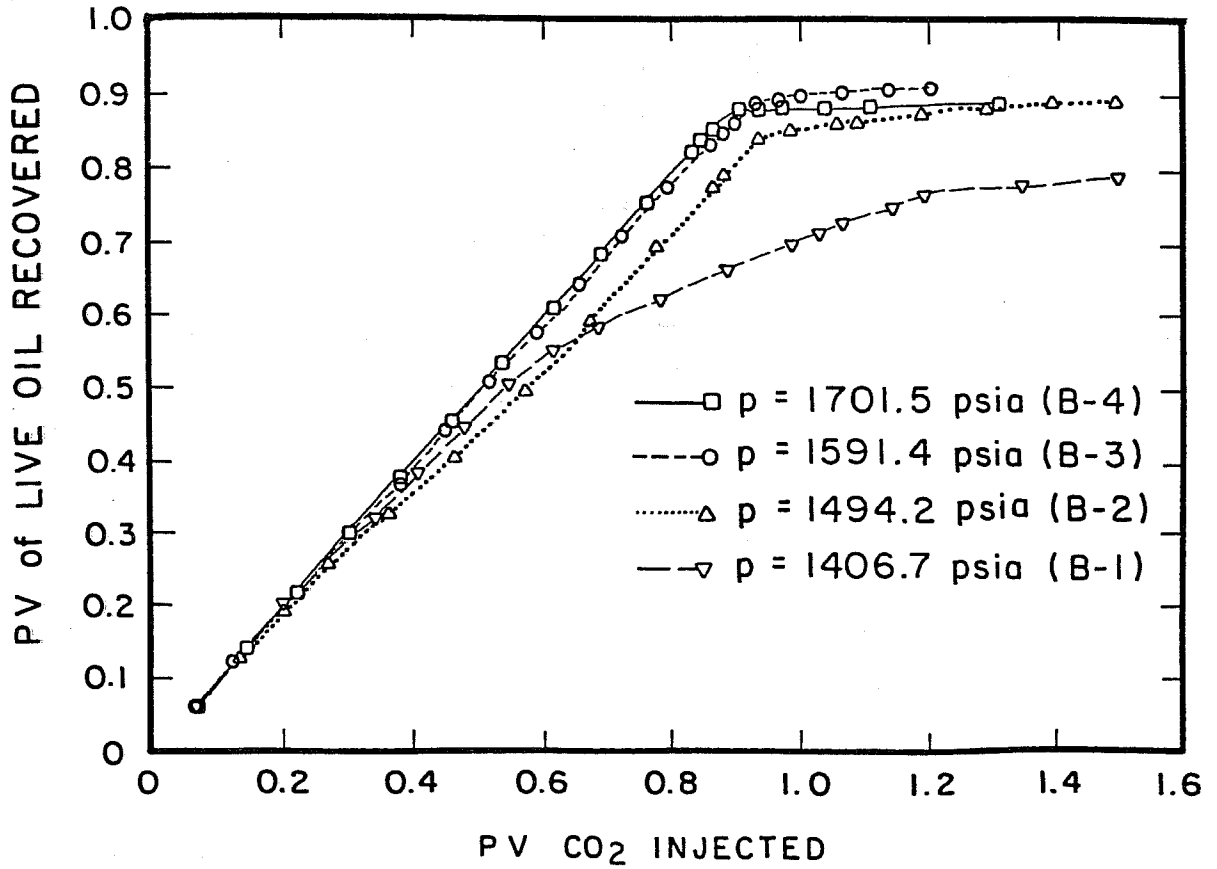


Figure 1.27. Slim tube recovery curves for Oil B.

(CO<sub>2</sub>-87-311)

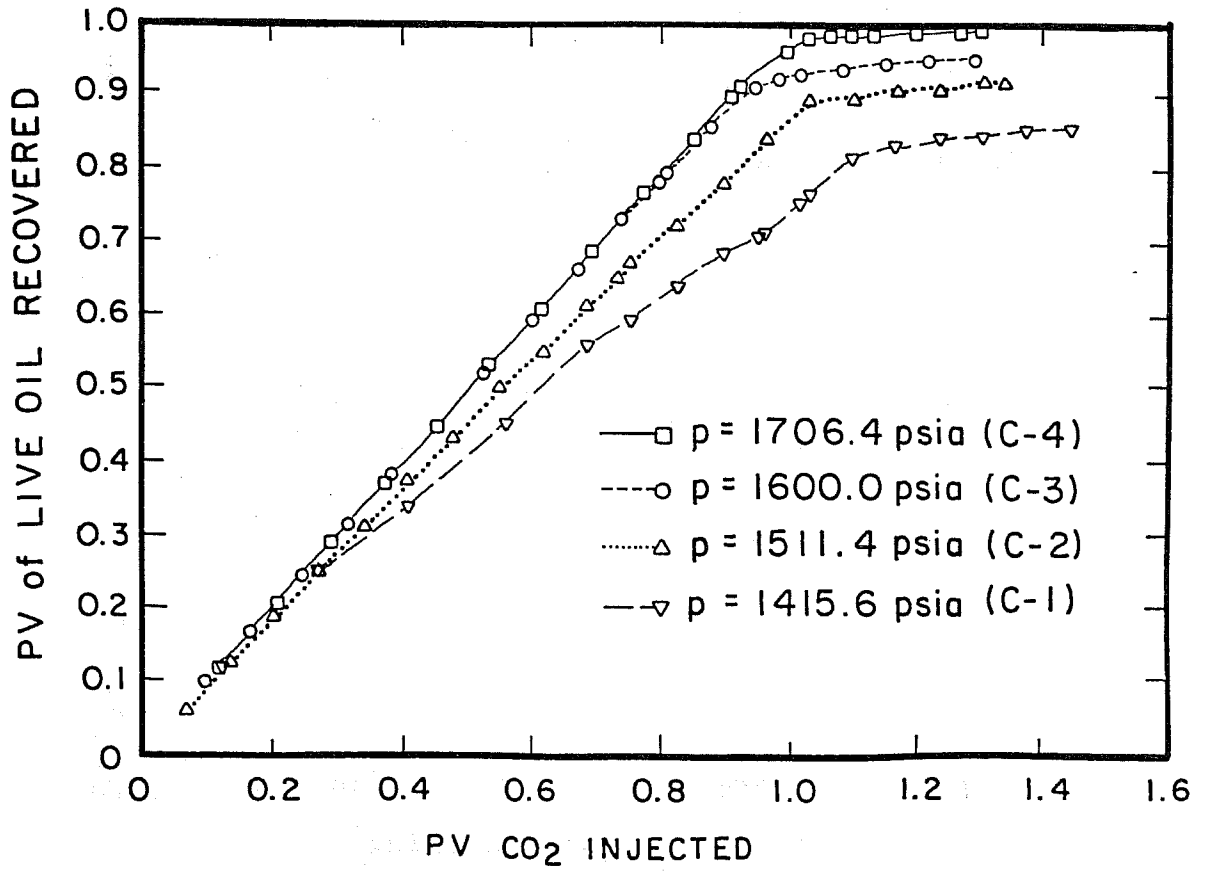


Figure 1.28. Slim tube recovery curves for Oil C.

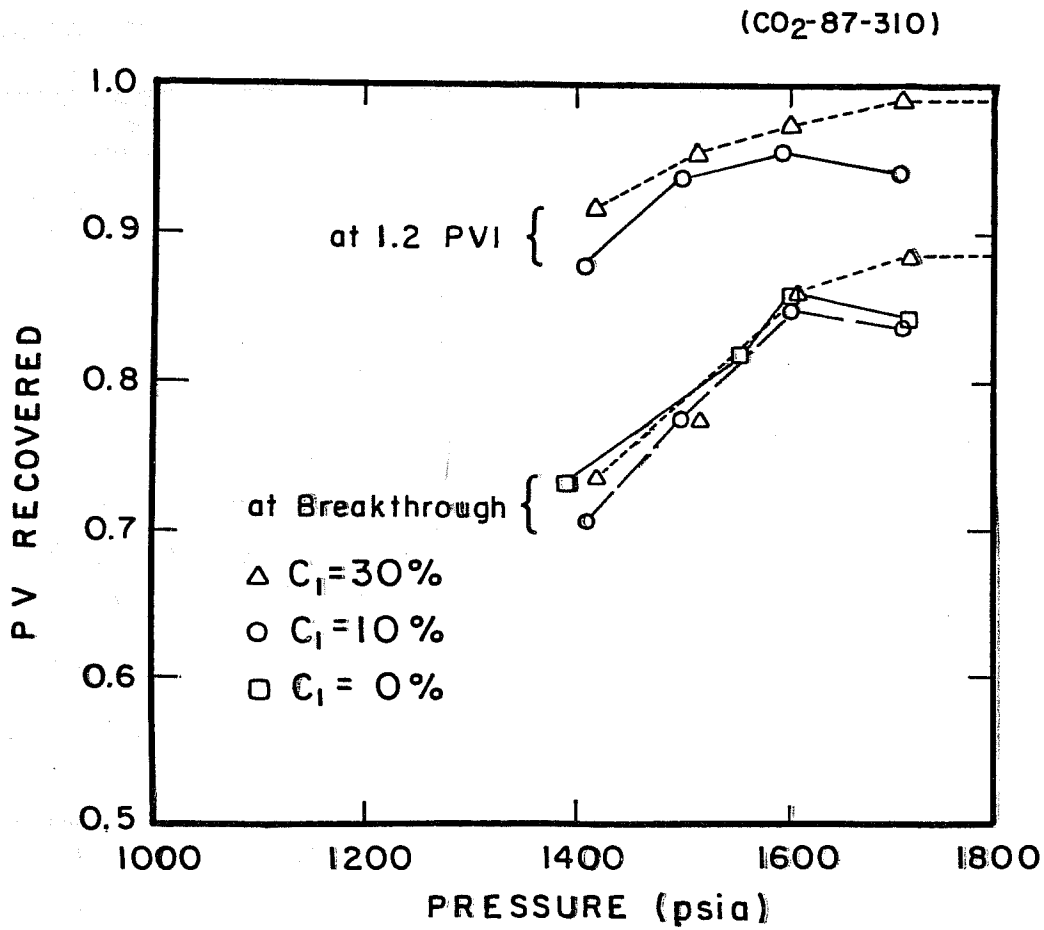


Figure 1.29. Minimum miscibility pressure of synthetic oil system (C<sub>1</sub>-C<sub>4</sub>-C<sub>10</sub>).

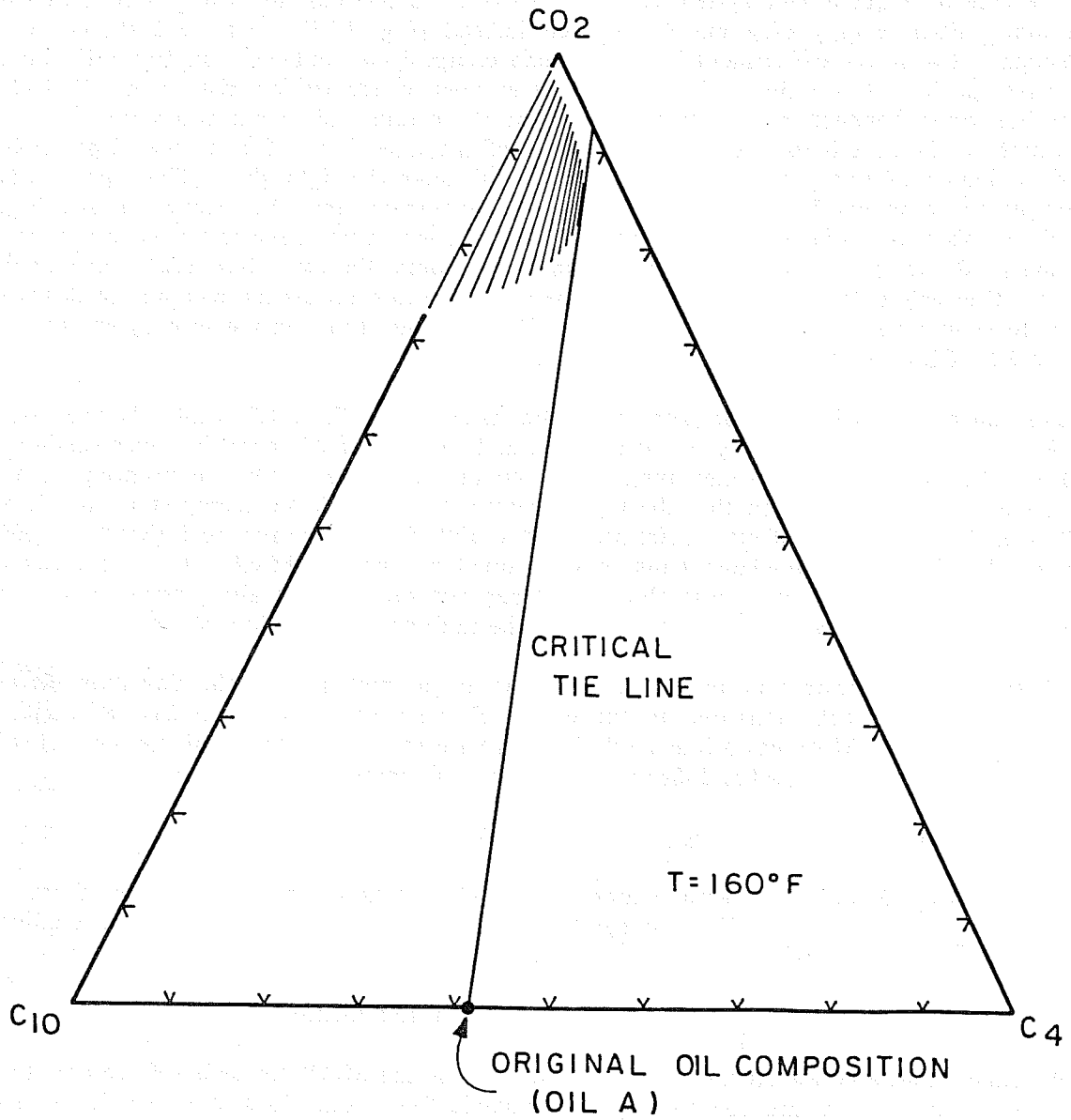


Figure 1.30. CO<sub>2</sub>-nC<sub>4</sub>-C<sub>10</sub> calculated ternary diagram (P = 1650 psia).

The case of a quaternary system (Oil B and Oil C) is difficult to visualize on a two-dimensional plot. Four ternary diagrams are plotted instead (Fig. 1.31). Fig. 1.32 shows the three-dimensional view of the experimentally determined composition route for Oil B-1 with the multiphase envelope in a dotted line. Table 1.8 is the effluent concentration history for Oil B-1. This composition route connects five compositions from the original oil composition (point 1) to pure CO<sub>2</sub> (point 5). Point 2 is the methane bank ahead of the CO<sub>2</sub> front. During the displacement, gas bubbles, evidence of two-phase flow, were observed through the sight glass. These gas bubbles did not completely disappear even at the MMP. So, it is speculated that the recovery is still high even when the composition route passes the two-phase region which has been indicated by several other researchers. Being able to follow a composition route around the two-phase region should increase recovery. One way to bypass the phase envelope would be to suppress the methane bank formation, perhaps in ways other than increasing pressure. Points 3 and 4 are on the ternary surfaces of 20% CO<sub>2</sub> and 80% CO<sub>2</sub>, respectively.

The concentration history for each component is shown in Figs. 1.33-1.38. In the case of Oil B (11.92% methane), there is a big methane bank, and the size of the bank becomes smaller around the MMP. For mixture C (30% methane), the C<sub>1</sub> concentration peak is not as pronounced as in Oil B. It should also be mentioned that the C<sub>1</sub> concentration peak did not completely disappear even at 1700 psia for mixture C (MMP is 1700 psia) and at 1701.5 psia for mixture B (MMP is 1600 psia). However, the size of the methane bank is very small around the MMP. For the concentration history of C<sub>4</sub> and C<sub>10</sub>, no peak was observed at any pressure. The trailing edges of C<sub>4</sub> and C<sub>10</sub> for the immiscible process are longer than that of the multicontact miscible process.

These results indicate that the effect of solution gas methane on the development of miscibility is relatively small compared to the effect of methane in injection gas (Kovarik, 1985). Kovarik reported that MMP has a linear relationship with the mole fraction of methane in injection gas. According to Kovarik (1985, 1986) for west Texas oil/impure CO<sub>2</sub> systems,

$$\text{MMP} \times 10^{-3} = 1.258 + 15.350 (y_{\text{N}_2}) + 4.994 (y_{\text{C}_1}) \quad (1.13)$$

For example, for 10% and 30% methane contaminated CO<sub>2</sub> streams, the MMP changes from 1757 psi to 2756 psi (a 57% increase). For the synthetic oil system (C<sub>1</sub>-C<sub>4</sub>-C<sub>10</sub>) we have studied here, changing the solution gas methane concentration from 10% to 30% changes the MMP from 1600 psi to 1700 psi, or a 6.25% increase. To our knowledge, this is the first time the effect of solution gas methane on the MMP of CO<sub>2</sub> has been documented in this manner.

We expect that a 40% methane system would increase the MMP between 100-150 psi (6.25% to 9.5%). For reservoirs that are operated at near miscible flood conditions (not considering effect of solution gas on MMP), an error of 6% to 10% underestimating the miscibility pressure could move the process into the immiscible condition and significantly reduce oil recovery. We are continuing our investigation into this area. In the case of impure CO<sub>2</sub> flooding, the injection gas composition lies deep in the multiphase region (Fig. 1.32). However, when methane is added to the oil mixture and the injection gas is pure CO<sub>2</sub>, the methane bank is usually generated and displaced ahead of the CO<sub>2</sub> bank.

#### 1.2.4.2 Crude Oil System

The second oil system investigated was Maljamar crude oil. Similar to the procedure used with the synthetic oil system, an increasing amount of methane was added to the Maljamar stock tank oil (STO). Preliminary results of these crude oil runs are shown in Table 1.9 and Fig. 1.39. With the addition of 20% methane, the recovery at 1200 psia was almost the same as the recovery

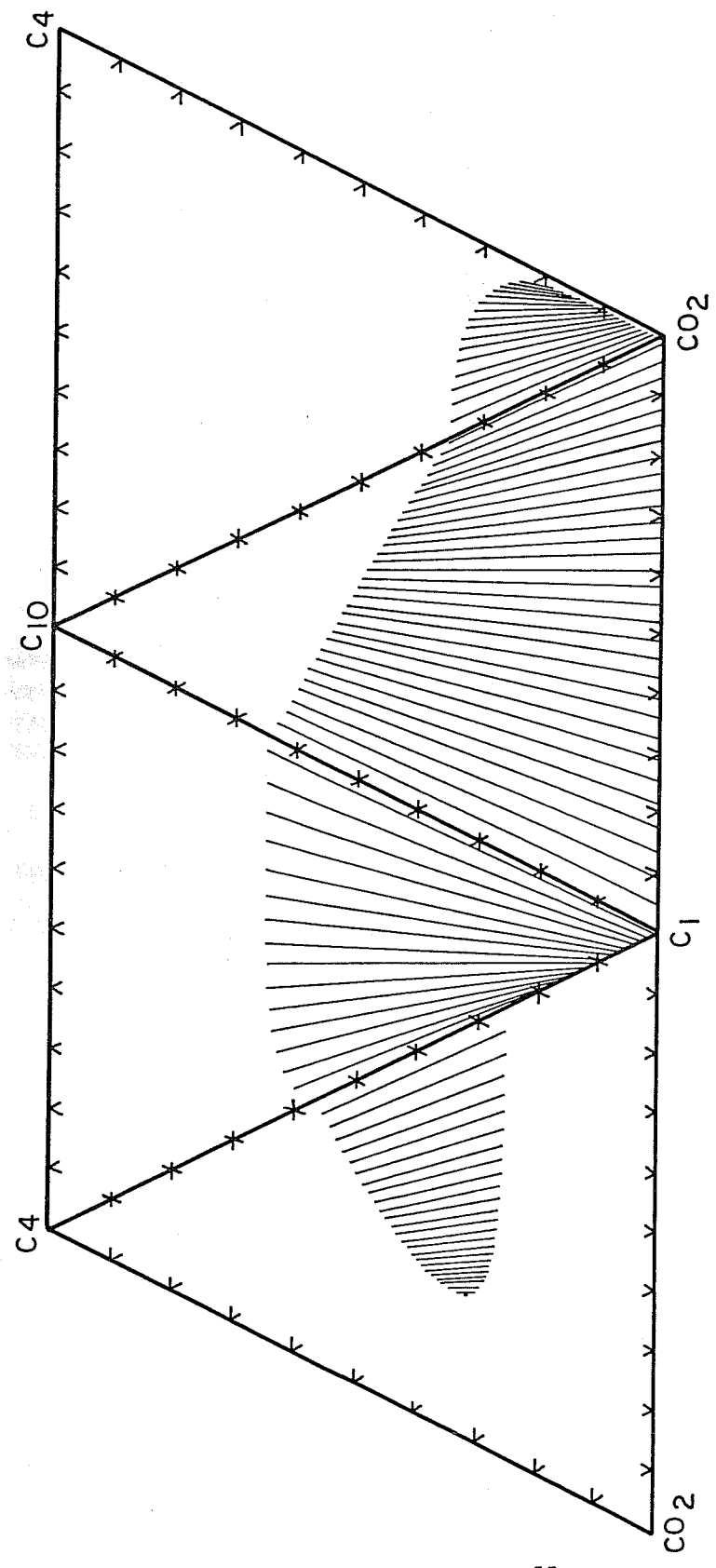


Figure 1.31. Ternary faces of quaternary system, Run B-1 (P = 1406.7 psia, T = 160°F).

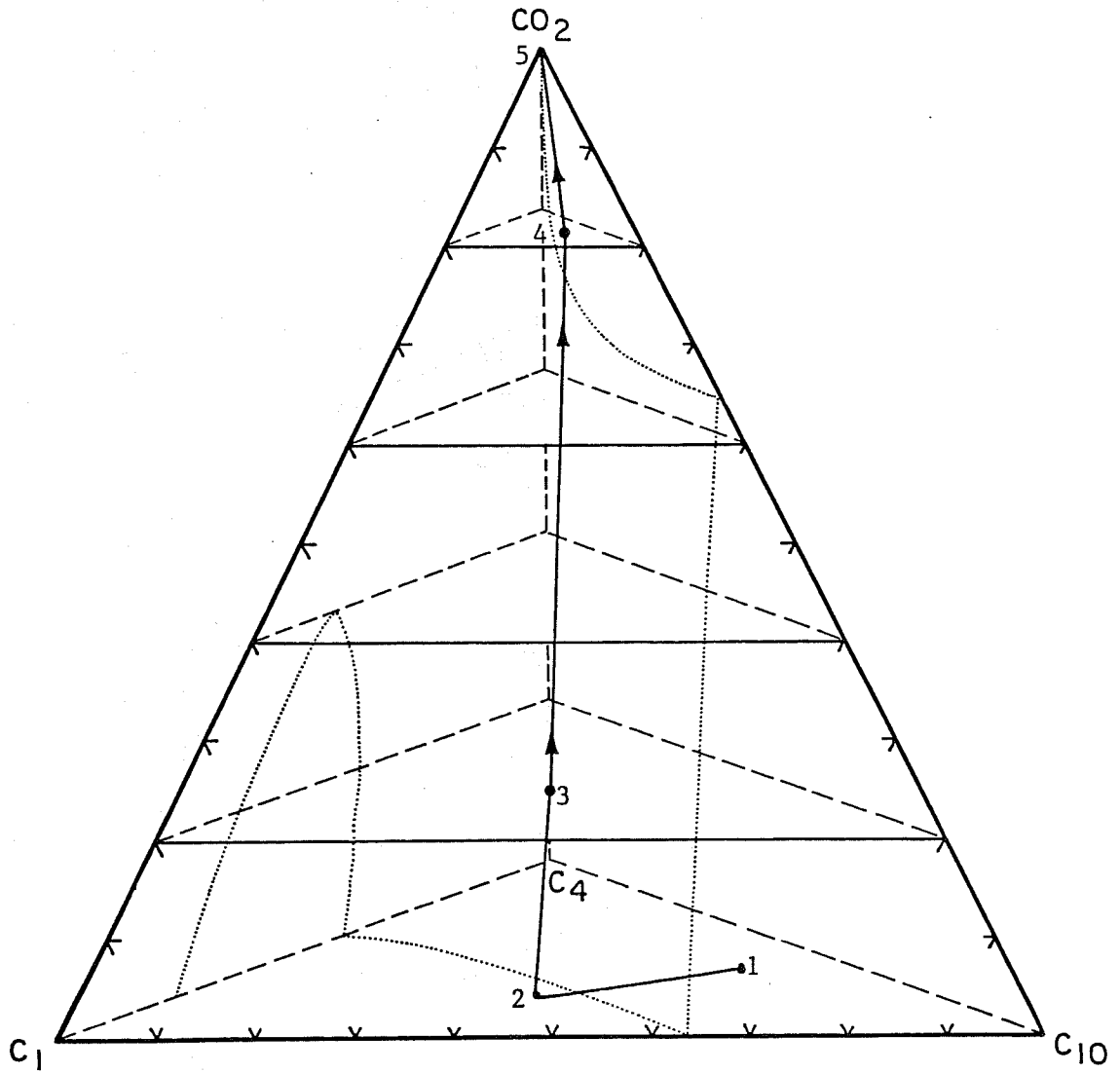


Figure 1.32. Composition route of Run B-1 (P = 1406.7 psia, T = 160°F).

Table 1.8

Effluent Concentration History for Oil B-1  
Used to Determine Composition Path in Figure 1.32

<u>P.V. of CO<sub>2</sub> Injected</u>	Effluent Composition (mole %)			
	<u>C<sub>1</sub></u>	<u>C<sub>4</sub></u>	<u>C<sub>10</sub></u>	<u>CO<sub>2</sub></u>
0.0680	11.92	37.98	50.10	0
0.2721	11.91	38.66	49.43	0
0.4762	12.15	38.63	49.22	0
0.6803	11.94	38.25	49.81	0
0.8798	12.49	38.25	49.26	0
0.9819	13.74	39.04	47.22	0
1.0601	31.86	33.50	34.47	0.17
1.1349	34.75	33.08	31.56	0.61
1.1859	25.47	26.13	26.85	21.55
1.3390	3.56	10.29	5.41	80.74
1.4921	0	8.32	2.05	89.63
1.7370	0	7.86	1.55	90.59

P = 1406.7 psia

T = 160°F

(CO<sub>2</sub>-87-309)

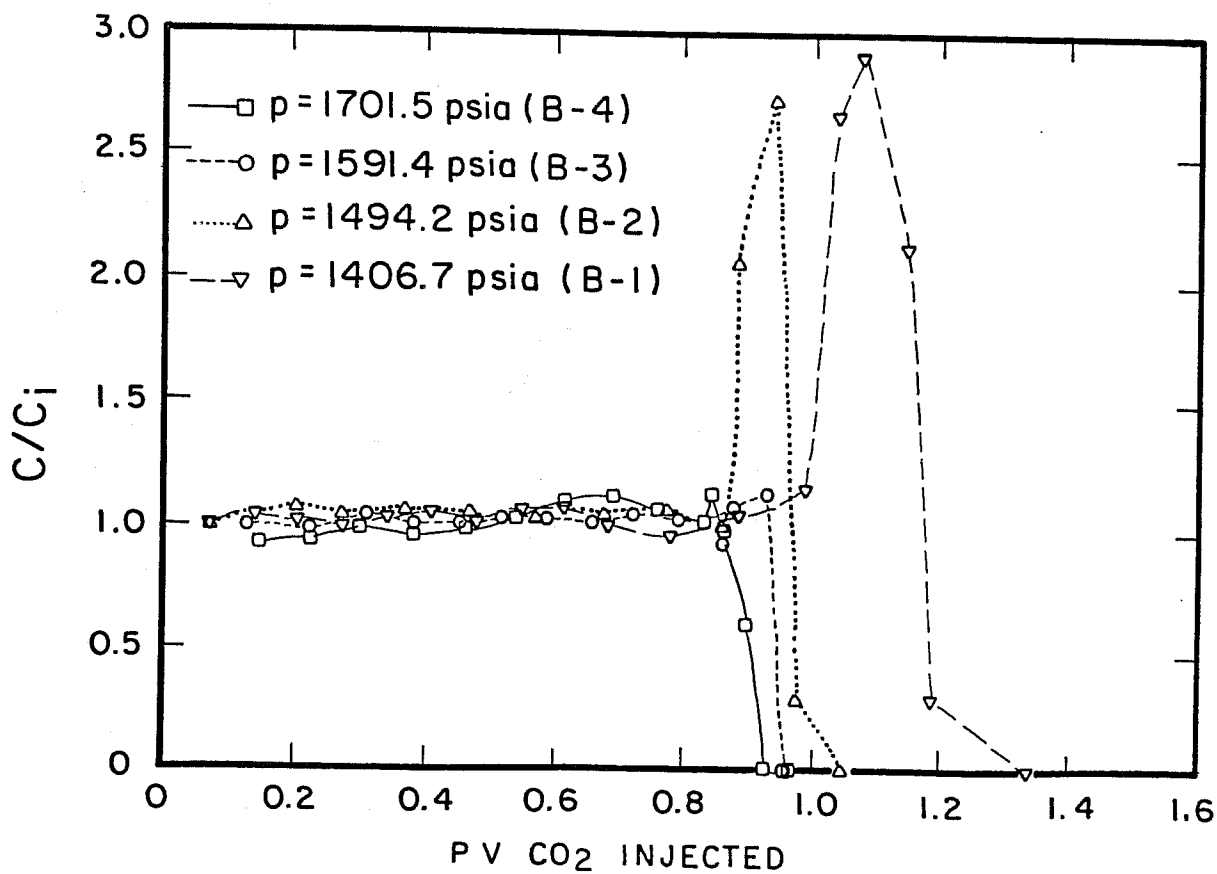


Figure 1.33. Concentration history of C<sub>1</sub>, Oil B (T = 160°F).  
C = effluent concentration (mole %)  
C<sub>i</sub> = initial concentration (mole %)

(CO<sub>2</sub>-87-308)

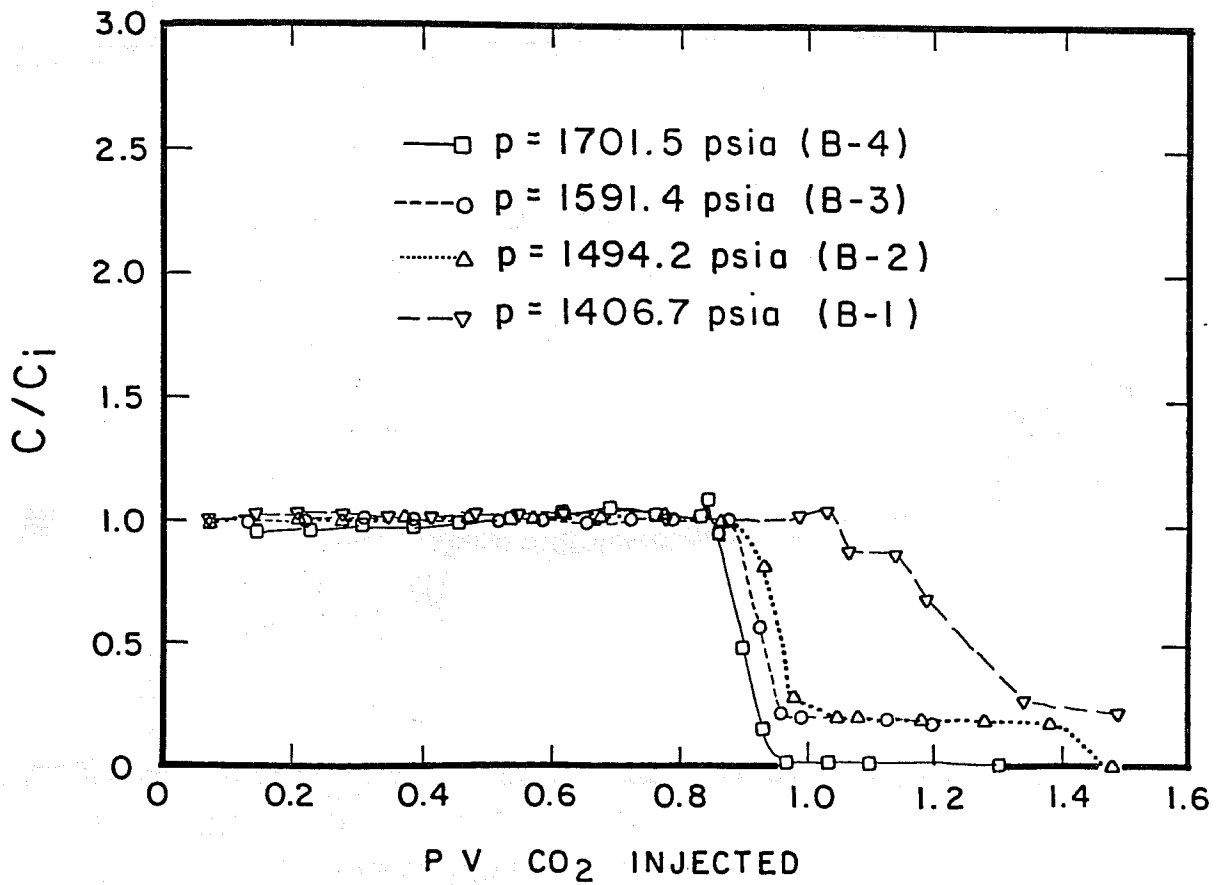


Figure 1.34. Concentration history of  $C_4$ , Oil B ( $T = 160^\circ F$ ).

(CO<sub>2</sub>-87-307)

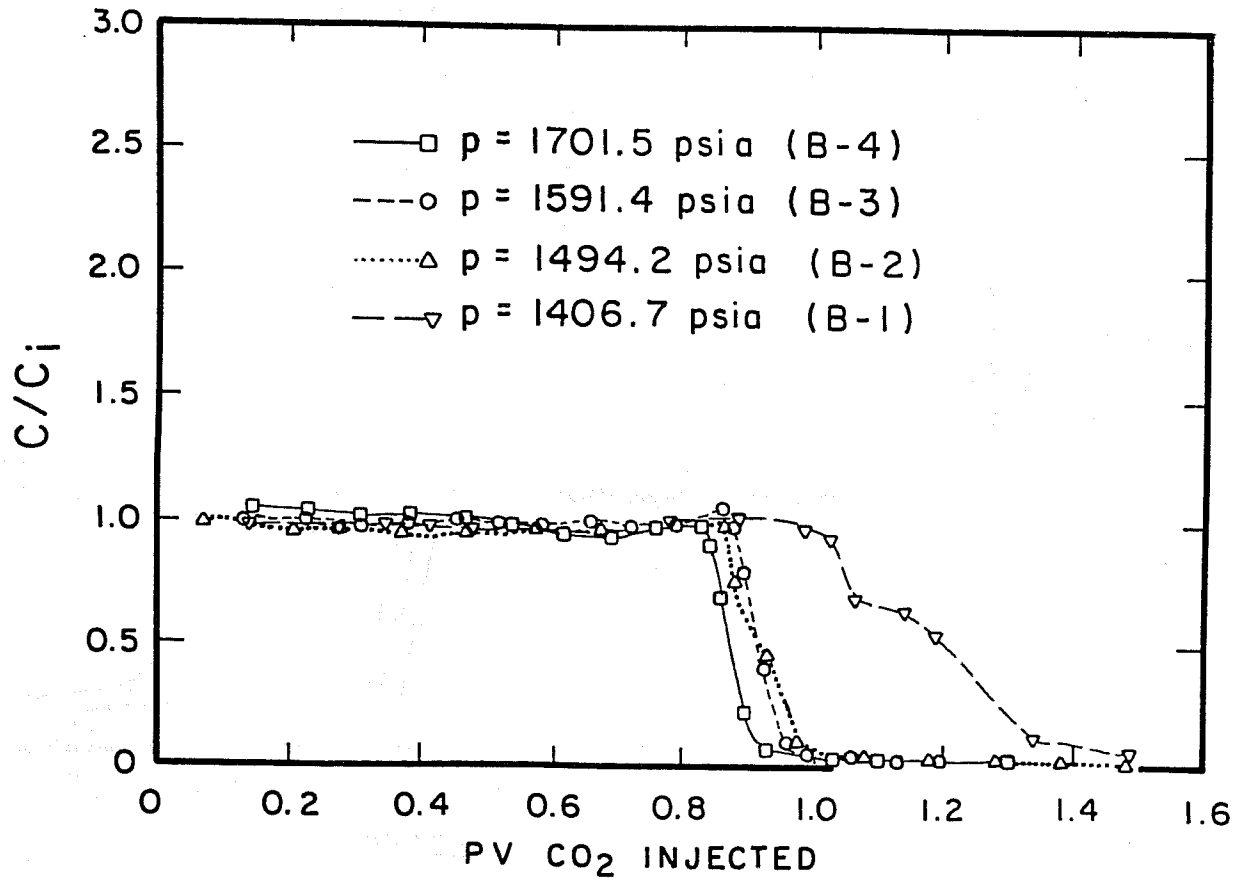


Figure 1.35. Concentration history of  $C_{10}$ , Oil B ( $T = 160^\circ F$ ).

(CO<sub>2</sub>-87-306)

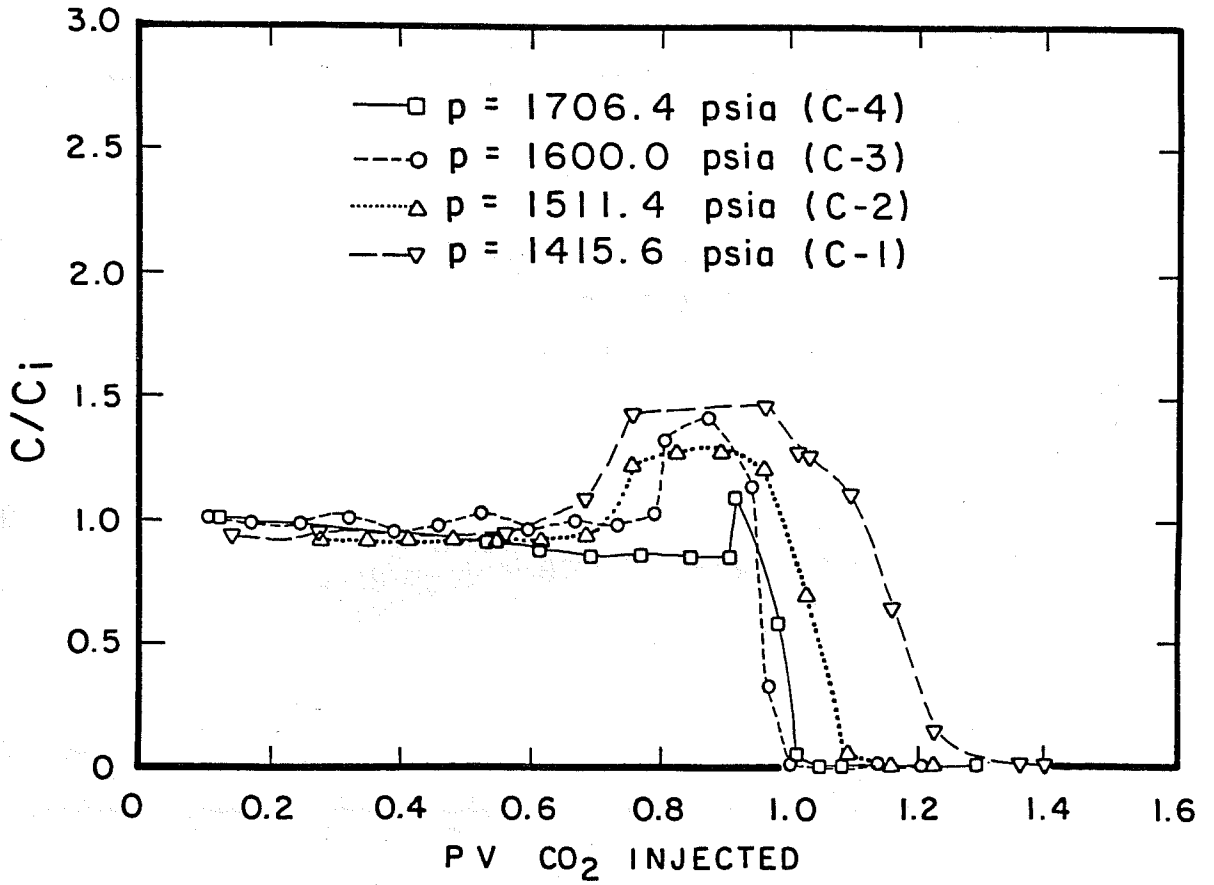


Figure 1.36. Concentration history of  $C_1$ , Oil C ( $T = 160^\circ F$ ).

(CO<sub>2</sub>-87-304)

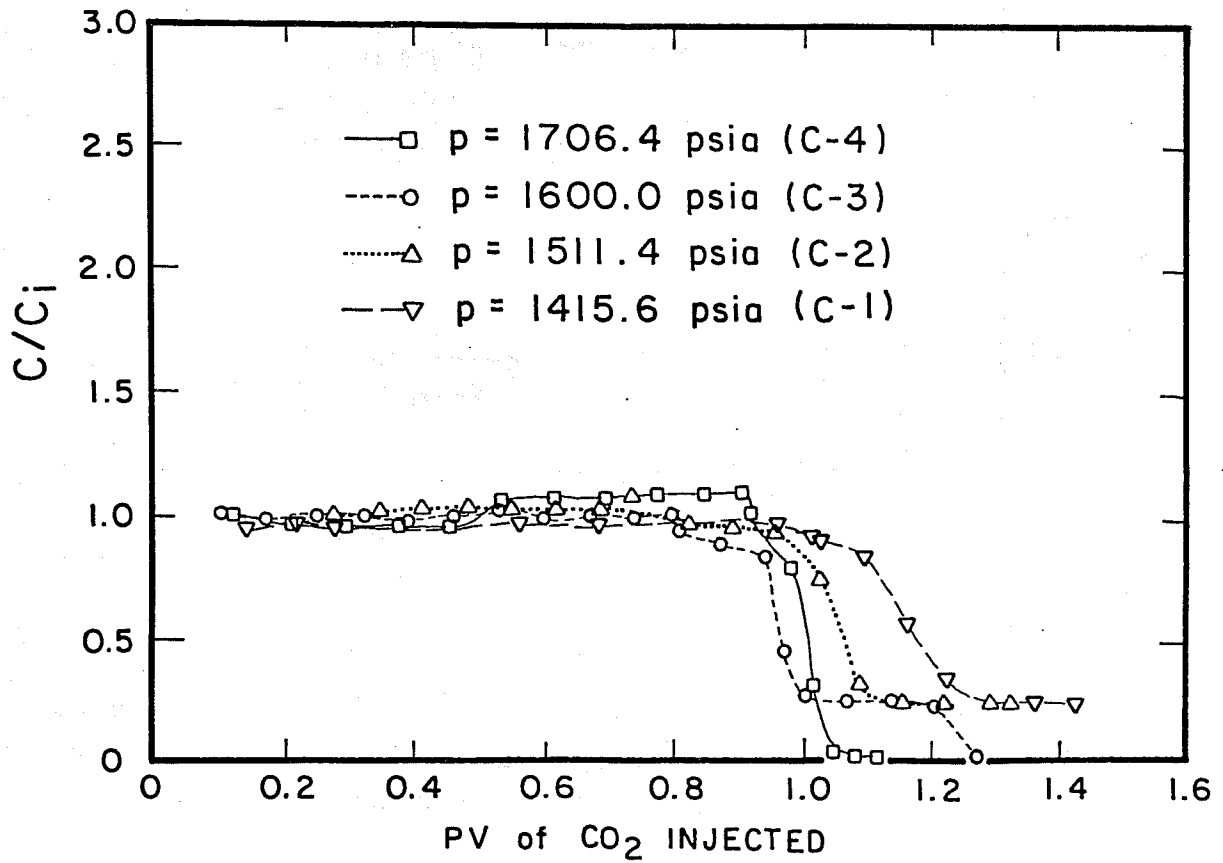


Figure 1.37. Concentration history of C<sub>4</sub>, Oil C (T = 160°F).

(CO<sub>2</sub>-87-303)

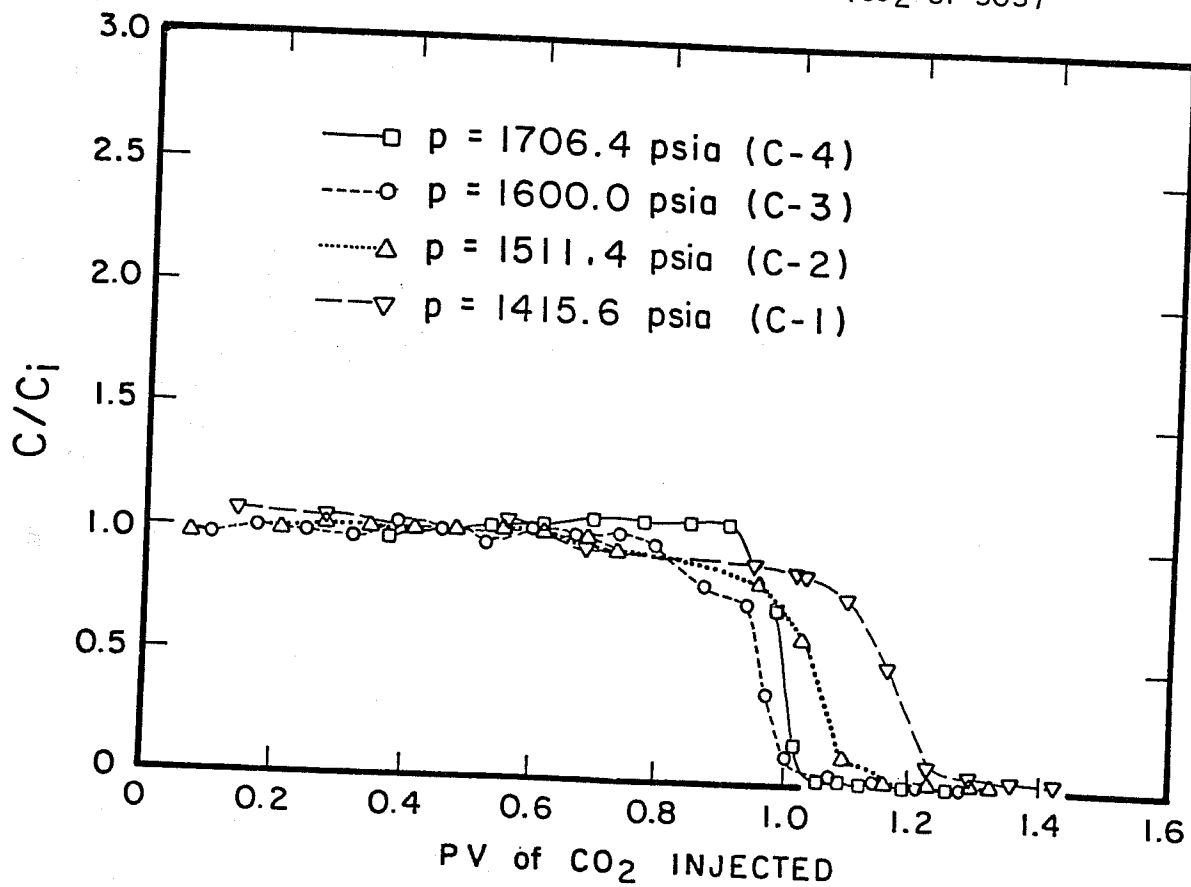


Figure 1.38. Concentration history of C<sub>10</sub>, Oil C (T = 160°F).

of the stock tank oil at the same pressure; however, we only ran one displacement. Addition of 30% methane resulted in a little lower recovery at 1500 psia compared to the recovery of STO at 1200 psia. We do not have enough data to determine if there is a shift in MMP. Added experiments are in process. Unlike the synthetic oil system, the density of CO<sub>2</sub> in the crude oil system (low temperature reservoir) was high enough to generate a dense CO<sub>2</sub> liquid phase. Since the dense CO<sub>2</sub> liquid phase is more efficient at extracting oil than the CO<sub>2</sub> vapor phase, this may be the reason for the high recovery at runs of E-1, E-2 and F-1. In high-temperature reservoirs, the addition of methane may increase the MMP if the density of CO<sub>2</sub> is not high enough to generate a dense CO<sub>2</sub> liquid phase. The concentration histories of methane in runs of E-1 and E-2 are shown in Fig. 1.40. Although the recoveries of these runs are high, the methane bank was still observed. These concentration histories are very similar to those of synthetic oil mixture C. Both oil mixtures contain 30% methane. Even in a complex crude oil system in a low-temperature reservoir, the effect of methane is not significant above the bubble point pressure of the mixtures but could be on the order of 10% as with the synthetic oil system, for methane concentrations typical of reservoir oils. However, below the bubble point pressure, we may see a more pronounced effect of methane in the free gas on the MMP. Future experiments are planned which will couple the slim tube runs (above the BPP) with coreflood runs (below the BPP). This research program is expected to extend the definition of MMP to the free gas condition which, we feel, would be more relevant to field operations.

### 1.2.5 Conclusions

In order to study the effect of solution gas on miscibility, MMP's of several synthetic and real oil mixtures with different methane compositions were measured. For our C<sub>1</sub>-C<sub>4</sub>-C<sub>10</sub> synthetic oil system, a 6.25% increase in MMP was observed when the methane composition was varied from 10% to 30%, while maintaining a constant C<sub>4</sub>-C<sub>10</sub> ratio. Preliminary results did not show significant increase in MMP with the addition of up to 30 mole % methane in the crude oil systems. However, a second order effect ( $\approx 10\%$ ) is still being investigated. If we choose the MMP above the pressure at which no methane bank is observed, the MMP may be too conservative. From the observation of the composition route, operation below the original bubble point pressure may result in high recovery even though this is an immiscible process. The physical meaning behind the Yellig and Metcalfe correlation was not found. We expect that the Yellig and Metcalfe correlation is accurate to the first order; thus, we are looking for secondary effects that for specific fields may play an important role and should be included in field flood design. For this reason, more experiments conducted below the bubble point pressure are needed.

### 1.2.6 Future Work

In a slim tube study, it is impossible to run an experiment below the bubble point pressure due to problems in interpreting the results. In other words, the recovery data are not available below the BPP of live oil when the calculated MMP of stock tank oil is less than the BPP of live oil. However, it may be possible to run the displacement experiments through a consolidated rock below the bubble point pressure of an oil mixture. A saturated reservoir (a reservoir below the BPP) will be simulated by lowering the pressure below the bubble point after saturation of a sample above the bubble point pressure. It may take a long time for the liquid and gas phases to reach equilibrium. The recovery curves below the bubble point pressure in a consolidated rock combined with the analysis of slim tube runs will tell us the the true MMP of the oil mixture and the physical meaning of the Yellig and Metcalfe correlation.

(CO<sub>2</sub>-87-302)

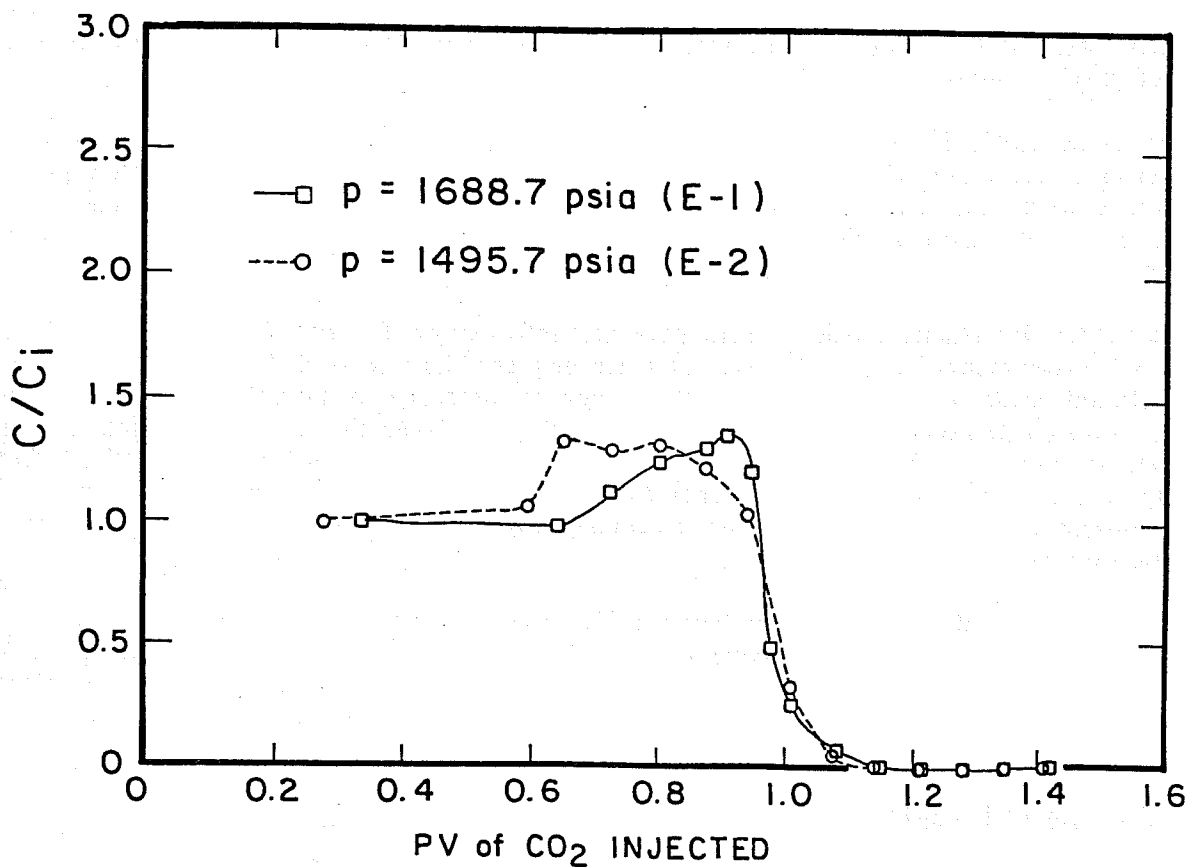


Figure 1.40. Concentration history of  $C_1$ , crude oil ( $T = 90^\circ F$ ).

## 2. AREA II - MIXING OF CO<sub>2</sub> AND OIL DURING FLOW IN RESERVOIR ROCK

### 2.1 Secondary and Tertiary CO<sub>2</sub>/Oil Coreflood Data: Experimental vs. Simulation

#### 2.1.1 Introduction

A series of gravity-assisted vertical CO<sub>2</sub> core displacements with a synthetic oil at first-contact miscible and immiscible conditions were conducted and simulated. Gravity-assisted displacements can, at low enough rates, result in a more stable flood front due to the dampening effect of gravity forces on viscous instabilities.

Orr et al. (1983) demonstrated through a series of phase equilibria measurements and slim tube displacements that a CO<sub>2</sub>-rich liquid phase is a more efficient solvent than a CO<sub>2</sub>-rich vapor at the same temperature and pressure. Not only does the CO<sub>2</sub>-rich liquid extract much heavier components, it can also dissolve significantly more hydrocarbon (as much as 30 wt %) than the CO<sub>2</sub>-rich vapor.

Calculated interfacial tensions from parachor information for the CO<sub>2</sub>-synthetic oil system used in the experiments indicate that the interface between the CO<sub>2</sub>-rich liquid phase (L<sub>2</sub>) and the oil-rich liquid phase (L<sub>1</sub>) is under very little tension as compared to the CO<sub>2</sub>-rich vapor phase (V) and L<sub>1</sub>. Strong interfacial forces between the displacing fluid and the fluid to be displaced renders the latter immobile in the fine pore networks of a reservoir rock. This immobilized fluid is virtually unrecoverable except by first-contact miscible displacements. Pressures under which first-contact miscibility is attained are often extremely high which makes it unattractive from the economic standpoint.

Since the type of phase behavior between the injected CO<sub>2</sub> and the reservoir oil will essentially determine the ultimate oil recovery, an insight is offered which here points towards the effectiveness of the dense CO<sub>2</sub>-rich liquid phase not only during multiple contact miscible displacements but possibly even under immiscible conditions.

#### 2.1.2 Experimental Aspects

The design of the experiments in this study was such that the run temperature is close to the CO<sub>2</sub> critical point temperature. A stable temperature is essential at this condition due to the sensitivity of the CO<sub>2</sub> density to slight thermal fluctuations in the vicinity of the critical point. Thus, the coreflood unit was redesigned, reconstructed, debugged, and validated in order to run gravity-stable secondary and tertiary CO<sub>2</sub> floods more accurately.

The airbath has been insulated with 1-inch thick polystyrene material with reflecting aluminum sheets covering both sides. Heat is provided by four 100-watt light bulbs connected in parallel to a variable transformer. Finer temperature control is achieved through a 60-watt light bulb connected to an automatic temperature controller (YSI Model 63RC). A shaded pole blower has been installed to provide air circulation. Resistance temperature devices (RTD), reliable to within  $\pm 0.1$  K, are used to monitor the temperature in several locations within the entire apparatus. The RTD's have been calibrated at ice-point and at various temperatures. Two RTD's which gave a reading of 32°F at the ice-point and consistently had identical readings for the range of temperatures measured were used as the reference standard.

The system pressure is monitored via pressure transducers, housed in the airbath, to minimize pressure calibration drift due to temperature fluctuations. The transducers are frequently calibrated against a dead weight gauge on site in the laboratory.

Changes have also been made in the plumbing to facilitate the operation of the apparatus. A core bypass loop has been installed to stabilize the flow of CO<sub>2</sub> prior to injection into the core. Fig. 2.1 is a schematic of the modified apparatus, and Fig. 2.2 shows the details of the back pressure regulator system. The following is an outline of the procedure for conducting the displacement experiments:

to start the displacement

- bring the back-pressure regulator (BPR) to the run pressure
- saturate the core with the synthetic oil mixture at the run displacement rate
- switch core bypass valves to "bypass" mode
- turn the strip-chart recorder on to record the volume of CO<sub>2</sub> produced
- turn the CO<sub>2</sub> pump to "run" mode and allow flow stabilization to proceed until two or three stable cycles have been recorded on the chart recorder
- switch core bypass valves to "inject" mode
- turn the rotary valve timer on
- make an event mark on the strip-chart paper and record the time of the start of the run

to end displacement

- close valves 8, 15, and 16 (see Fig. 2.2)
- turn off the switching valve (valve 10)
- turn off the strip-chart recorder, again making an event mark recording the time of the end of the run
- bring BPR down to atmospheric pressure and collect the blow down oil
- remove core and measure the final weight

The amount of oil recovered was determined by weight rather than by less accurate volumetric measurements.

The dead volume from the core effluent to the collection tubes has been carefully measured by saturating the line with water which is then displaced by nitrogen. This procedure was repeated several times, and the volume of water collected in each run was averaged to give the desired value.

### 2.1.3 Experimental/Simulation Results

A summary of the properties of the outcrop Berea sandstone core used in the displacements is presented in Table 2.1. The hydrocarbon fluid properties used in the calculation of the critical flow rate are listed in Table 2.2. These properties were obtained from the Transport Properties Prediction Program (TRAPP) of the U.S. National Bureau of Standards. The properties of CO<sub>2</sub>, also obtained from TRAPP, are shown in Table 2.3.

A summary of the experimental results is presented in Table 2.4. The run conditions, injection rates, critical rates, dimensionless injection rate (injection to critical rate ratio), recoveries at breakthrough and at 1.2 PV of the solvent injected are also tabulated in Table 2.4. The critical velocity, above which viscous forces dominate and frontal instabilities occur, was calculated for each run from the equation derived by Hill (1952):

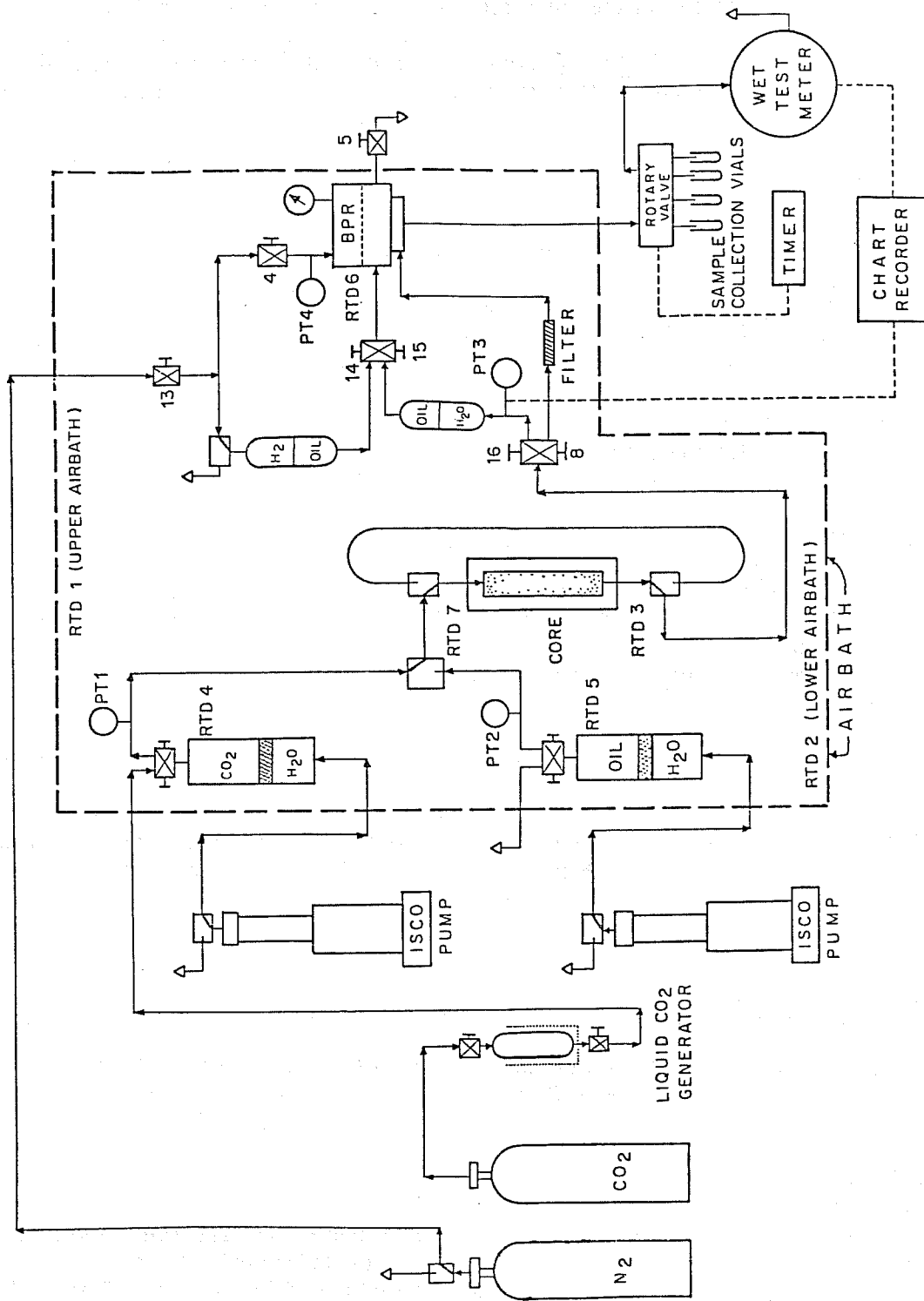


Figure 2.1. Schematic of the CO<sub>2</sub>/crude oil displacement apparatus.

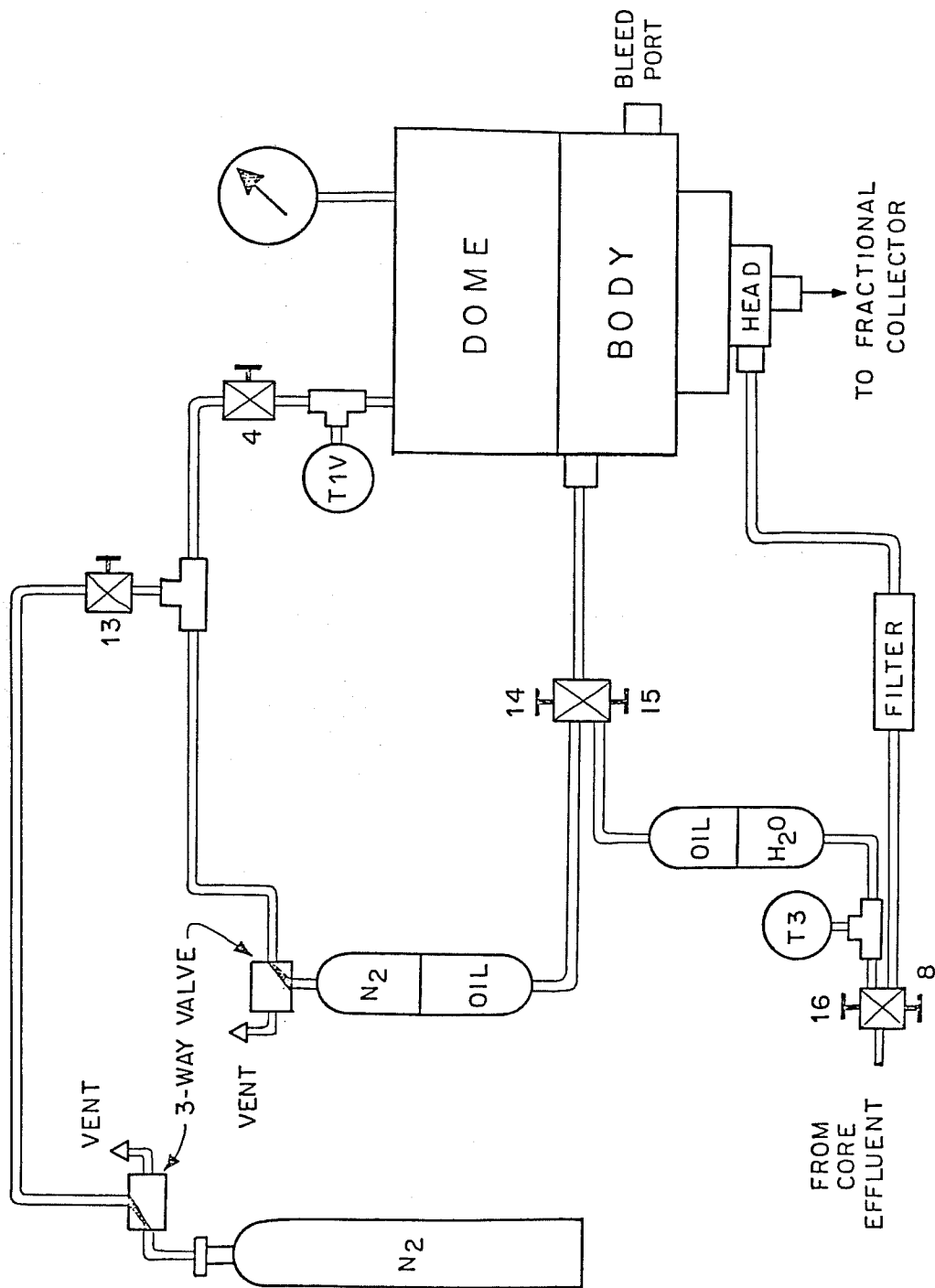


Figure 2.2. Schematic of the back pressure regulator system.

Table 2.1

Properties of Core B7

<b>Core Description:</b>	Outcrop Berea Sandstone
<b>Length:</b>	14.94 cm
<b>Diameter:</b>	3.790 cm
<b>Area:</b>	11.28 cm <sup>2</sup>
<b>Pore Volume:</b>	32 cm <sup>3</sup>
<b>Porosity:</b>	19%
<b>Absolute Permeability:</b>	216.5 md

Table 2.2

## Summary of Hydrocarbon Fluid Properties

Fluid	Run No.	P (psia)	T (°F)	Density (g/cc)	Viscosity (cp)
nC <sub>6</sub>	1	1014	93	0.6511	0.3038
nC <sub>6</sub>	2	1160	93	0.6523	0.3073
nC <sub>10</sub> + nC <sub>16</sub>	4	1634	93	0.7811	1.9671
nC <sub>10</sub> + nC <sub>16</sub>	5	1656	93	0.7812	1.9684
nC <sub>10</sub> + nC <sub>16</sub>	6	1202	93	0.7802	1.9359
nC <sub>10</sub> + nC <sub>16</sub>	7	1096	93	0.7799	1.9283
nC <sub>10</sub> + nC <sub>16</sub>	8	1100	93	0.7799	1.9285
nC <sub>10</sub> + nC <sub>16</sub>	9	1206	93	0.7802	1.9362
nC <sub>10</sub> + nC <sub>16</sub>	10	1212	93	0.7802	1.9367
nC <sub>10</sub> + nC <sub>16</sub>	11	1100	93	0.7800	1.9286

Table 2.3

Summary of CO<sub>2</sub> Properties

Run No.	P (psia)	T (°F)	Density (g/cc)	Viscosity (cp)
1	1014	93	0.2217	0.0210
2	1160	93	0.6433	0.0502
4	1634	93	0.7429	0.0699
5	1656	93	0.7821	0.0703
6	1202	93	0.6735	0.0543
7	1096	93	0.2965	0.0243
8	1100	93	0.3032	0.0246
9	1206	93	0.6756	0.0545
10	1212	93	0.6788	0.0549
11	1100	93	0.3032	0.0246

Table 2.4

Summary of Vertical CO<sub>2</sub> - Synthetic Oil Displacements

Run No.	T (°F)	P (psia)	Injection Rate			Recovery	
			Q (cc/hr)	Q <sub>c</sub> (cc/hr)	Q/Q <sub>c</sub>	@CO <sub>2</sub> BT	@ 1.2 PVI
1	93.0	1014	5.00	12.9	0.387	--	0.693
2	93.0	1160	4.00	0.298	13.4	--	0.491
4	93.0	1634	4.00	0.171	23.4	0.488	0.712
5	93.0	1656	1.46	0.171	8.54	0.560	0.884
6	93.0	1202	1.10	0.482	2.28	0.606	0.912
9	93.0	1206	1.22	0.473	2.58	0.417	0.713
10	93.0	1212	0.670	0.458	1.46	0.525	--
7	93.0	1096	4.20	2.16	1.95	0.309	0.491
8	93.0	1100	2.79	2.13	1.31	0.307	0.517
11	93.0	1100	2.46	2.13	1.16	0.472	0.485

$$v_c = \frac{3.481 \Delta\rho k \sin\theta}{\phi \Delta\mu} \quad (2.1)$$

where

- $v_c$  = critical velocity (cm/hr)
- $\Delta\rho$  = density difference (oil minus solvent) (g/cc)
- $k$  = core permeability (darcies)
- $\theta$  = dip angle measured from the horizontal
- $\phi$  = core porosity (fraction)
- $\Delta\mu$  = viscosity difference (oil minus solvent) (cp)

A sample calculation of the critical velocity and the critical injection rate is presented in Appendix A for Run No. 9. The complete experimental data presented as pore volume of CO<sub>2</sub> injected versus oil recovery (fraction original-oil-in-place) are found in Appendix B.

All the displacements were conducted with the less dense CO<sub>2</sub> solvent injected downward from the top of the core to take advantage of the dampening effect of gravity forces on frontal instabilities. Although the original intention was to perform gravity-stable displacements (i.e., to operate at or below the critical velocity), all of the experiments were conducted at supercritical flow rates. Operational difficulties were encountered due to the very small values of critical flow rates (see Table 2.4) which exacted the limiting operational capabilities of the experimental apparatus.

Two displacements (Runs 1 and 2) were performed on core B7 with n-hexane (nC<sub>6</sub>) for the purpose of acquainting the operators with the modified apparatus. Run 1 was conducted below the measured minimum miscibility pressure (MMP) of 1150 psia. The low recovery at 1.2 PV is characteristic of displacements performed below the MMP even though it is gravity-stabilized. An extreme case of a displacement dominated by viscous instability is shown by Run 2. The run was conducted at about 14 times the calculated critical velocity, and the adverse effect of viscous fingering is reflected in the low recovery (about 50%) at 1.2 PV. When the displacement is dominated by viscous instabilities, fingering of solvent results in gross bypassing of the oil, drastically reducing the overall efficiency of the process. The plot of the fraction of oil recovered versus pore volume of CO<sub>2</sub> injected for Runs 1 and 2 are shown in Fig. 2.3.

A series of immiscible displacements were performed to investigate the possibility of having what we refer to as "successful immiscible displacement." A summary of these displacements is also found in Table 2.4. The synthetic oil used in these experiments is a binary mixture of n-decane (nC<sub>10</sub>) and n-hexadecane (nC<sub>16</sub>) having a composition of 33.3 mole % nC<sub>10</sub>. This system, when mixed with CO<sub>2</sub>, exhibits a rich topography of multiphase equilibria behavior which can be rigorously represented on a ternary diagram.

A scan on the pressure-temperature space was conducted in a static PVT cell at a temperature of 93°F (slightly supercritical to CO<sub>2</sub>) to map out the location of the L<sub>1</sub>-V, L<sub>1</sub>-L<sub>2</sub>-V, L<sub>1</sub>-L<sub>2</sub>, and the single dense fluid phase region of the CO<sub>2</sub> + nC<sub>10</sub> + nC<sub>16</sub> ternary system. No attempt, however, was made to identify the boundaries of the different regions, i.e., the upper and lower critical end-points of the three-phase region and the upper critical solution temperature of the L<sub>1</sub>-L<sub>2</sub> region. Instead, the pressure was varied at fixed temperature, and the pressure was noted where the different regions were observed. Also, no density or composition measurements were made. A summary of the pressures and the corresponding type of phase behavior observed is presented in Table 2.5.

(CO<sub>2</sub> 87-278)

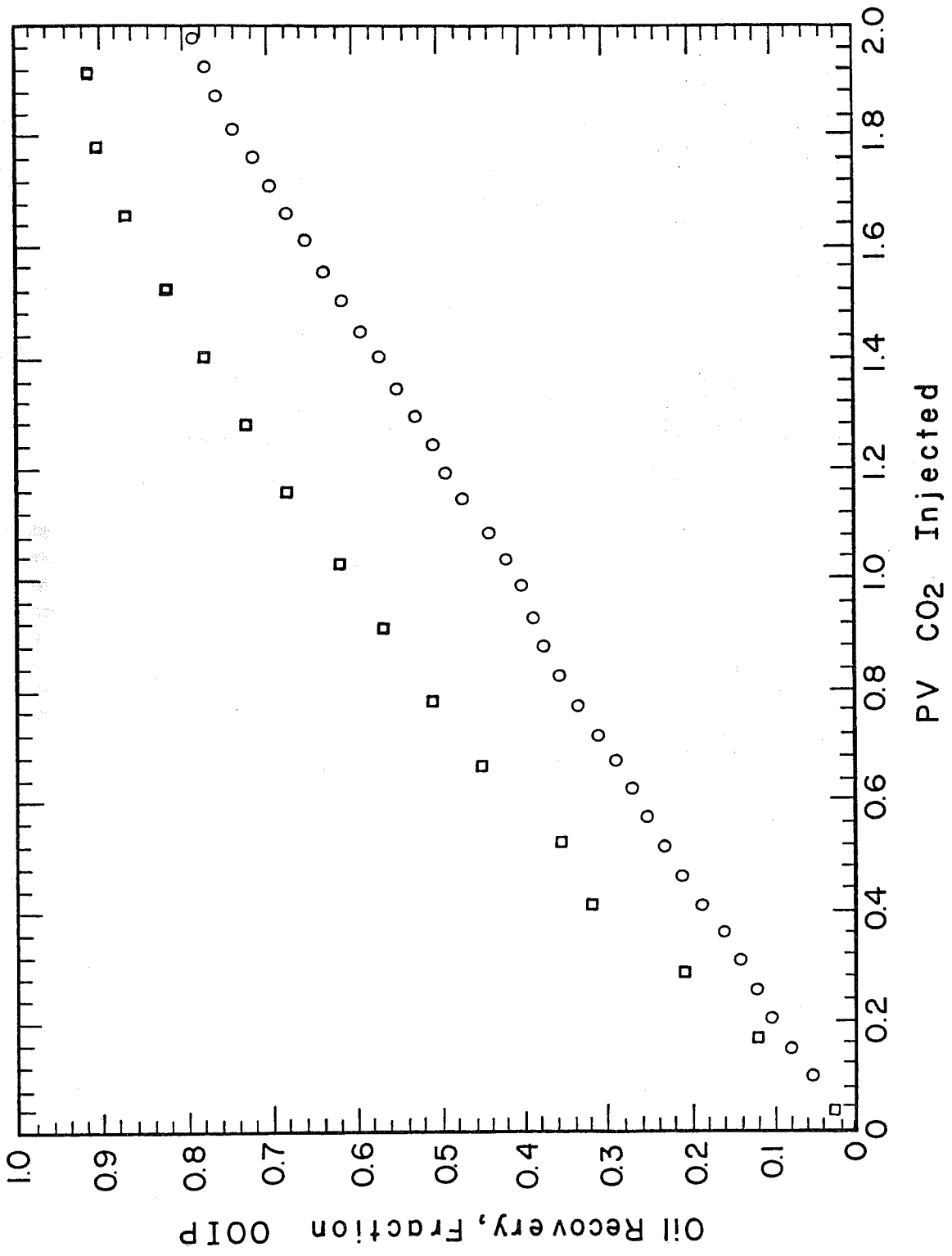


Figure 2.3. Experimental oil recovery curves - Run 1 ( $\sigma$ ) and Run 2 ( $\circ$ ); 1014 psia,  $Q/Q_c = 0.387$  and 1160 psia,  $Q/Q_c = 13.4$ .

Table 2.5

Summary of CO<sub>2</sub> + nC<sub>10</sub> + nC<sub>16</sub> Phase Behavior at 93°F

P* (psia)	Type of Phase Behavior
1068 - 1120	L <sub>1</sub> - L <sub>2</sub> - V
1192 - 1350	L <sub>1</sub> - L <sub>2</sub>
1647	single dense fluid

\*pressure intervals are not necessarily the end-points of the different regions

The phase equilibrium information needed to simulate the experiments was obtained using the Peng-Robinson equation of state. The ternary phase diagrams for the synthetic oil-CO<sub>2</sub> system are shown in Figs. 2.4, 2.5, and 2.6 at pressures where a single dense fluid phase, the two-liquid phase, and the three-phase regions are encountered, respectively. Also shown in these figures are the original oil composition, the dilution lines and limiting tie-lines.

Runs 4 and 5 were conducted at a pressure where the injected CO<sub>2</sub> is first-contact miscible with the synthetic oil. Laboratory first-contact miscible displacements are characterized by near 100%, if not 100%, recoveries at 1.2 PV of solvent injected provided the displacement is stable. Run 4 was conducted at 24 times the calculated critical rate which accounts for the poor recovery observed. The recovery at 1.2 PV was improved by as much as 17% when the injection rate for Run 5 was reduced to almost a third that of Run 4. Plots of the fraction of oil recovered and the volume of CO<sub>2</sub> produced at atmospheric conditions as a function of pore volume CO<sub>2</sub> injected for Runs 4 and 5 are presented in Figs. 2.7 and 2.8. Also shown in these figures are the simulation results.

The experimental result for Run 4 shows significant deviation from the simulation. Although the simulator used in this work (similar to Orr, 1980) has been shown to predict results accurately for simple flow settings such as encountered in a slim tube displacement, it suffers the inability to model viscous fingering. Better agreement between simulation and experimental result is evident for Run 5 where the value of the dimensionless velocity is about a third that of Run 4.

Three runs were performed at a pressure where two liquid phases were observed in the static PVT cell. Fig. 2.5 shows the ternary phase diagram for this system with its attendant limiting tie-line and original oil composition. The synthetic oil composition and the location of the limiting tie-line are such that an overall CO<sub>2</sub>-oil composition will be reached where an equilibrium tie-line extended through that point will also pass through the initial oil composition. Multiple-contact miscibility, therefore, will never be generated. Immiscible displacements are characterized by oil production rates that rapidly approach zero after gas breakthrough. Any additional CO<sub>2</sub> injected after breakthrough will invariably invade the swept regions, bypassing the residual oil. Even if contact with the oil occurs, miscibility will never be achieved because the residual oil is probably already saturated with CO<sub>2</sub>.

Figs. 2.9, 2.10, and 2.11 show both the experimental and simulated recovery curves for Runs 6, 9, and 10. A comparison between Runs 6 and 9 shows a dramatic increase in recovery (about 14% at 1.2 pore volume CO<sub>2</sub> injected) with about a 10% drop in the injection rate. Run 10 shows a slightly lower apparent recovery at CO<sub>2</sub> breakthrough despite the lower value of the dimensionless injection rate compared to Run 6. This discrepancy might be due to an unstable injection rate. The injection rate of 0.670 cc/hr is probably too low and has reached the limitations of the CO<sub>2</sub> pump used.

A comparison of experimental and simulated results for Runs 6 and 9 show that experimental oil production appears to increase beyond what was predicted by the simulator after gas breakthrough, i.e., the production rate does not drop as fast as expected for an immiscible displacement. What makes this comparison even more interesting is the fact that viscous fingering was not accounted for in the simulation, a phenomenon that is undoubtedly present in the experiments as indicated by the much earlier CO<sub>2</sub> breakthrough than predicted. This result seems to indicate the possibility of having an immiscible flood with recoveries characteristic of multiple-contact miscible displacements. The miscible-like behavior of displacements conducted at pressures where two liquid phases are observed in a static PVT cell might be related to the physical properties of the CO<sub>2</sub>-rich (L<sub>2</sub>) and hydrocarbon-rich (L<sub>1</sub>) phases of the CO<sub>2</sub> + nC<sub>10</sub> + nC<sub>16</sub> ternary system. Calculated interfacial tensions (IFT) between the two phases are in the range of 10<sup>-2</sup> - 10<sup>-1</sup> dynes/cm. Visual

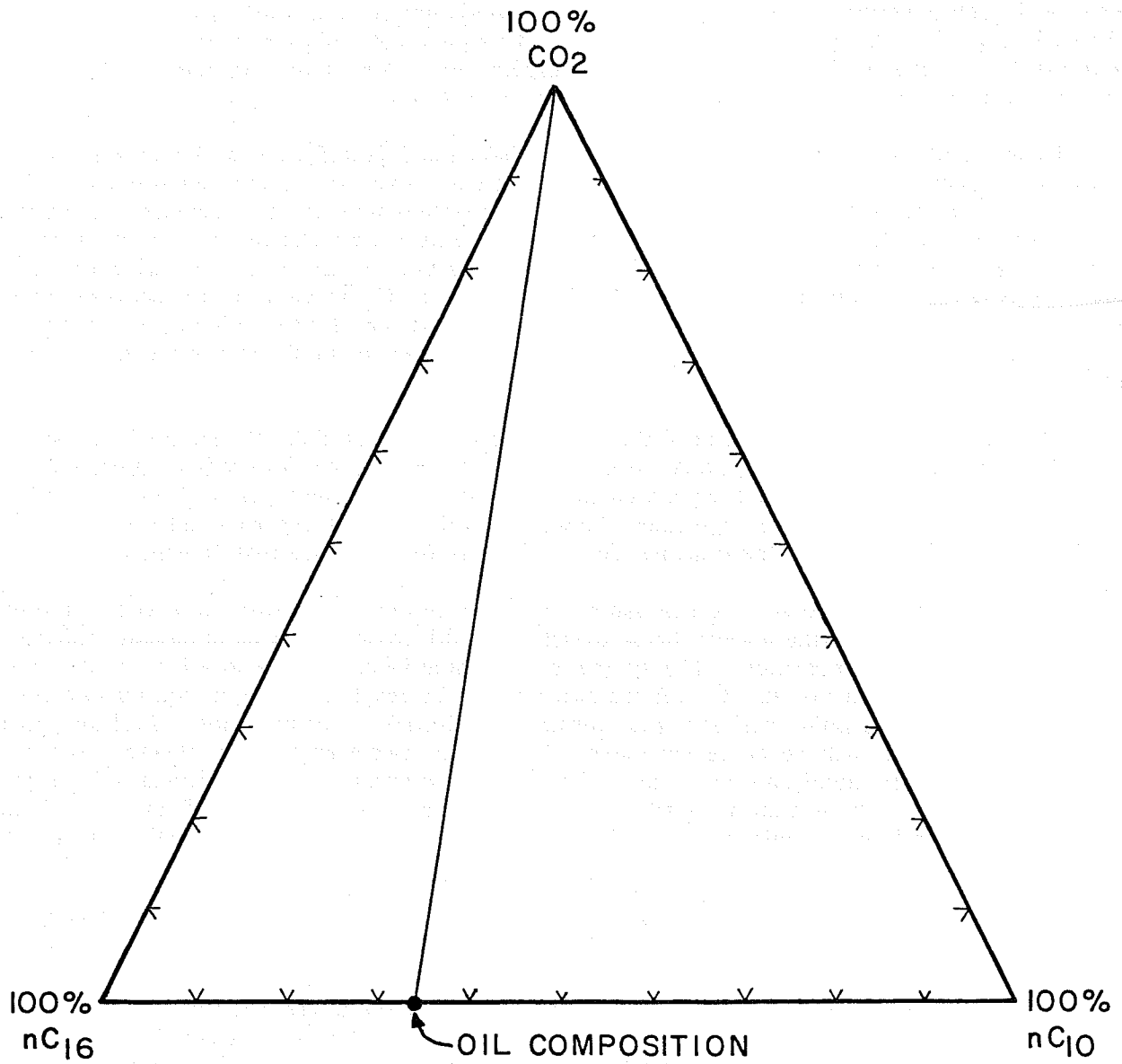
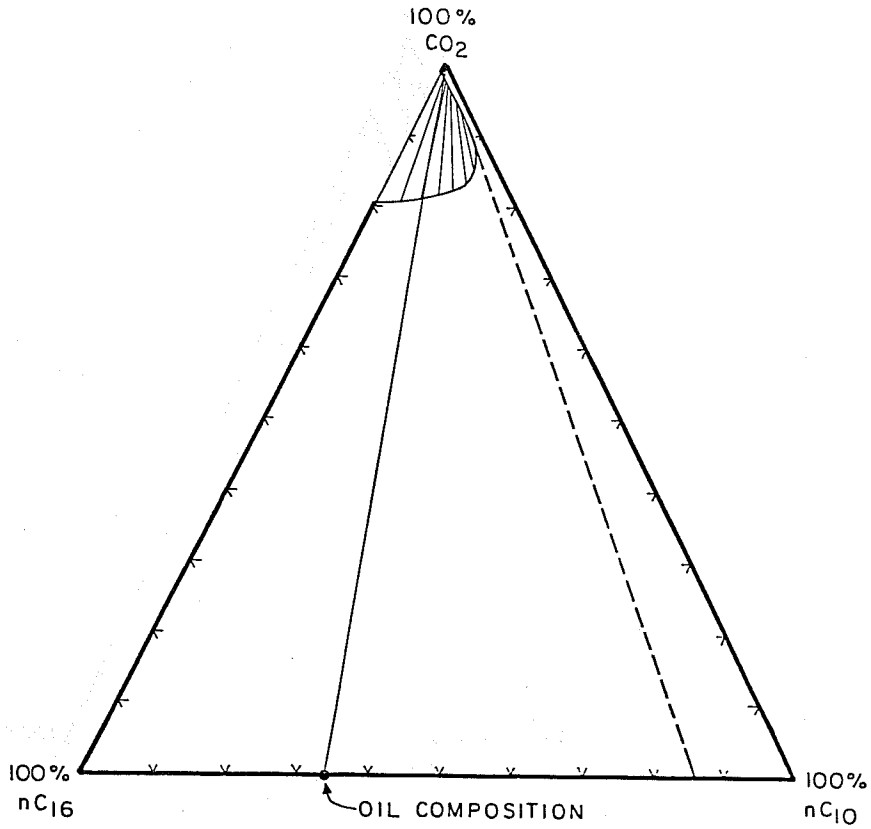


Figure 2.4. Ternary phase diagram of CO<sub>2</sub>+nC<sub>10</sub>+nC<sub>16</sub> at 1600 psia and 93°F.



(CO<sub>2</sub>-87-263)

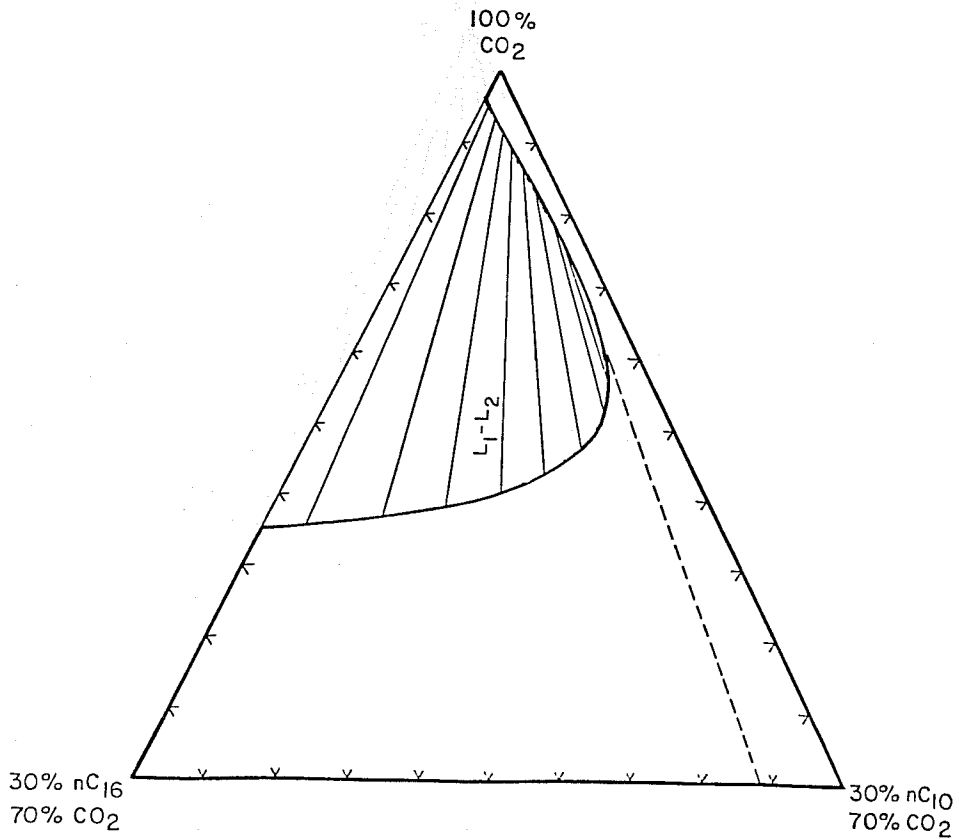
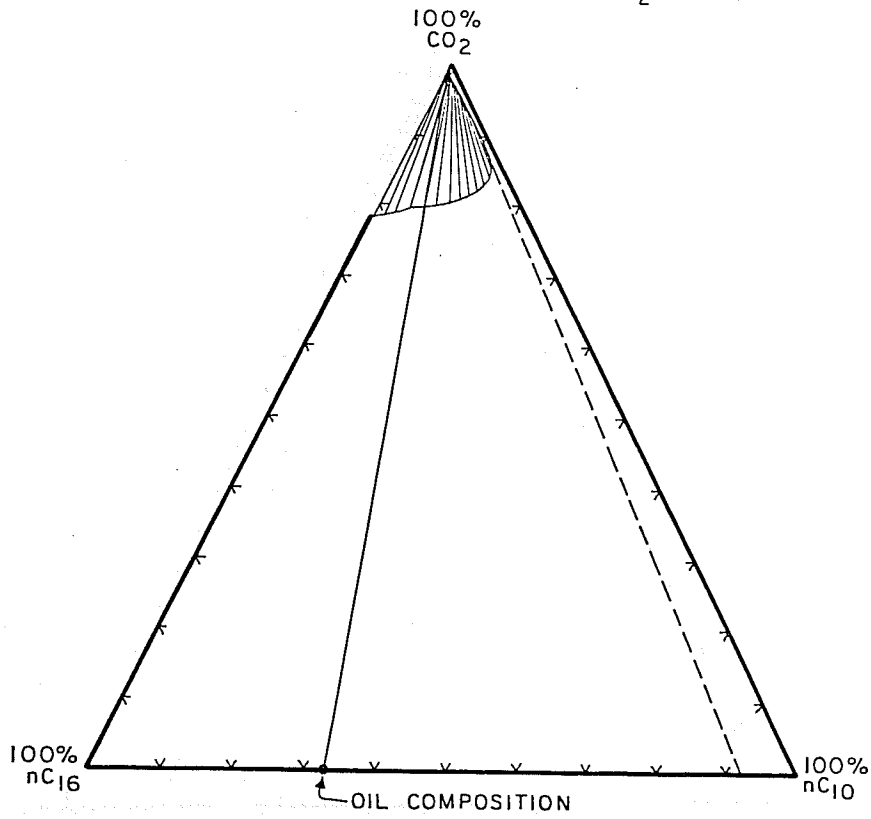


Figure 2.5. Ternary phase diagrams of CO<sub>2</sub>+nC<sub>10</sub>+nC<sub>16</sub> at 1200 psia and 93°F.

(CO<sub>2</sub>-87-265)



(CO<sub>2</sub>-87-262)

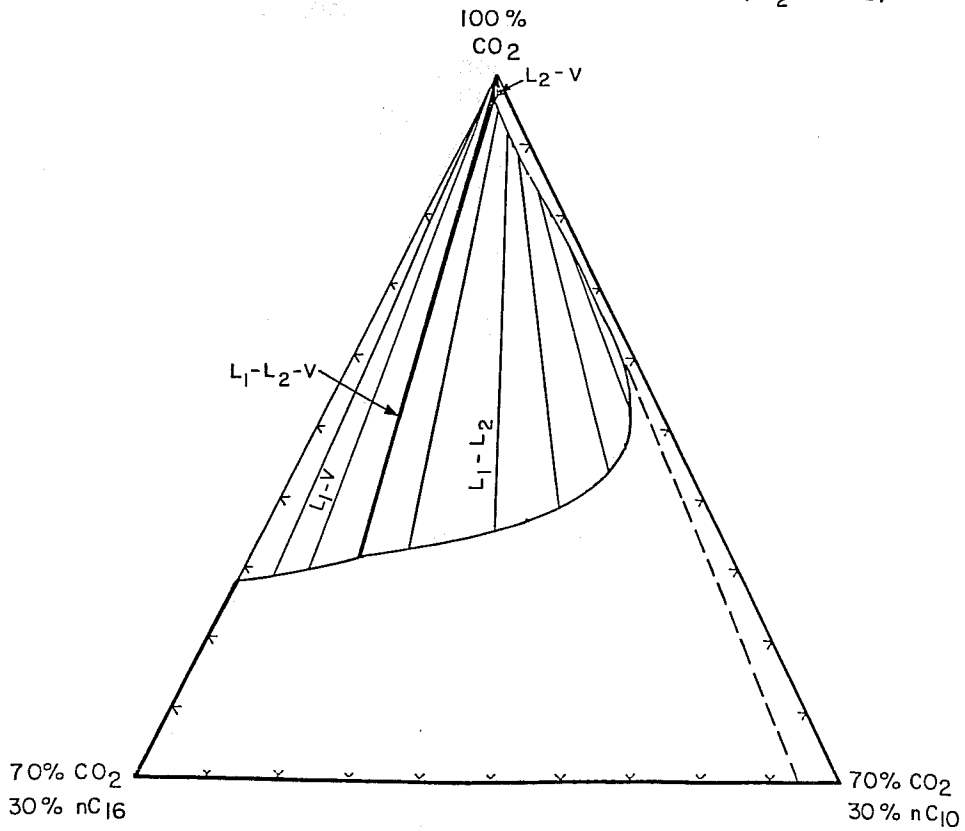


Figure 2.6. Ternary phase diagrams of CO<sub>2</sub>+nC<sub>10</sub>+nC<sub>16</sub> at 1100 psia and 93°F.

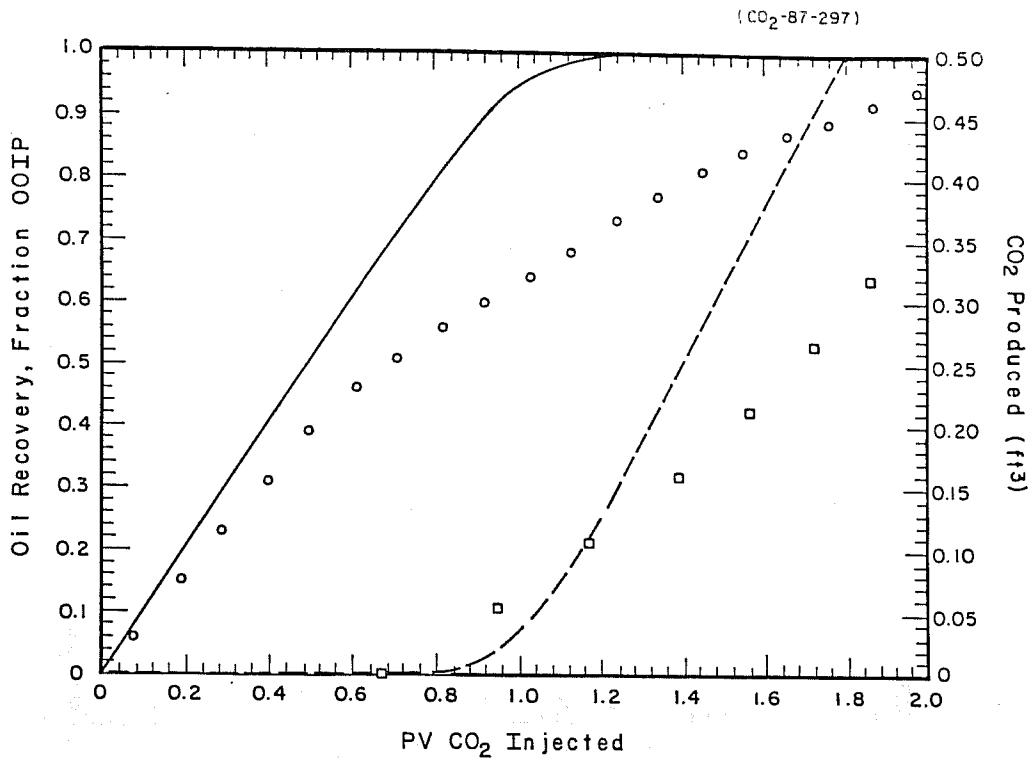


Figure 2.7. Experimental and simulated oil recovery and gas production  
 - Run 4, 1634 psia,  $Q/Q_c = 23.4$ .

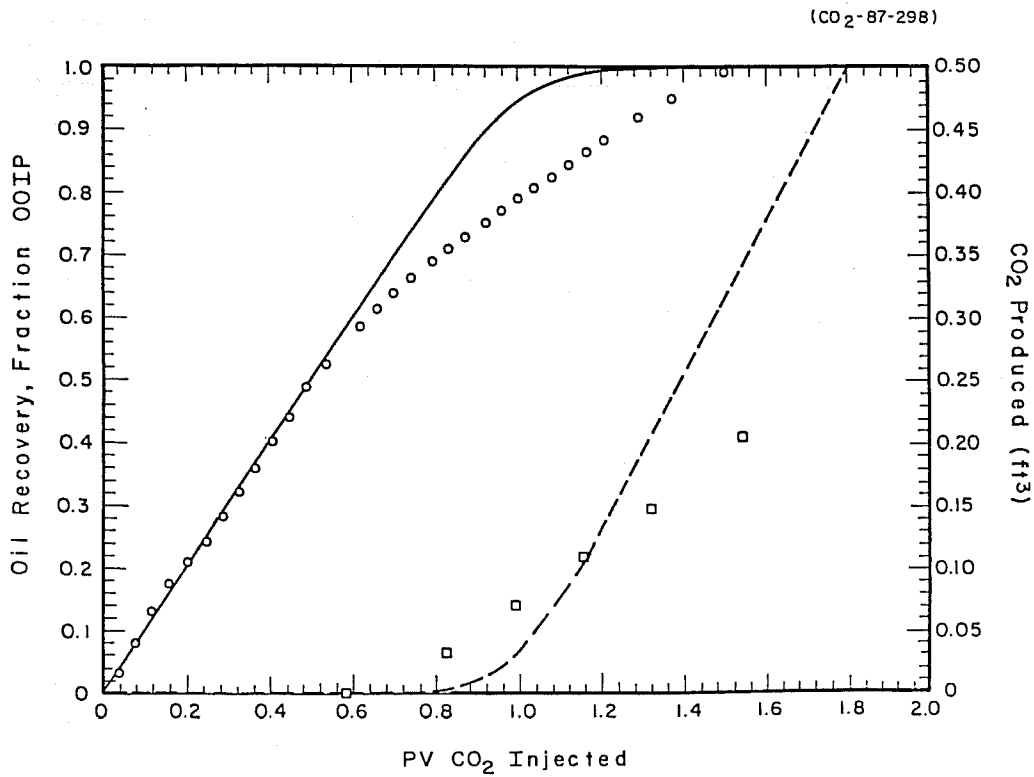


Figure 2.8. Experimental and simulated oil recovery and gas production  
 - Run 5, 1656 psia,  $Q/Q_c = 8.54$ .

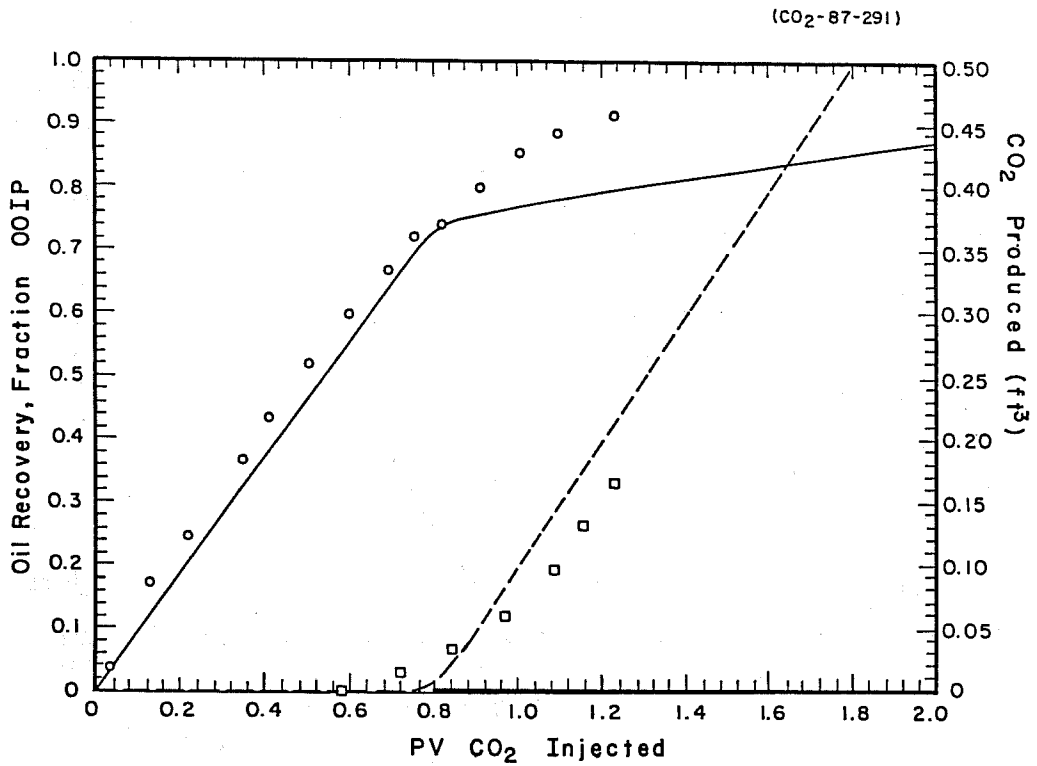


Figure 2.9. Experimental and simulated oil recovery and gas production - Run 6, 1202 psia,  $Q/Q_c = 2.28$ .

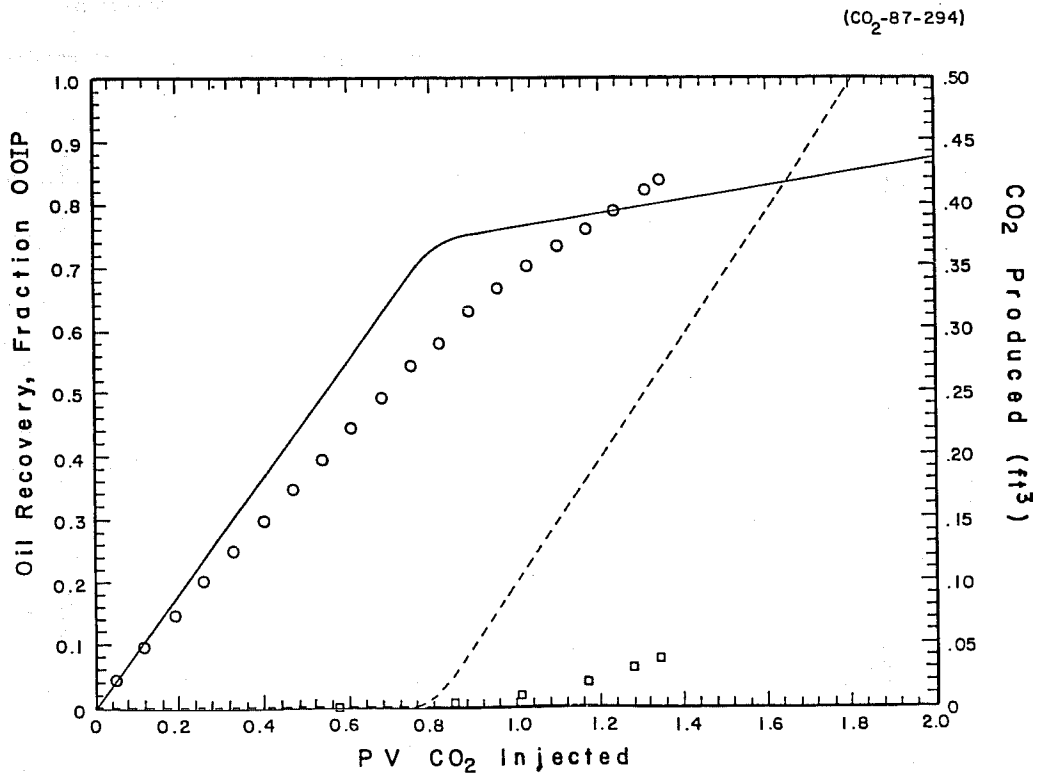


Figure 2.10. Experimental and simulated oil recovery and gas production - Run 9, 1206 psia,  $Q/Q_c = 2.58$ .

(CO<sub>2</sub>-87-295)

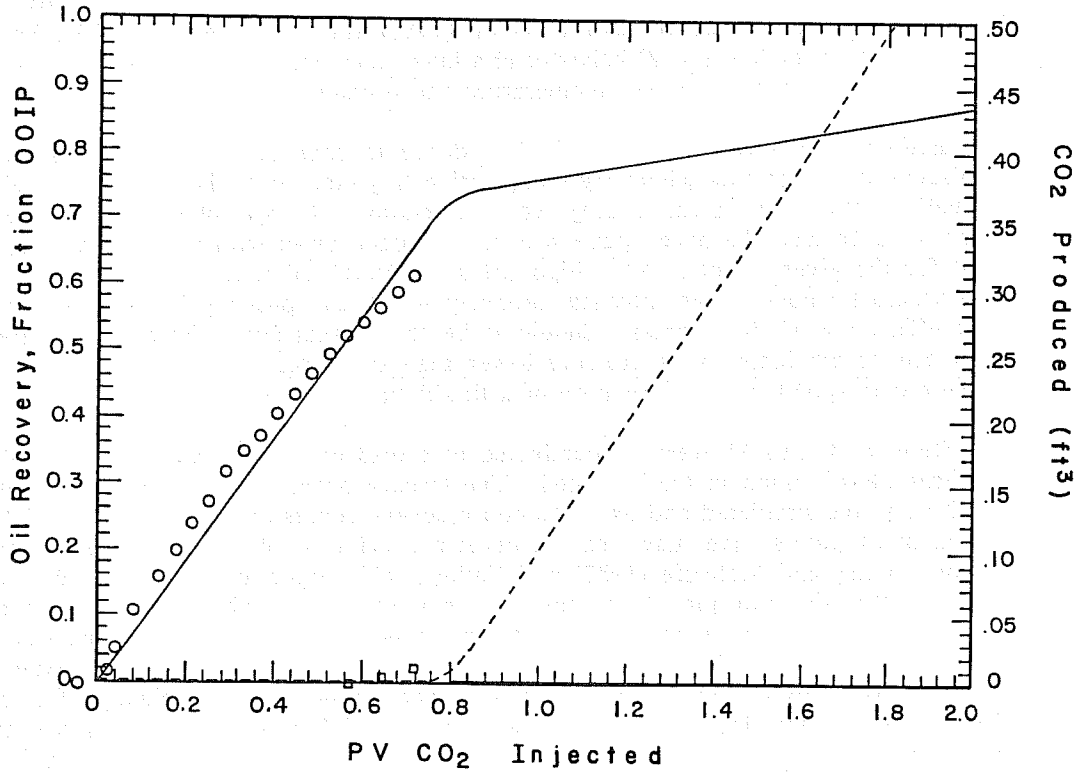


Figure 2.11. Experimental and simulated oil recovery and gas production - Run 10, 1212 psia,  $Q/Q_c = 1.46$ .

observations during phase equilibria experiments performed in a static PVT cell show a very flat meniscus between the two phases, a consequence of having low IFT. The process as a whole might be behaving like an ultra-low IFT flood.

Related findings by several investigators point to the beneficial effects of the  $L_2$  phase. Orr et al. (1983) published results of phase equilibria measurements which showed that the  $\text{CO}_2$ -rich liquid phase ( $L_2$ ) extracts hydrocarbons more efficiently than the  $\text{CO}_2$ -rich vapor at the same pressure. Lansangan et al. (1987) showed that the  $L_2$  phase is in itself responsible for the enhanced solubilizing capacity of a slightly supercritical dense fluid phase, a phenomenon referred to as supercritical extraction. The theory presented by Lansangan et al. also explains the hypothesis put forth by Charoensombut-amon (1985) and Huang et al. (1978), i.e., the presence of liquid-liquid-vapor ( $L_1$ - $L_2$ -V) behavior at a lower temperature is a prerequisite to the occurrence of supercritical extraction at higher temperature and pressure.

Even though there is very limited evidence to support the theory presented here regarding immiscible displacements where the composition trajectory cuts the binodal curve of  $L_1$ - $L_2$  region, we believe this is a research area worth pursuing. It will involve extensive phase equilibria experiments to map the exact location of the binodal curve with its attendant liquid-liquid critical point for the given system. Also, high-pressure interfacial tension measurements must be made to have accurate values of that physical property which can possibly be correlated with the displacement efficiency of the process. Should it be shown that such displacements are feasible, a  $\text{CO}_2$  flood can be conducted at a pressure lower than the MMP for the  $\text{CO}_2$ -crude oil system if that pressure corresponds to the formation of a liquid-liquid region.

Runs 7, 8, and 11 were all conducted at a pressure which corresponds to the observation of the three-phase region in the PVT cell. The ternary phase diagram for this system is presented in Fig. 2.6 and the simulated and experimental recovery curves are shown in Figs. 2.12, 2.13, and 2.14. Several investigators have suggested the beneficial effect of having multiple phases within the flow system. Henry and Metcalfe (1983) and Yellig (1982) suggested, based on very little experimental evidence, that the multiple phases can have a relative permeability effect on the mobility of the  $\text{CO}_2$ /oil transition zone which can lead to improved sweep efficiency of the flood. Their experiments were conducted above the measured MMP of the  $\text{CO}_2$ -oil system. The experiments conducted here, however, are all immiscible. Any improvement in sweep efficiency, if it occurred at all, is offset by a very low local displacement efficiency which resulted in a poor overall recovery. It is interesting to note, however, the increase in  $\text{CO}_2$  injection pressure by 5-7 psia above the initial injection pressure for these runs, a phenomena that was not observed with the other runs. This observation seems to be consistent with the reduced-permeability-effect theory as mentioned above. Tiffin and Kremesec (1986) published results which show that the critical velocity calculated from Eq. 2.1 is a sufficient criterion to predict the onset of viscous instabilities in vertical laboratory corefloods. They correlated the dimensionless injection velocity with the effective mixing length which is a ratio of the effective dispersion coefficient and the Darcy velocity. They found a sharp increase in the effective mixing coefficient at  $Q/Q_c = 1$  which shows that theory reliably predicts the formation of viscous fingers. One, therefore, can safely conclude, based on the values of  $Q/Q_c$  for these runs, that viscous fingers are indeed present during the experiment. Gardner and Ypma (1984) suggested the presence of what they termed "synergistic effect" between phase behavior and macroscopic bypassing (viscous fingering). These are all possible explanations for the very low ultimate recovery at 1.2 PV  $\text{CO}_2$  injection for Runs 7, 8 and 11.

Displacements of waterflooded residual synthetic oil ( $S_{orw} = 35\%$ ) at pressures which correspond to the formation of the  $L_1$ - $L_2$ -V and  $L_1$ - $L_2$  regions were also conducted. The immiscible tertiary displacement at the three phase pressure resulted in a very early  $\text{CO}_2$  breakthrough and a recovery of less than 36% of the post-waterflood residual oil after 2.0 pore volume of  $\text{CO}_2$  injected.

(CO<sub>2</sub>-87-292)

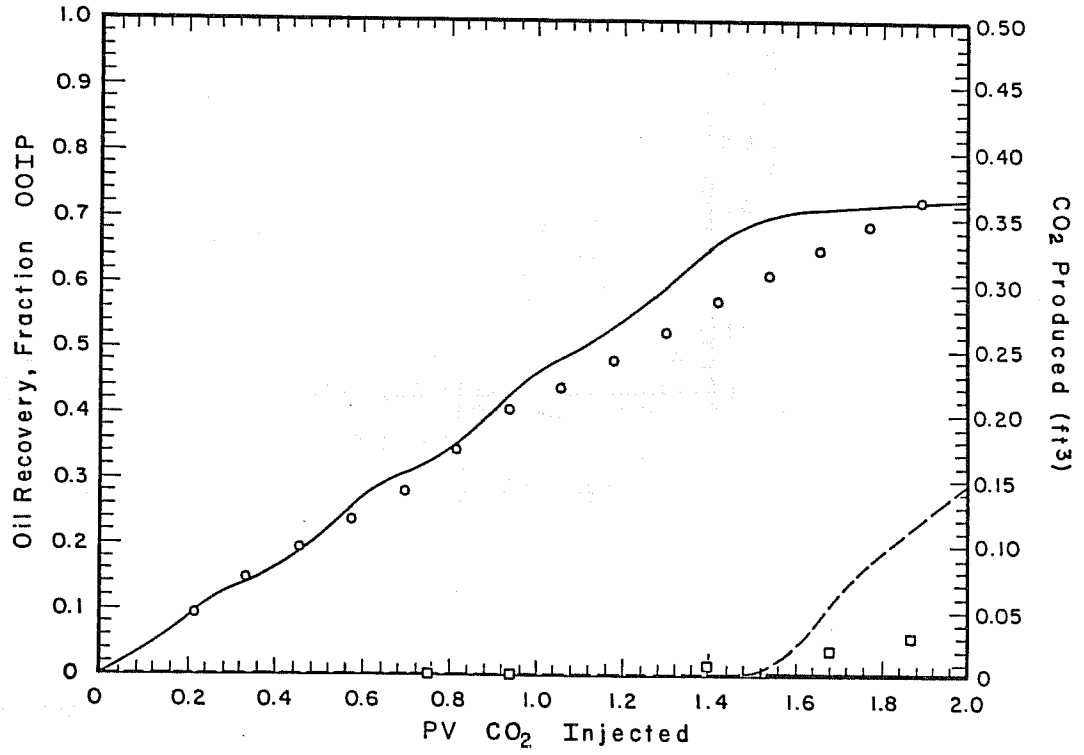


Figure 2.12. Experimental and simulated oil recovery and gas production - Run 7, 1096 psia,  $Q/Q_c = 1.95$ .

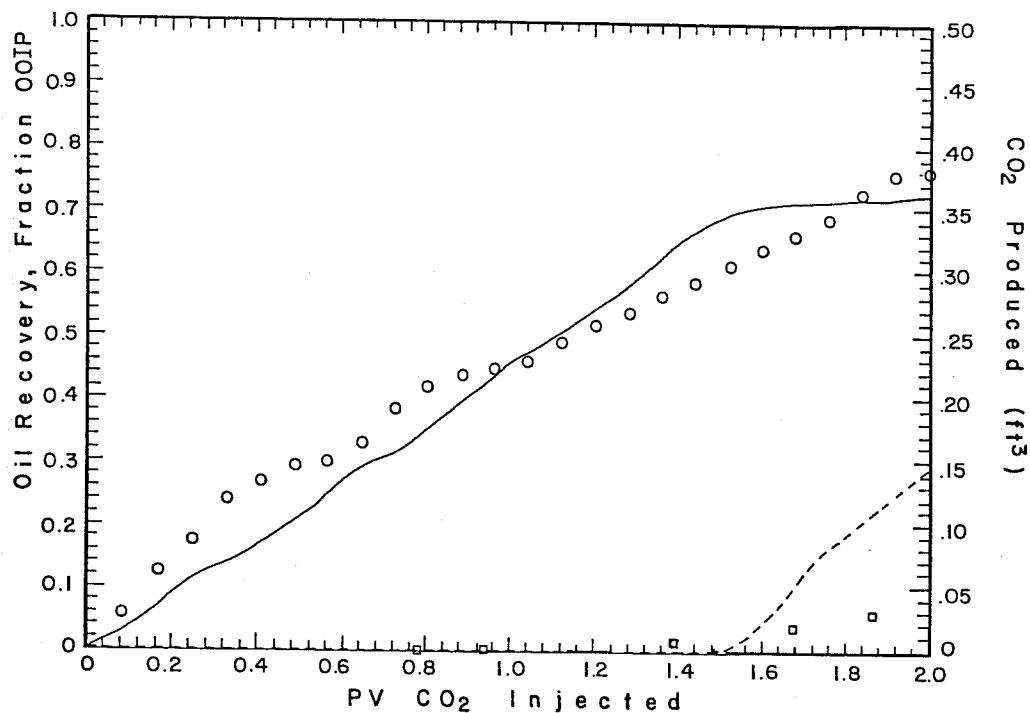


Figure 2.13. Experimental and simulated oil recovery and gas production - Run 8, 1100 psia, Q/Q<sub>c</sub> = 1.31.

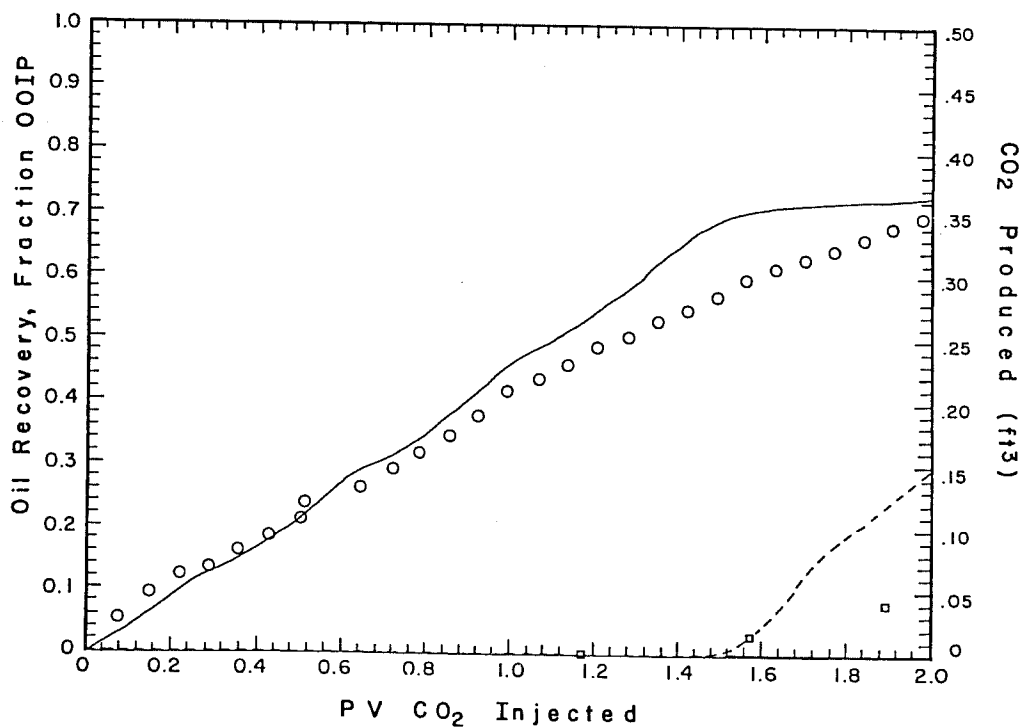


Figure 2.14. Experimental and simulated oil recovery and gas production - Run 11, 1100 psia, Q/Q<sub>c</sub> = 1.16.

Bahralolom (1985) conducted immiscible displacements of waterflooded residual Maljamar crude oil by CO<sub>2</sub> in a two-dimensional glass micromodel. His results showed that the initial distribution of crude oil and water was essentially the same at CO<sub>2</sub> breakthrough for the displacement at 800 psia and 25°C. The high water saturation in a water-wet system resulted in trapping of the oil in the form of blobs. The trapped oil remained largely uncontacted by the CO<sub>2</sub>, and recovery was essentially zero after the early breakthrough. The high interfacial tension between the different phases coupled with strong capillary forces forced the injected CO<sub>2</sub> through the regions occupied by the continuous water phase. Even if the experiment was carried on long enough to allow the CO<sub>2</sub> to diffuse through the water and eventually contact the oil, additional recovery, if any, will be minimal due to the immiscible nature of the displacement.

The tertiary flood at the two-liquid phase pressure showed a delayed CO<sub>2</sub> breakthrough and a recovery of about 63% at 1.6 PV CO<sub>2</sub> injected, almost double the recovery at the three-phase pressure. It is probable that the recovery would have increased further had the experiment been carried on longer. Bahralolom reported the results of displacements at 900 psia and 25°C on the same waterflooded residual Maljamar crude oil. His results showed that the flood performance at the early stage of the experiment was almost identical to the displacement conducted at 800 psia. A single flow channel was established, and most of the trapped oil remained uncontacted. A rather interesting phenomena was observed after about 1.5 PV of CO<sub>2</sub> was injected. A second phase, presumed to be a CO<sub>2</sub>-rich liquid phase, formed near the inlet of the micromodel and started to diverge from the main flow channel. The new phase was observed to flow through the oil films in the pore capillary grooves, dissolving in the crude oil while allowing more flow channels to be established. The relative ease by which the CO<sub>2</sub>-rich phase moved through the pore matrix is evidence that supports the low interfacial tension theory. The poor initial performance of the flood can be explained by the fact that not enough CO<sub>2</sub> was available at that point to generate the CO<sub>2</sub>-rich liquid phase.

The tertiary CO<sub>2</sub> flood at the L<sub>1</sub>-L<sub>2</sub> pressure was simulated and compared to the simulation of the tertiary displacement at the first-contact miscible pressure. The recovery curves for these displacements is shown in Fig. 2.15. Oil recovery is defined here as the fraction recovered relative to the post-waterflood oil saturation, S<sub>orw</sub>.

The one-dimensional simulator predicted a CO<sub>2</sub> breakthrough at about 0.36 and 0.5 PV injected for the displacements at 1200 psia (L<sub>1</sub>-L<sub>2</sub> pressure) and 1600 psia (first-contact miscible pressure) with recoveries of about 55% and 75%, respectively. The production rate for the first-contact miscible displacement declined rapidly after CO<sub>2</sub> breakthrough, the recovery approaching an asymptotic value of about 92%. Although the displacement at the L<sub>1</sub>-L<sub>2</sub> pressure only posted a 55% recovery at breakthrough, the production rate did not drop as fast, and recovery continued to increase substantially, approaching that of the displacement at 1600 psia. This result is consistent with the observations made by Bahralolom (1985) regarding the effectiveness of the CO<sub>2</sub>-rich liquid phase in recovering waterflooded residual oil.

Thus, there are evidences which show the effectiveness of the CO<sub>2</sub>-rich liquid phase in recovering oil even under high water saturations.

#### 2.1.4 Mixing Parameters Sensitivity Analysis

This part of the study examines the impact of microscopic heterogeneity due to rock pore structure on the performance of both miscible and immiscible one-dimensional CO<sub>2</sub> floods. The one-dimensional simulator used in this study was originally developed by Orr (1980) and Gardner et al. (1981). One important aspect of the simulator is that it models the effect of volume change on

(CO<sub>2</sub>-87-332)

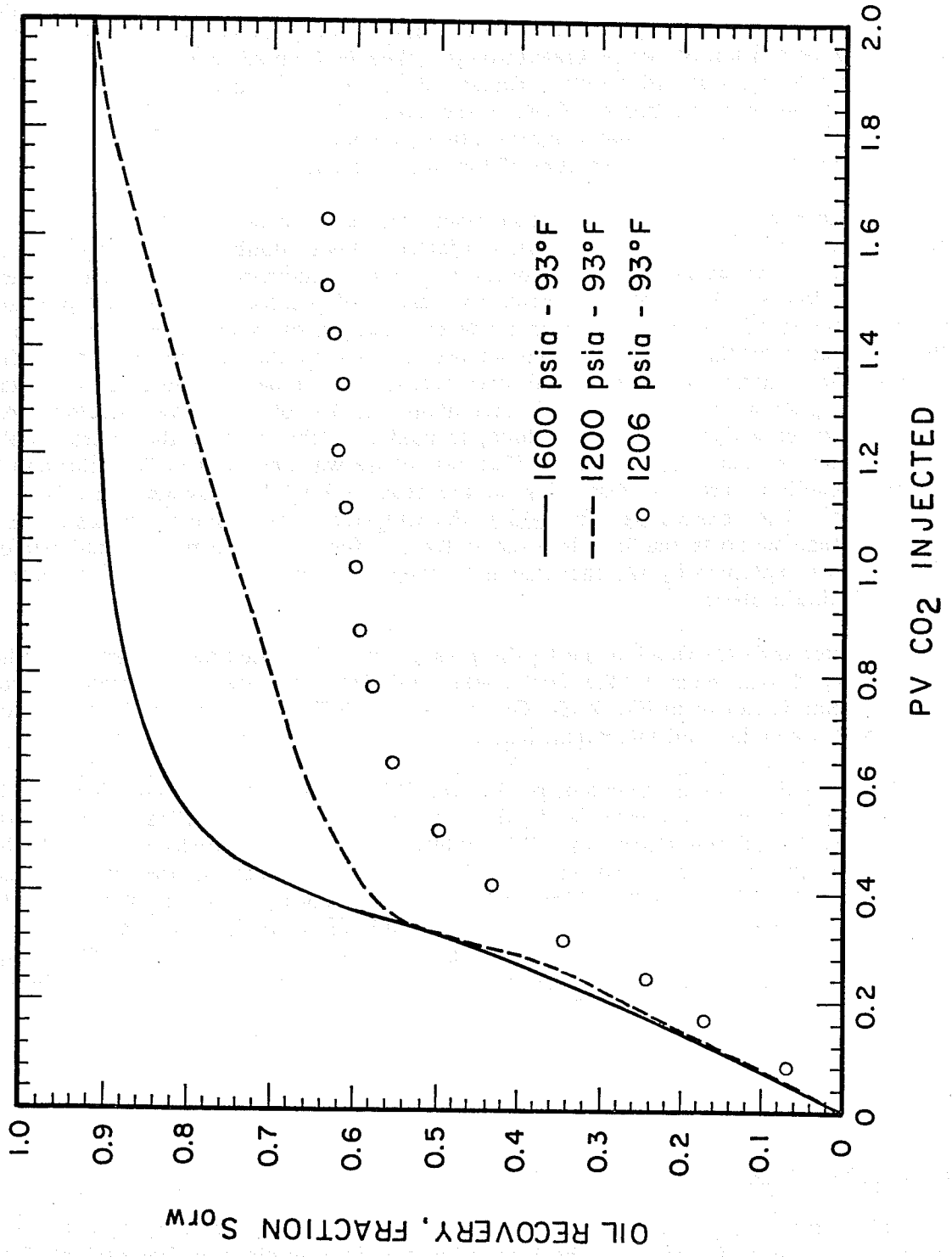


Figure 2.15. Experimental (o) and simulated (---) oil recovery of the tertiary CO<sub>2</sub> displacement.

mixing. This is accomplished by allowing the components ( $\text{CO}_2$ , light hydrocarbon, heavy hydrocarbon, and water) to have different densities in each of the four phases (V,  $L_1$ ,  $L_2$ ,  $\text{H}_2\text{O}$ ). It was later modified (Dai, 1984) to account for pore structure heterogeneity and alterations to mixing due to high water saturations. The flow system is essentially divided into a flowing fraction, a dendritic fraction which exchanges mass with the flowing fraction, and a trapped or isolated fraction largely unavailable for contact with injected fluids. Trapping of oil has been shown (Campbell & Orr, 1985) to occur in water-wet rocks under high water saturation. The simulator, at its heart, is the Coats-Smith model (1964) combined with a simplified phase behavior description of  $\text{CO}_2$ -crude oil mixtures.

In the simulation of the experiments performed in this study, no attempt was made to adjust the input parameters to the simulator to get a match between the experimental and simulated recovery curves. The simulations are the results of independent calculations of phase equilibria information, fluid properties, and measurement of mixing parameters. Phase equilibria information was calculated using the Peng-Robinson equation of state, and fluid properties were obtained from TRAPP (see Appendix C). The mixing parameters defined in the Coats-Smith model, namely the Peclet number, the flowing fraction, and the dimensionless mass transfer coefficient (Damköhler number) were obtained from a series of single-phase displacement studies of Bretz et al. (1986).

The application of the model to a series of displacements without the presence of water at pressures corresponding to the formation of a single dense fluid phase and two liquid phases are presented in the following sections.

Results of simulations of the displacement of  $n\text{C}_{10} + n\text{C}_{16}$  synthetic oil mixture by  $\text{CO}_2$  at 1600 psia and 93°F for nonuniform porous media are shown in Figs. 2.16, 2.17, and 2.18. Fig. 2.16 shows simulated recovery curves for the first-contact miscible displacement for three values of the flowing fraction. As expected, the presence of dendritic space causes earlier  $\text{CO}_2$  breakthrough and lower recovery at 1.2 PV injected. In the experiments performed in this study (Runs 4 and 5), the  $\text{CO}_2$  breakthrough occurred even earlier due to the presence of viscous fingering. Noteworthy, however, is that the recovery curves for simulation runs with flowing fraction less than one continue to increase towards 100% recovery. Thus, the effect of pore structure heterogeneity on first-contact miscible displacement in the absence of water is to lower the production rate after  $\text{CO}_2$  breakthrough; 100% recovery is possible if the experiment is carried on long enough to allow  $\text{CO}_2$  to recover the dendritic oil by the slow process of diffusion. This is consistent with the statement that phase behavior determines total recovery.

The effects of changes in the mass transfer rate are depicted in Fig. 2.17. Simulation runs were performed for three values of the Damköhler number with the Peclet number and flowing fraction held constant at 100 and 0.7 respectively. It is evident from Fig. 2.17 that changes in the rate of mass transfer have a dramatic effect on recovery during first-contact miscible displacement in the presence of pore structure heterogeneity. When mass transfer rate is very slow, the dendritic fraction acts as an inert, stagnant phase. The dendritic oil was left unrecovered even after 2 PV of  $\text{CO}_2$  had been injected. When the rate of mass transfer is increased, as in the case where the Damköhler number has a value of 5.0, mixing between the dendritic and flowing fraction is very efficient so that the displacement behaves as if no dendritic fraction is present.

Variations in the level of dispersion have very little effect on recovery compared to flowing fraction and mass transfer rate. Recovery curves for three values of Peclet number with Damköhler number and flowing fraction fixed at 0.5 and 0.7, respectively, lie virtually on top of each other as shown in Fig. 2.18.

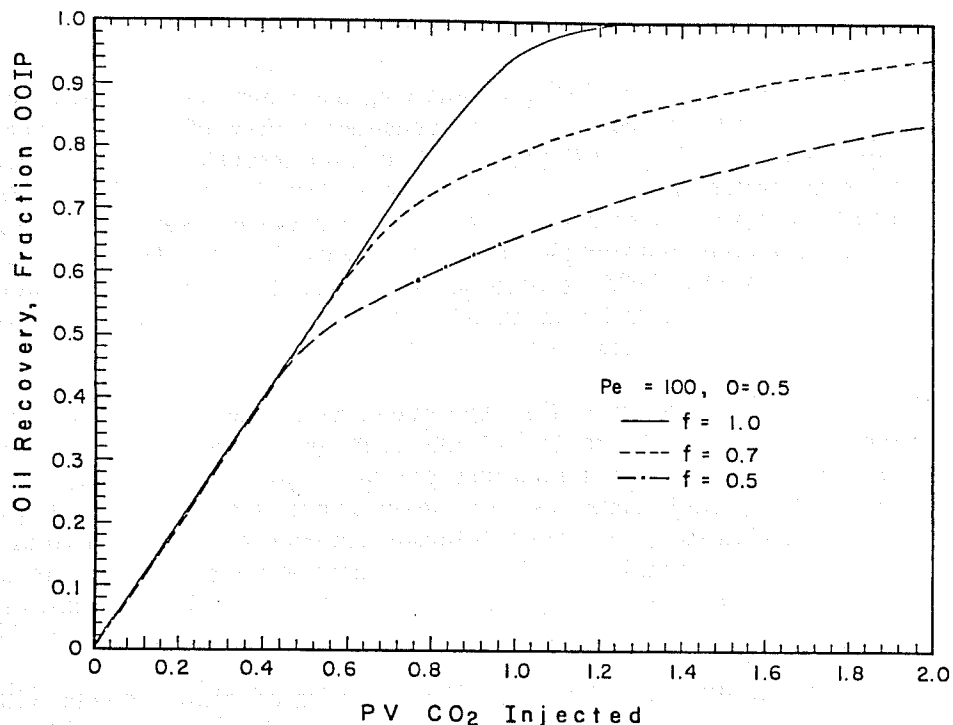


Figure 2.16. Effects of changes in flowing fraction on oil recovery during single-contact miscible displacements - 1600 psia, 93°F.

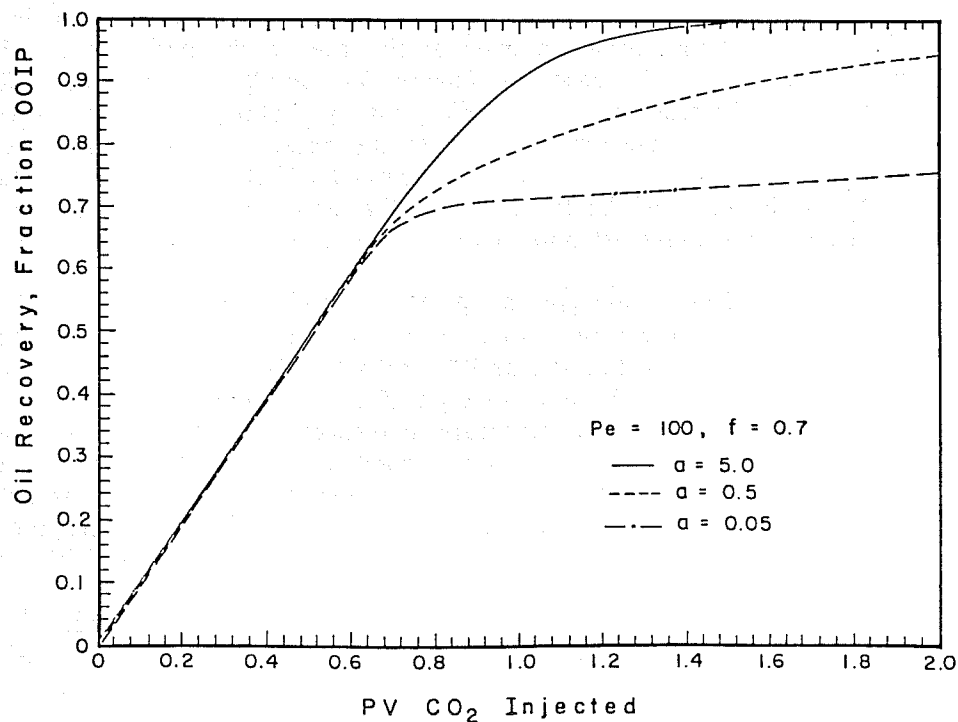


Figure 2.17. Effects of changes in mass transfer rate on oil recovery during single-contact miscible displacements - 1600 psia, 93°F.

(CO<sub>2</sub>87-301)

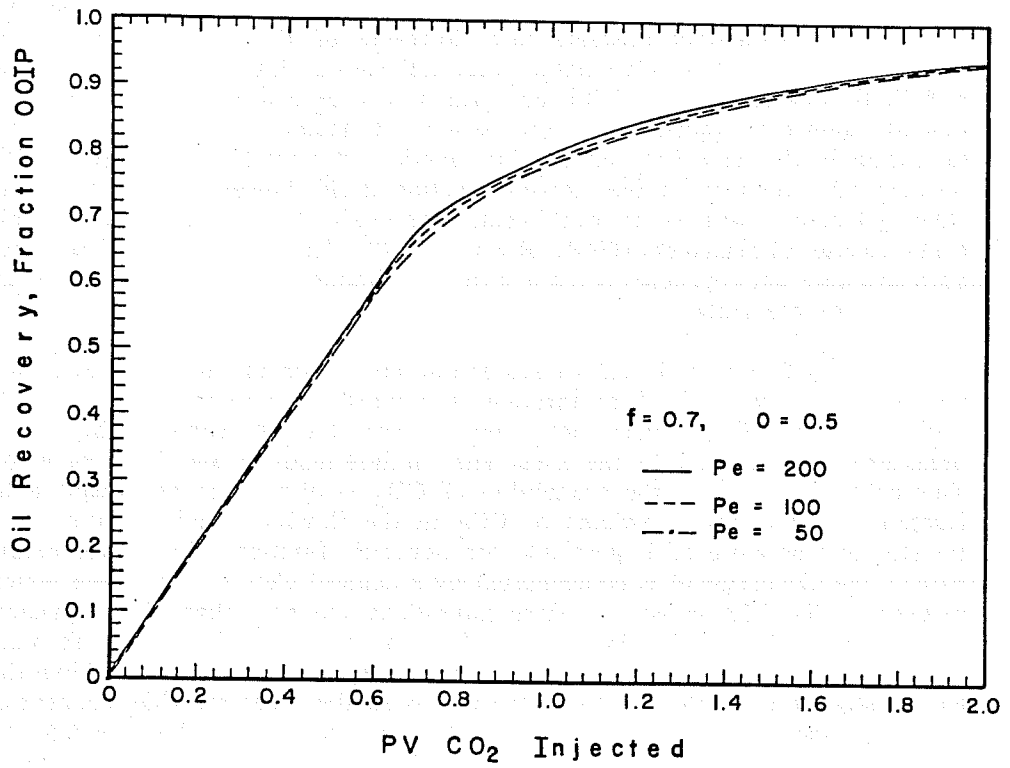


Figure 2.18. Effects of changes in longitudinal dispersion rate on oil recovery during single-contact miscible displacements - 1600 psia, 93°F.

The simulation of the displacements of the synthetic oil mixture by CO<sub>2</sub> at 93°F and 1200 psia, a pressure where the L<sub>1</sub>-L<sub>2</sub> phase separation occurs, is presented in Figs. 2.19, 2.20, and 2.21. Fig. 2.19 shows the calculated recovery curves for varying levels of pore structure heterogeneity. As in the first-contact miscible case, lowering of the flowing fraction reduces the recovery although the effect is less dramatic. Fig. 2.22 shows plots of saturations of the CO<sub>2</sub>-rich and oil-rich liquid phases, together with the normalized CO<sub>2</sub> concentration profile at 0.5 PV CO<sub>2</sub> injected plotted against the normalized core length. Calculations show that the combined residual oil saturation in the dendritic and flowing fractions decreases with increasing flowing fraction. The residual oil saturation in the flowing fraction itself, however, increases proportionately with the flowing fraction, whereas it would remain approximately constant for a miscible, in the multiple-contact sense, displacement (PRRC Report 84-10). Thus, the impact of restrictions to mixing due to pore structure heterogeneity is more severe for immiscible, or near miscible, than for multi-contact miscible displacements.

Effects of changes in mass transfer rate are shown in Fig. 2.20. A high rate of mass transfer results in a delayed CO<sub>2</sub> breakthrough as it transfers more efficiently into the dendritic fraction. The simulation with a very slow rate of mass transfer shows a higher recovery before CO<sub>2</sub> breakthrough compared to the runs with an intermediate and high value of mass transfer rate. This behavior is due to the availability of CO<sub>2</sub> to dissolve in and displace the oil in the flowing fraction. The effective volume of CO<sub>2</sub> in the flowing fraction decreases with increasing mass transfer rate as more of it goes into the dendritic fraction. The lower recovery during the early part of the displacement is compensated by a delayed CO<sub>2</sub> breakthrough which results in increased recovery. Fig. 2.23 shows the phase saturations and normalized CO<sub>2</sub> concentration profiles in all three cases at 0.5 PV injected. The effect of mass transfer on the formation of the CO<sub>2</sub>-rich liquid phase in the dendritic fraction is clearly depicted in Fig. 2.23. When the Damköhler number has a value of 0.05, the mass transfer rate is so slow that the CO<sub>2</sub> concentration in the dendritic fraction at the core inlet is only about 23% compared to 80% when  $a = 0.5$ . In both of these cases, however, not enough CO<sub>2</sub> has transferred into the dendritic fraction after 0.5 PV to allow the formation of the CO<sub>2</sub>-rich phase as it did in the case when  $a = 5.0$ . Thus, high mass transfer rate which results in high microscopic displacement efficiency can counteract the adverse effect of pore structure heterogeneity to yield favorable recovery.

The effects of changes in the level of dispersion are shown in Fig. 2.24. As in the first-contact miscible case, recovery is insensitive to the changes in the level of longitudinal dispersion.

These simulations demonstrate that microscopic heterogeneity due to rock pore structure and phase behavior interact in such a way as to reduce local displacement efficiency in a one-dimensional CO<sub>2</sub> flood.

### 2.1.5 Conclusions

A series of miscible and immiscible displacements of a synthetic oil by CO<sub>2</sub> in a Berea sandstone was conducted to assess the interaction of phase behavior and mixing in porous media. The experiments were simulated using a one-dimensional model with input parameters obtained from independent measurements or calculations. Further, the simulation was used to evaluate the impact of pore structure heterogeneity, mass transfer rate, and longitudinal dispersion when phase behavior is important.

(CO<sub>2</sub>-87-279)

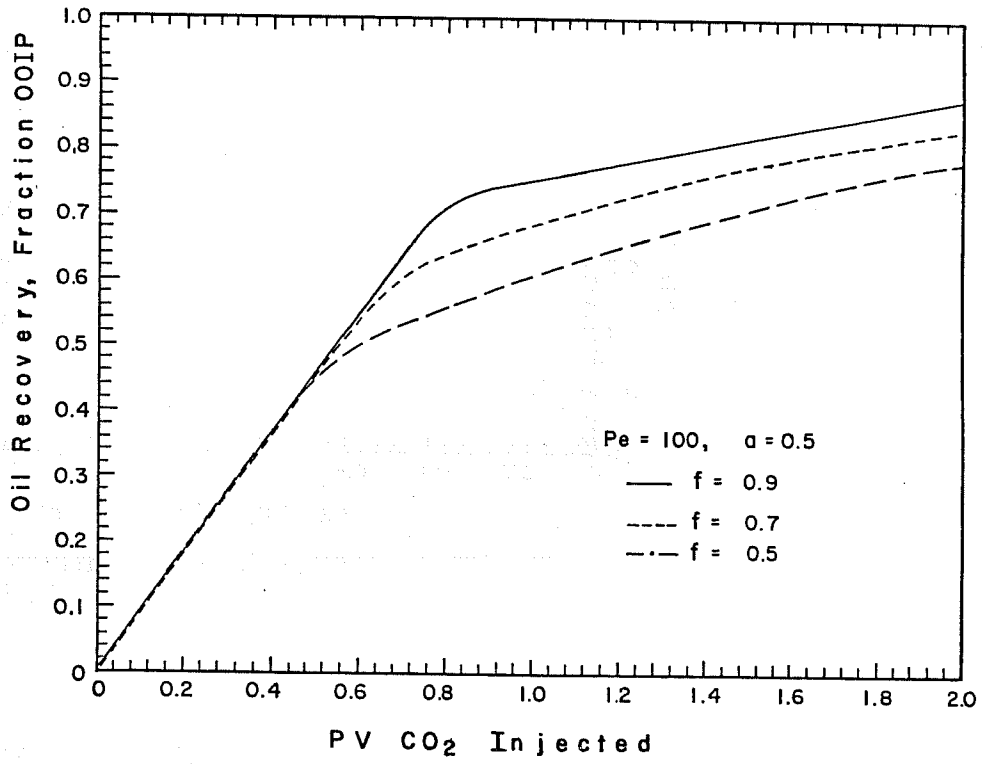


Figure 2.19. Effects of changes in flowing fraction on oil recovery during immiscible displacements - 1200 psia, 93°F.

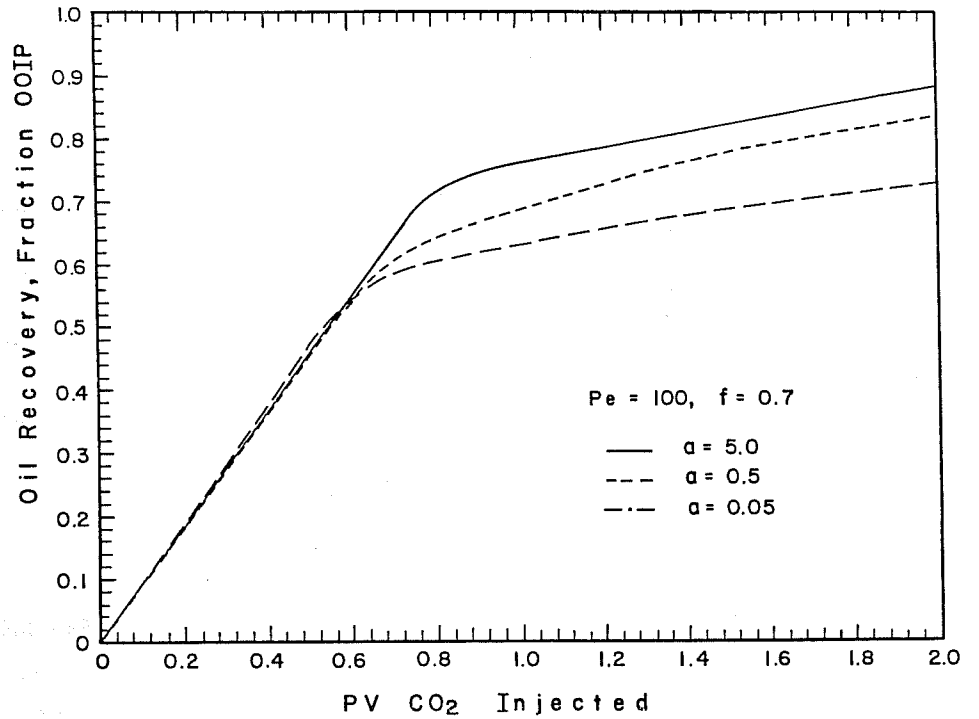


Figure 2.20. Effects of changes in mass transfer rate on oil recovery during immiscible displacements - 1200 psia, 93°F.

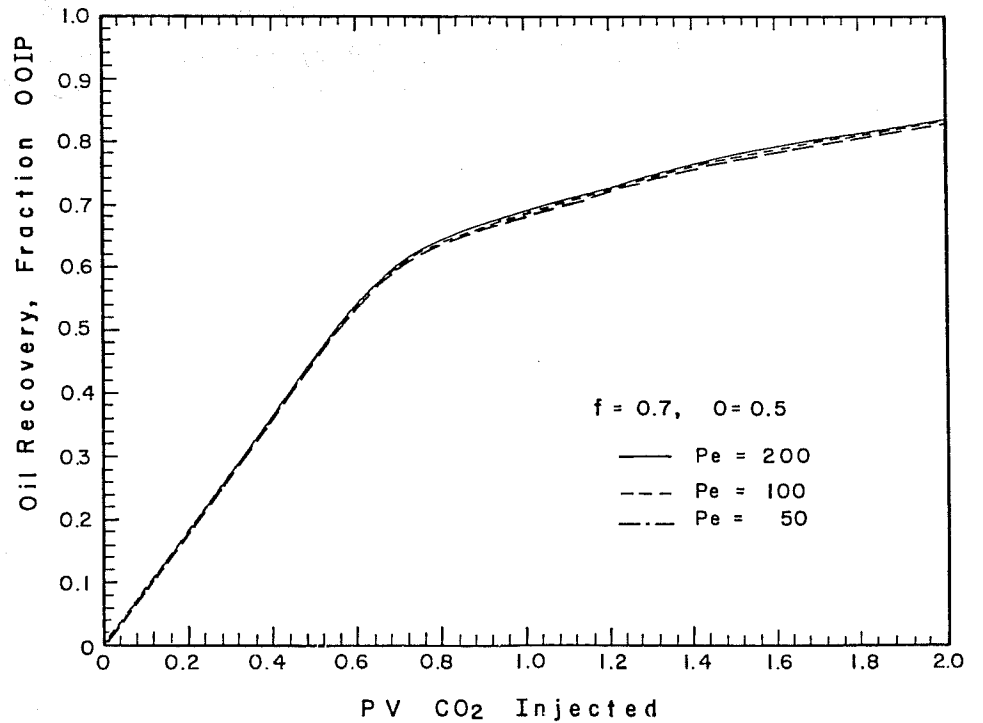
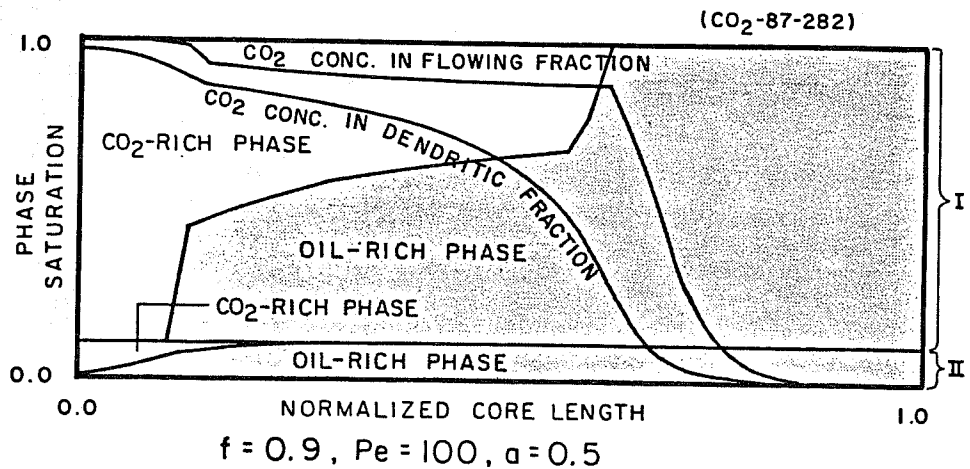
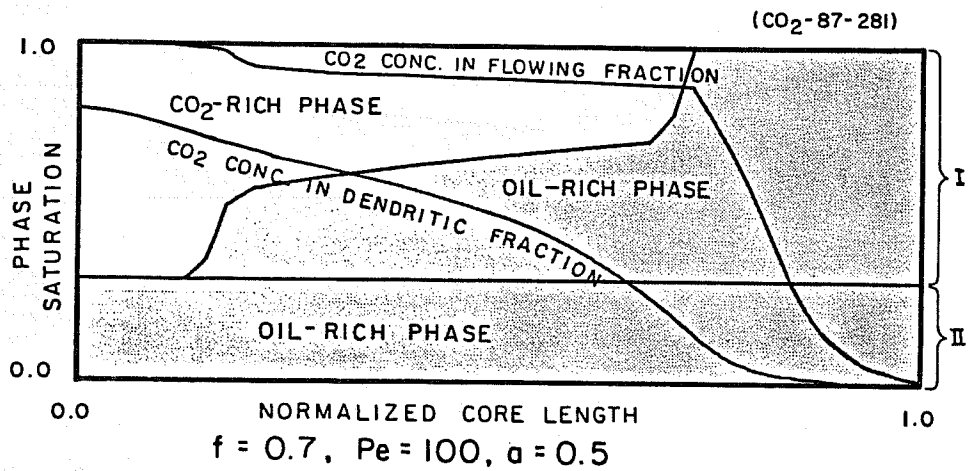
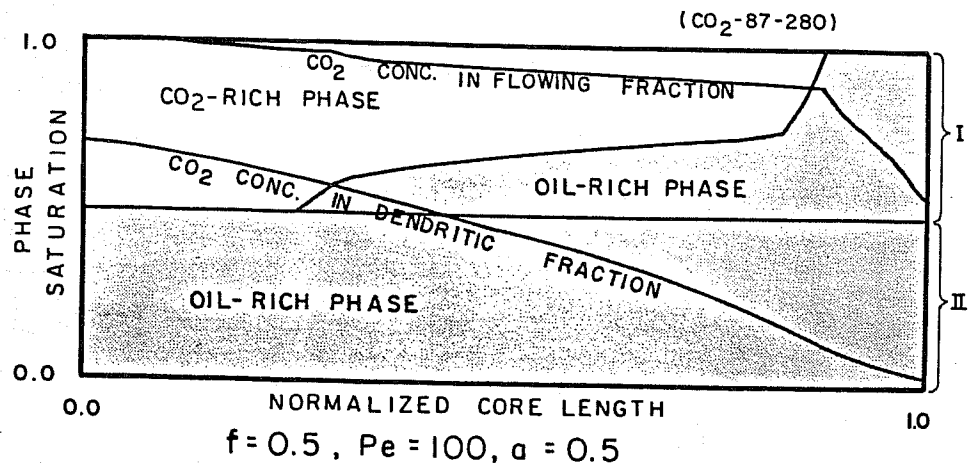


Figure 2.21. Effects of changes in longitudinal dispersion on oil recovery during immiscible displacements - 1200 psia, 93°F.



I = flowing fraction  
 II = dendritic fraction

Figure 2.22. Effects of flowing fraction on saturation distribution for displacements at the  $L_1$ - $L_2$  separation pressure at 0.5 PV injected.

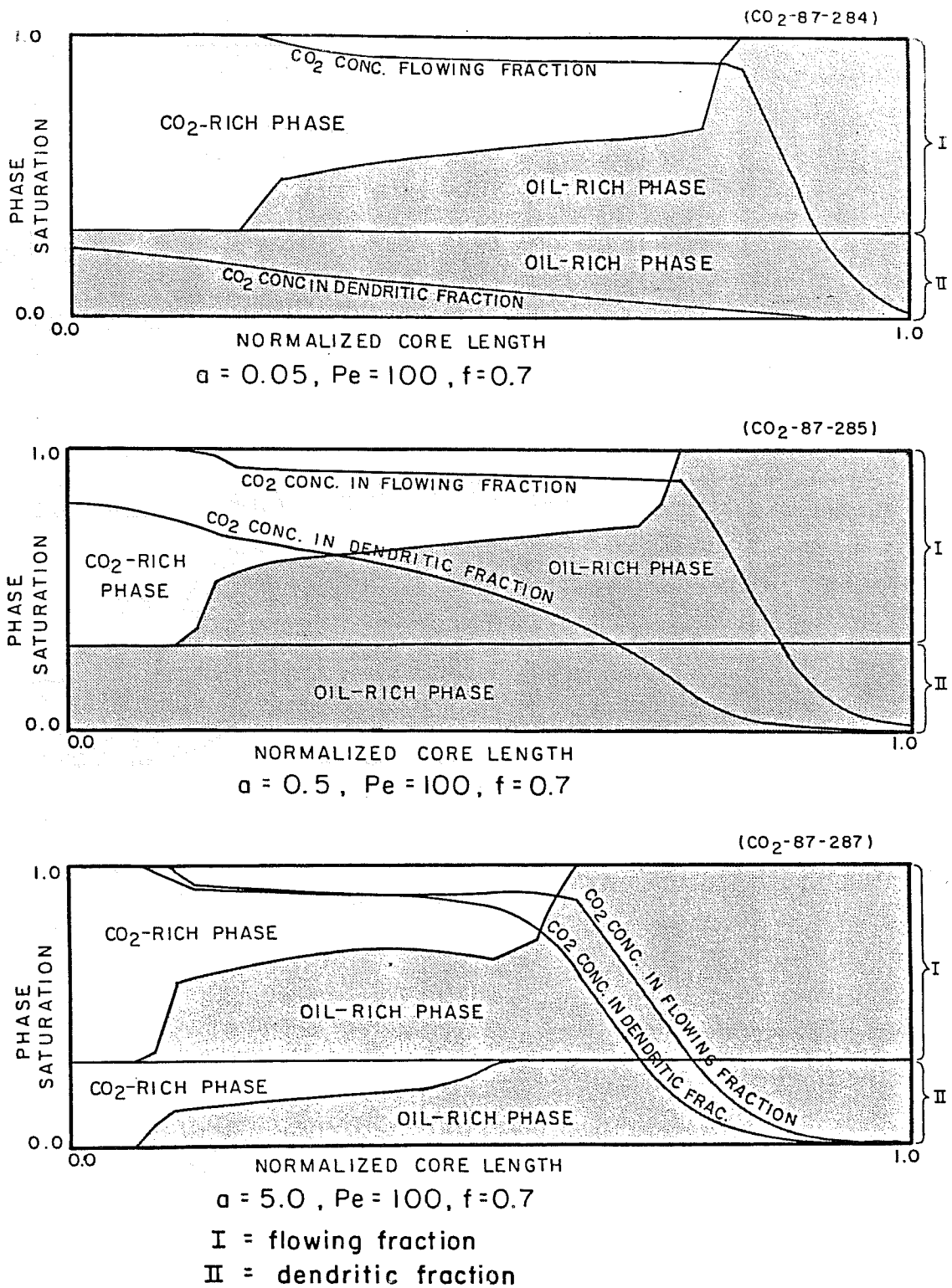
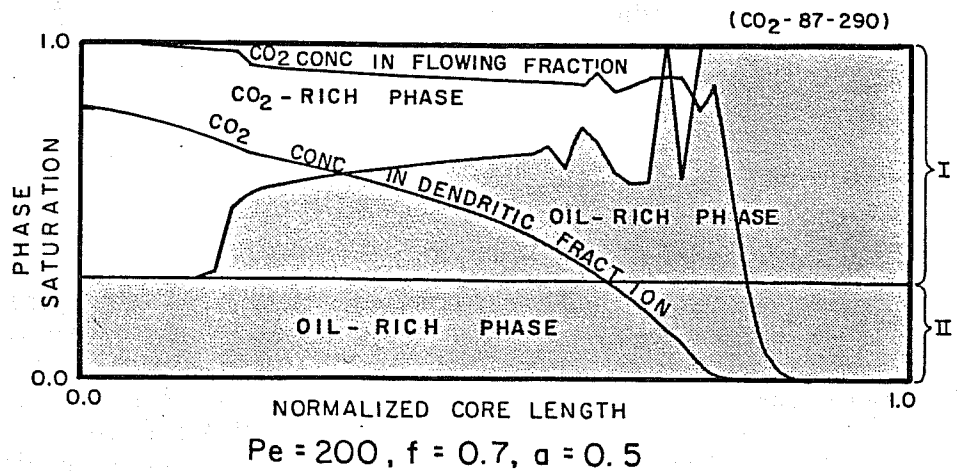
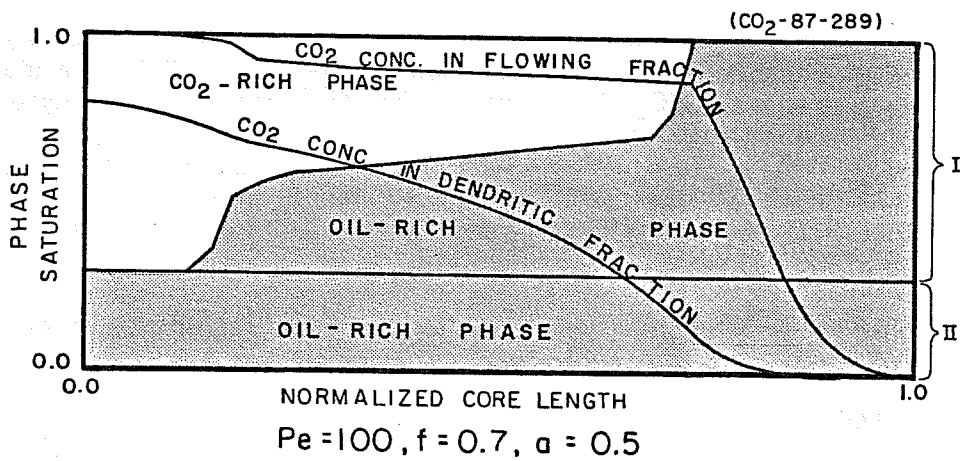
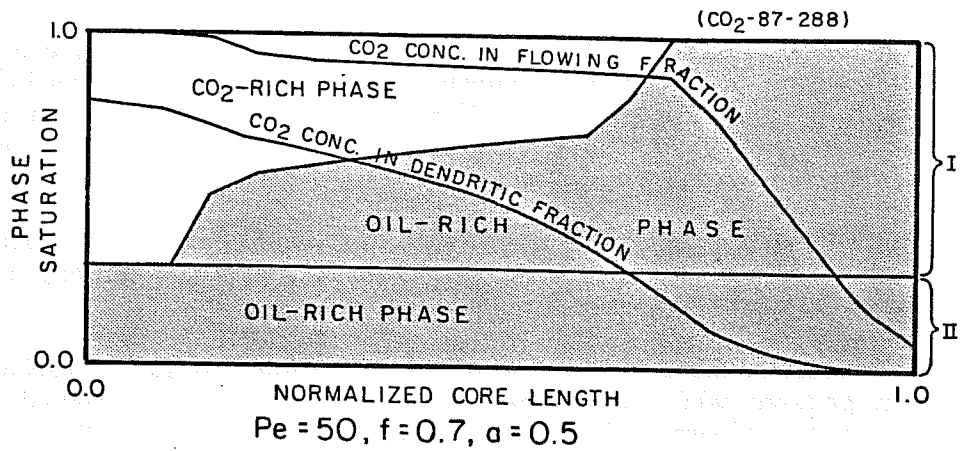


Figure 2.23. Effects of mass transfer rate on saturation distribution for displacements at the  $L_1$ - $L_2$  separation pressure at 0.5 PV injected.



I = flowing fraction  
 II = dendritic fraction

Figure 2.24. Effects of longitudinal dispersion on saturation distribution for displacements at the L<sub>1</sub>-L<sub>2</sub> separation pressure at 0.5 PV injected.

The following is an itemization of the salient points of this work:

- 1) There is experimental evidence which indicates the possibility of conducting immiscible displacements with recoveries characteristic of multiple-contact miscible displacements at pressures which correspond to the formation of a liquid-liquid type of phase behavior. This phenomenon can possibly be correlated with the very low interfacial tension between the CO<sub>2</sub>-rich and oil-rich liquid phases.
- 2) Experimental and simulation results show that the CO<sub>2</sub>-rich liquid phase can effectively displace and recover residual oil even under high water saturations such as encountered during CO<sub>2</sub> displacement of a waterflooded porous media.
- 3) An increase in the CO<sub>2</sub> injection pressure was observed during displacements conducted at a pressure where three-phase separation occurs: this supports the conjectured improvement of sweep efficiency in a multiphase flow setting.
- 4) The presence of substantial microscopic pore structure heterogeneity, correlated by a flowing fraction of less than one in the Coats-Smith model has a more adverse impact during immiscible CO<sub>2</sub> floods even if that displacement is conducted at the two-liquid phase separation pressure.
- 5) The effect in the changes of mass transfer rate is more severe during miscible displacements compared to near-miscible ones as indicated by a larger relative drop in recovery at 1.2 PVI.
- 6) Variations in longitudinal dispersion is practically insignificant in one-dimensional CO<sub>2</sub> floods.

### 2.1.6 Future Work

We are currently investigating the pursuit of two research fronts as a result of this study, namely, the successful immiscible-displacement theory and the multiphase-flow-effect-on-sweep-efficiency theory.

## 2.2 Flow Visualization Experiments

### 2.2.1 Introduction

The micromodel was used to study the effects of microscopic heterogeneity on foam flow. The apparatus allows unique visualization of foam flow in porous media in near-reservoir conditions. Efforts have been concentrated on the visualization of foam generated in-situ by simultaneously injecting an aqueous surfactant solution and dense CO<sub>2</sub> into a two-dimensional pore network etched in glass. First we attempted to isolate a set of conditions that allowed in-situ foaming in the presence of an oil phase. Next, the oil phase was removed, and foam generation conditions were studied, varying flow rates, and pore structures. A third set of experiments studied the effect of varying the heterogeneity of the pore structure on the mixing of the surfactant solution and CO<sub>2</sub>. The fourth set of experiments targeted the surfactant activity. The fifth set, using a higher surfactant concentration, produced stable foam. Modifications to the apparatus have dramatically improved the results obtained from a given displacement, and have reduced the time needed to perform displacements and the possibility of equipment failure.

The apparatus used in these experiments is shown in Fig. 2.25. This apparatus permits the videotaping of high-pressure displacements at the pore level. Mirror images of the pore networks are etched in glass, then fused together in a kiln. Inlet and outlet holes are drilled to allow flow in and out of the pore network. These pore networks are called micromodels. The apparatus includes an overburden chamber to maintain a low-pressure drop from the inside to the outside of the glass plates of the micromodel. Note that the gravity effect is minimized as the pore network lies horizontally (i.e., little or no flow is vertical).

In reporting these experiments, some terminology must be explained. Stable foam refers to clusters of CO<sub>2</sub> bubbles (discontinuous phase) when the average bubble diameter is less than the pore width and exists in the porous media for a significant length of time. Stable lamellae is the name given to the discontinuous phase when the bubbles are stable, but the average bubble diameter exceeds the pore diameter. These appear as films, oriented normal to the pore walls, that travel through the porous media without bursting. Unstable lamellae are exactly similar in appearance and performance to stable lamellae, but burst after a short period of time.

### 2.2.2 Generating In-situ Foam in the Presence of Oil

The first set of experiments consisted of four displacements. A heterogeneous micromodel, the MM-II (shown in Figure 2.26) was used. This model displays a preferential flow path running roughly through the middle and adjacent smaller pores surrounding a few larger vugs. The pore-size distribution of this porous media was described elsewhere (Bahralolom & Bretz, 1985). One aim of this study was to show how CO<sub>2</sub>-foam can be used to plug high permeability streaks. At 90°F and 1320 psia, CO<sub>2</sub> density and viscosity were 0.74 g/cc, and 0.064 cp. The oil viscosity and density were 2.8 cp and 0.83 g/cc (Orr, Yu, & Lien, 1981). In these experiments Maljamar separator oil at connate water was displaced by CO<sub>2</sub> and surfactant solution. The conditions of these displacements are reported in Table 2.6.

Displacement 1-1 was an attempt at generating foam in-situ using a surfactant solution preflush, followed by pure CO<sub>2</sub>. Presently this is the sequence of events used to generate foam in field-scale floods. The concentration of surfactant was kept low, at 0.038% (all surfactant concentrations presented are weight percent). This displacement did not prove effective under the given conditions, and no foam was generated.

Displacement 1-2 was an attempt to increase the mixing between the surfactant solution and the CO<sub>2</sub> by using a simultaneous injection method. A 4:1 flowing volumetric ratio of CO<sub>2</sub> to surfactant solution was used to displace the oil at connate water. The pressure was increased to make the CO<sub>2</sub> more dense, because previous studies showed foam stability to favor higher pressures and lower temperatures. Some unstable lamellae were observed to flow, but no stable foam was seen.

Displacement 1-3 combined a preflush and simultaneous flow in an attempt to maximize the mixing between the two foamable phases (CO<sub>2</sub> and surfactant solution). This resulted in more flowing unstable lamellae, but again no stable foam. This displacement did show fluid diversion on the pore level due to multiple interfaces. This effect was seen near the outlet of the micromodel, as oil, surfactant solution, and CO<sub>2</sub> interfaces blocked the preferential flow path, forcing the displacing fluids into adjacent pores.

Displacement 1-4 graphically demonstrated fluid diversion and showed some evidence of stable foam blockage. For this experiment, the surfactant concentration was increased to 0.38%, the temperature was decreased to 90°F, and fluids were injected simultaneously. The slug flow that

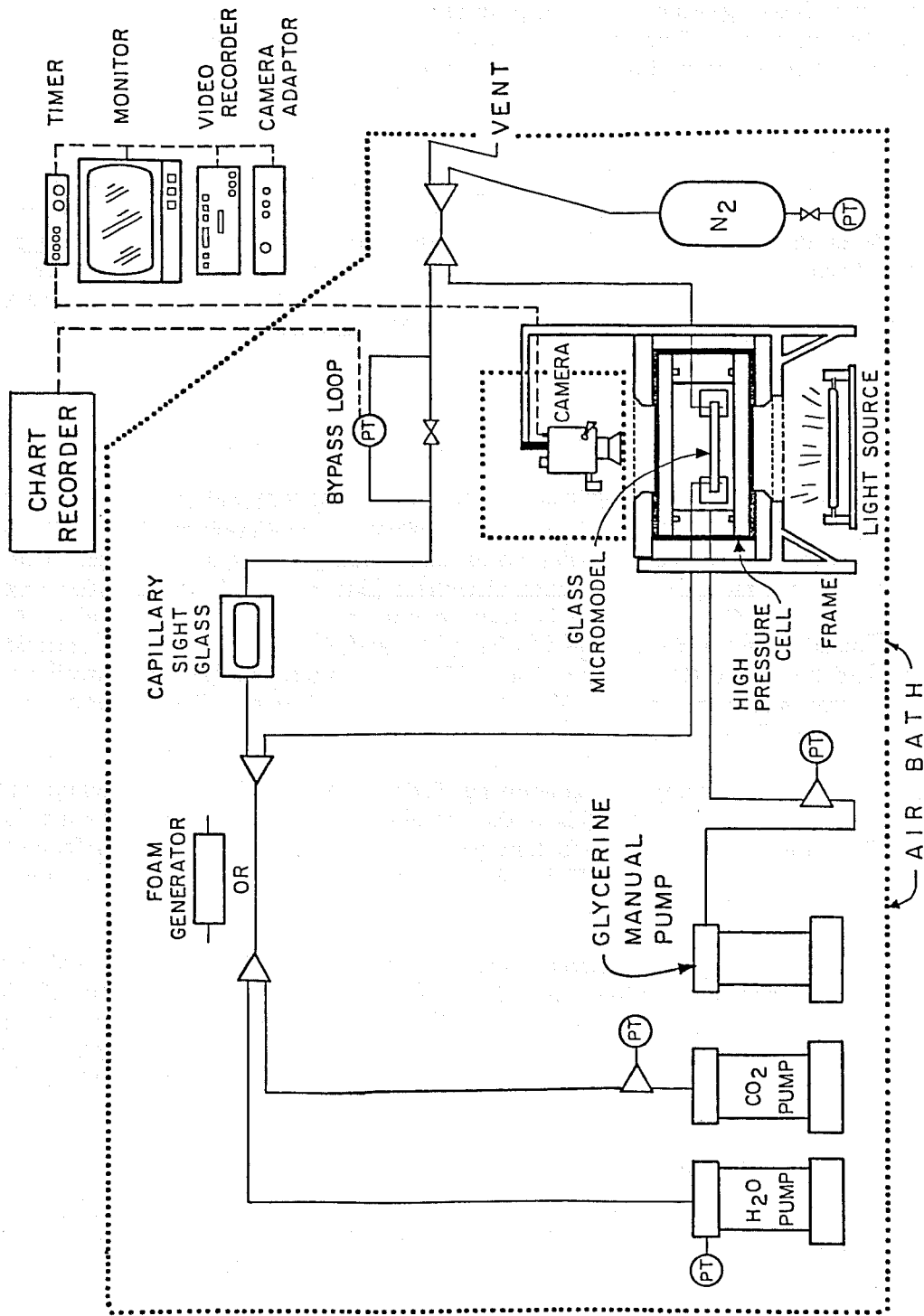


Figure 2.25. Micromodel apparatus.

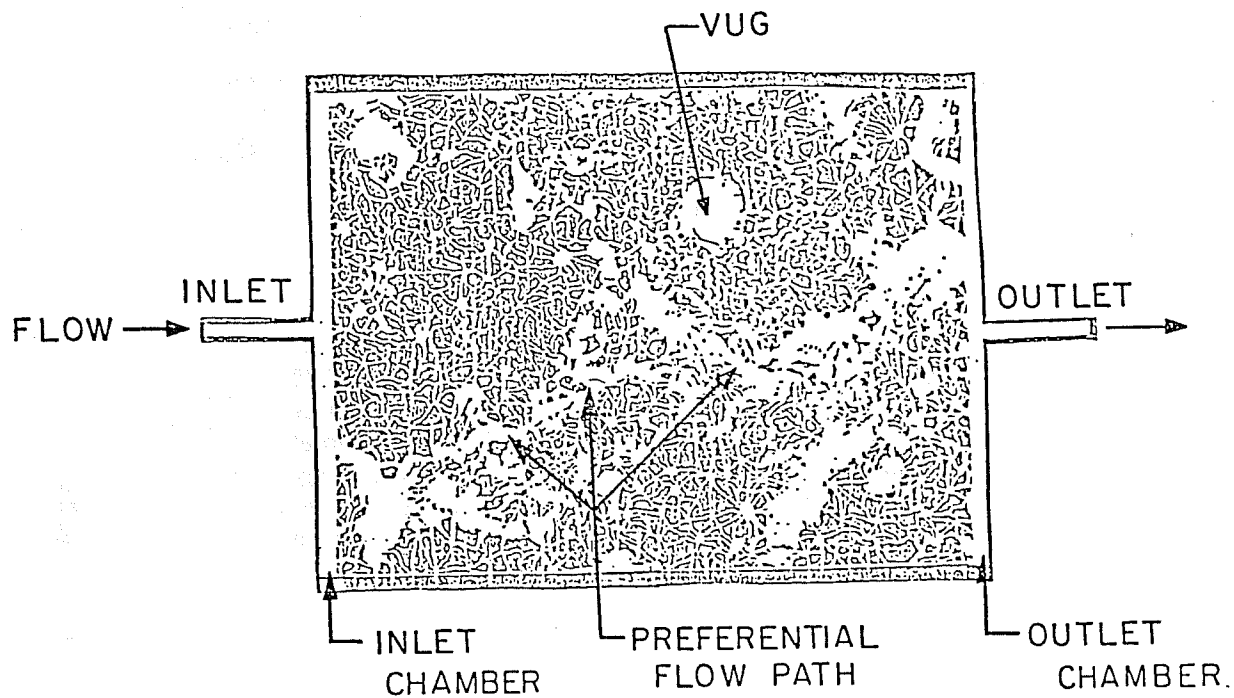


Figure 2.26. Heterogeneous pore network MM-II.

Table 2.6

## Displacements in the Presence of Oil

<u>Run</u>	<u>Surf. Conc. (wt. %)</u>	<u>S.S. Pre-flush PV</u>	<u>Displacing Fluids</u>	<u>Volume CO<sub>2</sub>/S.S. Ratio</u>	<u>Temp. °F</u>	<u>Pressure psia</u>
1-1	0.038	2.0	CO <sub>2</sub>	-	105	1000
1-2	0.038	-	CO <sub>2</sub> /SS	4/1	105	1320
1-3	0.038	2.0	CO <sub>2</sub> /SS	4/1	105	1320
1-4	0.38	-	CO <sub>2</sub> /SS	4/1	90	1320

micromodel  
surfactant  
oil  
water dye  
flow rate  
initial saturation  
S.S.

MM-II  
Alipal CD-128  
Maljamar separator  
0.05% methyl violet  
35.8 ft./day  
oil at connate water  
surfactant solution

developed in the inlet lines flowed into the micromodel. The pore volume of this micromodel is about 0.2 cc, and the mean pore size is about 1 to 2 mm<sup>2</sup>. The slugs that developed were on the order of 10 microliters. When a CO<sub>2</sub> slug followed a surfactant solution slug, some foam was generated at sites located from the middle to the production end of the model. Flow was blocked in the preferential flow path soon after, and displacing fluids were forced into the adjacent pores. More than 95% of the oil was quickly recovered. This was considered to be a successful foam displacement, since CO<sub>2</sub> sweep efficiency was increased by the blocking of the preferential flow path, and more oil was recovered. The fluid diversion that took place in this displacement is documented in Figs. 2.27-2.31 where the CO<sub>2</sub> flow paths are seen to change during the displacement.

A possible successive layer mechanism for foam flow was identified. First, oil was recovered from the preferential flow path. Next, this path was blocked by the CO<sub>2</sub> and surfactant solution. These displacing fluids then moved into a neighboring layer of the matrix. In this neighboring layer, the CO<sub>2</sub> and surfactant solution first displaced the oil, then blocked this layer. This continued until about 95% of the OOIP (original oil in place) was recovered. Some future studies directly target this phenomena. More information on this set of experiments is available in PRRC Report 87-6 (Quarterly Report for the period October 1, 1986 - January 31, 1987).

Based on the positive results of the last displacement, attempts were made to study in more detail the fluid diversion and increased CO<sub>2</sub> sweep efficiency process.

### 2.2.3 Generating In-situ Foam in the Absence of Oil

In our attempt to enhance the foam generated in the experiment, the micromodel MM-II was adapted to provide more foam generation sites near the inlet of the model. The resulting model is denoted MM-II<sub>f</sub>, as shown in Fig. 2.32. The cross-sectional area of the pores at the inlet of the preferential flow path was reduced. This forced the foaming agents to enter the preferential flow path through tighter pores. It was seen in earlier micromodel experiments and other studies that a site where a pore throat opens into a larger pore space is where the snap-off mechanism of foam generation can occur. This micromodel provided the opportunity to generate foam near the inlet of the model, instead of towards the outlet. By generating a foam near the entry, we have more porous media available in which to observe foam behavior.

Displacements 2-1, 2-2, and 2-3 were done in this micromodel and are listed in Table 2.7. The oil phase was eliminated to isolate the foaming agents and to see what effect the oil phase had on foam behavior.

Displacement 2-1 was done to compare to later displacements of surfactant solution. The result was a graphic demonstration of capillary forces and Haines jumps.

Displacement 2-2 demonstrated stable foam, and some diversion of CO<sub>2</sub> was seen. The entire model was initially saturated with surfactant solution. Foam was generated in the preferential flow path, and this path was blocked. The diverted CO<sub>2</sub> mixed with the surfactant solution in the new flow path, generated foam, and blocked the new flow path. As a result, the flow channeled back through the preferential flow path. With an oil phase present under the same conditions, the alternate paths were not blocked so quickly. This indicates that the presence of an oil phase inhibits foam stability, which is well known.

Displacement 2-3 was characterized by continuous foam generation. A flow path developed; then it was blocked. The following foam would flow through another path for a short time until it was blocked. This process continued over the life of the displacement.

## Heterogeneous Micromodel

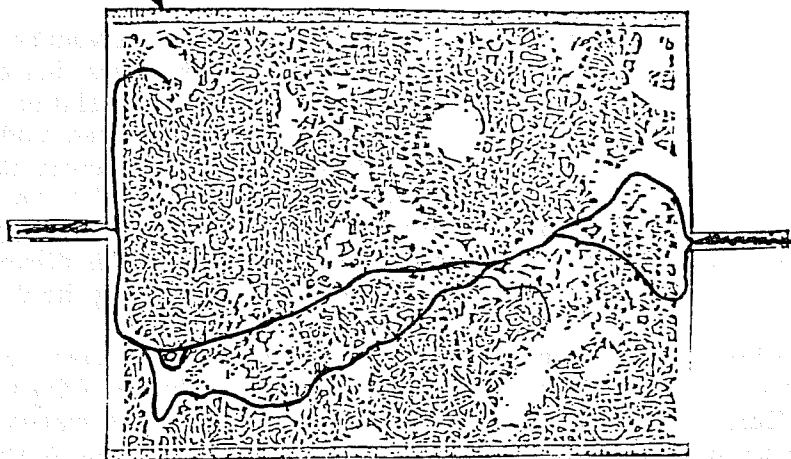


Figure 2.27. Micromodel experiment with CO<sub>2</sub>-foam displacing Maljamar crude (T = 90°F, P = 1320 psia, surfactant concentration 0.38 wt. %). Dark lines indicate initial CO<sub>2</sub> flow paths through high permeability streaks.

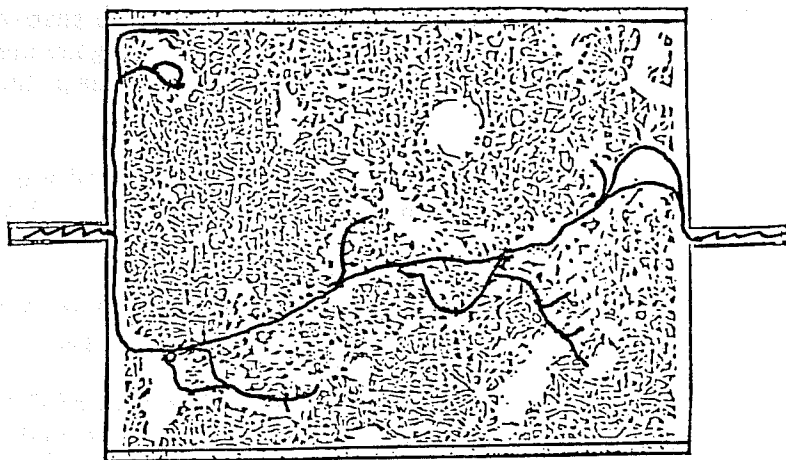


Figure 2.28. Micromodel experiment with CO<sub>2</sub>-foam displacing Maljamar crude. Same conditions as Fig. 2.27. Initial surfactant solution flow paths following the CO<sub>2</sub> slug indicated.

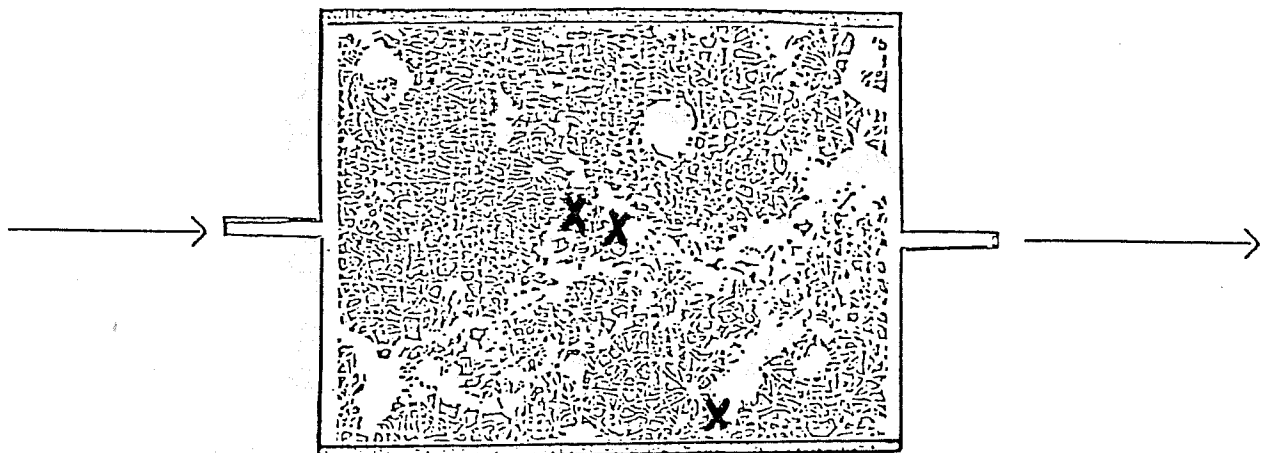


Figure 2.29. Micromodel experiment with CO<sub>2</sub>-foam displacing Maljamar crude. Same conditions as Fig. 2.27. Foam generation sites indicated by the Xs.

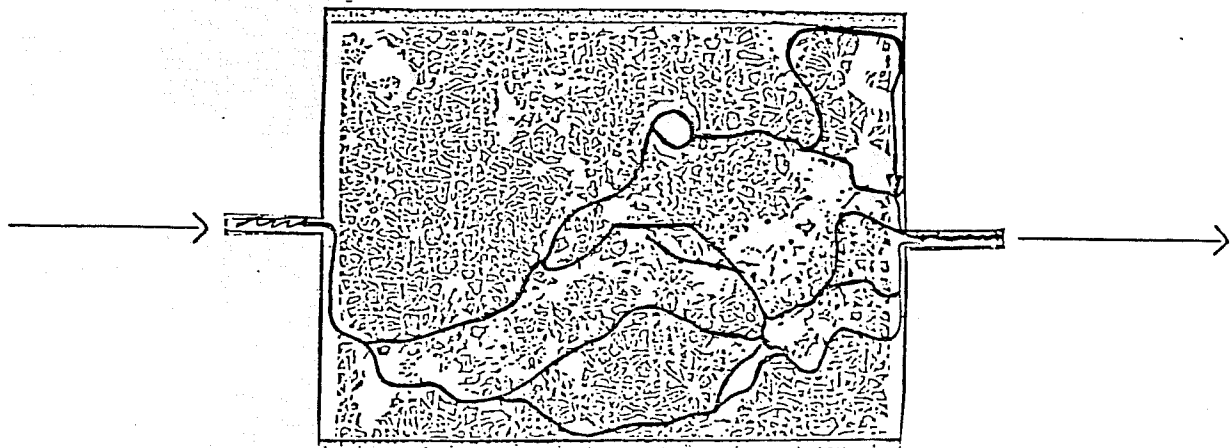


Figure 2.30. Micromodel experiment with CO<sub>2</sub>-foam displacing Maljamar crude. Same conditions as Fig. 2.27. Secondary CO<sub>2</sub> flow paths indicated.

General penetration  
of matrix

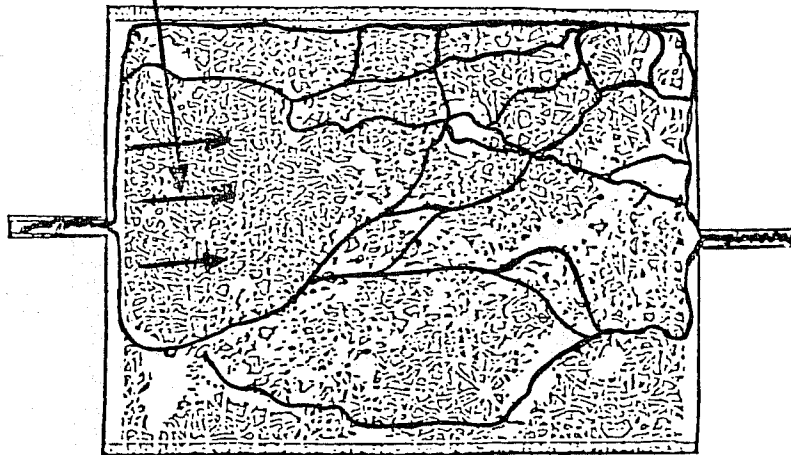


Figure 2.31. Micromodel experiment with CO<sub>2</sub>-foam displacing Maljamar crude. Same conditions as Fig. 2.27. Final CO<sub>2</sub> flow paths. There is general penetration of the matrix, with oil recovery estimated at 95% OOIP.

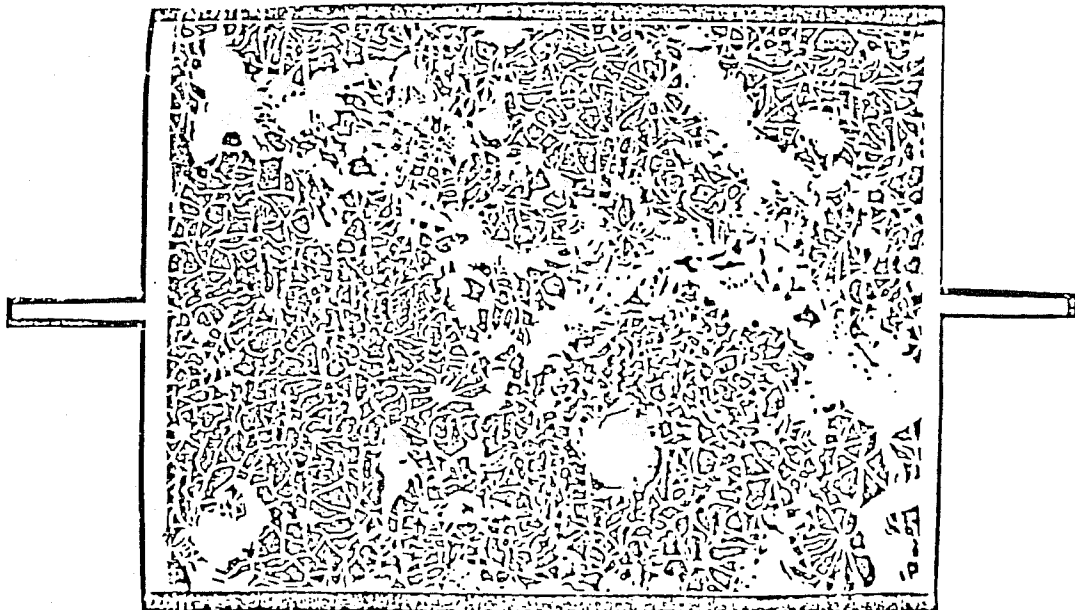


Figure 2.32. Heterogeneous pore network MM-II-f. Note the changes in pore structure near the inlet.

Table 2.7

Displacements in the Absence of Oil

<u>Run</u>	<u>Initial Saturation</u>	<u>Displacing Fluids</u>
2-1	100% water	CO <sub>2</sub>
2-2	100% S.S.	CO <sub>2</sub>
2-3	100% CO <sub>2</sub>	4/1 CO <sub>2</sub> /S.S.

micromodel	MM-IIIf
surfactant	Alipal CD-128
surfactant concentration	0.38 weight percent
water dye	0.05% methyl violet
flow rate	35.8 ft./day
pressure	1320 psia
temperature	90°F
S.S.	surfactant solution

These experiments showed that the reduction of pore width near the inlet of the model did produce a better pore network to study foam behavior. Foam was generated where the tighter pores opened to the preferential flow path, and foam flow behavior was studied over a greater portion of the model. This foam was more stable than foam in the presence of oil. We have also shown that our system, in the absence of an oil phase, can produce a stable foam in-situ. With this knowledge, the following experiments were undertaken to consider how heterogeneities would affect the mixing of CO<sub>2</sub> and surfactant solution during oil displacement.

#### 2.2.4 Effect of Microscopic Heterogeneity on Displacements

The third set of displacements was aimed at comparing the effect of heterogeneity and flow rate on foam flow. In these experiments, Maljamar separator oil at connate water was displaced by CO<sub>2</sub> and surfactant solution. The purpose of these experiments was to duplicate the conditions of the successful Displacement 1-4 in micromodels having different scales of heterogeneity. A strip chart recorder was added to the apparatus to monitor the pressure drop across the micromodel. The conditions for these displacements are shown in Table 2.8. These experiments used two new pore networks. MM-H, a homogeneous pore network, is shown in Fig. 2.33. MM-I is heterogeneous, but to a lesser degree than MM-II, and is shown in Fig. 2.34.

Displacement 3-1 demonstrated good sweep efficiency, but in the absence of stable foam. In this displacement the waterflood left an oil saturation distributed randomly throughout the model. There did not appear to be a distinct higher or lower oil saturation in any part of the model, though the residual oil saturation was found in local connected ganglia. Waterflood recovery was about 50%.

Under simultaneous injection, CO<sub>2</sub> first entered the model and established a few flow paths, contacting and displacing both water and oil. At this point, the CO<sub>2</sub> recovery mechanisms of swelling and extraction were in effect where the dense CO<sub>2</sub> and oil phases were adjacent. CO<sub>2</sub> continued to flow along these paths until a surfactant solution slug entered the model.

The surfactant solution established two paths through the porous media, one across the middle, and one in the lower portion (see Fig. 2.35). Unfortunately, CO<sub>2</sub> following these slugs flowed preferentially through the surfactant solution, not generating substantial foam, and severely limiting contact with the crude oil. CO<sub>2</sub> flowed through the surfactant solution from the inlet to outlet, forming very few unstable lamellae, and no foam.

The residual oil was seen to darken, as the CO<sub>2</sub> stripped away the lighter hydrocarbons. A large water saturation and a reduction in CO<sub>2</sub>-oil contact slowed this process. A relatively large residual oil saturation of 20 to 25% was left after 4.0 PV of CO<sub>2</sub> was injected.

In Displacement 3-2, a CO<sub>2</sub> slug was the first to enter the micromodel. During the initial CO<sub>2</sub> injection, the oil phase was seen to lighten as CO<sub>2</sub> dissolved in the oil. The displacement appeared stable, with a relatively even flood front when compared to a similar displacement (at 1200 psia and 75°F, Bahralolom & Bretz, 1985) done at a higher flow rate. When the oil was saturated with CO<sub>2</sub>, a distinct CO<sub>2</sub>-oil phase interface developed. The CO<sub>2</sub> then chose several paths through the oil phase, concentrated towards the center of the model. This left residual oil in the upper and lower parts of the model, and concentrated toward the outlet of the model (see Fig. 2.36).

After 0.86 PV of CO<sub>2</sub> was injected, a surfactant slug flowed preferentially through the center of the model, branching somewhat near the outlet of the model. The CO<sub>2</sub> that followed

Table 2.8

## Displacements in Different Micromodels

<u>Run</u>	<u>Initial Saturations</u>	<u>Flow Rate (ft./day)</u>	<u>Micromodel</u>
3-1	S <sub>or</sub> (waterflooded)	13.6	MM-H (shown in Fig. 2.33)
3-2	oil at connate water	27.2	MM-H
3-3	oil at connate water	10.6	MM-I (shown in Fig. 2.34)
3-4	oil at connate water	21.2	MM-I
*3-5	oil at connate water	21.2	MM-I
*3-6	oil at connate water	35.8	MM-II (shown in Fig. 2.26)
†3-7	oil at connate water	35.8	MM-II

\* without methyl violet dye in surfactant solution

† without surfactant or dye

surfactant	Alipal CD-128
surfactant concentration	0.38 weight percent
water dye	0.05% methyl violet
oil	Maljamar separator
pressure	1320 psia
temperature	90°F
volumetric injection ratio	4/1
displacing fluids	CO <sub>2</sub> /S.S.
S.S.	surfactant solution

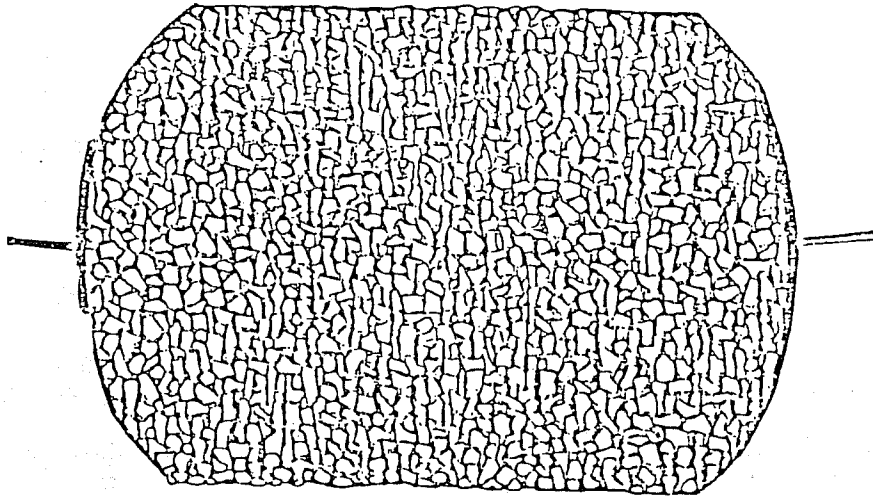


Figure 2.33. Homogeneous pore network MM-H.

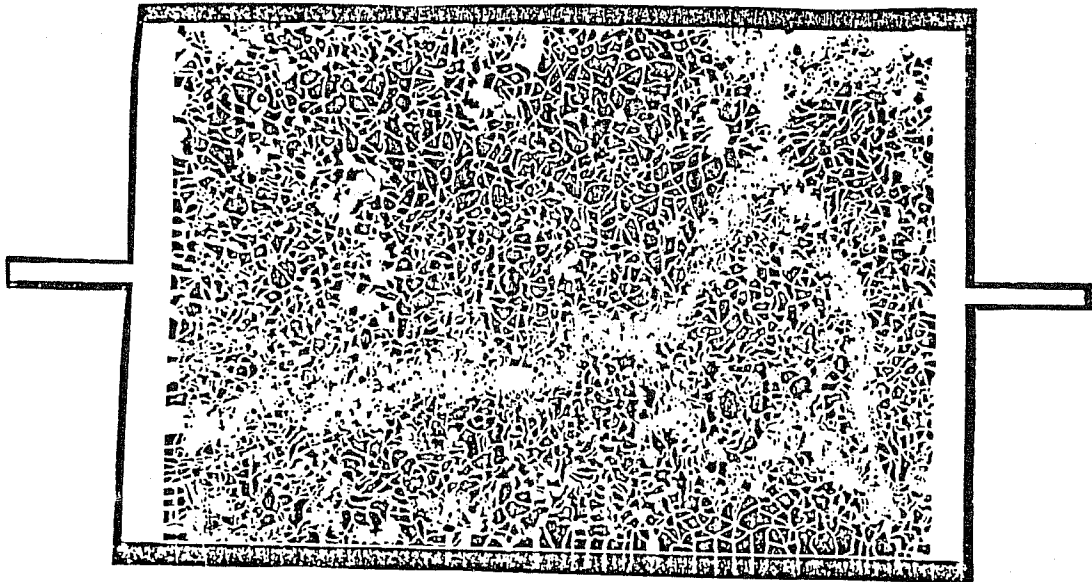


Figure 2.34. Heterogeneous pore network MM-I.

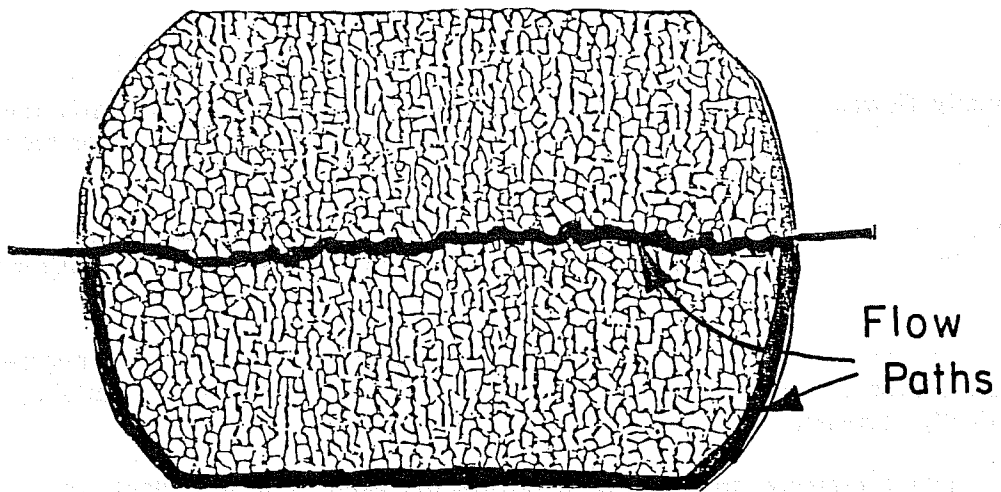


Figure 2.35. Flow paths of surfactant solution through middle and lower portions of MM-H.

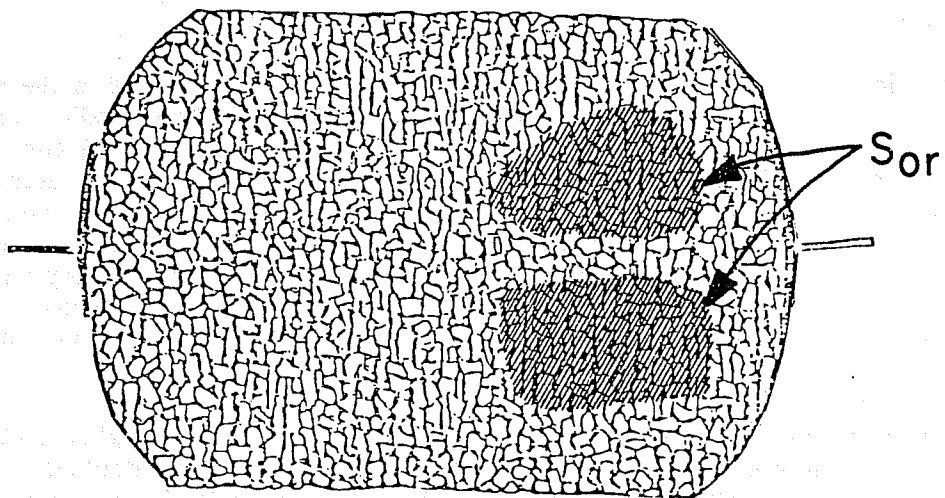


Figure 2.36. Residual oil in the upper and lower portions of MM-H concentrated toward the outlet.

preferentially flowed through the surfactant solution, which conducted it nearly the length of the model. Upon exit from the surfactant solution, no significant stable foam was seen, though some flowing lamellae were produced.

Successive slugs of CO<sub>2</sub> and surfactant solution produced some branching of surfactant solution paths, but little incremental oil recovery. Recovery after 3.0 PV was estimated at 80% to 85%.

Some observations were correlated with the pressure drop (across the micromodel) history. The pressure drop increased by up to 100% when CO<sub>2</sub> followed a surfactant slug. The pressure drop gradually decreased with continued pure CO<sub>2</sub> injection to a minimum.

The highest pressure drop was seen during the flow of a surfactant slug, when two CO<sub>2</sub> bubbles became trapped in the flow path. The surfactant solution flowed around the trapped bubbles at approximately three times the normal pressure drop.

This displacement showed that pressure drop history can be correlated directly to observations to make important conclusions about local fluid flow phenomena with this experimental system.

In Displacement 3-3 excellent recovery was seen, as the presence of multiple interfaces in the preferential flow path forced CO<sub>2</sub> and surfactant solution into the tighter pores in the media. Small amounts of foam bubbles were seen. Ultimate recovery was 85% to 90%. Higher recovery was limited by a water saturation (mostly surfactant solution) that protected some oil ganglia from the CO<sub>2</sub>. Extended exposure to the CO<sub>2</sub> may have recovered more of this oil by diffusion and swelling. This displacement showed that multiple interfaces can produce good sweep efficiency.

In Displacement 3-4, a CO<sub>2</sub> slug was the first to enter the model, and a transition zone developed. Compared to the displacement at the slower flow rate, larger slugs of CO<sub>2</sub> and surfactant solution were seen.

Again, high recovery was seen, as the presence of multiple interfaces in the preferential flow path forced CO<sub>2</sub> and surfactant solution into the tighter pores in the media. Small amounts of foam were generated in-situ. Ultimate recovery was 90 to 95%, with recovery continuing until after 4 PV was injected. The recovery at the higher displacement rate was actually slower, but ultimately more efficient, as CO<sub>2</sub> and surfactant solution developed more flow paths. This delivered CO<sub>2</sub> to most of the oil ganglia, allowing recovery by extraction, diffusion, and swelling during the life of the experiment. The earlier delivery of the surfactant solution to many parts of the model initially inhibited CO<sub>2</sub>-oil contact, but added surfactant solution to the system that provided the means for later fluid diversion. This process explains why the recovery was slower, but more extensive.

The chart record of the pressure drop across the model showed higher pressure drop when CO<sub>2</sub> immediately followed a surfactant solution slug. The pressure drop doubled during this part of the displacement because CO<sub>2</sub> was trying to displace through multiple interfaces (CO<sub>2</sub> displacing surfactant solution, oil, or lamellae) and was usually routed into a reduced cross-sectional area of flow. These same mechanisms allowed fluids to be diverted into alternate paths. The pressure was reduced toward the end of a CO<sub>2</sub> slug, by which time a good portion of the surfactant solution had been displaced.

The conditions of Displacement 3-4 were duplicated in Displacement 3-5, with the exception of the removal of the methyl violet dye from the surfactant solution. The results developed in a similar way with a few exceptions. In this displacement, no foam was generated. The tendency of

the CO<sub>2</sub> to flow through the surfactant solution was enhanced. This effectively sealed oil from the CO<sub>2</sub>, and reduced the ultimate recovery. After some initial fluid diversion, nearly all flow was channeled into the preferential flow path. This indicated that the dye in the surfactant solution was affecting the displacement to some degree.

One important feature of Displacements 3-1 through 3-5 is that the CO<sub>2</sub> flowed preferentially through the surfactant solution, avoiding the surfactant solution/oil interface. The effect was more pronounced in Displacement 3-5, where the dye was omitted from the surfactant solution. This phenomenon will be analyzed later, when comparisons to systems without surfactants can be made.

Displacement 3-6 was an attempt to duplicate Displacement 1-4 exactly but without the methyl violet dye. The results were the same; however, it became evident that the foam we saw was neither very stable, nor the only source of fluid diversion. This observation will spark later investigations into the optimum concentration of the surfactant.

The important result of these displacements is that substantial amounts of stable foam were absent. There are a variety of factors included in these displacements that may cause this behavior.

Studies have shown that the aspect ratio of a pore system directly affects the snap-off mechanism of foam generation. The best site for foam generation is where a smaller pore throat opens into a larger porespace. When CO<sub>2</sub> exits the pore throat, the surfactant solution closes in behind. The CO<sub>2</sub> in the pore space then snaps-off from the CO<sub>2</sub> in the pore throat and becomes a bubble.

Also, the presence of a hydrocarbon phase can inhibit foam generation or stability. In these displacements, heavy hydrocarbons resulting from the CO<sub>2</sub> stripping were found in the preferential flow path where foam generation must take place. Displacements 2-2 and 2-3 showed that under these conditions, but in the absence of oil, stable foams were generated. These heavy hydrocarbons in the preferential flow path probably inhibited foam generation to some degree.

Large water saturations, such as were encountered in the tertiary Displacement 3-1, may have served to dilute the surfactant solution to a point where it was unable to produce foam. However, at a 0.38% concentration, we were well above the critical micelle concentration (CMC) of Alipal CD-128 which is around 0.12%. This would allow a 3:1 dilution of surfactant solution without seriously impairing the ability of the surfactant solution to generate foam. Also, most flow of surfactant solution took place in the preferential flow paths. This served to increase continually the surfactant concentration in this area and reduce the dilution effect.

Flow rate has been seen to have an effect on foam generation. However, in this set of displacements, the flow rate was varied considerably from run to run. Also, at the end of some runs, the flow rate was increased to even higher values, which did not produce a better foam.

In order to evaluate further the systems studied, it was decided to eliminate the surfactant completely from Displacement 3-7, keeping all of the other conditions the same.

In comparison to Displacements 3-1 through 3-6, the CO<sub>2</sub> showed less tendency to flow through the water in Displacement 3-7. We speculate that this may have been due to the higher CO<sub>2</sub>/water interfacial tension in 3-7. In Displacements 3-1 through 3-6, the presence of surfactant (and the resulting reduction of the CO<sub>2</sub>/water interfacial tension) may have reduced the energy needed for the CO<sub>2</sub> to flow through the water phase.

### 2.2.5 Surfactant Solution Tests

Differences in performance between two systems were similar except that the presence of the methyl violet dye had some effect on the displacement. It was seen when Displacements 3-4 and 3-5 were compared. In the system without the dye, CO<sub>2</sub> flowed more strongly through the surfactant solution. Some tests were run to study the effect of the dye on the surfactant system. Also, in order to measure the CMC, surface tension of this surfactant solution was measured.

The method for foamability testing is identical to that presented by Dr. Lee in PRRC Report 87-6 (Quarterly Report for the period October 1, 1986 - January 31, 1987, page 34). The surfactant system was placed in a sealed vial with isooctane and inverted by a machine. Foam volumes in cc's were measured after 100 and 500 inversions and recorded. The surfactant concentration tested was 0.38 weight percent. Two samples were tested; one undyed, and the other with a 0.1% weight concentration of methyl violet. This experiment was used as part of a screening process for surfactants. The observation of stable emulsion with isooctane at atmospheric pressure does not guarantee foaming will take place with CO<sub>2</sub> at high pressure. The test does, however, give evidence of the ability of a surfactant to generate emulsions. The results are shown in Table 2.9.

The results show that the dye has a distinct effect on the foamability of solution. It is interesting to note that the dyed solution produced more than the reported volumes, but in a few seconds, coalesced to values shown in Table 2.9. Given this information, it was desirable to determine exactly the characteristics of the system we were dealing with.

Surface tension measurements were made at different concentrations of surfactant, with and without dye. The Rosano surface tensiometer was used to determine the static surface tension of the given surfactant solution in the presence of air. Again, Alipal CD-128 was used, with and without a 0.1% concentration of methyl violet. (Concentrations are in weight percent.) The results of this test are given in Figure 2.37.

The results show that the dye impaired the ability of the surfactant to reduce surface tension. We can conclude that it would also impair its ability to reduce the interfacial tension at the CO<sub>2</sub>-surfactant solution interface. Reduction of the interfacial tension allows an interface to be lengthened and snap-off into foam. Also, we can see that a CMC of around 0.12 weight percent can be deduced from the test.

### 2.2.6 Stable Foam Displacements

The concentration was increased to 1.9 weight percent for another set of displacements to see if this improved foam stability.

For the next set of displacements, the volumetric injection ratio was maintained at 4:1 CO<sub>2</sub>/surfactant solution. The temperature was 90°F. The displacement rate was 35.8 ft/day. Maljamar separator oil or Soltrol® was used to displace distilled water to irreducible water saturation. This was followed by simultaneous injection of CO<sub>2</sub> and surfactant solution. Oil type (Maljamar separator or Soltrol®), absolute pressure, and heterogeneity of pore structure were varied in order to see the effects of these parameters on the behavior of foam.

Displacements 5-2 and 5-3 were aimed at identifying wettability effects. The solid film-forming material that is produced with the Maljamar oil at 1320 psia was absent at 1800 psia. Displacement 5-3 was done as a reference to see what effects this phase would have on the other displacements. In Displacement 5-2, the Soltrol®-water was used to see what effect strong water

Table 2.9

Foamability Test of Alipal CD-128

<u>sample</u>	<u>foam volume, cc</u>	
	<u>100 inversions</u>	<u>500 inversions</u>
without dye	4	10
with dye	1	3

(CO<sub>2</sub>-87-330)

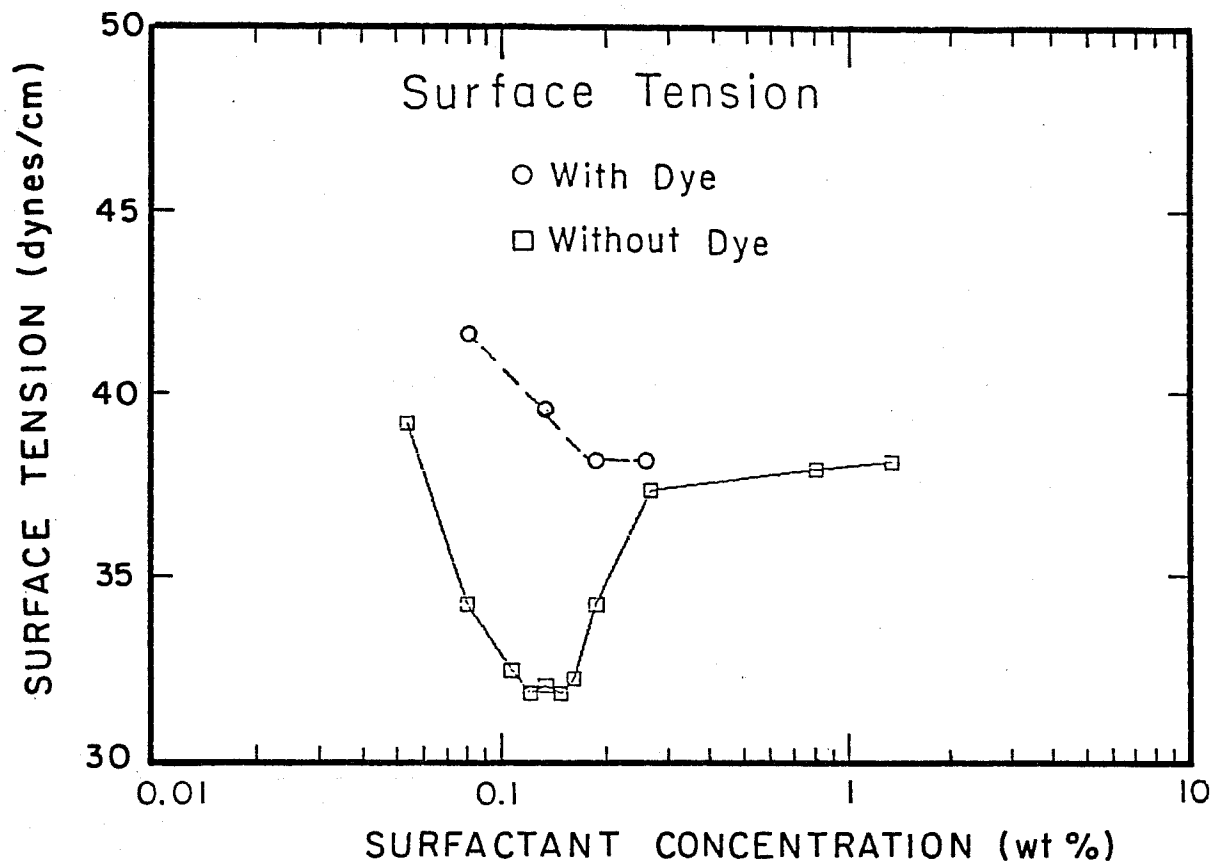


Figure 2.37. Plot of surface tension vs. surfactant concentration of Alipal CD-128 sample.

wettability (characteristic of the Soltrol<sup>®</sup>/water system) could have on a displacement. Displacements 5-1, 5-4, and 5-5 were designed to study the effect of pore heterogeneity. The conditions of these displacements are listed in Table 2.10.

#### 2.2.6.1 Results Common to Displacements 5-1 Through 5-5

Some results were common to all displacements. All produced stable foam, fluid diversion, and therefore good recovery. When a foam bubble invaded any substantial oil saturation, the bubble coalesced. In some instances, oil propagated through the porous media as a film surrounding a CO<sub>2</sub> bubble in the surfactant solution. As the displacements progressed, a trapped gas saturation was established. It was seen that a mobile surfactant solution saturation was necessary for foam generation and fluid diversion.

In the presence of stable foam, flow velocities of surfactant solution varied from that of the CO<sub>2</sub> bubbles. Any given bubble would be propagated by the surfactant solution and bubbled around it. Surfactant solution flowed with a volume of bubbles, or in a channel where the bubbles were stationary (a channel having no mobile CO<sub>2</sub> saturation). Both phenomena were observed occurring, simultaneously in separate flow channels in some instances.

#### 2.2.6.2 Results Common to Maljamar Oil Displacements

In Displacements 5-1, and 5-3 through 5-5, Maljamar separator oil was used. Slugs of CO<sub>2</sub> and surfactant solution entered the model, and foam was generated in-situ. Mixing at the front ends of surfactant solution and CO<sub>2</sub> slugs resulted in foam generation by the snap-off mechanism. After a CO<sub>2</sub> slug generated foam, it swept out a continuous phase flow path through the model.

Foam was generated during flow of surfactant solution. At the front of a slug, the surfactant solution flowed around the end of the previous CO<sub>2</sub> slug in a flow path. It then constricted the pore downstream of the CO<sub>2</sub> and pinched off a CO<sub>2</sub> bubble. This process was repeated, and with bubble division, generated notable quantities of foam at the leading edge of a surfactant solution slug.

At the trailing edge of a surfactant solution slug, CO<sub>2</sub> entered the surfactant-solution--saturated pores. The surfactant solution then closed in behind the CO<sub>2</sub>, and a bubble snapped-off.

The slug flow foam generation was very effective for fluid diversion. The residual oil saturation in all the Maljamar oil displacements was less than 10.0% total pore volume.

A chart record of the pressure drop across the porous media was made. In the early stages of the displacement, the pressure drop was lower as the oil saturation in the preferential flow paths inhibited foam generation. As the oil saturation in the porous media was reduced, more foam was generated, and the pressure drop increased. When the CO<sub>2</sub> established a continuous phase flow path through the porous media, the pressure drop fell to a minimum. This corresponded to a near-static condition in the porous media in all but the CO<sub>2</sub> flow path. When surfactant solution flowed, foam was generated, and the pressure drop rose to a maximum. These displacements showed stable foam, fluid diversion, good sweep efficiency, and provided meaningful insight into foam flow behavior.

### 2.2.7 Conclusions

The following conclusions can be drawn from these experiments.

1. Continuous foaming was obtained in the Soltrol<sup>®</sup>/water system after oil was displaced, as opposed to slug flow and in-situ foam generation for the Maljamar oil/water system.
2. Foam bubbles coalesced, and foam generation was inhibited when foaming agents flowed into an oil saturation. However, if there is a large enough water barrier between the oil and the foam, the oil may not cause coalescence. So, in systems where waterflooding is an important mechanism, the dissolvability effect that oil has on foam may be reduced.
3. Continuous foaming can be inefficient in diverting fluids into unswept pores.
4. Cycles of in-situ foaming, followed by a CO<sub>2</sub> sweep of continuous phase paths, were effective in diverting fluids into unswept pores.
5. Foam was generated at the front of both CO<sub>2</sub> and surfactant solution slugs.
6. Pressure drops across the model were higher when foam was generated, and fluid diversion took place.
7. The condition where a small pore throat opened into a larger pore space aided the generation of foam in glass micromodels.
8. Higher surfactant concentrations improved foamability over the range of concentrations studied.
9. Fluid diversion can be caused by not only foam and lamellae but also by multiple interfaces of oil, CO<sub>2</sub>, and surfactant solution.
10. In the absence of a discontinuous CO<sub>2</sub> phase (foam), surfactant solution inhibits oil/CO<sub>2</sub> contact and oil recovery because the CO<sub>2</sub> preferentially flows through the surfactant solution phase.
11. At low surfactant concentrations, the presence of a methyl violet dye increases surface tension. Also, it was shown that this dye depressed the ability of the surfactant solution to form emulsions with isooctane.

### 2.2.8 Future Experiments

We have found a system in which we can study stable foam flow and generation behavior. Future studies were focused on the effect of microscopic heterogeneity on foam flow behavior. A uniformly heterogeneous pore network will be incorporated into this study. A more accurate means of measuring pressure drop has been installed. Future studies will also target foam stability under different conditions, such as pure water or WAG floods.

The purpose of this investigation was to study the behavior of high-pressure CO<sub>2</sub> foams in porous media having different scales of heterogeneity. This foam visualization study will aid the development of a mathematical model for foam flow. In future studies, the effect of hydrocarbons

on foam stability will be investigated, as will the stability of a blocking foam during waterfloods and CO<sub>2</sub> injection.

### 3. SUPPLEMENTARY RESEARCH IN AREA II -- TRANSITION ZONE LENGTH

#### 3.1 Introduction

In this work, measurements were made of the output fluid concentration from a number of miscible displacements in small-diameter tubes with glass bead packings. These experiments were performed with various mobility ratios on each side of unity to obtain more data on the factors that influence the growth and apparent length of the transition zone between the fluids. While this research has implications for laboratory corefloods, its major application is in the evaluation of the design of slim tube tests and in the interpretation of results from them. The major conclusions available at this time concern the fact that often the flow in a slim tube is not uniform, but is afflicted with serious lateral variations of flow velocity, about which the following summarizing statements can be made:

These lateral velocity variations can arise from frontal instability and from non-uniform permeability.

The anomalous transition zone due to frontal instability first grows in proportion to the distance traveled, but then its growth slows, and the zone eventually reaches a limiting length that is set by transverse dispersion across the column, and which is subject to no further growth due to the instability.

For a column of sufficient length, a stabilized transition zone is reached that grows longer by longitudinal dispersion alone. This rate is generally much less than those observed previously.

The length of the stabilized zone that can result from an unstable flood has been derived in two ways. In either case, the stabilized transition zone length is proportional to a driving function for instability (the sum of a viscous and a gravitational part), to the square of the tube diameter, and to the reciprocal of the transverse dispersion coefficient.

Anomalously lengthened transition zones that arise from permeability stratification in this geometry are also stabilized by transverse dispersion.

These results are applicable in miscible and developed miscibility displacements. In some slim tube tests, transition zones are artificially lengthened by these flow circumstances, leading to overestimation of the minimum miscibility pressure in a CO<sub>2</sub> or solvent flood. To guard against this possibility, the strong recommendation is made that slim tube apparatus should be periodically tested with first-contact miscible floods (of the mobility ratio of interest) so that the breakthrough curve in this "base case" can be observed.

Because much of the earlier part of this work, including an extensive experimental section, was described in the second annual report of this project, it is only summarized here.

### 3.2 The Minimum Length of Transition Zone, Due to Longitudinal Dispersion Alone, in a Uniform Pack

In a miscible displacement run with fluids of matched density and viscosity in a uniformly packed column, an initially sharp transition zone between the fluids will become more diffuse as flow proceeds. In the mathematical solution of the partial differential equation, the variation of concentration with time and distance is given by the so-called "error function complement," abbreviated  $\text{erfc}(z)$ . The curve of this function describes the variation of concentration with a dimensionless distance  $z$  along the column from the center of the transition zone. Authors have shown that this "concentration profile" remains the same shape but is "stretched out" as flow proceeds, so that the real distance between the 10% and 90% concentration points increases in proportion to the square root of the time (or of the distance traveled).

$$\Delta x = 3.625\sqrt{(D_L t)} \quad (3.1a)$$

$$= 3.625\sqrt{(D_L \phi x / U)} \quad (3.1b)$$

Here,  $D_L$  is the longitudinal dispersion coefficient,  $\phi$  is the rock porosity fraction,  $U$  is the Darcy velocity through the column,  $x$  is the lengthwise distance along the column, and  $t$  is the time since the sharp front was started into the column at  $x=0$ . The number 3.625 comes from the choice of 10% and 90% as convenient points between which to measure the transition zone. The longitudinal dispersion coefficient at very small flow velocity is simply a fraction of the molecular diffusivity. At higher velocities, a second term proportional to the Darcy velocity becomes dominant. Definitive papers on this variation were published some years ago by Blackwell et al. (1959), Perkins and Johnston (1963), and others.

Because the value of  $D_L$  is fairly small, the transition zone length given by Eq. 3.1a is also small. But from the form of the variation, it is seen that the relative size of  $\Delta x$  grows continually smaller as  $x$ , the total length of travel, increases.

$$\Delta x/x = 3.625\sqrt{(D_L \phi / xU)} = 3.625\sqrt{(1/Pe)} \quad (3.1c)$$

Here, the dimensionless number,  $Pe$ , is the macroscopic Peclet Number, which is proportional to the length of the system.

It turns out that for a forty-foot slim tube packed quite uniformly with well-sorted glass beads, this formula would predict a transition zone length of only a few inches. Although chromatographic columns are often packed to this degree of perfection, this ideal is not always achieved in the slim tubes used for determination of minimum miscibility pressure. While the concentration profile is seldom measured, the transition zone length is inferred from the breakthrough curve, that is, from the amount of fluid, in pore volumes, that must be injected to change the output concentration from 90% to 10%. There are two reasons for the more slowly varying breakthrough curve from many columns that are briefly discussed below.

### 3.3 Stratified Packing

It often occurs that for some reason of asymmetry in packing or handling, even a small-diameter column may have noticeably greater permeability along one side than the other. Even a rather small relative variation of permeability, if distributed in such a consistent way along the column, could cause a large increase in the inferred transition zone length.

If the permeability varied linearly across the column diameter with a total difference of 10%, the Darcy velocity would also be expected to vary by the relative amount. An initially sharp transition zone could be represented by a close collection of isoconcentration surfaces, all plane and all perpendicular to the tube. As the flow proceeded, these isoconcentration surfaces would not remain perpendicular to the tube if the velocity were distributed as postulated over the whole length of the column. Instead, the surfaces of constant concentration would rotate about a diameter as they moved along the tube so that when the output port was reached, the observed breakthrough curve would indicate a transition zone about 10% as long as the tube.

In the absence of any relief from the correlated permeability variation, and without the restraint of transverse dispersion, we can expect that in contrast to the ideal transition zone described in Eq. 3.1c, the length of this anomalous transition zone will, in a stratified pack, grow in simple proportion to the distance traveled.

### 3.4 Non-uniform Flow Resulting From Frontal Instability

Even in a small diameter column, gravitational and viscous effects can give rise to secondary flow effects--overriding, if the column is horizontal, and frontal instability, if the displacing fluid is less viscous or if the tube is vertical and the heavier fluid is above. From a general mathematical point of view, these cases were treated in an early paper (Heller, 1963) in terms of the rate of rotation of the isoconcentration surfaces. In that paper, a "determining vector" was defined; its cross product with the concentration gradient gave the curl of the Darcy velocity.

It may be more helpful here to discuss a convenient approximation method that can be used to calculate the rate of growth of the non-uniform concentration distributions in several distinct cases. This shortcut is based on an observation first published by van Meurs and van der Poel (1958), that the pressure gradient in a developed finger has the same value as in the moving fluid adjacent to the finger. This generalization is based on the fact that no flow is occurring perpendicular to the side boundary of the finger and means that (in a matched density system) the ratio of the flow velocities inside the finger to that alongside it is equal to the mobility ratio.

With this principle and the assumption that boundaries between the parts of the column that are saturated with the two fluids remain sharp, it is possible to calculate the growth rates of extensions on the front.

The viscosities, densities, and velocities of the two fluids are subscripted  $u$  and  $\ell$  for upper and lower. After fingers are well developed in a vertical column, the (upward pointing) darcy velocities inside and alongside them are

$$U_u = (2\mu_\ell Q / A + gk(\rho_u - \rho_\ell)) / (\mu_u + \mu_\ell) \quad (3.2a)$$

$$U_\ell = (2\mu_u Q / A - gk(\rho_u - \rho_\ell)) / (\mu_u + \mu_\ell) \quad (3.2b)$$

The rate at which the finger grows in length is then the difference between these, divided by the porosity. If the finger growth velocity is  $V_f$ , and the mean Darcy velocity in the core  $Q/A$  is denoted by  $U$ , then:

$$\begin{aligned} V_f &= (U_\ell - U_u) / \phi \\ &= 2(M-1)U / (\phi(M+1)) + 2kg(\rho_u - \rho_\ell) / (\phi(\mu_u + \mu_\ell)) \end{aligned} \quad (3.3)$$

Here,  $M$  is the ratio of the displaced to the displacing fluid viscosities (that is, for an upward displacement,  $\mu_u/\mu_\ell$ ), and the unsubscripted  $U$  is the mean Darcy velocity. The presence of the gravitational acceleration,  $g$ , is a reminder that consistent units (like SI, or cgs) must be used in this formula.

We note that in a matched density system, the growth rate of the fingers is proportional to the mean displacement velocity. This means that, subject again to the same restrictions about the absence of transverse dispersion, the observed length of the anomalous transition zone due to viscous fingering would be proportional to the length of the column.

### 3.5 Dispersive Stabilization of Anomalous Transition Zones

In both of the situations described above, and contrary to the simplified rules given, the growth of the anomalous transition zone is actually restrained by transverse dispersion. The longer that such a channeled or fingered zone grows, the greater will be the influence of the dispersion. Eventually, such a stepped transition zone becomes so long that all of the excess fluid that goes into the fast channel (by reason of the higher velocity there) will be carried over into the other channel by transverse dispersion. One way of calculating what this length will be is to set equal the expressions for the two values of flux. One cannot expect an exact solution from this procedure, because the values of the flux are not constant but depend on the actual concentration profiles across the tube.

Approximate values for the fluxes can be given, however. The excess convected fluxes, in the two cases above, are:

$$\Gamma_C = \phi V_f AC/2 = QC\Delta k/(2k) \quad (3.4)$$

for the case of a column with a lengthwise correlated permeability variation from one side to the other ( $Q$  is the flow rate and  $C$  is the concentration difference of the fluids), and

$$\Gamma_C = CA(U(\mu_\ell - \mu_u) + kg(\rho_\ell - \rho_u))/(\mu_u + \mu_\ell) \quad (3.5)$$

for the case in which frontal instability (due to both viscosity and density differences between displacing and displaced fluids) produces a long finger in a vertically oriented column.

As the anomalous transition zone grows longer, the area for transverse dispersion increases. The dispersive flux can be estimated as

$$\Gamma_D = 2aLD_T\phi C/h = LD_TC\phi \quad (3.6)$$

Here,  $L$  is the length of the channel or finger,  $D_T$  is the transverse dispersion coefficient, and the assumption has been made that the variation of the concentration  $C$  takes place over the entire width of the tube.

At the limiting length of these anomalous transition zones, the convective excess flux is equal to the dispersive. Setting  $\Gamma_D = \Gamma_C$  to obtain this length, we have  $L_{nuk}$  in the first case, in which the anomalous transition zone is the result of nonuniform permeability (with variation from one side of the column to the other)

$$L_{nuk} = (Q/2D_T\phi)(\Delta k/k) \quad (3.7)$$

In the second case, setting  $\Gamma_D = \Gamma_C$  gives a formula for the dispersion stabilized transition zone length  $L_{DS}$ , in the presence of frontal instability:

$$\begin{aligned} L_{DS} &= (\pi a^2 / 2D_T \phi) (2U(M-1)/(M+1) + kg(\rho_\ell - \rho_u) / \mu) \\ &= (\pi a^2 / 2D_T \phi) E^* \end{aligned} \quad (3.8)$$

where  $E^* = 2U(M-1)/(M+1) + kg(\rho_\ell - \rho_u) / \mu$  (3.9)

and  $\pi a^2$  has been inserted for  $A$ , the cross-sectional area. The quantity  $E^*$  can be viewed as the driving function for frontal instability. It is a scalar version of the "determining vector" mentioned earlier.

In anomalous transition zones, the flow velocity is greater on one side of the column than the other. In the two cases discussed in this section, formulas have been presented for the maximum lengths to which transverse dispersion will allow such transition zones to grow. After the zones have reached these lengths, one could expect in the second case that the isoconcentration surfaces that describe the frontal region would gradually rotate, until they finally became perpendicular to the column. From this situation, the frontal region would continue to expand by longitudinal dispersion alone, as the spacing between the isoconcentration surfaces very slowly increased. Thus there would be no further growth resulting from the instability; the initial fingers would have been first restrained and eventually suppressed completely by transverse dispersion.

It is also of interest to consider a different initial configuration, in which the isoconcentration surfaces are closely spaced but perpendicular to the column, and in which the instability has not yet given rise to perceptible fingering.

### 3.6 The Onset of Fingering From a Graded Concentration Front

Because the sharp front assumed for convenience in the preceding sections is only a crude picture of the actual situation, it is worthwhile to consider a next higher level of approximation. In such a more refined image, the concentration can be considered to be a continuous function of position and time, and one can consider the fate of perturbations impressed onto a set of evenly spaced isoconcentration surfaces. Such a perturbation calculation was presented in the second annual report of this project for the case of a miscible transition zone in a cylindrical tube.

The purpose of the calculation was to deduce the rate of initial growth of perturbations of different types, considering the opposing effects of the "driving function" for instability, and of transverse dispersion. A major result was that one of the perturbation modes (that in which the flow rate is increased on one side of the column and decreased on the other) was least restrained by transverse dispersion, and therefore showed the greatest net rate of growth.

This result can then be used to provide a formula for the particular length,  $\delta_{DS}$ , of such a ramp-shaped transition zone that will have a growth rate of exactly zero. This formula is

$$\delta_{DS} = Ea^2 / (\phi D_T \lambda_{11}^2) \quad (3.10)$$

Here  $\lambda_{11}$  is dimensionless growth rate of the fastest growing perturbation mode and has the value 1.84. The driving function for instability that is used in this formula has a somewhat different form than that in Eq. 3.9 but the same limiting value for low values of the mobility ratio.

$$E = U \ln M + kg(\rho_L - \rho_U) / \mu \quad (3.11)$$

The similarities of the expressions in Eqs. 3.8 and 3.10 are more significant than the differences. In both formulas, the transition zone length is proportional to the square of the tube radius. In both, a driving function is proportional to the sum of a term containing the Darcy velocity through the column and one containing the density difference of the fluids. In both, the transverse dispersion coefficient is contained in the denominator.

### 3.7 Conclusions

These calculations have shown the extent to which transverse dispersion can limit the growth of a transition zone during a slim tube test, and they quantify the common qualitative opinion that fingers and permeability stratification must be less important in smaller diameter columns.

They also point toward the situations in which these effects can still be large enough to influence the results of an MMP test.

The same conclusions are given here as appeared in the second annual report:

1. In a "slim tube test" for minimum miscibility pressures, the characteristics of the pack do need to be considered to be sure that the stabilized zone in a first contact miscible displacement is short compared to the zones produced by phase behavior.
2. A slimmer slim tube does not need to be so long to meet this criterion.
3. It is important to pack the tube carefully because a lengthwise-stratified packing, in which the permeability is greater along one side of the tube than the other, can significantly increase the length of the transition zone and the magnitude of the apparent MMP.
4. When in doubt about the characteristics or quality of a particular slim tube system, it is prudent to perform two first-contact-miscible displacements in it--one at matched viscosity and one at an unfavorable mobility ratio near that of the floods contemplated.

## 4. AREA III - MOBILITY CONTROL IN CO<sub>2</sub> FLOODS

### 4.1 Introduction

As noted previously in reports of this work, two distinct meanings of the phrase "mobility control" are in current use. Both describe procedures or injection strategies designed to increase the uniformity of displacement in floods where the injected fluid is more mobile than the fluid to be displaced. As a consequence of such an unfavorable mobility ratio, the displacement front becomes unstable and increasingly non-uniform. The non-uniformity of displacement leads to early breakthrough, which is followed by production of the injected fluid, at an escalating rate and economic penalty, throughout the remaining life of the flood.

One meaning of the phrase "mobility control" refers to the use of radical methods of thickening the injected fluid in an attempt to decrease the flow into those horizons that

communicate more directly to the production wells. This procedure can be very effective in highly stratified formations in which the "thief zones" can be distinguished, and in which flow of the thickened material can be directed preferentially.

The second meaning of the phrase, which is mostly used here, concerns the attempt to decrease the mobility of the injected fluid by a more modest amount. The optimum mobility reduction would be just sufficient to decrease significantly the negative economic significance of frontal instability, but not so great that the overall injectivity--and profitability--of the flood would be seriously reduced. In order to make this ideal economic choice (of the proper degree of thickening to be used) the engineering management would need good technical information on the cost and effect of the available mobility control additives and procedures.

Obvious overlap exists between these two interpretations, and the distinction drawn above may be superfluous or entirely empty in some sub-areas of the research or field applications.

Our research goals in this area of the project, as expressed in the list of tasks included in the original proposals, have been concerned with the development of mobility control methods specifically designed for the improvement of CO<sub>2</sub> flood performance.

First among these goals are laboratory measurements and experiments designed to develop additives by which dense CO<sub>2</sub> can be thickened by a predetermined amount. There are two general types of additives that we are working to perfect: "CO<sub>2</sub>-foam" and "direct thickeners." Our development efforts and extensive results concerning these two types of mobility control additives are presented below.

A second goal is to design and conduct experimental tests to verify, as far as is possible in the laboratory, the effectiveness of these additives and flood procedures. A further specific purpose of these tests is to verify the survivability of the thickeners at reservoir conditions.

A third goal is concerned with the design of engineering procedures for the optimum use of the additives that are developed. This goal involves reservoir calculations as well as the consideration of operational conditions.

Each of these goals has involved mathematical analysis of flow processes in rocks and the modes by which the additives influence it. As noted, the three research goals correspond to those tasks enunciated at the beginning of this three-year project.

Substantial progress has been made on each of the goals; detailed accounts of the research findings are presented in this report. At the same time, it must be recognized that further research work is needed on some of these topics, as well as on new ones that have been recognized as a result of the clarifications accomplished by this and other research projects. These remaining and continuing questions are pointed out where appropriate in each of the following sections.

## 4.2 Background

It is generally recognized that effective mobility control could increase substantially the oil recovery from CO<sub>2</sub> flooding. This recognition is based on fairly common knowledge of the behavior of miscible flood-fronts, especially under conditions of frontal instability. There are a few important features of this behavior, however, which have not been described in the literature with sufficient detail to be generally useful in reservoir calculation. Because any field recommendations

to be made must take into account the processes that shape the frontal behavior, it is useful to consider all of these processes here.

The need for mobility control is often more evident (though not always more economically pressing) in miscible or near-miscible floods than it is in a waterflood or in immiscible gas floods. This is because of the absence of the relative permeability effects that, in immiscible displacements, are sometimes able to decrease the mobility of the injected fluid. Because there are no interfaces in the porespace between the displaced and displacing fluids during a miscible flood, the mobility ratio is simply the ratio of viscosities.

It is well known that a mobility ratio greater than unity causes a miscible displacement front to become unstable. The speed with which the resulting fingers or protrusions grow on the front is subject to two influences that depend differently on time and distance scales--convection and dispersion. Calculation of the course of these processes requires the simultaneous solution of Darcy's equation (using the imposed pressures and well rates) and the convection-dispersion equation. The latter equation describes the change in the distribution of the fluid components during the flow regime specified by the former. It is the coupling of the two equations (resulting from the viscosity and density differences between the displaced and displacing fluids) that admits the possibility of frontal instability.

In the displacement of miscible fluids, a "sharp front" between the displaced and displacing fluids is impossible to maintain because of the influence of molecular diffusion. In consequence of this continual thermal agitation of the molecules that constitute the fluid, they do not exactly follow the average streamlines of flow. Instead, the molecules can readily migrate from one streamline to adjoining ones. By this means, diffusion reduces the very large dispersion effects that would follow from the extreme differences of velocity between the streamlines that lead through the centers of porespace and those that are close to the grains of rock. The change in concentration distribution thus becomes subject to a much more moderate dispersion, the coefficient of which is the sum of a term containing the molecular diffusivity and one proportional to the average flow rate.

The resulting dispersive widening of a diffuse transition zone between the displaced and displacing fluids is proportional to the square root of the time (or the distance traveled). The important result of this is simply that the larger the flow system, the smaller will be the fractional volume of this dispersed zone.

In contrast, frontal structure due to viscosity instability (and to correlated distributions of permeability heterogeneity) grows in direct proportion to the distance traveled. The fractional volume containing these features is independent of the size of the flow system.

Consequently, there is a great difference in the relative importance of dispersive effects between laboratory floods and field-scale miscible displacements. Whereas in smaller scale displacements, the effect of dispersion on the growth of frontal instabilities is significant, the diffuseness of the edges of relatively large fingers can be ignored while considering their shapes and growth rates. In calculating flow rates in a larger scale geometry, the finger boundaries can often be considered as mathematical discontinuities.

While the "sharp front" approximation can be appropriate for reservoir situations, it never provides a good description of laboratory experiments. As is seen in the next two sub-sections on the development of additives to thicken the displacing fluid, much of our research effort must temporarily be directed toward the basic processes that occur at poresize or smaller scales.

After detailed accounts of the current progress in our two additive-development efforts, this section of the report on mobility control returns to the broader questions of the laboratory assessment of such additives and their applications in the oil field.

### 4.3 CO<sub>2</sub>-Foams

#### 4.3.1 Overview

The addition of surfactant to the flowing water during the flood reduces CO<sub>2</sub> mobility and should improve both areal and vertical sweep efficiencies by reducing frontal instability and flow through the more permeable zones (Bernard, Holm, & Harvey, 1980). Numerous laboratory studies have demonstrated that if contact is made with the oil, dense supercritical CO<sub>2</sub> can develop multicontact miscibility with many crudes (Whorton, Brownscombe, & Dyes, 1952; Holm, 1959, 1963; Holm & Josendal, 1974). Most of the time, though, oil recoveries with CO<sub>2</sub> have been much higher in the laboratory than in the field because the field conditions are more severe for all oil recovery processes, permitting much more non-uniform flow.

CO<sub>2</sub>-foam presents an immediately available, and perhaps a more efficient, method of reducing CO<sub>2</sub> mobility because a foam consists of at least 80% CO<sub>2</sub> and the cost of needed surfactant promises to be minor. Furthermore, foam possesses favorable properties for oil recovery, especially by CO<sub>2</sub> flooding. The apparent viscosity of foam in porous rock is greater than the actual viscosities of its components and increases with the rock permeability. To emphasize that the apparent viscosity in this case is very dependent on the rock, and is not simply a fluid property, our results are given in terms of the mobility and relative mobility of the foam through the rock. The apparent viscosity is the reciprocal of the relative mobility. Also, foam lamellae increase trapped gas saturation. As gas saturation increases, oil saturation decreases. Usually, a high trapped gas saturation reduces gas mobility.

In the case of CO<sub>2</sub> floods, a partially compensating feature has been reported by Patel, Christman, & Gardner (1985). They have observed unexpectedly low mobilities during CO<sub>2</sub> injection in field and laboratory experiments and conclude this effect is caused by "mixed-wettability" of the rock. The decreased mobility also might possibly be connected with the high solubility of CO<sub>2</sub> in crude oil, which adds to the effectiveness of transverse dispersion in tending to dissipate at least the closely spaced fingers. Despite these mitigating features, most CO<sub>2</sub> floods do show early breakthrough, indicating higher flow rate in a CO<sub>2</sub> finger or channel connecting the injection and production wells. So long as this finger expands laterally, thereby entraining enough additional oil to make continuing the flood economic, the produced CO<sub>2</sub> can be reinjected. The costs of gathering, processing and recompressing are an additional operating expense that must necessarily hasten the day of abandonment. Because of this, the overall recovery efficiency is reduced--a loss of oil that can be considered a result of the unfavorable mobility ratio.

Foam flooding is a method that modifies the flow mechanism by changing the structure of the displacing fluid at the pore level. The use of foam-like dispersions or CO<sub>2</sub>-foams is a useful method in enhanced oil recovery.

This method of decreasing the mobility of a low-viscosity fluid in a porous rock requires the use of a surfactant to stabilize a population of bubble films or lamellae within the pore space of the rock. The degree of thickening achieved apparently depends to some extent on the properties of the rock. These properties probably include the distance scale of the pore space and the wettability, and so can be expected to differ from reservoir to reservoir, as well as to some extent within a given field.

Major emphasis has been on measurement of the mobility of CO<sub>2</sub>-foam in rock core samples. Our work on this method of thickening has also included the testing of several features of surfactant suitability: the compatibility of the surfactant with oilfield brines at reservoir temperatures and its adsorption on the rock. The work reported describes the development of apparatus and methods and presents results available at this time.

#### 4.3.2 Past Work

Much of the past work was on calibration of the foam mobility measurement apparatus and improvement of the experimental set-up. As for the surfactant screening testing, a standard experimental procedure was developed. Also, a standard device was built to obtain consistent results in foam height measurement. In adsorption studies on rock samples, time was spent to optimize the experimental set-up and perform preliminary testing.

In foam mobility measurements, two basic and important calibrations were performed. Compressibility of CO<sub>2</sub> was measured at a number of temperatures and is shown at 20°C in Fig. 4.1. The relatively high values of compressibility, even at higher pressures, made it apparent that independent measurement of the CO<sub>2</sub> flow rate are required during the experiments, even though the Ruska pump was operated at a constant rate.

For this purpose, calibration of the flow of dense CO<sub>2</sub> through the capillary tube was carried out. The pressure drop across the capillary tube was measured by use of time-averaged readings from a Validyne differential pressure transducer, after steady pressure drops were reached at various Ruska pump flow rates. The linear relationship observed is consistent with the Hagen-Poiseuille equation. Fig. 4.2 shows this calibration data in a plot of flow rate of CO<sub>2</sub> vs.  $\Delta p_{cap}/\mu_{CO_2}$ . During subsequent mobility experiments, the flow rate of CO<sub>2</sub> was computed from this calibration line.

Flow of the dense CO<sub>2</sub> is laminar up to 90 cc/hr; at higher rates we observed a transition region between laminar and turbulent flow and finally the upper dashed curve that presents the turbulent region. The break in the calibration curve is at an approximate Reynolds number of 2500, and the curve is used only in the laminar flow region below this break. More detail of the measurements will be described later in this section under "CO<sub>2</sub>-Foam Mobility Measurements."

Screening of past and current surfactant results will be summarized in tabular form under the heading of "Surfactant Screening." Preliminary results were also collected and will be presented under "Adsorption Studies," along with other results.

#### 4.3.3 Description of the Foam Mobility Measurement Apparatus

A schematic of the CO<sub>2</sub>-foam mobility measurement apparatus is given in Fig. 4.3. The Ruska pump pressurizes the liquid CO<sub>2</sub>, maintained at a constant temperature by circulating antifreeze inside the jacketed pump. The CO<sub>2</sub> flows through the capillary tube; the pressure drop across the tube is measured by a Validyne differential pressure transducer. An Isco pump is used to pressurize the brine surfactant solution, which also flows through the foam generator and the core. As a matter of procedure, the core is first fully saturated with brine-surfactant solution. The foams are generated inside the short core used as a foam generator, where the mixing between CO<sub>2</sub> and surfactant solution occurs. The mixed CO<sub>2</sub>-foam flows through the core. The pressure drop across the core is recorded by a second Validyne differential pressure transducer. In addition to

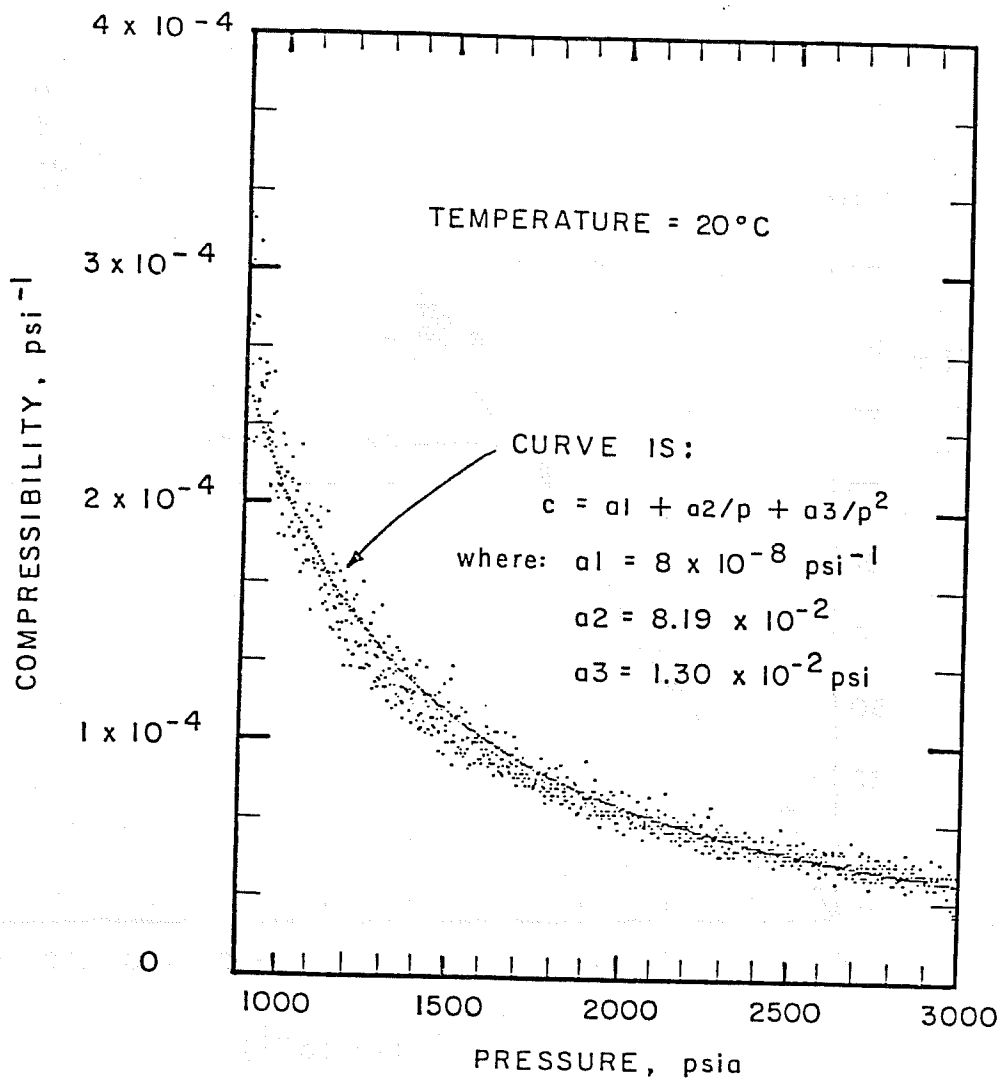


Figure 4.1. Compressibility of CO<sub>2</sub> at 20°C.

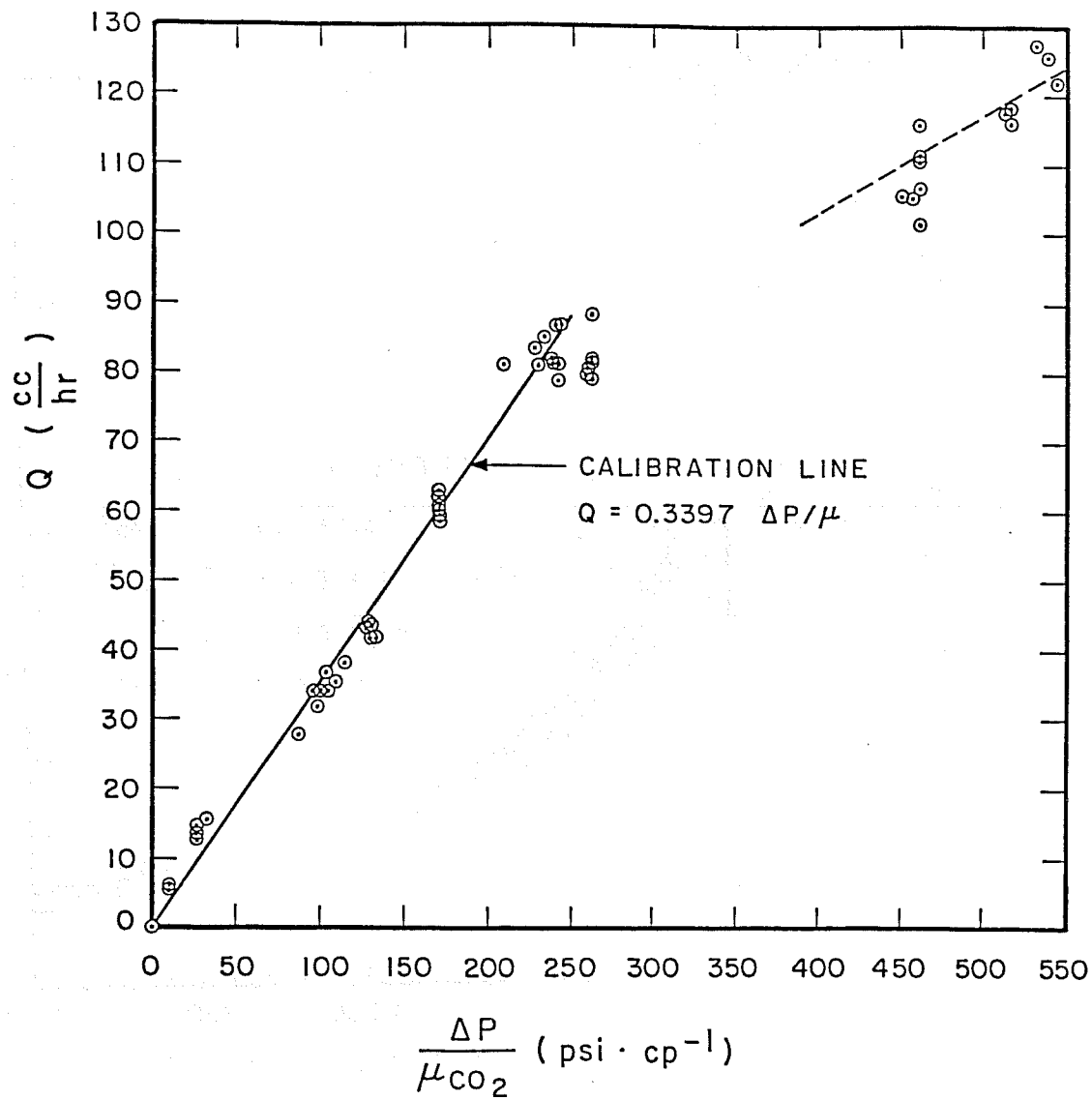


Figure 4.2. Calibration of capillary tube flowmeter.

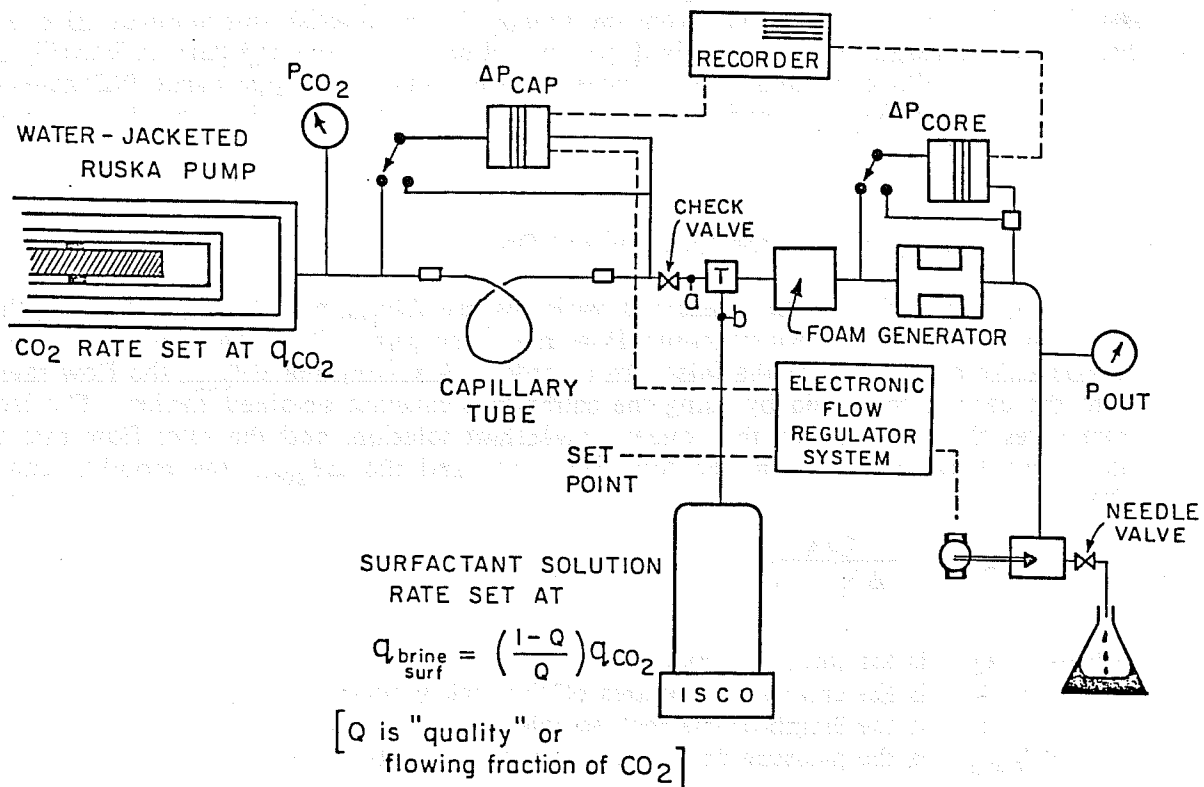


Figure 4.3. Schematic of the CO<sub>2</sub>-foam mobility measurement apparatus.

the digital readout of the values of  $\Delta P_{\text{cap}}$  and  $\Delta P_{\text{core}}$ , a two-pen recorder is used to record the simultaneous measurements. The needle valve is operated by the electronic flow regulator system.

To maintain the macroscopic steady-state of the flow of dense  $\text{CO}_2$  through the capillary tube, several tests have been made to come up with an optimum flow device. Two fine tapered needle valves in series were used to regulate the flow rate of the  $\text{CO}_2$  at high pressure. A fine adjustment dial on one of the valves permits repeatable manual settings. Steady state is accomplished manually by setting the dial to give a desired pressure drop across the calculated capillary that carries dense  $\text{CO}_2$  from the pump. To accomplish this automatically, a controller set point that corresponds to the desired pressure drop across the capillary is chosen. After opening the manual needle valve to an approximately desired value, the appropriate PID gains (proportional, integral, differential) are optimized to open or close the motorized needle valve electronically, according to the set point.

#### 4.3.4 Interpretation of the Experimental Data

In this experiment, the measured variables are  $\Delta P_{\text{cap}}$  and  $\Delta P_{\text{core}}$ . Besides these variables, other data, such as the Ruska pump flow rate, Isco pump flow rate, inlet pressure of  $\text{CO}_2$ , and temperature of the  $\text{CO}_2$  at the inlet, are recorded. Knowing the  $\Delta P_{\text{cap}}$ , the flow rate of pure  $\text{CO}_2$  into the core is computed by using the calibration constant obtained earlier. The Isco pump flow rate gives the flow rate of the aqueous surfactant solution, and the total flow rate is the sum of these two flow rates. From the total flow rate and the  $\Delta P_{\text{core}}$ , the mobility can be evaluated from:

$$\lambda = \frac{Q/A}{\Delta P_{\text{core}}/L} \quad (4.1)$$

where

- Q is the total flow rate
- A is the cross-sectional area of the rock sample
- L is the length of the rock sample
- $\Delta P_{\text{core}}$  is the pressure drop across the rock sample

#### 4.3.5 $\text{CO}_2$ -Mobility Measurements

##### 4.3.5.1 The Effect of Surfactant Concentration

The effect of the concentration on foam mobility for a particular surfactant has been studied extensively. The surfactant under investigation for this effect was Varion CAS from Sherex.

Varion CAS is a zwitterionic surfactant which contains both anionic and cationic functional groups. The rock under study was Berea sandstone, which has a permeability of 308 md measured by using 1% brine solution. The permeability using  $\text{N}_2$  gas was  $1000 \pm 6.2$  md [measured at atmospheric pressure].

Among the types of surfactants, we want to avoid the cationic type, which, because sandstone is negatively charged, may be subject to excess adsorption in the rock. The nonionic surfactant is relatively sensitive to temperature, and some anionic surfactants can react strongly with brine solution, leaving undesirable salt deposits in the rock. Taking these factors into consideration, we decided to start this series of tests with a well-defined system, incorporating the zwitterionic surfactant.

The effect of concentration of the Varion CAS was studied extensively. The initial concentration (0.001 wt% active) was selected from the graph of surface and interfacial tensions in Figs. 4.4-4.7 and lies in the range of CMC values for these measurements.

Strictly speaking, CMC values of surface and interfacial tensions are only slightly different, and one can talk about the range of CMC. Also, we are well aware that good foamers are most effective well above the CMC. The initial concentration was in this case selected at 0.001 wt%, and in subsequent tests the concentrations were increased well above that range.

Two definite conclusions were made from this experiment. Fig. 4.8 demonstrates the effect of concentration, and clearly the mobility decreases as the surfactant concentration is increased from  $10^{-3}$  to  $10^{-2}$  wt% active of surfactant concentration. For concentrations above a particular value, in this case, 0.03 wt% active, further increase in concentration did not reduce the magnitude of the foam mobility. These are very important points to realize since we do not want to use more than the necessary amount of surfactant to obtain the desired mobility values. More details of each concentration, with its necessary information, are listed in Table 4.1.

As far as reproducibility of the results is concerned, we have repeated some of the data points. Also, we can see that the order of magnitude of the mobility is the same for a particular concentration. This demonstrates the sensitivity and viability of the present foam mobility apparatus.

One of the major difficulties in carrying out such an experiment is to maintain a constant fractional flow of  $\text{CO}_2$ , or "foam quality." The experimental difficulty is presumably due to the compressibility of dense  $\text{CO}_2$ . Also, the length of the core and the heterogeneities of the rock could be contributing factors. Each time in this experiment when we have increased the concentrations, sufficient pore volumes have been used to wash the core thoroughly.

Some observations were recorded during the experiment. Through the transparent, low-pressure outlet tubing, no foam lamellae were observed for concentrations between 0.001 wt% and 0.01 wt% active. The chart recorder showed a fairly straight line of pressure drop across the core but a relatively irregular line for the pressure drop across the capillary tube. It seemed as if insufficient foam lamellae were passed through the rock to have an appreciable effect on the flow resistance in the core.

With 0.03 wt% active or more, well-formed foam lamellae were observed in the output tube as we washed the core with each concentration before the actual experiment with dense  $\text{CO}_2$ . With the simultaneous run of dense  $\text{CO}_2$ , elastic bubbles were seen through the outlet tubing.

As we increased the concentrations to 0.03 wt% and more, the pressure drop across the capillary tube became quite regular, and more fluctuations were recorded in pressure drop across the core. This indicates the presence of sufficient foam lamellae.

Varion CAS foams well, but the foam also dies out rather quickly. It must be a fast draining foam. In general, we have observed that at some threshold concentration that is well above the CMC range, mobility does not decrease any further. (The performance of Varion CAS as a foamer is shown later in Table 4.6.)

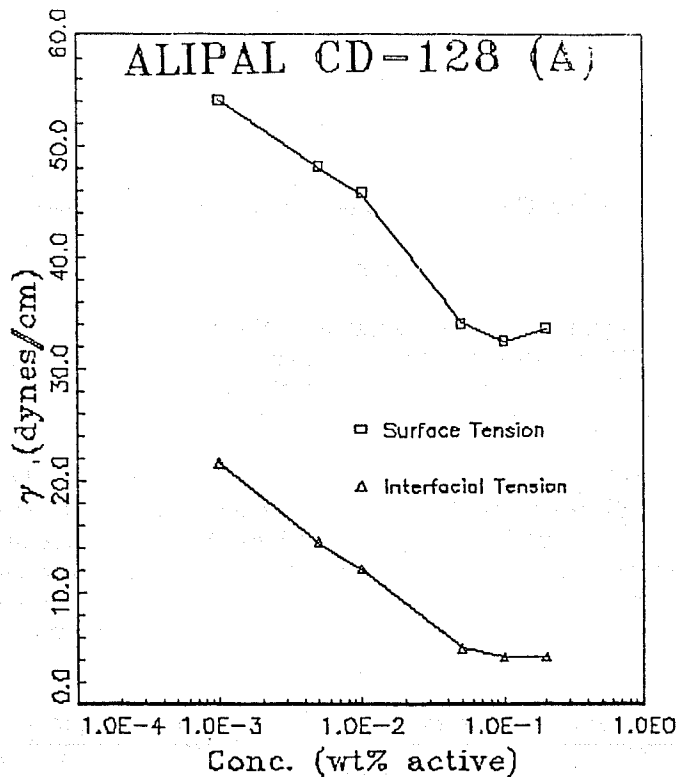


Figure 4.4. Measurements of surface and interfacial tensions, Alipal CD-128 (A).

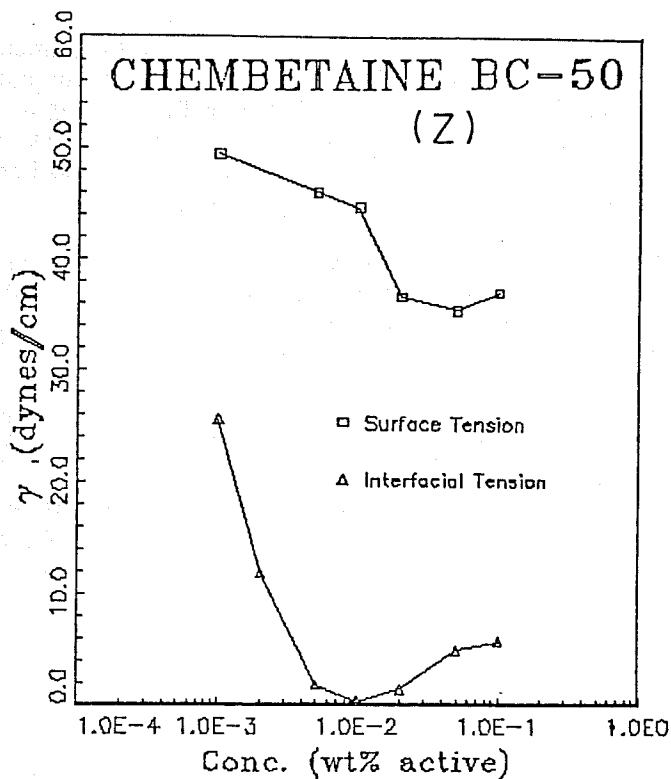


Figure 4.5. Measurements of surface and interfacial tensions, Chembetaine BC-50 (Z).

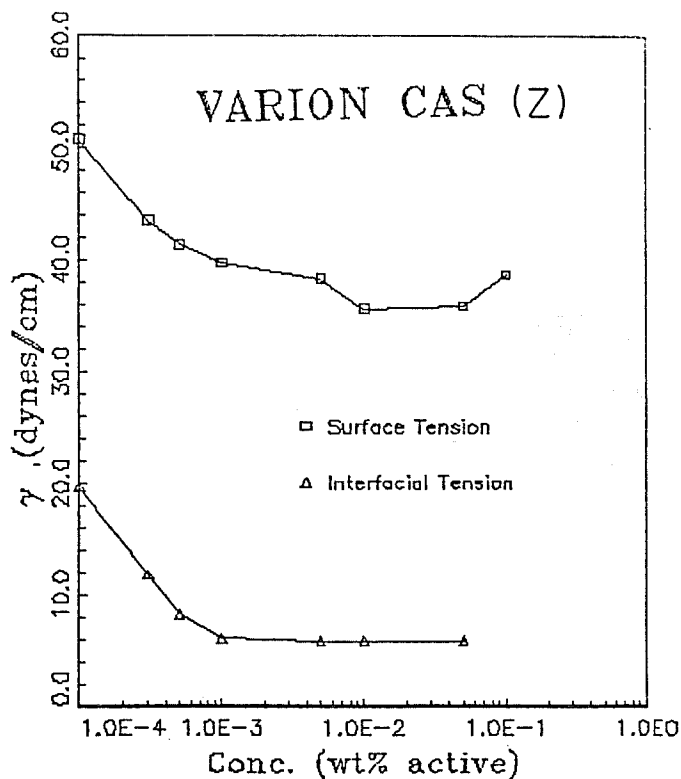


Figure 4.6. Measurements of surface and interfacial tensions, Varion CAS (Z).

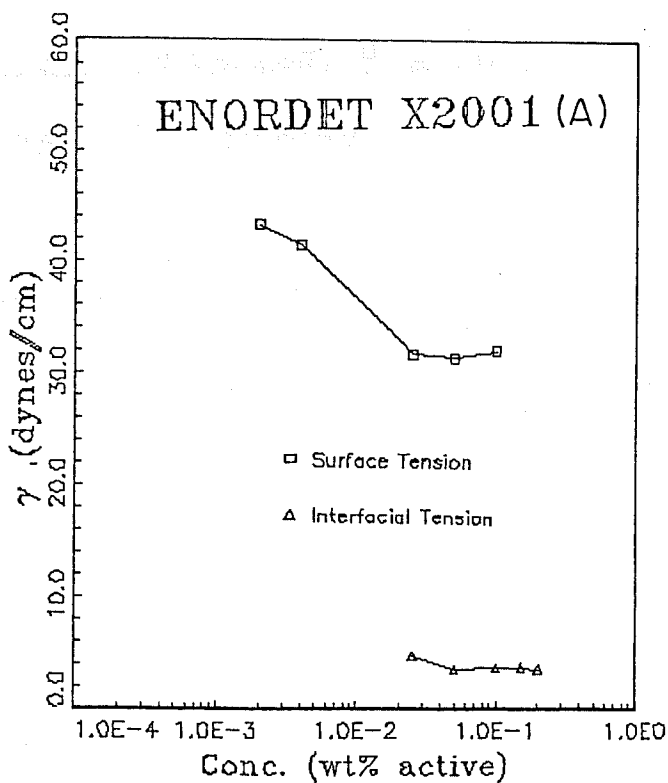


Figure 4.7. Measurements of surface and interfacial tensions, Enordet X2001 (A).

# $\lambda$ vs. $V$

(CO<sub>2</sub>-87-276)

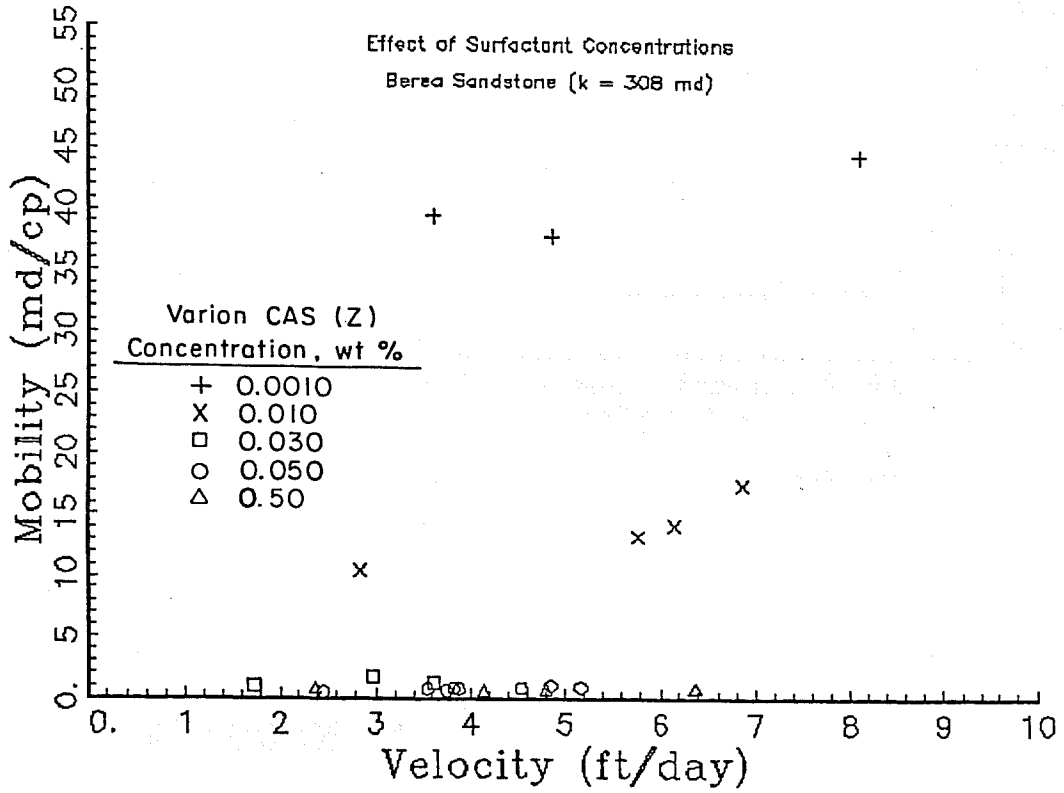


Figure 4.8. Effect of surfactant concentrations.

Table 4.1

CO<sub>2</sub>-Foam Mobility MeasurementsEffect of Surfactant Concentrations  
Varion CAS (Z) in 1% Brine\*

Rock type: Berea Sandstone

Permeability of the rock: 308 ± 9 md

Inlet pressure of the pumps: 1615 ± 5 psia

Temperature of the CO<sub>2</sub> in Ruska pump: 25.0 ± 0.2°C

Concentration (wt% active)	v (ft/day)	λ (md/cp)	λ <sub>r</sub> (cp <sup>-1</sup> )	CO <sub>2</sub> (quality,** %)
0.0010	3.60	39.4	0.128	82.7
	4.86	37.8	0.123	80.8
	8.10	44.5	0.144	81.5
				81.7 ± 1.0
0.010	2.84	10.5	0.0340	78.1
	5.76	13.2	0.0428	78.4
	6.14	14.2	0.0461	81.7
	6.86	17.5	0.0568	82.2
				80.1 ± 2.1
0.030	1.73	0.953	0.00309	81.2
	2.97	1.64	0.00531	83.2
	3.60	1.28	0.00414	82.7
				82.4 ± 1.0
0.050	2.46	0.520	0.00169	79.7
	3.54	0.643	0.00209	82.4
	3.74	0.582	0.00189	83.3
	3.82	0.755	0.00245	83.7
	3.88	0.662	0.00215	83.9
	4.53	0.762	0.00247	83.5
	4.85	0.927	0.00301	83.3
	5.16	0.854	0.00277	83.1
				82.9 ± 1.4
0.50	2.37	0.743	0.00241	81.0
	4.14	0.549	0.00178	81.9
	4.80	0.648	0.00210	81.8
	6.36	0.753	0.00244	80.7
				81.4 ± 0.6

\*Standard brine solution is made of 0.5% NaCl and 0.5% CaCl<sub>2</sub>.\*\*Quality is the volume fraction of the CO<sub>2</sub>.

#### 4.3.5.2 The Effect of Flowing CO<sub>2</sub> Fraction (Foam Quality)

The effect of CO<sub>2</sub> fraction on foam mobility measurements has been studied. The surfactant under the investigation was the anionic Enordet X2001 from Shell.

Four different CO<sub>2</sub> fractions were tested at constant surfactant concentration of 0.05 wt% active. Again, the concentration of 0.05% was chosen from Fig. 4.7, the measurements of surface and interfacial tensions. The rock sample used was Berea sandstone with  $k = 302 \pm 16$  md. The variation of foam mobility with different values of CO<sub>2</sub> fraction is clearly seen in Fig. 4.9. The corresponding numerical data are shown in Table 4.2 for convenience. In Fig. 4.9, the effect of CO<sub>2</sub> fraction is definitely distinctive. As has been expected, the foam mobility decreases with decreasing CO<sub>2</sub> fraction. This verifies the fact, long known in the literature, that the presence of surfactant solution along with CO<sub>2</sub> lowers the mobility.

It is also interesting to observe that the slope of the fitted lines (that is, the dependence of mobility on overall flow rate) decreases as the surfactant fraction increases. A possible explanation is that the lamellae formed by the CO<sub>2</sub> and surfactant mixture become more stable as the water (surfactant) fraction is increased. From a macroscopic viewpoint, more uniform displacement would be expected as a result of the decreased mobility.

Furthermore, more scattering of data is observed for the CO<sub>2</sub> fraction of  $81.1 \pm 1.0\%$ . It is likely that this particular ratio may not be favorable for this surfactant and rock type.

In previous experiments, such as with Varion CAS (Z) and Chembetaine BC-50 (Z), this variation of mobility with CO<sub>2</sub> fraction has also been observed. Those data are not presented here, although similar behavior consistent with such a significant decrease in mobility with increase in surfactant fraction was observed. An extensive study with Enordet X2001 (A) has also supported the previous observations.

In this experimental system, we can expect two limiting case results which are well known. One is the pure dense CO<sub>2</sub> flow, and the other is the water flow only.

In our laboratory, we have investigated these limiting cases. One limiting case, namely the flow of pure dense CO<sub>2</sub> on the presence of residual brine, was carried out by using Rock Creek sandstone. Fig. 4.10 shows that the pure dense CO<sub>2</sub> has high mobility compared to that of a simultaneous flow of 0.1% Chembetaine BC-50 and dense CO<sub>2</sub>. Also, Fig. 4.11 shows the mobility measured during simultaneous immiscible flow of surfactant-free 1.0% brine with dense CO<sub>2</sub>. It shows also that this mobility is higher compared to 0.05% Enordet X2001. These two figures actually verify the amount by which the surfactant solution lowers the mobility. Tables 4.3 and 4.4 show the apparent foam mobility magnitudes for both cases.

#### 4.3.5.3 The Effect of Rock Sample Permeability

The effect of rock sample permeability has also been investigated. Two different kinds of sandstone were studied--Rock Creek sandstone with a permeability of 14.8 md and Berea sandstone with an average permeability of 305 md. The permeability of these rocks was measured by using 1% brine solution. Fig. 4.12 presents graphically the effect of rock sample permeability. The numerical values of the points on the figure are presented in Table 4.5. We can see from the figure that the magnitude of the relative mobility for the Rock Creek sandstone is approximately 36 times higher than the Berea sandstone, although the inverse ratio of permeabilities is only about 21.

# $\lambda$ vs. $v$

(CO<sub>2</sub>-87-272)

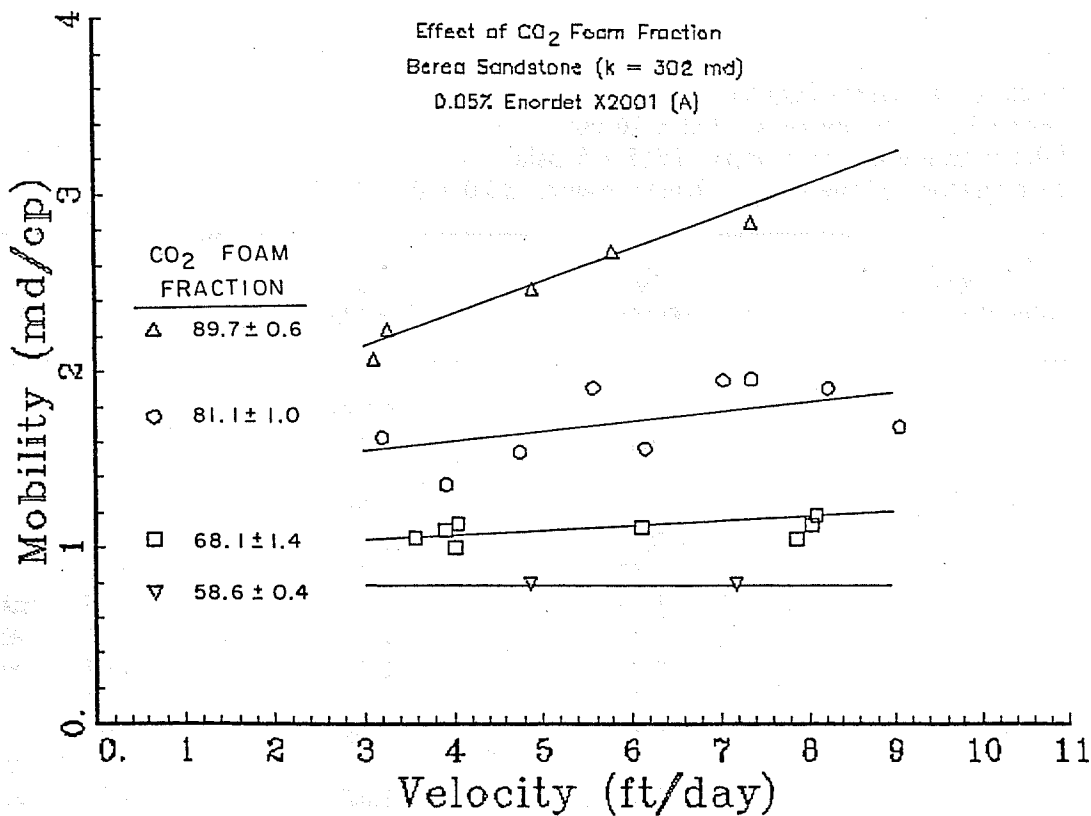


Figure 4.9. Effect of CO<sub>2</sub> fraction.

Table 4.2

CO<sub>2</sub>-Foam Mobility Measurements

Effect of CO<sub>2</sub> Foam Fraction  
0.05% Enordet X2001 (A) in 1% Brine\*

Rock Type: Berea Sandstone  
Permeability of the rock: 302 ± 16 md  
Inlet pressure of the pumps: 1615 ± 5 psia  
Temperature of the CO<sub>2</sub> in Ruska pump: 25.0 ± 0.2°C

CO <sub>2</sub> (Quality,** %)	v (ft/day)	λ (md/cp)	λ <sub>r</sub> (10 <sup>-3</sup> x cp <sup>-1</sup> )
58.6 ± 0.4	4.86	0.785	2.60
	7.17	0.791	2.62
68.1 ± 1.4	3.57	1.05	3.48
	3.91	1.10	3.64
	4.02	0.998	3.31
	4.05	1.13	3.75
	6.12	1.11	3.67
	7.86	1.05	3.47
	8.04	1.13	3.73
	8.10	1.18	3.91
81.1 ± 1.0	3.20	1.62	5.37
	3.92	1.35	4.48
	4.75	1.54	5.10
	5.57	1.91	6.32
	6.17	1.56	5.16
	7.03	1.95	6.46
	7.36	1.96	6.49
	8.23	1.91	6.32
	9.04	1.69	5.60
89.7 ± 0.6	3.12	2.07	6.85
	3.27	2.24	7.42
	4.88	2.47	8.18
	5.79	2.68	8.87
	7.36	2.85	9.44

\*Standard brine solution is made of 0.5% NaCl and 0.5% CaCl<sub>2</sub>.

\*\*Quality is the volume fraction of the CO<sub>2</sub>.

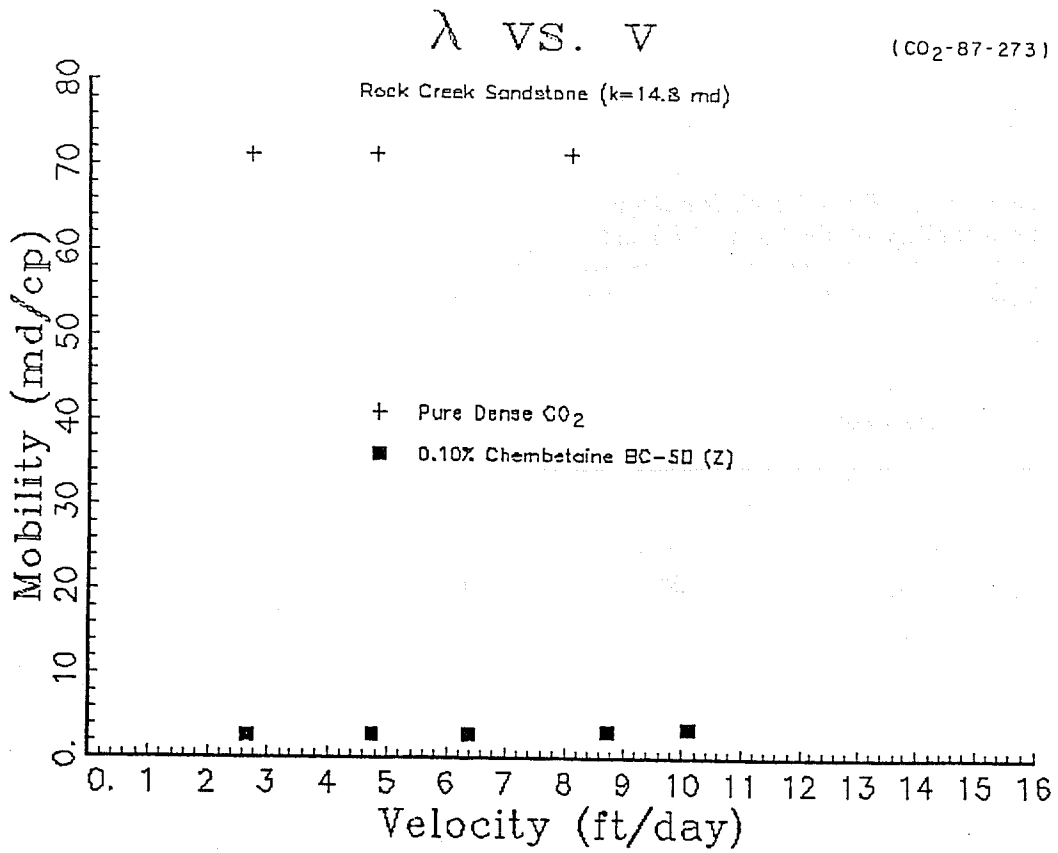


Figure 4.10. Pure dense CO<sub>2</sub> flow.

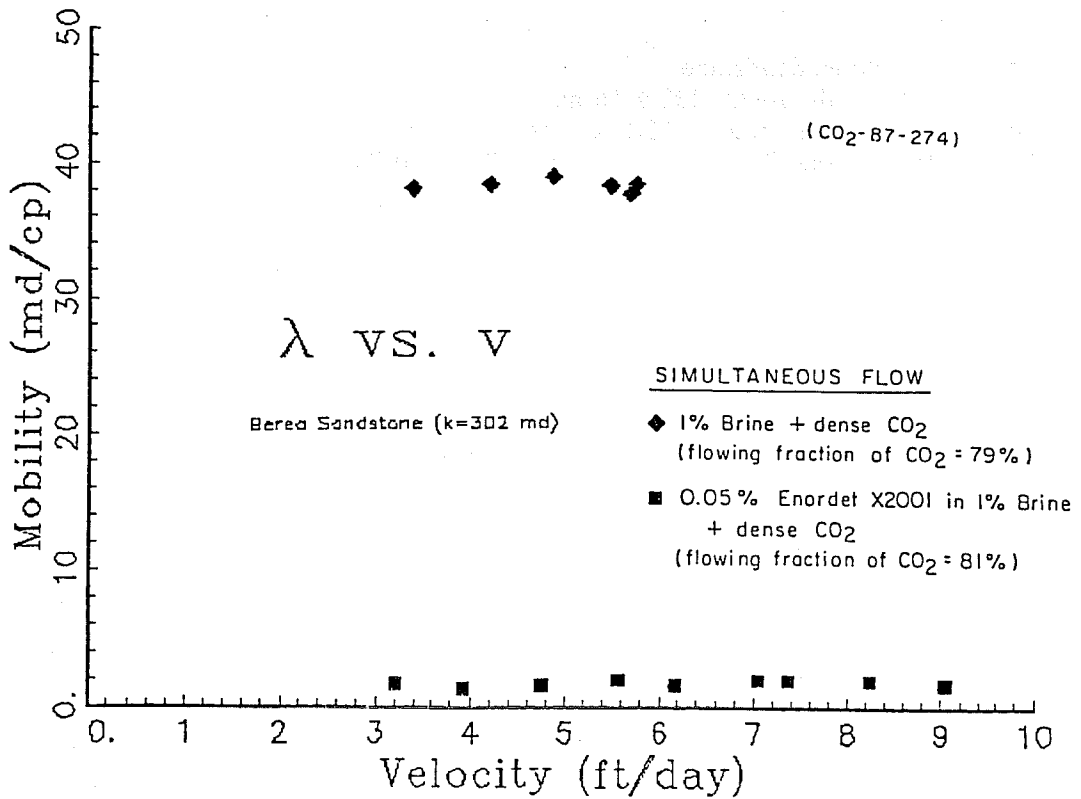


Figure 4.11. Immiscible simultaneous flow of brine and dense CO<sub>2</sub>.

Table 4.3

Pure Dense CO<sub>2</sub> Flow

Rock type: Rock Creek Sandstone

Permeability of the rock: 14.8 md

Inlet pressure of the pumps: 1615 ± 5 psia

Temperature of the CO<sub>2</sub> in Ruska pump: 23.0 ± 0.2°C

v (ft/day)	λ (md/cp)	λ <sub>r</sub> (cp <sup>-1</sup> )
2.72	71.3	4.82
4.82	71.3	4.82
8.10	71.3	4.82

Table 4.4

Immiscible Simultaneous Flow of CO<sub>2</sub> and 1% Brine \*

Rock type: Berea Sandstone

Permeability of the rock: 302 ± 16 md

Inlet pressure of the pump: 1615 ± 5 psia

Temperature of the CO<sub>2</sub> in Ruska pump: 25.0 ± 0.2°C

v (ft/day)	λ (md/cp)	λ <sub>r</sub> (cp <sup>-1</sup> )	CO <sub>2</sub> (quality,** %)
3.37	38.1	0.126	75.9
4.19	38.5	0.127	77.7
4.86	39.1	0.129	87.2
5.46	38.5	0.128	77.1
5.68	37.9	0.125	78.0
5.74	38.6	0.128	78.3

\*Standard brine solution is made of 0.5% NaCl and 0.5% CaCl<sub>2</sub>.\*\*Quality is the volume fraction of the CO<sub>2</sub>.

$\lambda_r$  VS.  $V$

(CO<sub>2</sub>-87-275)

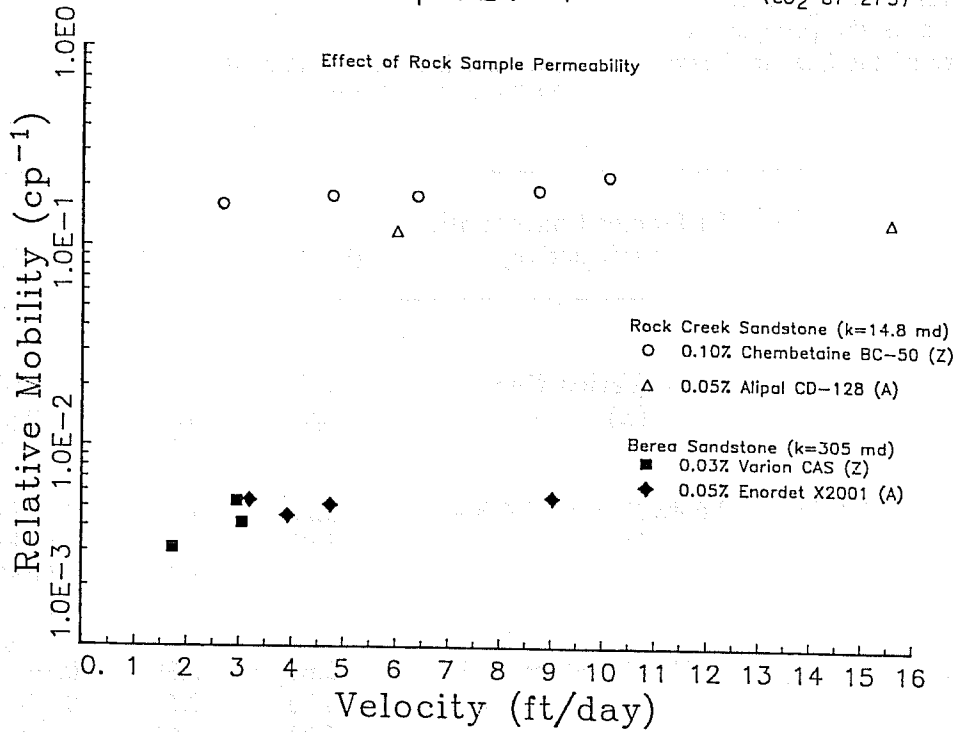


Figure 4.12. Effect of rock sample permeability.

Table 4.5

CO<sub>2</sub>-Foam Mobility Measurements

## Effect of Rock Sample Permeability

Foam fraction of CO<sub>2</sub>: 81.0 ± 0.92

Inlet pressure of the pumps: 1615 ± 5 psia

Temperature of the CO<sub>2</sub> in Ruska pump: 25.0 ± 0.2°C (Berea Sandstone)

23.0 ± 0.2°C (Rock Creek Sandstone)

Rock Type (Sandstone)	k (md)	Surfactant Concentration (wt% active)	v (ft/day)	λ (md/cp)	λ <sub>r</sub> (cp <sup>-1</sup> )
Berea	308 ± 9	0.03% Varion CAS (Z)	1.73	0.953	0.00309
			2.97	1.64	0.00531
			3.60	1.28	0.00414
Berea	302 ± 16	0.05% Enordet X2001 (A)	3.20	1.62	0.00537
			3.92	1.35	0.00448
			4.75	1.54	0.00510
			9.04	1.69	0.00560
Rock Creek	14.8	0.10% Chembetaine BC-50 (Z)	2.66	2.39	0.161
			4.76	2.63	0.178
			6.38	2.67	0.180
			8.73	2.87	0.194
			10.1	3.41	0.230
Rock Creek	14.8	0.05% Alipal CD-128 (A)	6.00	1.78	0.120
			15.6	2.07	0.140
			37.5	2.22	0.150
			75.0	2.07	0.140
			141	2.75	0.186
			212	3.70	0.250
		278	4.23	0.286	

Furthermore, two different kinds of surfactant were tested with each rock sample. Concentrations of 0.1% Chembetaine BC-50 (Z) and 0.05% Alipal CD-128 (A) were used along with Rock Creek sandstone. With Berea sandstone, 0.03% Varion CAS (Z) and 0.05% Enordet X2001 (A) were used. It is evident that the effect of sample permeability overshadows that of surfactant type, at least in these sandstone samples.

Fig. 4.13 shows the plot of relative mobility versus velocity using Alipal CD-128 (A). This test was done by using Rock Creek sandstone with flow rates up to 280 ft/day. This and the higher flowing fraction curves on Fig. 4.9 show a somewhat similar trend--that the relative mobility increases with increasing velocity. It seems this feature is more clearly developed at high flow rates.

The classical shear thinning or pseudoplastic behavior exhibits a nearly constant  $Q/\Delta P$  ratio for small values of  $\Delta P$ , although it increases by as much as two orders of magnitude with increasing  $\Delta P$ . Thus the resistance of such fluids to the applied  $\Delta P$  is decreasing as if these materials are "yielding." The dependence of  $\text{CO}_2$ -foam mobility on velocity is not this extreme, but some "shear thinning" is evident.

#### 4.3.5.4 Conclusions

At this stage, it is premature to make any comments on the effect of the type of the surfactant, such as anionic, zwitterionic, etc. However, from our research on  $\text{CO}_2$ -foam mobility measurements, we have drawn a few significant conclusions on foam flooding.

Apparently, rock sample permeability has a very strong effect on foam mobility. The tests show that  $\text{CO}_2$ -foam is not equally effective in all porous media. They indicate that the relative reduction of mobility caused by foam is much greater in the higher permeability rock. Although the quantitative exploration of this effect cannot be considered complete on the basis of these tests alone, the result raises two important points. One is the hope that by this mechanism, displacement in heterogeneous rocks can be rendered even more uniform than could be expected by the decrease in mobility ratio alone. The second point is that because the effect is not linear, the magnitude of the ratio cannot be expected to remain the same at all conditions. Further experiments of this type are therefore especially important in order to define the numerical bounds of the effect.

The effect of concentration on foam mobility can be clearly seen from Fig. 4.8. In the case of Varion CAS (Z), an increase beyond 0.03% of its concentration seemed to secure no further decrease in mobility. A similar result has also been observed with Chembetaine BC-50 (Z) where 0.05% and 0.1% had similar magnitudes of mobility, although results are not shown here. At this time, we have only tested Enordet X2001 (A) at the 0.05% concentration level. We plan to run some higher concentrations to see whether a similar effect will be evident for that surfactant. In general, these tests have demonstrated that only minor reduction of  $\text{CO}_2$ -foam mobility occurs when the surfactant concentration is less than the Critical Micelle Concentration (CMC) measured in the classical macroscopic laboratory test. The mobility decreases continuously as the concentration is increased above the CMC, however, until it reaches a minimum value when the surfactant concentration has reached about twenty-five times the CMC (the number may only be precise for the particular surfactant used in this detailed test). No further appreciable mobility reduction results from increases in surfactant concentration beyond this level. Only further tests can determine whether this ratio of the "maximum useful level of concentration in the rock" will itself depend on rock type or other variables. This variation promises to be of great value in tailoring the desired amount of mobility reduction in a particular reservoir situation.

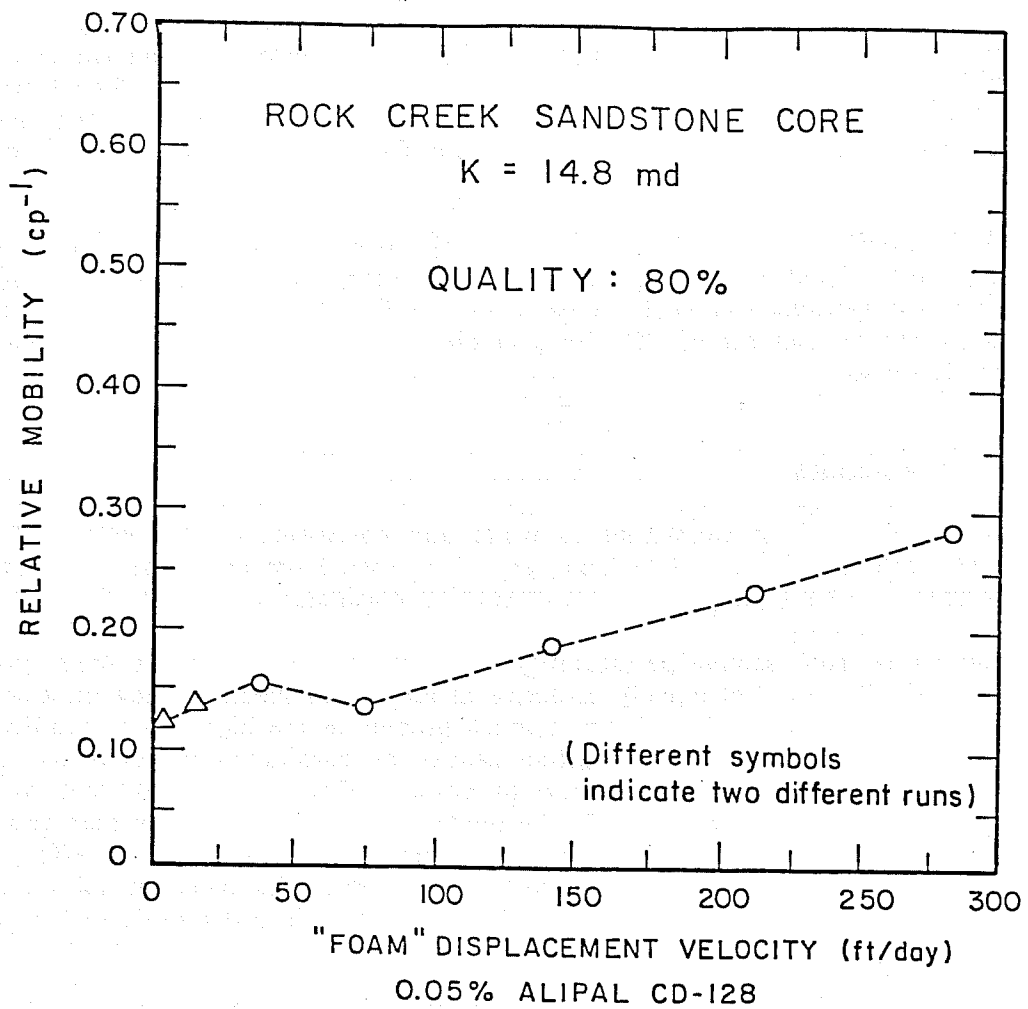


Figure 4.13. Relative mobility of CO<sub>2</sub>-foam at high velocity range.

The effect of the CO<sub>2</sub> flowing fraction or foam quality was well demonstrated by using Enordet X2001 (A). We also observed the same trend with other surfactants, such as Chembetaine BC-50 (Z) and Varion CAS (Z), even though the data were not presented here. Generally, when a significant variation was found - the measured mobility was higher when the flowing ratio was higher (that is, when the "foam" contained a higher proportion of CO<sub>2</sub>). Thus, a greater mobility reduction in foam mobility can be expected in the field by the use of a higher proportion of surfactant solution in the injected mixture.

In addition to the above experiments, Figs. 4.10 and 4.11 show the effect of surfactant in the aqueous phase. The figures support the idea that in the presence of surfactant solutions, the dense CO<sub>2</sub> becomes discontinuous as foam lamellae are formed by the aqueous phase. This, it is postulated, is the mechanism responsible for lowering mobility. As shown in Fig. 4.10, pure dense CO<sub>2</sub> flow has very high mobility even in the presence of residual brine, and mixed flow of immiscible brine with dense CO<sub>2</sub> flow also has high mobility because without surfactant no foam lamellae can be produced.

Furthermore, the effect of velocity or total flow rate on relative mobility has been investigated and is shown in Figs. 4.12 and 4.13. These display some shear thinning or pseudoplastic behavior, which is, of course, the more favorable "non-Newtonian" behavior for foam mobility control.

This shear thinning behavior seems quite minimal in the low velocity range, but can be observed at very high flow rate, as with Alipal CD-128 (A) on Rock Creek sandstone as shown in Fig. 4.13.

To verify the reproducibility of all these experimental points, some of the measurements were purposely repeated. A typical data set, such as those with a CO<sub>2</sub> fraction of  $81.1 \pm 1.0\%$  and of 0.05% Enordet X2001 (A) was used to do some standard error analysis. The relative error on the mobility measurements was approximately 4%. The error was judged to arise primarily from the uncertainties in the total flow rate, due to the difficulty of maintaining "ideal" steady state, because CO<sub>2</sub> is a compressible fluid. In addition, the flow rate is measured by using a Validyne differential pressure transducer, which produces some uncertainty even though it has been calibrated against a dead-weight tester, and its zero is frequently checked during the experiment. The small magnitude of the measured pressure drop across the capillary tube means that many measurements are made at the lower end of the range of sensitivity of the Validyne, so that these errors are increased in importance.

A final remark on the surfactants is in order. Both Varion CAS (Z) and Enordet X2001 (A) performed very well on the foam height measurement. Both also showed very promising results on the thermal aging test. These results are tabulated in Table 4.6. Yet, surprisingly, on foam mobility measurements, Enordet X2001 (A) performed far better than Varion CAS (Z). The Enordet X2001 (A) formed a more durable foam and consequently had more elasticity, and it was a slow draining foam. Regretably, Varion CAS (Z) did not do as well as the results shown below in the surfactant screening tests.

These measurements of CO<sub>2</sub>-foam mobility under different conditions have demonstrated the great complexity that exists in the phenomenon of foam flow. While the experiments certainly satisfy the original expectations of the project as expressed in the listed tasks, they do not yet offer completely finalized information by which the reservoir engineer can confidently design a flood. In fact, they point to fruitful directions for further research.

Table 4.6

## Results of Surfactant Screening

Name	Ionic Type	% Active	Estimated CMC Range* (wt% Active)	Foamability**			pH**		
				77°F	150°F	175°F	77°F	150°F	175°F
<u>American Cyanamid Co.</u>									
Aerosol 18	A	35.0	0.005 ~ 0.01	P***	-	-	----not tested----		
Aerosol 22	A	35.0	0.005 ~ 0.01	P	E	E	3.44	2.94	2.68
Aerosol C61	C	70.0	{0.005 (1) 0.1 (2)}	A	A	A	7.64	8.08	8.46
Aerosol OS	A	75.0	0.005 ~ 0.01	P	-	-	----not tested----		
Aerosol MA	A	80.0	0.01 ~ 0.1	P	P	P	2.96	2.80	2.69
<u>Arjay Incorporated</u>									
Arfoam 2386	C	100	0.005	P	E	E	9.03	7.89	7.45
Arnox 930-70	N	100	0.01	P	P	P	3.10	2.86	2.83
<u>Armak Industrial Chemicals Division</u>									
Aromox T/12	Amp.	100	{0.005 ~ 0.01(1) 0.1 (2)}	P	A	A	6.10	6.76	7.24
Aromox C/12	Amp.	50.0	0.005 ~ 0.01	P	A	A	6.32	7.28	crystallized
Aromox DM16	Amp.	40.0	0.005	E	E	E	6.81	7.03	7.35
Aromox DMC	Amp.	40.0	0.005	P	E	E	7.44	7.72	8.06
<u>BASF Wyandotte Corporation</u>									
Plurafac C17	N	100	0.05 ~ 0.1	E	--not tested--		----not tested----		
Pluronic L64	N	100	0.05 ~ 0.1	P	X	X	----not tested----		
Pluronic P85	N	100	{0.01 (1) 0.01 (2)}	A	--not tested--		----not tested----		
<u>Chemron Corporation</u>									
Chembetaine BC-50	Z	40.5	0.01 ~ 0.1	E	E	E	4.15	4.14	4.19
<u>Chevron</u>									
Chevron Chaser® SD 1000	A	42.5	0.001 ~ 0.005	P	X	A	7.55	X	3.48
Chevron Chaser® XP-100	A	12.5	-not tested-	----not tested----		----not tested----			

Table 4.6

(continued)

Name	Ionic Type	% Active	Estimated CMC Range* (wt% Active)	Foamability**			pH**		
				77°F	150°F	175°F	77°F	150°F	175°F
<b>Shell Development (continued)</b>									
Enordet X2002	A	32.5	0.01 ~ 0.05	A	E'	E'	3.04	2.45	2.35
Enordet X2003	A	24.3	0.02 ~ 0.1	E	P	P	3.34	2.62	2.40
Nonanol 2-S	N	50.0	0.3	P	E'	E'	3.83	2.66	2.29
Neodol 25-12	N	100	0.005	E	P	P	2.97	2.48	2.46
Neodol 45-13	N	100	0.005 ~ 0.05	E	E'	E'	2.95	2.40	2.40
Neodol 23-6.5	N	100	0.01 ~ 0.2	E	E'	P	2.94	2.51	2.51
Neodol 91-8	N	100	0.02 ~ 0.1	A	E'	E'	2.97	2.52	2.36
Neodol 25-3A	A	59.5	0.01 ~ 0.05	E	P	P	3.00	1.89	1.78
Neodol 91-2.5 S/32	N	100	0.05 ~ 0.1	E	E'	E'	2.98	2.29	2.57
<b>Sherex Chemical Company</b>									
Arosurf 66-E10	N	100	0.005 ~ 0.05	E	P	P	2.91	2.78	2.63
Arosurf 66E-20	N	100	0.005 ~ 0.05	A	P	P	2.93	2.72	2.32
Varamide MA-1	N	100	0.005 ~ 0.01	E	P	P	2.91	2.71	2.98
Varion CADG-LS	Z	35.0	0.005 ~ 0.01	E	E	E	3.75	3.89	4.07
Varion CAS	Z	35.0	0.001	E	E	E	2.90	2.91	2.96
Varonic 320	N	100	{ 0.001 (1) 0.01 (2)	P	P	E	2.75	2.77	2.69
<b>Stepan Chemical Company</b>									
Biosoft EA-10	N	100	0.01 ~ 0.1	E	E	E'	2.96	2.56	2.54
Makon 4	N	100	0.05 ~ 0.1	P	-	-	----not tested----		
Makon 6	N	100	0.05 ~ 0.1	P	-	-	----not tested----		
Makon 8	N	100	0.01	E	E	E	2.96	2.73	-
Makon 12	N	100	0.005 ~ 0.01	E	E	E	2.98	2.43	2.49
Makon 14	N	100	0.005 ~ 0.01	E	E	E	2.93	2.28	2.72
Makon NF-5	N	100	0.05 ~ 0.2	P	-	-	----not tested----		
Makon NF-12	N	100	0.01 ~ 0.1	P	-	-	----not tested----		
Stepanflo 20	A	40.0	0.005	A	A	A	7.57	3.03	3.03
Stepanflo 50	A	60.0	0.1	E	E	E	3.05	2.35	1.83
Stepanflo 60	A	30.0	0.005 ~ 0.05	E	E	E	2.96	3.69	3.94
Stepanflo 1313	N	100	0.05	E	P	E'	7.03	7.03	3.95
Stepanflo 1343	A	50.0	0.01 ~ 0.1	P	-	-	----not tested----		

Table 4.6

(continued)

Name	Ionic Type	% Active	Estimated CMC Range* (wt% Active)	Foamability**			pH**		
				77°F	150°F	175°F	77°F	150°F	175°F
<u>Westvaco</u>									
Polyfon T	A	100	{ 0.001 (1) 0.01 (2)	P	-	-	----not tested----		
<u>Witco Chemical Corporation</u>									
Witcolate 1247-H	A	40.0	0.05	E	P	P	2.84	2.85	2.91
Witcolate 1259	A	40.0	0.05 ~ 0.1	E	P	P	2.83	1.94	2.59
Witcolate 1276	A	40.0	0.005 ~ 0.01	E	E	E	2.93	2.63	2.33

\*Estimated CMC range includes both surface and interfacial tension measurements at room temperature.

\*\*Foamability and pH are measured at 28th day of thermal aging.

\*\*\*E = excellent; A = average; P = poor; X = not tested;

' = highest concentration; - = no further test necessary.

In particular an exciting new possibility has been opened up. This is the possibility that a new mechanism may exist, by which CO<sub>2</sub>-foam can further improve displacement uniformity, in the proper ranges of operating parameters. Additional laboratory and analytical work is needed, and is planned in the continuation of the project.

#### 4.3.6 Surfactant Screening

##### 4.3.6.1 Review of Surface Chemistry and Surfactant for Foams

Surfactants are molecules that consist of a hydrophilic group with a strong attraction for the solvent, and a hydrophobic group with very little attraction for the solvent. For oil-soluble surfactants, the terms are lyophilic and lyophobic, respectively. Water-soluble surfactants are generally classified according to the nature of their solubilizing or hydrophilic group. They are commonly distinguished as anionic, cationic, nonionic (polyethylene-oxide types), and amphoteric surfactants. Zwitterionic surfactants contain both functional groups and have also been identified as amphoteric. Anionic surfactants ionize in solution with a head group carrying a negative charge, and cationic surfactants ionize in solution with a positively charged head group. Nonionic surfactants, of course, do not ionize in solution. Amphoteric or ampholytic surfactants ionize in solution with the ion carrying either a positive or negative charge depending upon the pH of the solution.

The amphipathic nature of surfactants causes the molecules adsorbed at the interface to be oriented (usually) with the hydrophilic portions turned towards the water and the hydrophobic portions oriented away from the water. This orientation is an important factor in determining the change in the properties of the interface produced by the surfactant upon adsorption there. The properties of an interface with adsorbed molecules may vary greatly, depending upon the particular orientation of these molecules with respect to the interface (Schwartz, Pery, & Berch, 1952; Osipw, 1962).

Surface tension reduction in aqueous media depends upon the replacement of water molecules from the interior of the solution; the adsorption at the surface of surfactant molecules results in a lowering of the surface tension of the water.

For many surfactants, and in the lower range of concentration, the surface tension of the solution decreases almost linearly with the logarithm of the concentration. In this range, the surfactant molecules dissolve as individual molecules. However, as the amount of the surface active agent in solution is increased, a critical concentration is reached (the value of which is dependent upon the structure of the surfactant) at which a further increase in the amount of dissolved surfactant causes no significant changes in the surface tension measurements. This abrupt change coincides with the first formation of the micelles and is dependent upon the critical micelle concentration (CMC), the narrow concentration range in which surfactant ions or molecules begin to aggregate and form micelles. Above the CMC, the surface tension stays nearly constant because the concentration of the individual molecules at the surface remains nearly constant, even when the surfactant concentration increases significantly. Other physical properties, such as osmotic pressure, electrical conductivity, viscosity, etc., also show sharp changes at the CMC (Rosen, 1972).

##### 4.3.6.2 Surfactant Screening Results

The above-described steady-state measurements of CO<sub>2</sub>-foam mobility were carried out with several surfactants, in part to reveal the differences between them. Prior to these more time-consuming experiments, however, a much larger set of surfactants was screened in other tests, to

indicate their general suitability for use in this EOR process. In the tests described below, we have screened 88 surfactants from various manufacturers.

As a general indication of the ability of the surfactant to produce a "foam-like dispersion" with a dense non-polar fluid, atmospheric pressure tests are run in a standard shaking apparatus, using the light hydrocarbon isooctane to simulate high-pressure, dense CO<sub>2</sub>. With the aid of this device, and utilizing an acidified surfactant solution rich in calcium as well as sodium ions as a synthetic oilfield brine in contact with CO<sub>2</sub>, the effectiveness and chemical stability of the surfactants was tested by prolonged exposure to moderately high temperatures. These tests were also supplemented by measurements of the surface tension (against air) and the interfacial tension (against isooctane) in order to obtain consistent values of the CMC for each surfactant, for comparison to the mobility measurements as noted above. Our general goal was to understand the nature of the surfactants and to classify them as excellent, average, and poor foamers. The tests and their outcomes are described below.

Three characteristics have been tested: surface and interfacial tensions; foam height at room temperature (77°F), and after 28 days of thermal aging at 150°F and 175°F; and pH, measured before and during the thermal aging process.

All results are presented in Table 4.6. Also, a few good foamers have been selected and grouped according to their functional types, for display here of the variation of the surface and interfacial tensions with concentration. These are shown in Figs. 4.14 to 4.31. These measurements were made as described in the next section. Using the basic techniques of analytical chemistry, 1% brine solution was prepared. Its pH value was initially adjusted to 2.88. All of the various concentrations of surfactants were prepared by using the above described "acidified brine" solution.

#### 4.3.6.3 Measurements of Surface and Interfacial Tensions

The measurements of surface and interfacial tensions were done by using the Wilhelmy plate method in a Rosano surface tensiometer. A standard procedure described in the manual was carefully followed. Surface tension was measured against air, whereas interfacial tension was measured against isooctane. Figs. 4.14-4.31 present the apparent equilibrium surface/interfacial tensions as functions of concentration. These are the typical plots which are also reported in column 4 in Table 4.6, to observe the CMC range.

We have classified the surfactants into five categories: anionic (A), amphoteric (Amph.), cationic (C), nonionic (N), and zwitterionic (Z). The anionic (Figs. 4.14-4.17) and nonionic surfactants show a typical standard curve. All of these surfactants show a distinctive CMC range (Figs. 4.14-4.17), with smooth curves that indicate almost pure surfactant.

The amphoteric surfactants showed relatively low interfacial tension measurements. All of the four interfacial tension curves presented in Figs. 4.18-4.21 show values of zero on the scale of the graphs. We have obtained zero values due to the limitation of the plate method measuring device, which is incapable of measuring tensions less than about 1 dyne/cm. For such low values, the spinning drop tensiometer would be more suitable, if an exact value in this range had been sought.

Figs. 4.22 and 4.23 present the cationic surfactants. Because cationic surfactants are not favorable for use in sandstones, we have not tested many of these samples. The surfaces of sandstone are negatively charged, and we wanted to avoid excessive adsorption of surfactant on the rock sample. One of the cationic surfactants shows two CMC values, a commonly observed feature. These multiple values of CMC are probably due to the presence of more than one functional group.

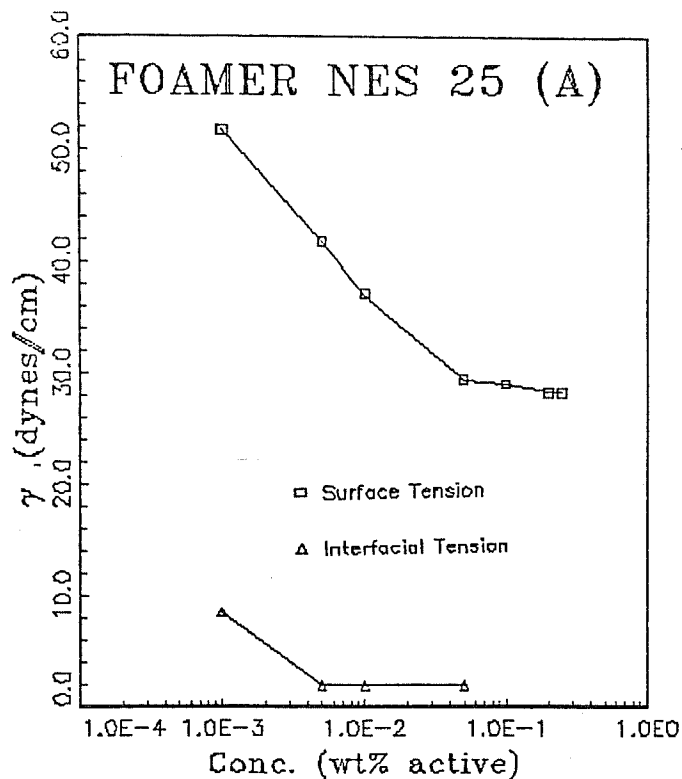


Figure 4.14. Measurements of anionic surface and interfacial tensions, Foamer NES 25(A).

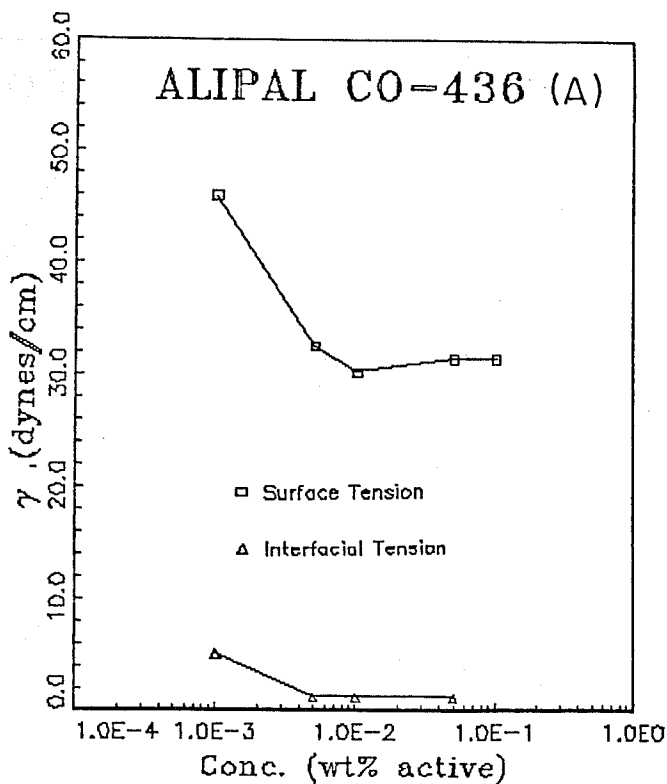


Figure 4.15. Measurements of anionic surface and interfacial tensions, Alipal CO-436 (A).

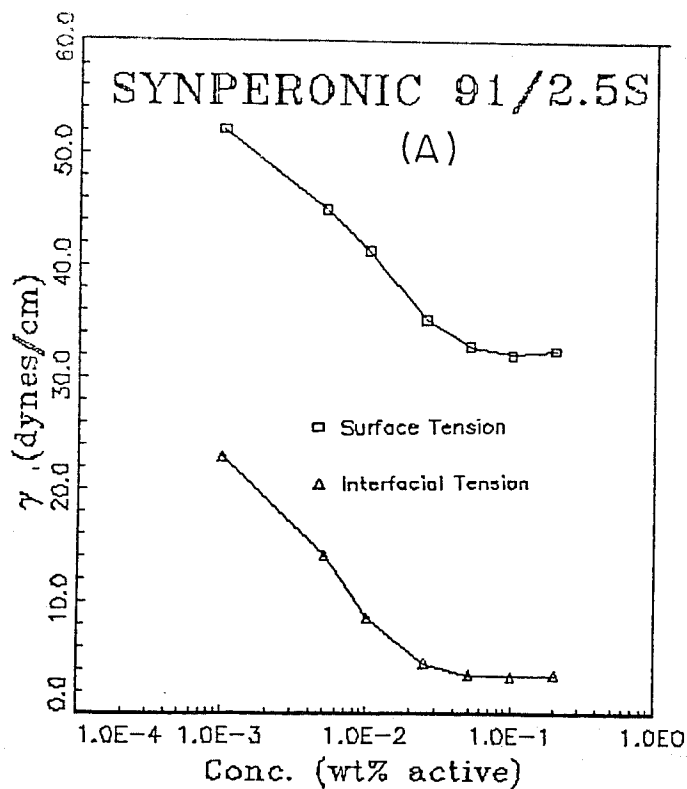


Figure 4.16. Measurements of anionic surface and interfacial tensions, Synperonic 91/2.5S (A).

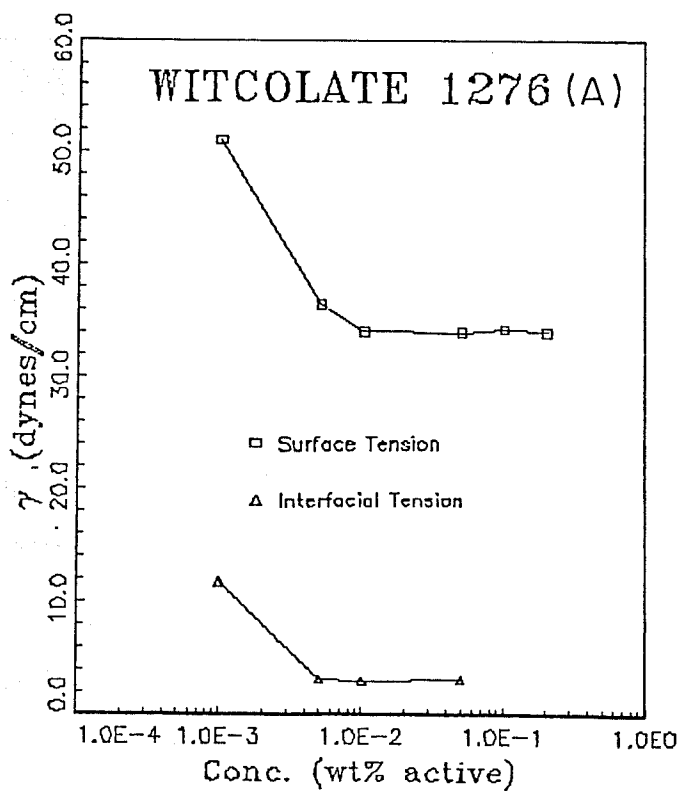


Figure 4.17. Measurements of anionic surface and interfacial tensions, Witcolate 1276 (A).

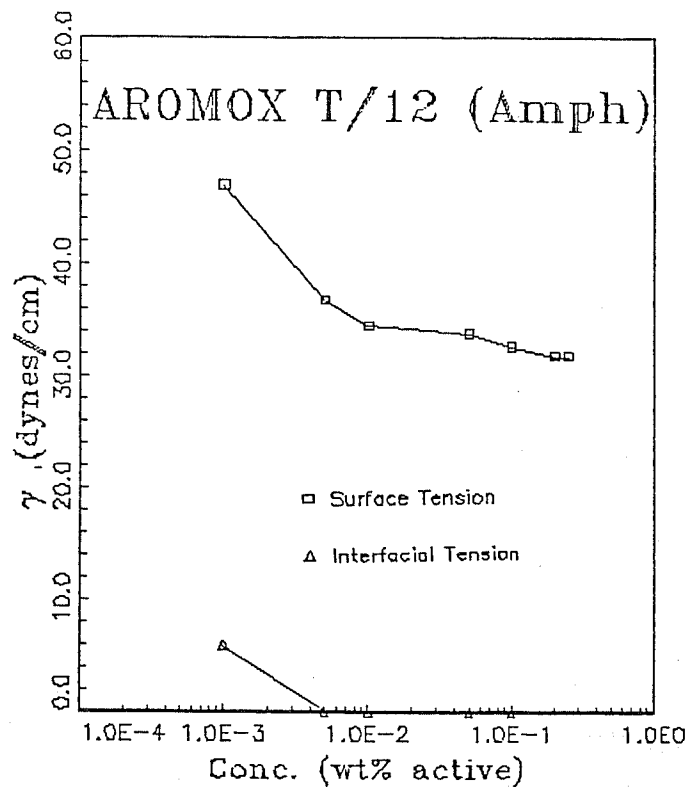


Figure 4.18. Measurements of amphoteric surface and interfacial tensions, Aromox T/12 (Amph).

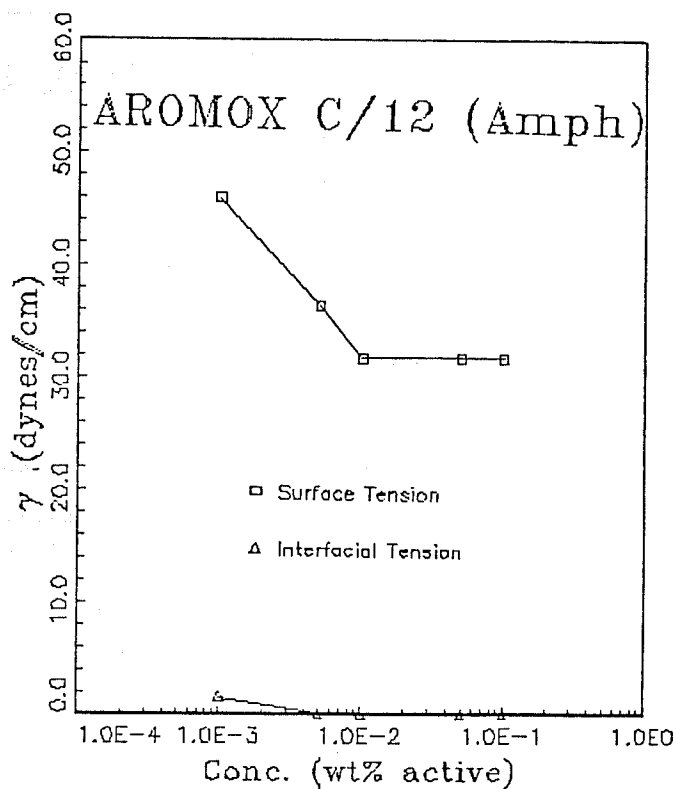


Figure 4.19. Measurements of amphoteric surface and interfacial tensions, Aromox C/12 (Amph).

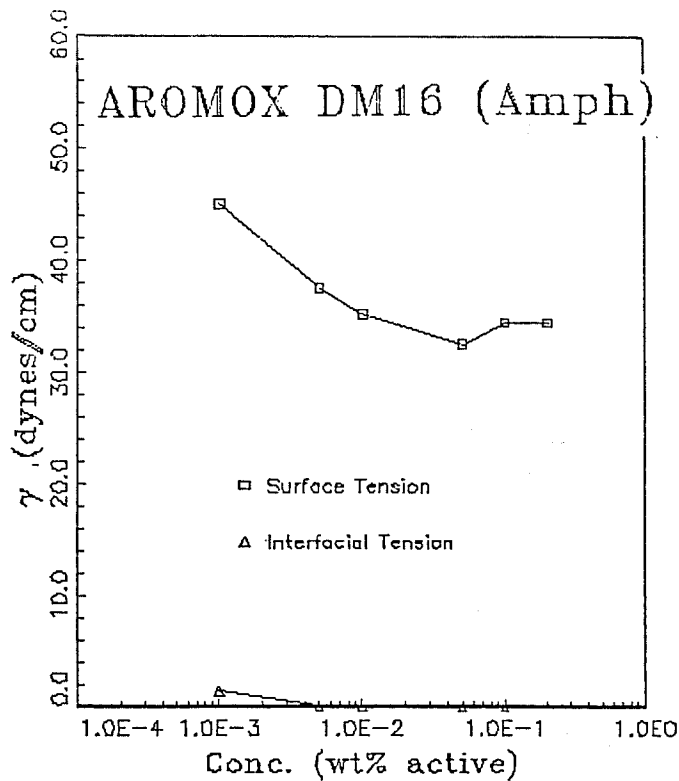


Figure 4.20. Measurements of amphoteric surface and interfacial tensions, Aromox DM16 (Amph).

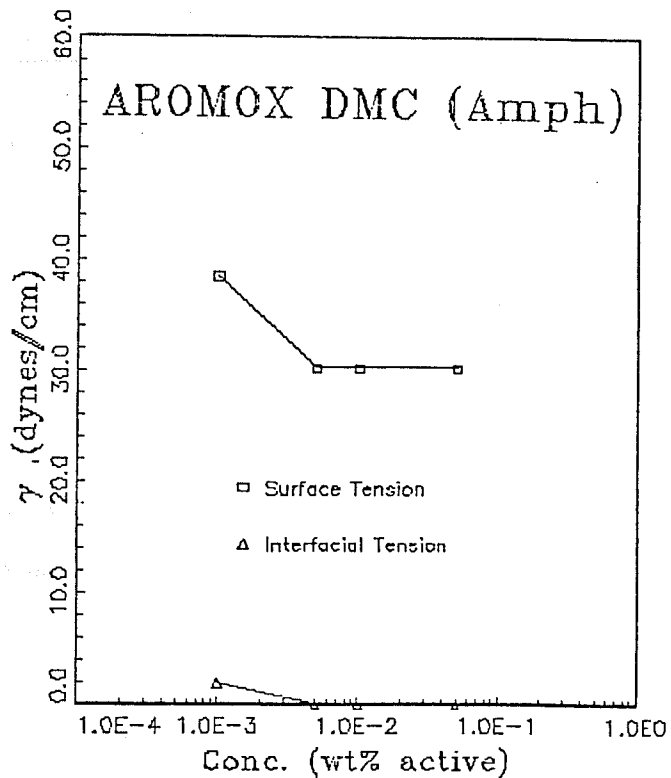


Figure 4.21. Measurements of amphoteric surface and interfacial tensions, Aromox DMC (Amph).

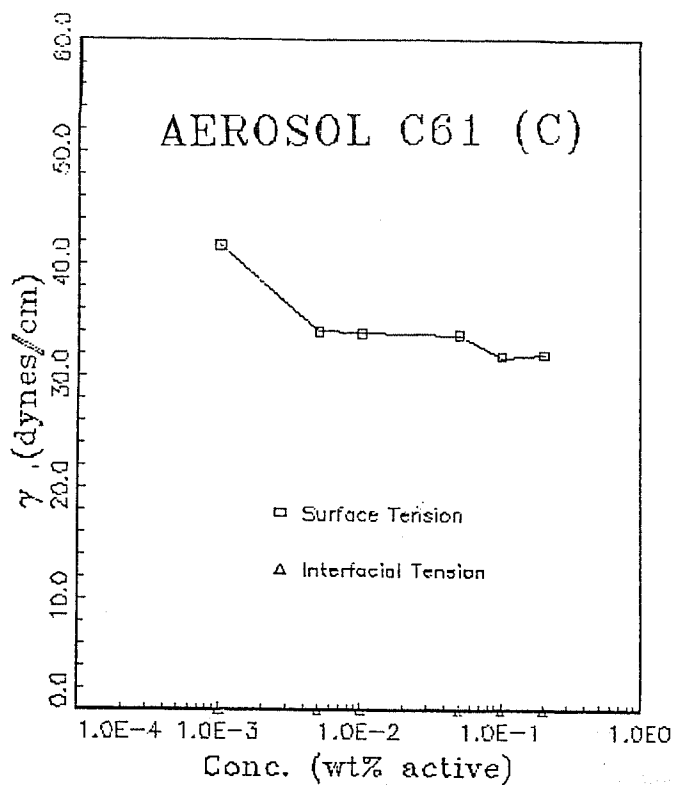


Figure 4.22. Measurements of cationic surface and interfacial tensions, Aerosol C61 (C).

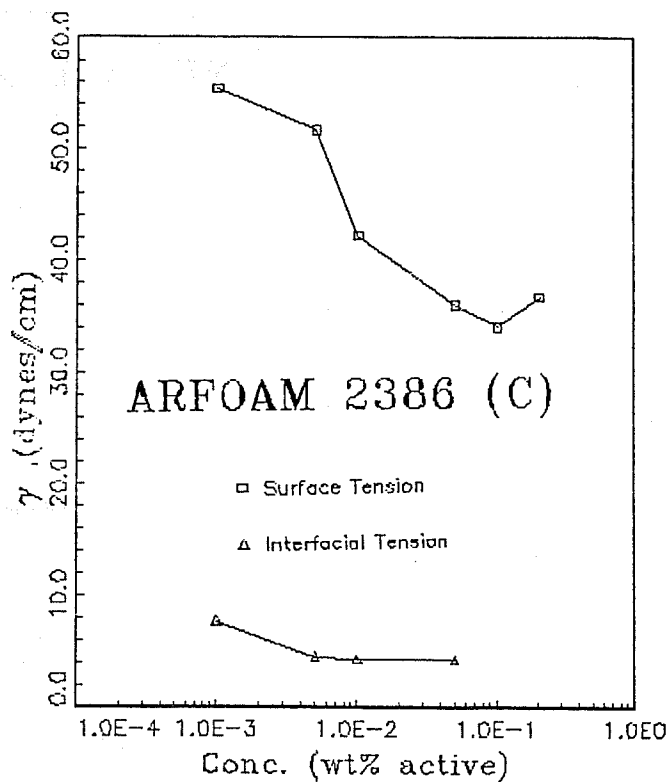


Figure 4.23. Measurements of cationic surface and interfacial tensions, Arfoam 2386(C).

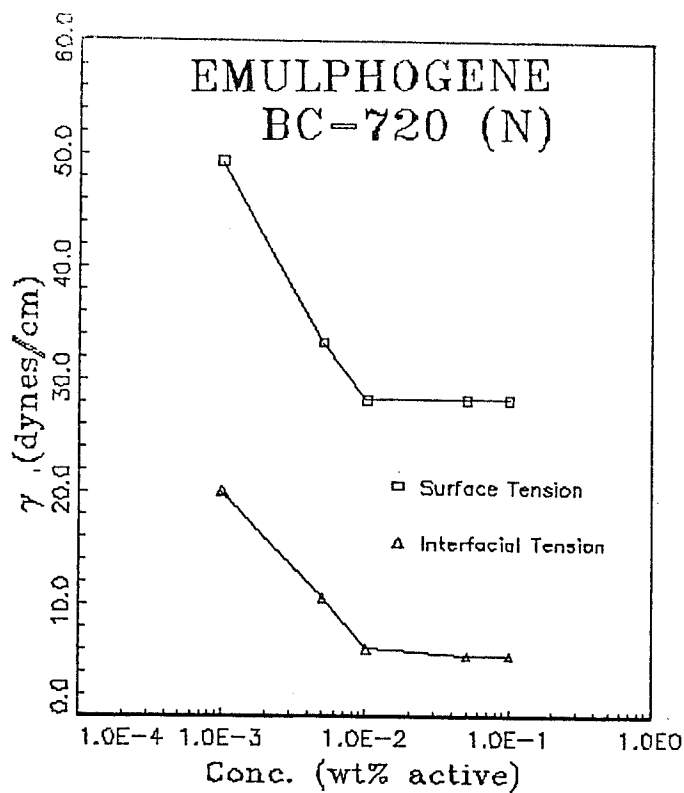


Figure 4.24. Measurements of nonionic surface and interfacial tensions, Emulphogene BC-720 (N).

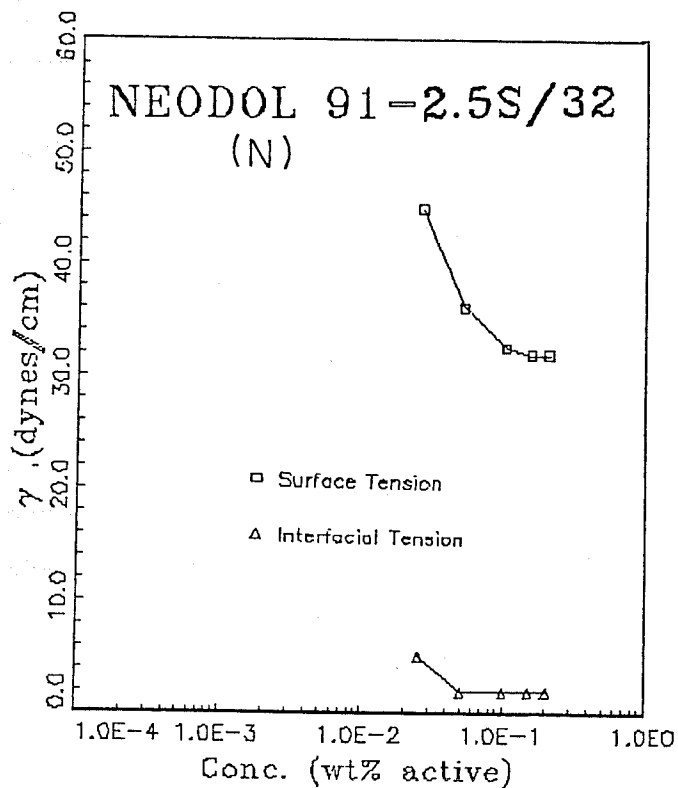


Figure 4.25. Measurements of nonionic surface and interfacial tensions, Neodol 91-2.5S/32 (N).

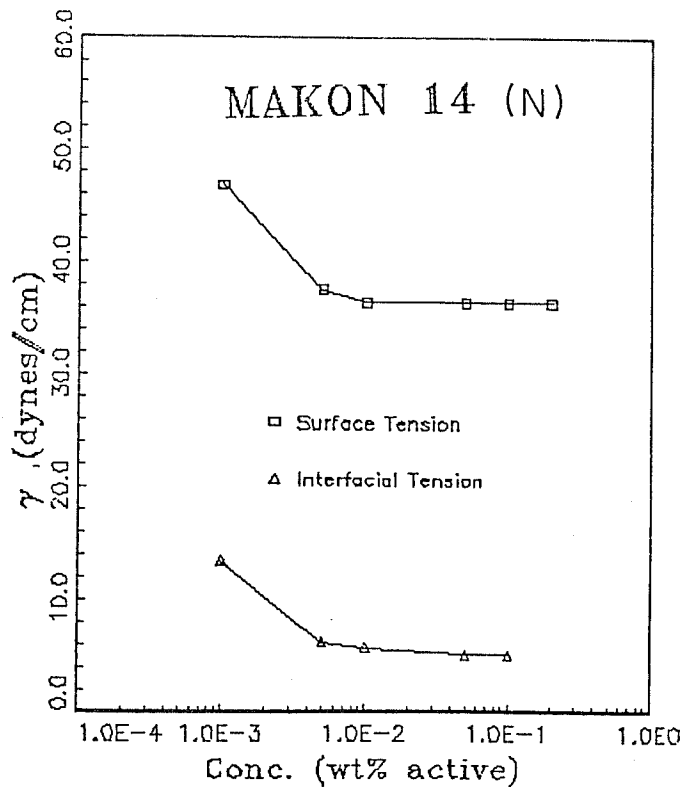


Figure 4.26. Measurements of nonionic surface and interfacial tensions, Makon 14 (N).

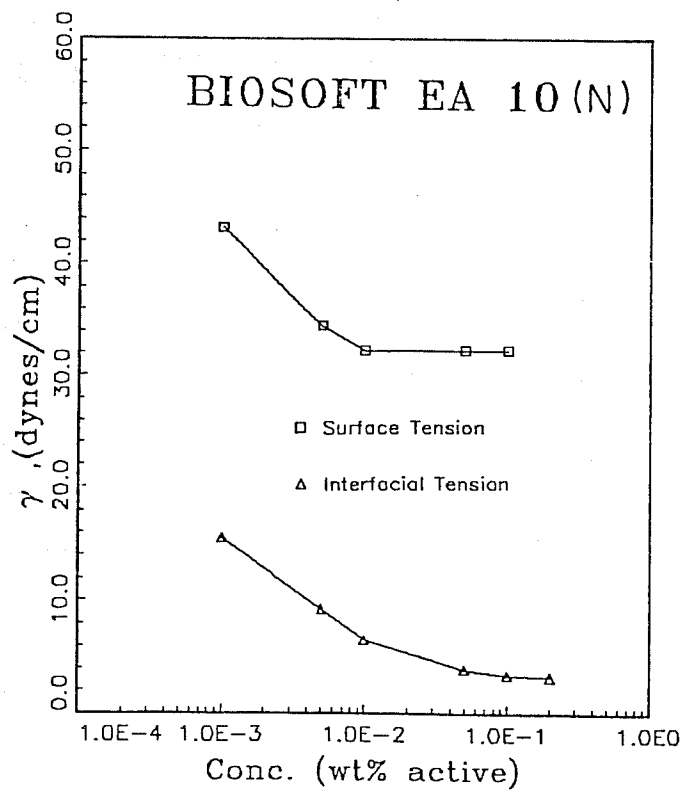


Figure 4.27. Measurements of nonionic surface and interfacial tensions, Biosoft EA 10 (N).

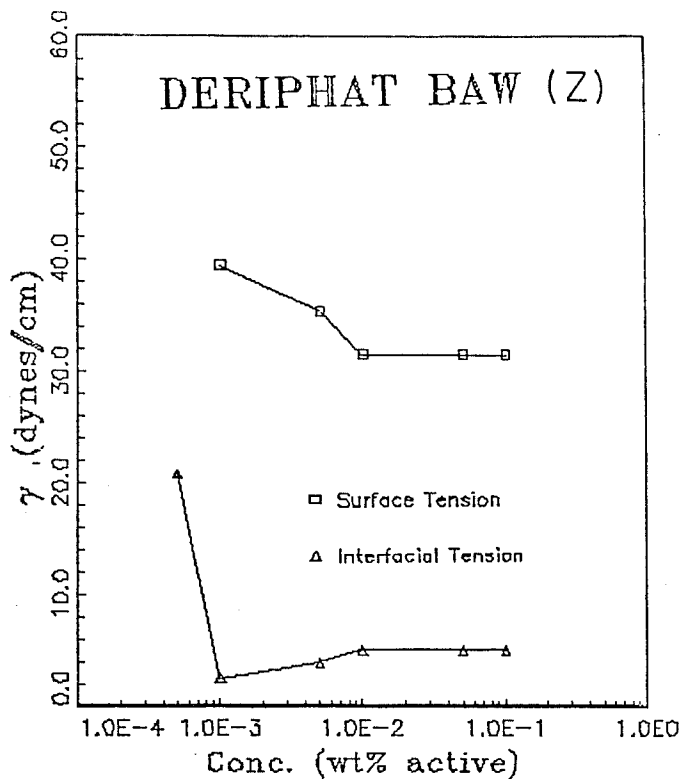


Figure 4.28. Measurements of zwitterionic surface and interfacial tensions, Deriphat BAW (Z).

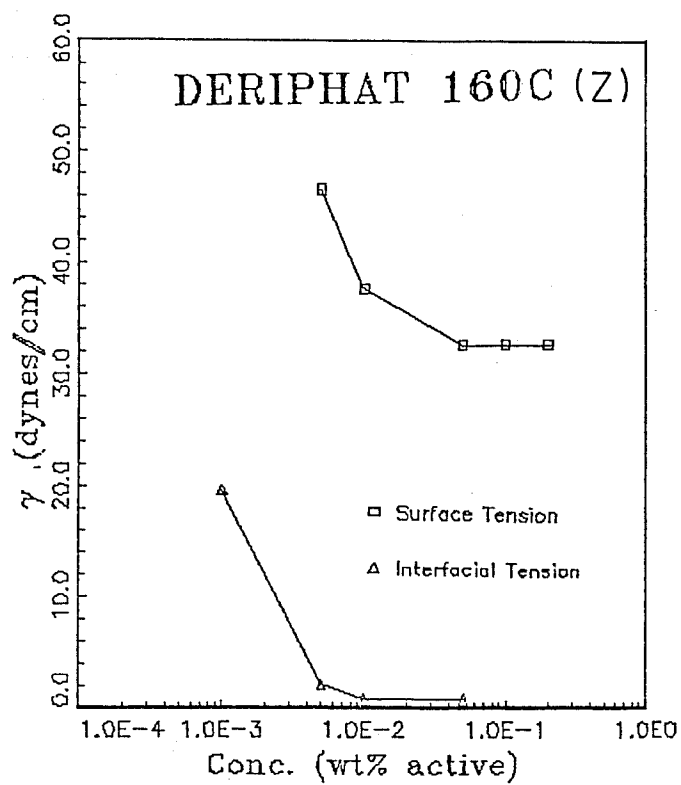


Figure 4.29. Measurements of zwitterionic surface and interfacial tensions, Deriphat 160C (Z).

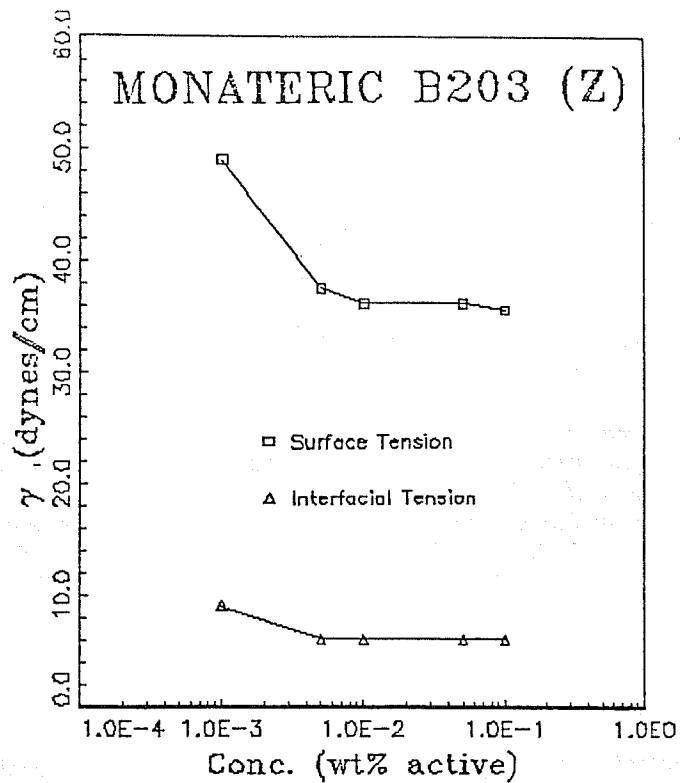


Figure 4.30. Measurements of zwitterionic surface and interfacial tensions, Monateric B203 (Z).

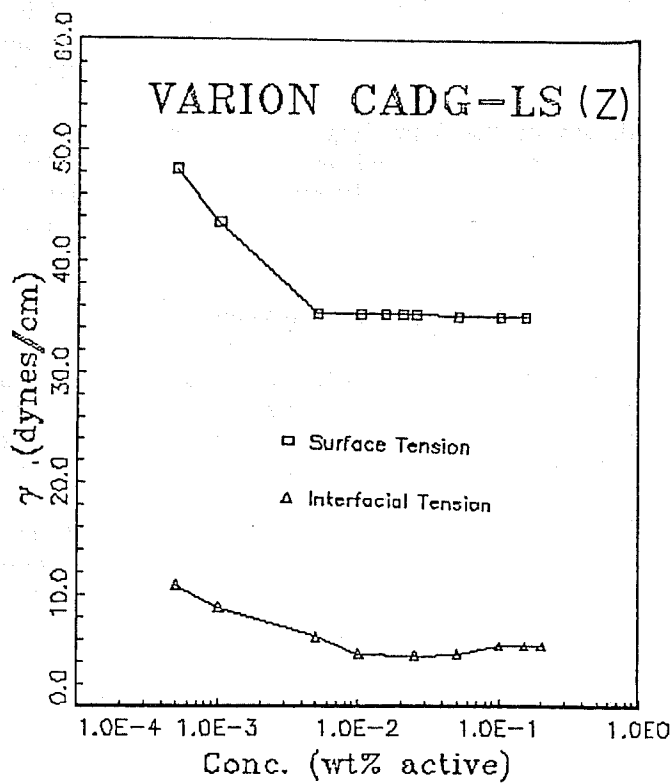


Figure 4.31. Measurements of zwitterionic surface and interfacial tensions, Varion CADG-LS (Z).

The nonionic surfactants are presented in Figs. 4.24-4.27. Again they all showed some standard features. One caution to be observed in using nonionic surfactants is to know the cloud point; it is necessary to avoid the cloud point temperature when carrying out the experiment.

The last category is the zwitterionic surfactants shown in Figs. 4.28-4.31. In many of the cases, the zwitterionic surfactants have a very sharp slope which results in some minimum value.

Although we have measured surface and interfacial tensions of these 88 surfactants, the results for only those surfactants which had the best performance in thermal aging and foam height measurement are presented. All have a clear CMC range with a standard feature: the surface/interfacial tension decreases as the surfactant concentration is increased and eventually reaches a plateau. The start of the plateau marks the CMC range, beyond which no further addition of surfactant can lower the surface or interfacial tensions. As mentioned earlier, this standard feature is an indication of the purity of the surfactant.

#### 4.3.6.4 Measurements of Foam Height

Foam height was measured by a standard measuring device shown in Fig. 4.32. This machine, developed in earlier work on this project, enables consistent reproducible results. These measurements were carried out at room temperature with freshly made solution. Also, the foam height was measured after thermal aging of day 1 and day 28. Here we have reported only the results of foam height at 28 days of thermal aging. We have aged the surfactants at 150°F and 175°F.

The thermal aging test indicates whether the surfactant can withstand high reservoir temperature and still perform well as a foamer. The results are listed in Table 4.6 under "Foamability." The letter E stands for excellent, A for average, and P for poor performance. A letter with prime mark designates that a high concentration was used to test for that particular surfactant.

On the zeroth day of the foam height measurement tests, several concentrations were tested at room temperature. For the thermal aging test, we used only those concentrations which had above-average foam height (from 0 ~ 10 scale on a testing vial). Therefore, for surfactants with poor performance at room temperature, we did not test any further.

#### 4.3.6.5 Measurements of pH after Thermal Aging

The measurements of pH were made with fresh solution and also after an interval of one week. Before the actual pH measurements were made, all solutions were cooled to room temperature. The pH values were recorded to note any thermal decomposition of the surfactants during the process of thermal aging. The precision of our pH meter was to  $\pm 0.02$ .

The initial pH of 2.88 changed during thermal aging, either slightly or drastically according to the surfactants. For instance, all the amphoteric surfactants showed an increase in pH values during aging. On the other hand, most of the anionic and nonionic types remained around the vicinity of the initial pH values. The zwitterionic type showed some deviations from the initial pH value. This difference in pH value shows somewhat the characteristic of the type of surfactant. Again, we did not measure pH values for those surfactants which gave poor foam height performance on the zeroth day.

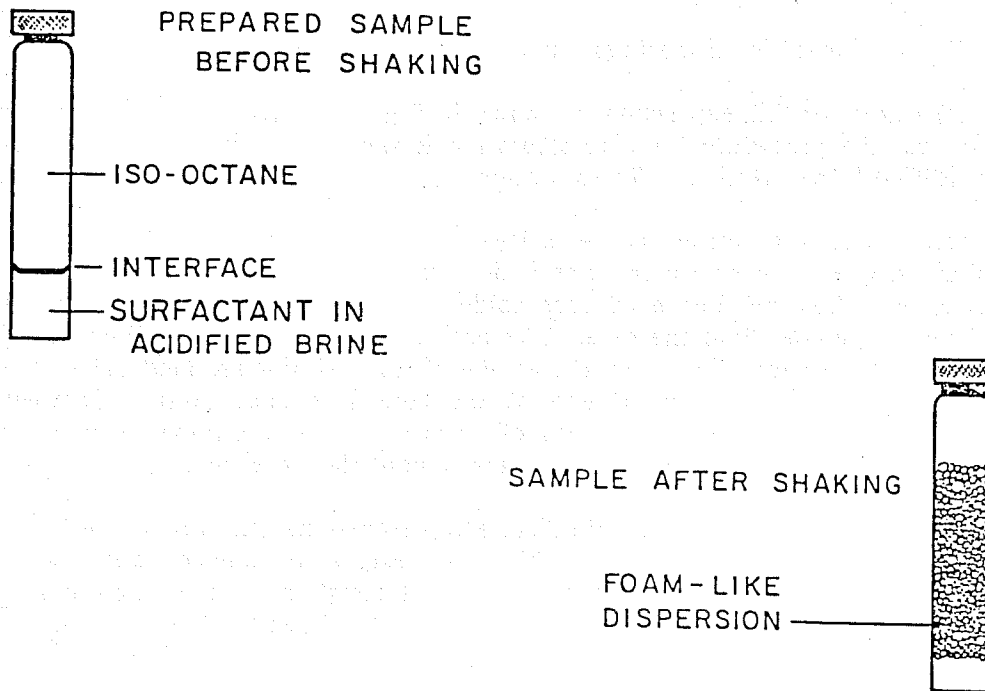
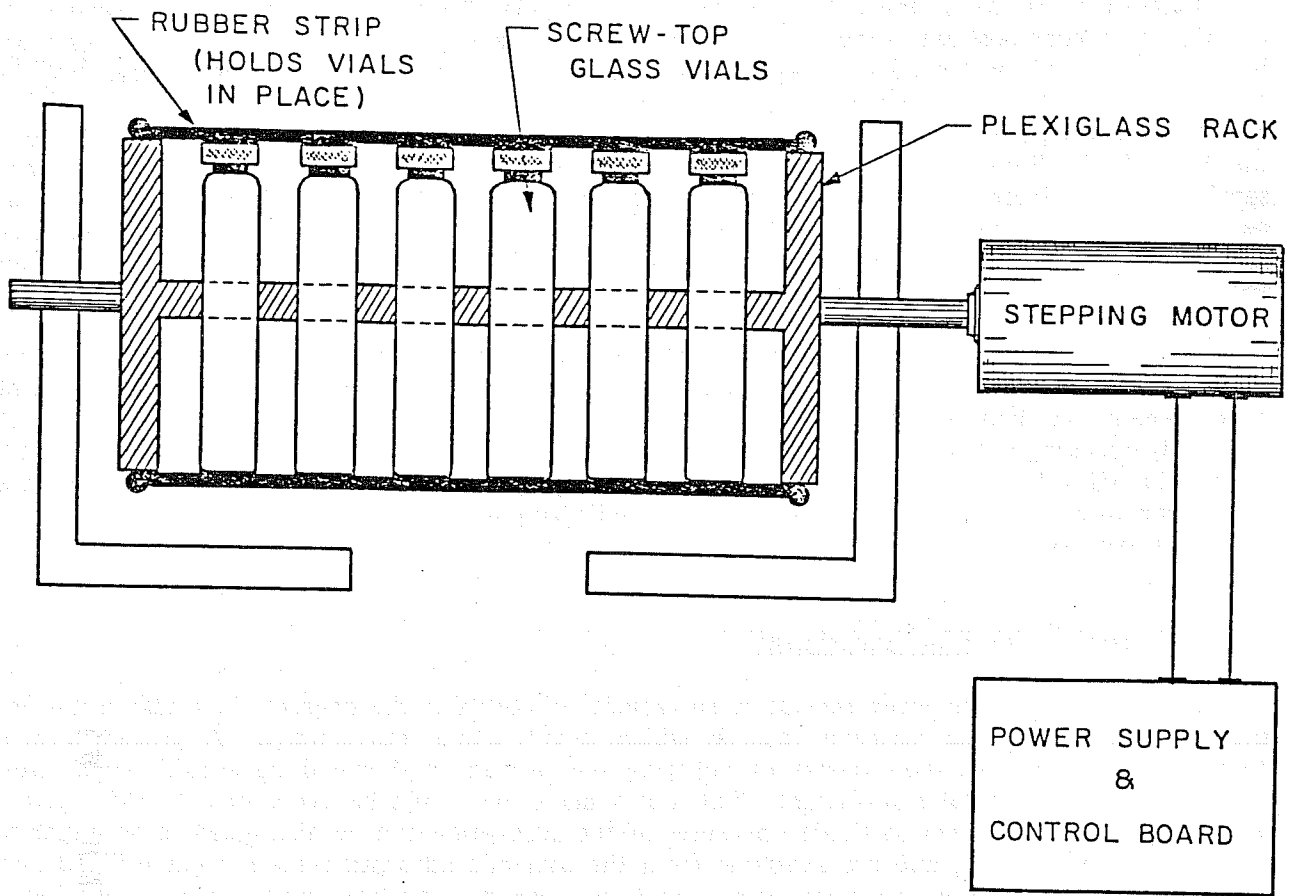


Figure 4.32. Sample shaking machine.

In most of the cases, the pH value decreased with the thermal aging. This demonstrates that the thermal decomposition is occurring during the course of time at the elevated temperature. Some values of pH increased after aging. We suspect that it may be due to the interaction with air since in our standard measurement procedures we open the vial cap weekly as we measure pH. To verify this hypothesis, we prepared a few samples and aged them without opening the vial until the 28th day. From the testing results, we found that some surfactants seemed to be more sensitive to the interaction with air while others were not. The insensitive surfactants did not change much in pH values as we compared with and without opening the cap. On the other hand, the sensitive ones showed that the interaction of surfactant with air sometimes lowered and sometimes raised the pH values during the thermal aging process.

The screening of surfactants gave insight into their performance. We have observed that thermal decomposition does happen during the course of thermal aging, and foam height measurement can help us to distinguish this feature between a good foamer and a poor one. Generally speaking, surfactants with excellent performance on foam height tests showed almost no change in pH values during the period of thermal aging. Also, most of the surfactants showed more drop in pH values at 175°F than at 150°F, indicating an accelerated rate of decomposition, as would be expected.

#### 4.3.7 Dynamic Adsorption Experiment

A further important measurement of surfactant suitability is the degree of its adsorption onto the pore surfaces of the reservoir rock in which it will come into contact. A greater level of adsorption will increase the expense of applying the process, and would be considered a strong mark against any particular surfactant. But it is a mark that could be overcome, if other features were very favorable. Two particular measures of the adsorption can be distinguished as important in reservoir calculations, and are available from the dynamic adsorption experiment utilized here. This experiment, preliminary results from it, and the method of analysis used, are described below. All experiments in this area are not yet complete, and in fact, continuing experiments with different rock types and surfactants are anticipated in the continuing phase of this research.

##### 4.3.7.1 Description of the Experiment and Apparatus

The apparatus for this experiment is shown in Fig. 4.33. At the left side of the figure, inside the dashed box, the procedure for core saturation is shown. Initially, the core tested is saturated with 1% acidified brine solution. The saturation of the core is achieved in the following manner.

The core is put in a Hassler sleeve inside a core holder where overburden pressure is applied outside of the sleeve by using water. Gas is not used, since it has the potential to diffuse through the rubber sleeve. The overburdened core holder is connected to the Isco pump, from which 1% acidified brine is pumped into the core. The needle valve that restricts flow from the output end of the core is opened slightly to allow the escape of air and air-saturated brine. The needle valve which restricts flow from the input end of the core is opened fully. Complete saturation is attained after two or three pore volumes of brine have been pumped through the core under pressure, and this fully saturated core is used throughout the experiment.

The first of two large circles in the figure represents the sampling valve (from Valco Instruments Corp.). This valve has six ports which are designated alphabetically. The sample loop is filled with a slug injection of the sample solution through port C at the "load" position of the valve. During this operation, flow within the valve is as shown by the solid lines. The excess of

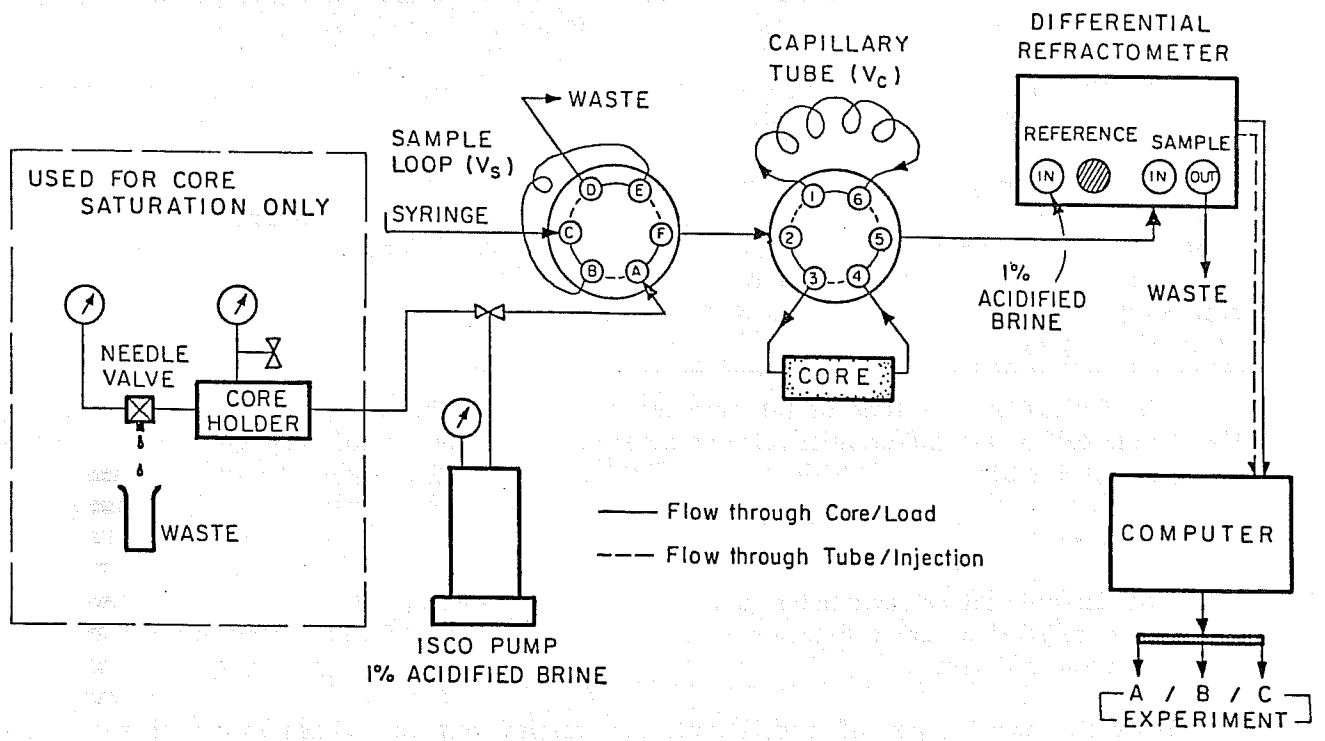


Figure 4.33. Dynamic adsorption apparatus.

Table 4.7

## Preliminary Results of Dynamic Adsorption Experiment

	<u>Velocity Ratio*</u>	<u>Area Ratio**</u>
Brine	(1.00)	
Enordet AE9-12	0.994	0.753
Enordet AE9-6	0.955	0.668
Emulphogene BC-720	0.993	0.587

$$*\text{Velocity Ratio} = \frac{V_{\text{surfactant}}}{V_{\text{brine}}}$$

$$**\text{Area Ratio} = \frac{\text{Peak Area (core)}}{\text{Peak Area (loop)}}$$

Table 4.8

## Calibration Results with Modified Set-Up

## Refractometer Information

Range: 64

Time Constant: 0.25

Isco Pump Rate: 8 cc/hr

Chart Speed: 1 cm/min

Sample Solution: 1.3% acidified brine

Reference Solution: 1.0% acidified brine

<u>Area (cm<sup>2</sup>)</u>	<u>Peak Time (min)</u>
47.65	3.17
44.18	3.17
44.45	3.17
44.03	2.50
47.32	2.95
49.44	2.80
50.41	2.95
47.34	2.80
47.05	2.95
<u>49.67</u>	<u>3.00</u>
47.15 ±2.3	2.95 ±0.21

Relative error on area under the peak: 4.9%

Relative error on peak time: 7.1%

From the chart recorder output the peak showed near symmetry as expected because this was a non-adsorption experiment. At this time, we have not yet run the experiment using the rock samples. It is our goal to run the experiment with the various rock samples and surfactants in the near future.

#### 4.4 Future Foam Studies

Our goal for the future is to emphasize foam mobility measurements and adsorption studies on the rock samples.

We hope to collect more data on foam mobility measurements by using several different types of surfactants to see their effect. Also, we want to continue the previous tests to see the effect of surfactant concentration as well as the effect of CO<sub>2</sub> fraction. Furthermore, we wish to come to some definite conclusion on the dependence of velocity on mobility at low and high flow rates. In addition, different rock samples, such as carbonate type, cannot be neglected.

The other major task for future investigations is a complete study on the adsorption of surfactant on the rock samples. We hope to test a series of surfactants at different concentrations. Also, the dependence of adsorption on flow rate will be considered.

We have completed the described surfactant screening tests on all available surfactants that showed any promise. Although these results are fairly conclusive, their empirical nature is such that we are still seeking further tests that might be more definitive. The ability of a surfactant to produce a useful foam-like dispersion under reservoir conditions can be evaluated, on a preliminary basis by means of the series of atmospheric-pressure tests we have described.

To conclude this discussion on the development of CO<sub>2</sub>-foam: we have clearly shown some very positive results, and described effects that should greatly improve the uniformity of CO<sub>2</sub> floods by use of these additives. But our studies have shown that both mobility reduction and the other possible front-smoothing mechanism due to foam are non-linear. This non-linearity strongly suggests that the most effective ranges of values for the surfactant concentration and CO<sub>2</sub> flowing fraction cannot be chosen in advance. The optimum ranges will be very dependent on the particular reservoir rock, and on the character of the surfactant that is best able to survive the particular reservoir environment with acceptably low adsorption and decomposition rates. Thus, to take maximum advantage of CO<sub>2</sub>-foam where it can be applied, an operator is advised to invest in preliminary laboratory work, to determine the optimum conditions of its use. For finalizing the design decisions for a field test, it would undoubtedly be prudent to perform actual mobility measurements with CO<sub>2</sub> at high pressure, in core samples from the actual formation.

#### 4.5 Direct Thickeners

The first goal of this research, the synthesis and testing of promising types of dense CO<sub>2</sub>-soluble polymers, was accomplished early in the project. The initial polymers investigated were atactic polyalphaolefins. It was soon realized that the only known types of catalysts that could be used for the intended polymerizations were those belonging to the Ziegler-Natta class. Accordingly, in completing sub-task 3.3, exploratory syntheses with several members of this class were performed, from which a catalog was constructed of suitable catalyst combinations, concentrations, times and temperatures for the polymerizations. Detailed summaries of this work were published in the first and second annual reports of this project.

The search was then extended to include more complex co- and ter-polymers with the goal of synthesizing the highest molecular weight polymers that retain appreciable solubility in dense CO<sub>2</sub>. Most of these more complex hydrocarbon polymers were also synthesized, characterized and tested in the earlier years of the Project, and a most complete account of the work on them is given in the Second Annual Report of this Project. For the purposes of the survey, random hydrocarbon polymers having highly irregular structures were synthesized. This was accomplished through the copolymerization of  $\alpha$ -olefins of varying chain lengths, using Ziegler-Natta catalysts. The solubility of some of these copolymers in hydrocarbons and in dense CO<sub>2</sub> was measured with the aid of a device that was developed at the PRRC, and which has been described in previous reports. Briefly, previous qualitative factors have been verified and described more quantitatively in the recent work that has been done on this completed sub-task. Because the high pressure solubility measurement is time consuming and we have as yet been unable to replace a full-time chemist technician who had done most of this work, we have not completed all of these measurements that we would wish. A part-time student is now performing the experiment, and we expect him to continue, at a slower rate, to collect further solubility data.

In consequence of discoveries made during the course of the work, the scope of the research to develop direct thickeners has been considerably expanded from that envisaged when the proposal was first written.

In the first place, it was realized early in the work that the condensed light hydrocarbons ethane, propane and butane might also be usefully included, along with CO<sub>2</sub>, as possible non-polar solvents for direct thickening polymers, and that the solvent power of these fluids increases in the order given, from an apparently close similarity between ethane and CO<sub>2</sub>. Accordingly, we have also tested the solubility of many of the synthesized materials in butane and propane, and measured the viscosity of these solutions.

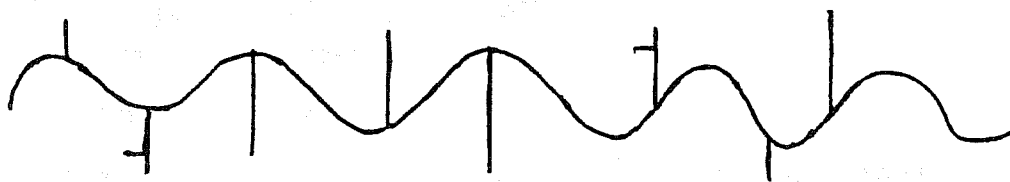
Secondly, with the initially defined directions of search for direct thickeners classified as Method I, the work has been expanded to include the study of an entirely different class of viscosifiers. These, the so-called associative polymers, are described below under the headings Method II and Method III. They form polymeric solution even though some of the bonds between the individual monomers may be of only a transient nature. The work performed under Method I has been useful in these areas as well, because it enabled the classification of structural features that are favorable for dense-gas solubility of the associative as well as of classical polymers.

The search for a suitable direct thickener for CO<sub>2</sub> is thus conveniently classified into three different areas identified as Methods I, II and III. In Method I, high-molecular-weight, multicomponent polymers were synthesized using various 1-olefins. In Method II, ionomers have been synthesized from higher 1-olefins. These polymers contain some ionic groups pendent to the hydrocarbon chain backbone and can form associative cross links in nonpolar solvents. Method III, which pursues a different route to associative viscosifiers, has produced organotin fluorides that effectively viscosify nonpolar compressed gases like n-butane and propane at a concentration of less than 0.5%. Method III appears to be very promising at this time as advances are being made to improve the solubility of organotin fluorides by tailoring their structure. In the sections below, progress in these three directions is described.

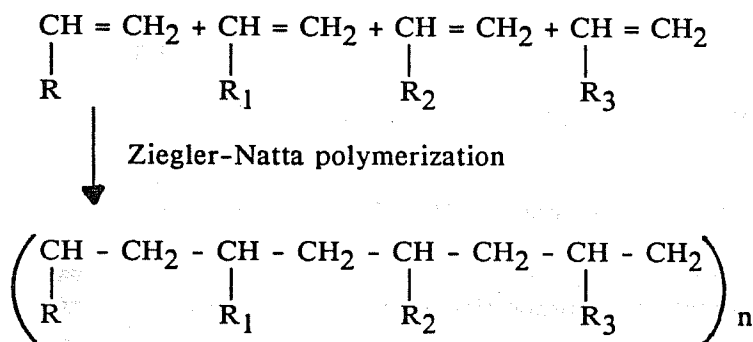
#### 4.5.1 Method I

Based on the earlier studies (Heller et al., 1985; Dandge, Heller, & Wilson, 1985; and Heller & Taber, 1983), it was hypothesized that a random hydrocarbon polymer having highly irregular

structure may have enough solubility in CO<sub>2</sub> to increase its viscosity sufficiently. The hydrocarbon polymer molecule that we desired to obtain can be schematically represented as follows:



Probably the only way to synthesize this molecular structure of high molecular weight was to copolymerize  $\alpha$ -olefins of varying chain lengths using Ziegler-Natta catalysts. The scheme for the synthesis of this structure is given below.



Scheme for the synthesis of multicomponent hydrocarbon polymers

where  $\text{R} \neq \text{R}_1 \neq \text{R}_2 \neq \text{R}_3$  and, for example,  $\text{R} = n\text{-C}_3\text{H}_7$ ,  $\text{R}_1 = n\text{-C}_4\text{H}_9$ ,  $\text{R}_2 = n\text{-C}_8\text{H}_{17}$ ,  $\text{R}_3 =$  branched alkyl group.

Although numerous Ziegler-Natta polymerizations of ethylene, propylene and various other  $\alpha$ -olefins have been carried out at laboratory and plant scale in the last three decades, data on the multicomponent  $\alpha$ -olefin polymerizations are very scarce. Therefore, several 1-hexene polymerizations were carried to standardize the reaction conditions for the synthesis of multicomponent polymers. The different molecular weight poly 1-hexenes obtained in the process were examined for solubility in CO<sub>2</sub>. It was found that the CO<sub>2</sub> solubility of poly-1-hexenes was dependent on polymer intrinsic viscosity (and hence the molecular weight) and was independent of polymer microstructure. These results have been published (Dandge, Heller, & Wilson, 1986).

Having obtained appropriate reaction conditions to produce amorphous polymers soluble in *n*-pentane and *n*-hexane (these solvents were used to simulate CO<sub>2</sub> under atmospheric conditions), we developed a gas chromatographic (GC) technique to follow the course of higher  $\alpha$ -olefin polymerization. Details regarding this technique have been reported in the literature (Dandge et al., 1986). The GC technique allowed us to determine instantly the approximate composition of the multicomponent hydrocarbon polymers. Several co-, ter-, and multicomponent polymers were synthesized using 1-hexene, 1-pentene, 1-decene, 2,4,4-trimethyl-1-pentene and 2,3-dimethyl-1-butene monomers. The intrinsic viscosities of these polymers ranged from 1.00 to 3.00 dl/g. Most of the polymers had broad molecular weight distribution (MWD). The ability of various poly-1-olefins to viscosify compressed *n*-butane and propane was 1) directly proportional to the intrinsic viscosity despite broad MWD of the samples, and 2) independent of polymer composition (Heller, Kovarik, & Taber, 1987). The data in Table 4.9 indicate that the viscosity of *n*-butane and propane solutions

Table 4.9

Viscosities of Poly  $\alpha$ -Olefins in Dense Hydrocarbon Gases

No.	Polymer Composition*	[ $\eta$ ] dl/g	Drop Time of Bar (sec.)	
		25°C n-hexane	1200 psi, 25°C n-butane†	propane†
-	--	--	0.86	0.77
77I	D-64; H-19; P-16#	1.14	1.08	0.87
90I	D-58; P-42	1.88	2.15	1.08
87I	D-63; H-37	2.01	2.75	1.09
94I	H-53; P-47	2.29	2.6	1.43
97Ia	D; H; P; TP; DB	2.84	3.18	1.35
78I	D-34; H-47; P-19	2.87	3.27	1.53

\*D = 1-decene; H = 1-hexene; P = 1-pentene; DB = 2,3-dimethyl-1-butene;  
TP = 2,4,4-trimethyl-1-pentene

†Under test conditions, the approximate properties of these solvents are:

	Density	Viscosity
n-butane	0.57 g/ml	0.15 cp
propane	0.51 g/ml	0.11 cp

#Composition of initial monomer feed.

of a given polymer changed in proportion with solvent power. For example, the drop time of the bar (an indicator of viscosity of the medium) for a given polymer at identical concentration was higher in the case of the n-butane solution compared to the propane solution. This was due to enhanced expansion of the polymer coil in n-butane which is a better solvent than propane.

The CO<sub>2</sub>-solubilities of selected poly-1-olefins synthesized in this work have been reported (Heller, Kovarik, & Taber, 1987). It was concluded from this work that the solubility of these polymers in CO<sub>2</sub> was inversely proportional to polymer molecular weight and, to a certain extent, was independent of polymer composition. This polymer structure (composition) dependence of solubility was not observed, probably due to high molecular weights of these polymers. To observe the structure dependence of CO<sub>2</sub>-solubility, a few low-molecular-weight poly-1-olefins are being synthesized. The synthesis and properties of those already synthesized are given in Table 4.10. Their solubilities in CO<sub>2</sub> are being studied now.

#### 4.5.2 Method II

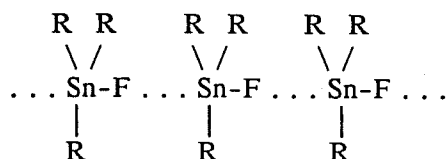
The synthesis of several diene-containing terpolymers was carried out; details are given in Table 4.11. As the column for the GC analysis of unreacted monomers was not available at this time, only monomer feed ratios are reported in Table 4.9. As would be expected, the polymers obtained using the TiCl<sub>4</sub>/AlEt<sub>3</sub> system were of relatively higher molecular weight compared to those produced by AlCl<sub>3</sub>/2-butanone catalyst. More polymerizations using other 1-olefins are planned.

The procedure for the sulfonation of diene-containing terpolymers has been standardized. A commercially available ethylene-propylene-diene terpolymer was used in the standardization experiments. The sulfonation of the polymers reported in Table 4.11 is now being carried out. Preliminary results on the solubilities and viscosities of these ionomers in CO<sub>2</sub> and lower hydrocarbons should be available in the next few months.

#### 4.5.3 Method III

A novel approach to viscosify nonpolar solvents is being studied in this method. It consists of solubilization of triorganotin fluorides (R<sub>3</sub>SnF, where R = alkyl, aryl or alkylaryl group) in solvents with zero or negligible dipole moment.

It is reported in the literature (Dunn & Oldfield, 1970) that tributyltin fluoride (Bu<sub>3</sub>SnF) slowly dissolves in n-hexane and increases its viscosity from 0.3 cst to 300 cst at a concentration of 10 g/L at 37°C. This viscosification was explained on the basis of formation of transient polymeric chains having the following structure:



The large difference in the electronegativity of tin and fluorine atoms causes the triorganotin fluoride molecules to auto-associate provided appropriate R groups are present, and the solvent is nonpolar. For example, Bu<sub>3</sub>SnF and its lower homologues have been shown to exist as auto-associated species, in solid as well as solution states (Clark, O'Brien, & Trotter, 1964; Dunn & Oldfield, 1970). Trineophyltin fluoride, however, does not auto-associate because of the steric

Table 4.10

## Synthesis of Low Molecular Weight Poly-1-olefins

<u>No.</u>	<u>Monomer(s)*</u>	<u>Catalyst</u>	<u>[<math>\eta</math>] dl/g n-hexane, 25°C</u>
108	1-H	↓	0.02
109	1-H		0.06
102	1-P:1-H:1-D 30:30:40	AlCl <sub>3</sub> :2-butanone 1:1 mole ratio	0.33
104	4-methyl-1-pentene	↑	0.20
113	1-P, 1-H, 1-D	↑	0.09
114	1-P, 1-H, 1-D	↑	0.17
106	4-methyl-pentene	AlCl <sub>3</sub>	0.42

\*P = 1-Pentene, H = 1-Hexene; D = 1-Decene

Table 4.11

## Synthesis of Diene-Containing Terpolymers

<u>Polymer No.</u>	<u>Monomers* (feed composition)</u>	<u>Catalyst</u>	<u>[<math>\eta</math>] dl/g n-hexene, 25°C</u>
58	P,H,ENB	TiCl <sub>4</sub> /AlEt <sub>3</sub>	1.51
98	H,D,ENB (45:45:10)	TiCl <sub>4</sub> /AEt <sub>3</sub>	0.62
111	H,D,ENB (47.5:47.5:5)	AlCl <sub>3</sub> /2-butanone	0.13
112	H,D,ENB (47.5:47.5:5)	AlCl <sub>3</sub> /2-butanone	--

\*...as in Table 2.10

ENB = 5-Ethylidene-2-Norbornene

hindrance due to bulky neophyltin groups near the tin-fluorine bond. In polar solvents, dipole-dipole interactions between solvent molecules and the  $R_3SnF$  molecules deny an opportunity for the latter to pentacoordinate with each other, preventing the formation of long polymer chains.

Dunn and Oldfield (1970) had reported an intriguing solubility behavior of  $Bu_3SnF$ , which was reported to be soluble in *n*-hexane and not in *n*-heptane. We found that this compound dissolved in and effectively viscified lower normal alkanes up to propane. It was, however, meagerly soluble in ethane and  $CO_2$ .  $R_3SnF$  compounds with  $R \leq 4$  are known to be almost insoluble in most organic solvents. Therefore, we decided to study the effect of an increase in the alkyl chain length on the solubility and viscosity of  $R_3SnF$  in various solvents. Accordingly, we synthesized the following novel compounds; tri-*n*-amyltin fluoride ( $Am_3SnF$ ), tri-*n*-hexyltin fluoride ( $Hex_3SnF$ ), tri-*n*-octyltin fluoride ( $Oct_3SnF$ ), tri-*n*-decyltin fluoride ( $Dec_3SnF$ ), and di-*n*-amyl-*n*-butyltin fluoride ( $Am_2BuSnF$ ). The following data on these compounds have been reported (Heller & Taber, 1986; Heller, Kovarik, & Taber, 1987): 1) synthesis scheme, 2) characterization by physical constants, elemental analysis, infrared (IR) and nuclear magnetic resonance (NMR) spectroscopy, 3) x-ray diffraction, and 4) solubility and viscosity behavior in various solvents.

The major findings of this work were:

1. Increasing the chain length of the R group from 4 to 10 decreased the crystallinity of the compound and increased the overall solubility in most non-aqueous solvents.
2. The critical concentration (loosely defined here as the concentration after which viscosity increases asymptotically) for most of the trialkyltin fluorides studied was between 0.3 and 0.5 g/100 ml.
3.  $Am_2BuSnF$ , an unsymmetrical fluoride, seemed to be very effective in increasing solvent viscosity at low concentrations.
4. The purity of  $R_3SnF$  has a very substantial influence on the extent of viscosification.
5. An increase in temperature decreased the viscosity of the solution.
6. *n*-Hexane solutions of these compounds would retain much of their viscosity on contact with distilled water but lose much of the viscosity on contact with high concentration brine. Despite such loss in viscosity, the brine-treated solutions were at least 20-fold more viscous than the solvents.
7. The solubility in  $CO_2$  did not exceed 0.17 g/100 ml; whereas a solubility of 0.3 to 0.5 would suffice to increase its viscosity by more than 10-fold.

During the last year, two new unsymmetrical trialkyl-tin fluorides ( $R_2R'SnF$ ) were synthesized: di-*n*-hexyl-*n*-butyltin fluoride ( $Hex_2BuSnF$ ) and di-*n*-hexyl-*n*-amyltin fluoride ( $Hex_2AmSnF$ ). The steps involved in the synthesis are outlined in Fig. 4.34. Both  $Hex_2BuSnF$  and  $Hex_2AmSnF$  are soluble in lower hydrocarbons ( $C_3-C_{10}$ ) and many other organic solvents. Their solubility in  $CO_2$  and ethane is being investigated.

The viscosity vs. concentration curves of  $Hex_2BuSnF$  in various hydrocarbons (see Fig. 4.35) show the effectiveness of this compound even at lower concentrations (0.5%). Table 4.12 shows the drop time of the bar (which is a measure of the viscosity of the medium) for propane solutions of various trialkyltin fluorides at a given concentration. The data in Table 4.12 indicate that most of the trialkyltin fluorides are effective in increasing the viscosity of propane at a concentration of 0.35%. The unsymmetrical ones, however, seem to have lower critical concentration. It became

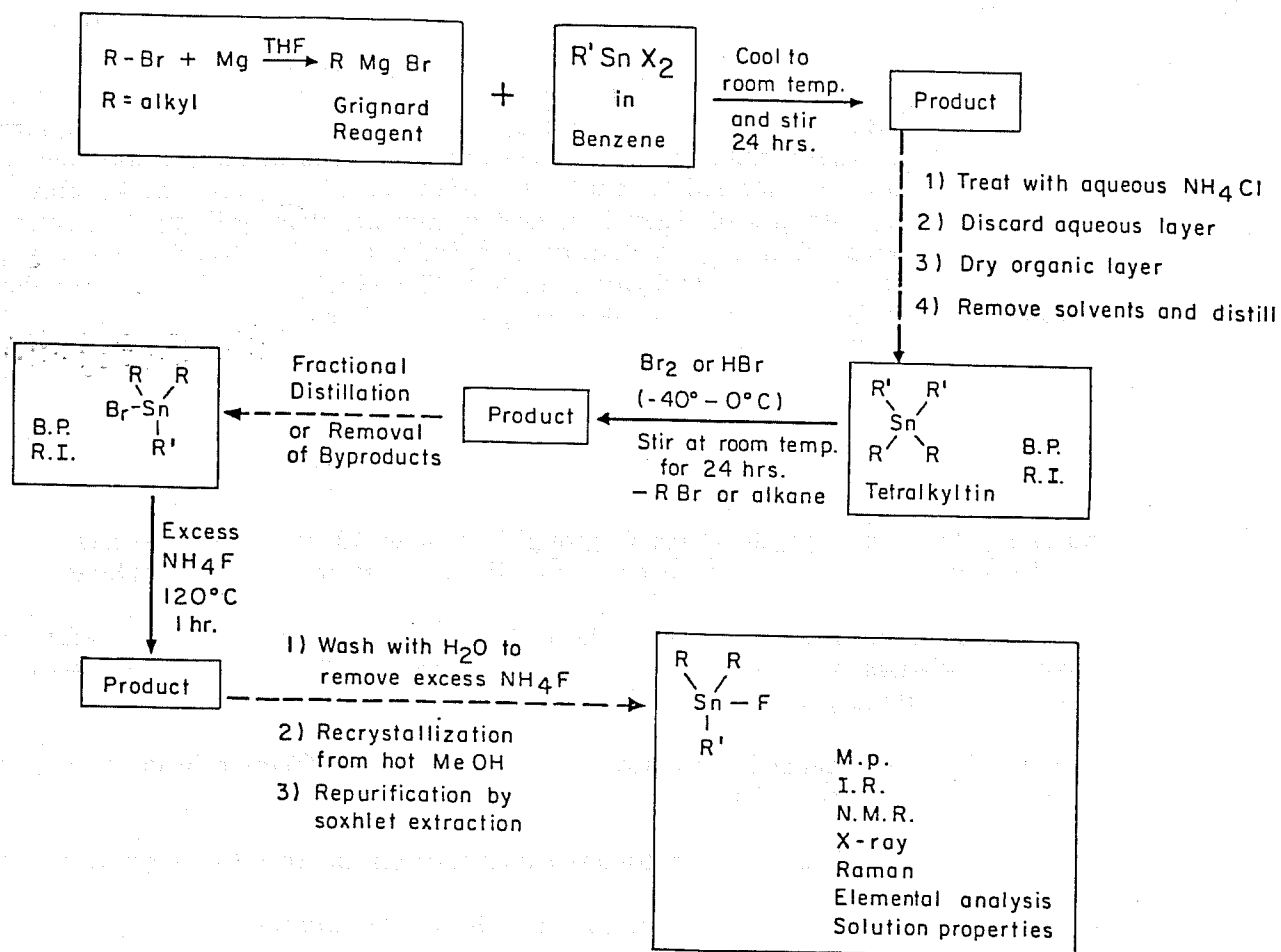


Figure 4.34. Steps involved in the synthesis of unsymmetrical trialkyltin fluorides.

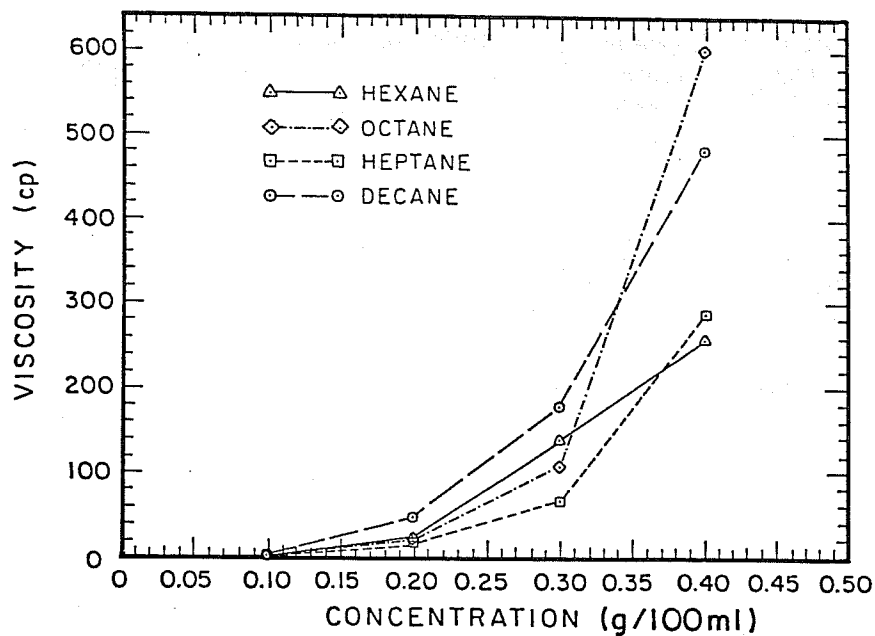


Figure 4.35. Viscosity of Hex<sub>2</sub>BuSnF in various hydrocarbons.

Table 4.12

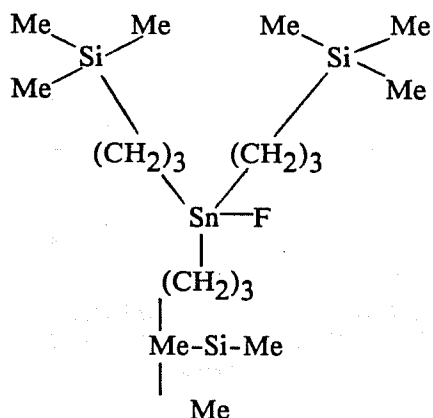
Viscosity of Various Trialkyltin Fluorides in Propane\*  
at a Concentration of Approximately 0.35%

<u>No.</u>	<u>Trialkyltin Fluoride</u>	<u>Exact Conc.</u> <u>%</u>	<u>Drop Time of Bar</u> <u>(sec.)</u>
1	di-n-hexyl-n-butyltin fluoride	0.35	17
2	di-n-amyl-n-butyltin fluoride	0.35	11
3	tri-n-amyltin fluoride	0.38	6
4	tri-n-octyltin fluoride	0.32	4

\*Pressure 1200 psi  
 Temperature 25°C;  
 Density 0.51 g/ml  
 Viscosity 0.11 cp

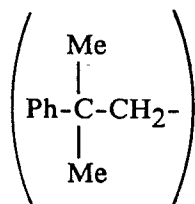
very clear from this work that organotin fluorides are a special class of compounds in that solubility and viscosity behavior can be changed dramatically with very little structural manipulation. Therefore, the synthesis of novel compounds has been continued.

Our previous work (Heller et al., 1985) had shown that silicon-containing polymers had high solubilities in CO<sub>2</sub>. Therefore, it was thought that the introduction of Si-containing groups in trialkyltin fluorides may enhance the solubility of these compounds in CO<sub>2</sub>. Accordingly, a compound with the following structure was synthesized:



Tris-(trimethylsilylpropyl)tin fluoride

A complete characterization of this compound is underway. Tris(trimethylsilyl-propyl)tin fluoride (TTF) instantly dissolved in normal alkanes. This was in sharp contrast with the solubility behavior of most trialkyltin fluorides which dissolve slowly in nonpolar solvents. Thus, the influence of trimethylsilyl groups on improving the solubility of R<sub>3</sub>SnF was immediately evident. The viscosity behavior of this compound, however, was much different than trialkyltin fluorides and is exemplified in Figs. 4.36 and 4.37. It is clear from these figures that the critical concentration of this compound is above 0.7% compared to <0.5% for most of the trialkyltin fluorides. This may be due to some steric hindrance by bulky trimethylsilyl groups present in the vicinity of Sn-F bond. The steric hindrance to auto-association, offered by the Me<sub>3</sub>Si-group in TTF, however, is much less than that by a neophyl group



in trineophyltin fluoride, as the latter is known to be soluble in various nonpolar solvents but does not increase their viscosity. It may be possible to reduce the steric hindrance of Me<sub>3</sub>Si-groups by pushing them further away from Sn-F bond. The synthesis of such compounds is being attempted. These compounds can be expected to have higher solubilities in nonpolar solvents due to the presence of Me<sub>3</sub>Si-groups and may effectively viscosify solvents at a concentration lower than TTF. The solubility of TTF in CO<sub>2</sub> and ethane is being studied.

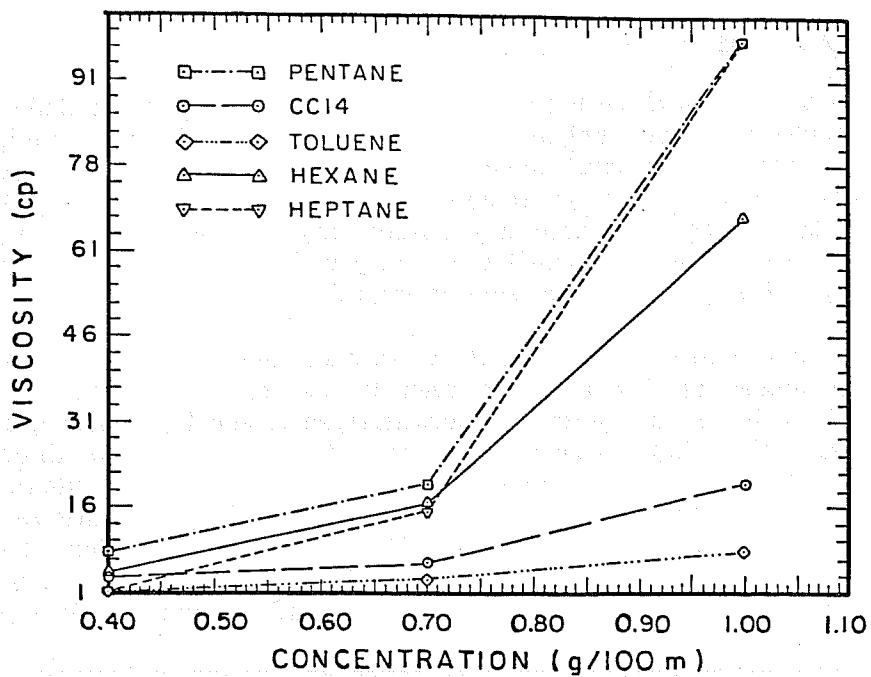


Figure 4.36. Viscosity vs. concentration curves for tris (trimethylsilylpropyl)tin fluoride in various solvents at 25°C.

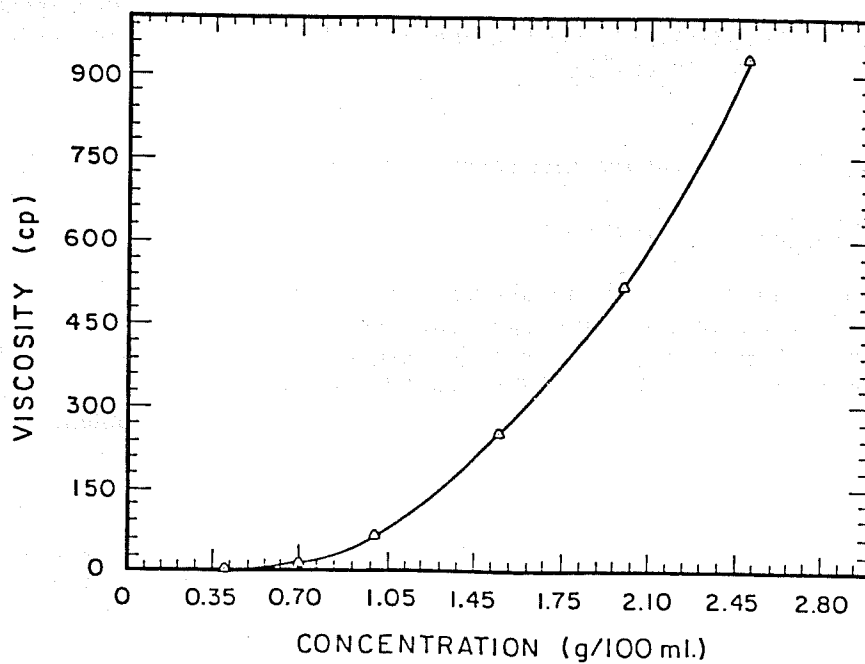


Figure 4.37. Viscosity of tris (trimethylsilylpropyl)tin fluoride at high concentrations; solvent n-hexane; temp. 25°C.

#### 4.5.4 Conclusions

We have apparently exhausted the possibilities of atactic, straight chain hydrocarbon polymers with side branches. Method I polymers have been explored as far as the limits originally envisaged. However, some work in this area will continue, to answer a few remaining questions concerning the relationship between polymer structure and solubility in dense CO<sub>2</sub>. Our investigations of this class of polymers has served as a necessary introduction to work on associative polymers for this application. It also serves as a valuable guide by which to narrow the field of synthesis to those compounds most likely to fulfill the requirements of successful direct thickeners.

In the general area of Method II, there are many more unknowns yet to be discovered. The pace of our studies on ionomers has been limited to some extent to the unavailability of appropriate GC columns to monitor the polymerizations, and by personnel changes during the last several months. Nevertheless, the potential usefulness of this type of direct thickener cannot be ignored, and it is expected that Method II research will receive more attention in the future. The variety of approaches that might be productive in Method II, to synthesize the ionomeric type of associative thickeners, has only commenced. The research we have done there has shown that the initial synthesis schemes we have laid out are viable, and can be used to produce many different kind of ionomers that may yet prove to be the most practical direct thickeners.

It has been in the synthesis, characterization and testing of Method III compounds that the closest approaches have yet been made to the goal of synthesizing practical direct thickeners for CO<sub>2</sub>. We have already found and patented a class of compounds which would be presently feasible for this purpose, in Liquified Petroleum Gas (LPG) floods. Although the solubility of these trialkyltin fluorides in CO<sub>2</sub> is not high enough, they do point out some very promising directions.

It is clear that a great deal of research has already been devoted to the study of Method III compounds. This emphasis will continue as small variations in the structure of R<sub>3</sub>SnF produce strikingly different solubility behavior. It may, therefore, be possible to substantially improve the solubility of R<sub>3</sub>SnF in CO<sub>2</sub> by introducing appropriate R groups. With an increase in CO<sub>2</sub> solubility would come its viscosification, as CO<sub>2</sub> is a nonpolar solvent. These compounds would then be the first direct thickeners for use in CO<sub>2</sub>.

#### 4.6 Laboratory Procedures for the Assessment of Mobility Control Additives in CO<sub>2</sub> Floods

##### 4.6.1 Introduction and Background

The use of physical models to simulate and elucidate the displacement behavior of oil reservoirs is no longer a common activity among the research and technical service activities in oil company research laboratories. This is a major change from the situation of only two decades ago when the operation of several kinds of flow models was common. The most important reason for the change is economic; it has followed from the continuing development of the hardware and software by which numerical simulation of non-linear, partial differential equations can be performed rapidly and at relatively low cost.

Calculated solutions of complicated sets of equations do not always carry with them the answers to all of the problems facing reservoir engineers in their choice and application of production methods. In particular, this is the case in the use of mobility control methods. There are two distinguishable causes for the difficulty.

One of these is that the course of a miscible or partially miscible flood and the behavior of an unstable displacement front in a large-scale, non-uniform reservoir are incompletely described by the numerical representation used in the simulator. The effect of mobility ratio in these floods, while well known and understood in general from classic studies, is commonly represented in reservoir simulators by the use of an overall recovery factor or by a change in some other reservoir-wide parameter. But to evaluate reliably the economic utility of a particular mobility control agent, it will be necessary to know what is the effect of design changes in the displacing fluid mobility and in the slug volume on the recovery efficiency and the scheduling of production.

A second reason why any computer simulation method would have difficulty in evaluating mobility control agents and procedures is that no simulator can take into account all of the chemical and physical interactions between the additives and the reservoir environment. For instance, the effectiveness on the reservoir scale of the lowered mobility of CO<sub>2</sub>-foam involves many aspects of the interaction of water, surfactant, CO<sub>2</sub> and crude oil on the rock surfaces. These cannot yet be described in the list of reservoir properties given to a simulator program.

Having pointed out that the usefulness of CO<sub>2</sub> mobility control procedures and additives cannot be adequately evaluated by use of current reservoir simulation techniques, it becomes necessary to consider what alternative methods are available for this task - the task of evaluating the effectiveness of particular mobility control additives or procedures.

It is clear that a physical flow system is required. Such a system should duplicate essential reservoir conditions so that displacement experiments performed would be sufficiently credible for petroleum engineers to use the results in making predictions for the field. In addition, the flow system should be at risk in the same sense as is the reservoir. In other words, the oil recovery should be subject to the same general causes of displacement inefficiency as are expected in the field. The poor sweep caused by viscous fingering occurs in laboratory cores as well as in oilfields, but does not necessarily lead to the same degree of sweep inefficiency. The differences include both geometric effects, due to the different shape of the laboratory system and the reservoir, and scaling effects caused by their considerable size difference. The causes for the differences include both those mechanisms that operate at the pore level and those which become important at reservoir scale and in reservoir geometry.

Because of the constraints of time and expense, it is also difficult to design, construct, and operate an exact physical model of a reservoir. As has been noted in the literature, it is not possible merely to reduce the distance scale and to modify the time scale accordingly to attain a miniaturized "working model" of the oilfield. A major obstacle in the case of miscible floods is the contrast between the two mixing processes that occur in porous rock. These two processes, convection and diffusion, proceed at rates that depend differently on the distance scale.

Mixing by convection depends on the convective fluid velocities--those which are driven by the rates of injection and production as modified by any large-scale fluid drift rates. In fact, so long as Darcy's Law is applicable, and in the absence of drift, the rates are proportional to these pressure forces. The motions contribute to mixing to the extent that they are not uniform. The non-uniformities that are most effective in mixing are the variations of flow velocities transverse to the flow. They arise because of heterogeneities in the rock properties at all scales, and as a result of the growth of viscous fingers, and they are directly responsible for convective fluid mixing.

Generally, these flow non-uniformities have come to the attention of the industry only indirectly during the interpretation of production or breakthrough curves from large-scale miscible displacement experiments. An attempt was even made by C. Johnson (1971) to analyze such curves

solely on the basis of channels of different permeabilities. Attention is also called to a photograph (Heller, 1963) of a sectioned Berea core showing the non-uniform progress of a miscible displacement of clear styrene by blue-dyed styrene.

Very recently, some results of computer tomographic studies, in which rock and flow processes are examined, have appeared in the literature. These have been performed in oil industry labs, by Wellington and Vinegar (1987) and others, such as S.Y. Wang et al. (1984), and indicate that the extent of the flow non-uniformities is greater, perhaps, than had been generally realized. The direct influence of the non-uniformities of natural convective flow, and the consequent importance of such inhomogeneities in the mixing processes in rocks are thus becoming increasingly more apparent.

Mixing by diffusion is essentially based on the random motions of the fluid molecules. The statistics of the process dictate that the net rate of transport by diffusion is nearly proportional to the gradient of concentration. These net rates thus vanish between areas with the same concentration and become very low between regions that are far apart. Thus, the direct contribution of diffusion to mixing occurs only over very short distances or very long timescales. Direct diffusive mixing of displacing and displaced fluids at the boundaries of large regions containing them is relatively minor.

In spite of this and the fact that molecular diffusion is independent of convective flow in the velocity range of interest, the interaction of the two mixing processes is significant. Paradoxically, but as explained by Taylor (1953) and other authors, the interaction causes a reduction in the degree to which a displacing fluid mixes with the displaced one.

The apparent paradox arises because the flow of fluids through the porous system (like that through a capillary tube) entails extreme variations of velocity transverse to the streamlines on a microscopic scale. Were it not for the effect of molecular diffusion, these variations would produce very extensive mixing during displacement. The time for nearly complete diffusive mixing within any individual pore is short in comparison to the average residence time in the pore at reservoir flow rates. Consequently the convective mixing that would otherwise occur, due to these great variations of streamline velocity, is almost eliminated. Insofar as their effect on large-scale mixing is concerned, the effective fluid velocities through a pore are all equal to the average of the velocities along nearby streamlines.

The combined influence of molecular diffusion and the variations of convective flow on the mixing of miscible fluids at a macroscopic concentration boundary are often identified under the label "dispersion." In bodies of porous media that can be considered to be "uniform," classical experiments and analysis by Day (1956), von Rosenberg (1956), Aronofsky and Heller (1957), Blackwell et al. (1959) and others have found that the gradual spreading of initially sharp mixing fronts can be described reasonably well with a single dispersion coefficient.

In more heterogeneous or fractured flow systems such as many, if not all, reservoir rocks, convection and diffusion interact in more complicated ways. This is still an area of active research, but it is apparent that the description of mixing behavior must include the effects of large-scale velocity variations. A familiar attempt was originated by Deans (1963), developed by Coats and Smith (1964), and used by Batycky et al. (1980), and Bretz et al. (1986). It deals with the observed dispersive behavior by assuming a fraction of the sample to have zero flow velocity, and to be in communication with the flowing fraction only by diffusive mass transfer. A different way of taking the velocity variations into account is explored in a recent thesis completed at New Mexico Tech by Sultan (1987). This thesis examines the mixing zone after displacement through a sample that contains three parallel channels of different permeabilities.

#### 4.6.2 Considerations of Model Design (for Assessment of CO<sub>2</sub> Mobility Control)

Because it is not possible to design an "exact model" by which to test all features of mobility control additives for CO<sub>2</sub> displacement, the necessary compromises must be chosen with care and an awareness of the effects of the unavoidable differences between model and reservoir. In light of the discussion above, it is clear that the direct effect of diffusion is much less than that of convection in determining the frontal mixing behavior in a reservoir. The thicknesses of dispersed boundaries between displaced and displacing fluids will be much smaller fractions of the overall flow distances in the reservoir than they are in any laboratory model. On the other hand, and because of the long time scale, the actual values of the concentration gradients in most parts of an oilfield are much less than they are in a model. One can expect that diffusive equilibrium will generally have been established not only in the porespace but between nearby pores, in rock in the reservoir.

The geometrical shape of a model can also have a great effect on the recovery obtained in displacement runs. There are two main geometric differences between a well-to-well flood and one in which fluid enters and leaves through rock faces as large as the cross section of the flow system. The first of these is a consequence of the much greater Darcy flow velocity near the wells. If there is any non-Newtonianism in the rheology of the fluids, or if there are any other influences of velocity on fluid properties, the occurrence of these in the reservoir, and not in this type of model, must be taken into account. Secondly, because the flow times along the different Darcy streamlines are neither constant or uniform from one to the next in a well-to-well flow, this difference in arrival times of fronts must also be taken into account.

An ideal physical model for our purpose might be square, to have the same shape as the symmetry unit of a five-spot pattern. In this or similar geometries, the extremely large ratio of flow velocities, between those near the well and those in the center of the pattern, could be simulated. So also could be the great difference between the flow times along different streamlines, which is quite important in this application.

In spite of these advantages, the special construction problems introduced by the choice of a "two-dimensional pattern" model would cause additional problems. The designer might, for instance, consider the consequences of a choice of radius for the "wells" in the model. Geometrical similarity would demand these ports into the model to have radii measured in hundredths of an inch, a size so small that the experimenter would be asking for trouble from plugging and contamination. In addition, because the ratio of well size to pore size would be much different than near a real well, doubt would be cast on the effectiveness of the modeling in the neighborhood of the wells.

Although compromise on well size could be justified, other questions remain that cannot be so easily settled. One such problem concerns the procedures to be used to achieve uniform saturation. In any physical model, the ability to repeat runs and measurements is vital. Yet the boundary conditions by which to saturate initially and repeatedly the porous model (with fluids simulating the reservoir contents) is almost incompatible with the well geometry needed to simulate field floods. To overcome this difficulty with a model designed to use high-pressure CO<sub>2</sub> as the displacing fluid would require a great deal of mechanical effort and expense.

In this case, the decision was made that design and construction of a five-spot model would bring additional uncertainties in the use of a CO<sub>2</sub> mobility control experiment and that it would not be worth the effort. Instead, a traditional sample shape was selected in which "fluid spreaders" could be used at the inlet and outlet ports so that the Darcy velocities on all streamlines would be the same. A linear model does not possess the very important and distinctive characteristic of a

five-spot model as mentioned above. The considerable variation in velocity, between the Darcy streamlines that are directed toward the producing well, and those which leave the injection well aimed at another injector, is not simulated. An allowance for this difference can to some extent be made in subsequent calculation.

The ratio of sizes of model and reservoir is important because the mixing of displaced and displacing fluids proceeds both by convection and diffusion. Final, irreversible mixing, leading to compositional equilibrium on a molecular scale, occurs only by the latter process. The time required for this approach to equilibrium is proportional to the square of the distance involved. Thus a fairly large core model is required if the fingers are not to disappear, or be considerably diminished, by the process of molecular diffusion alone. Consideration of the effect of sample size is here related to the rate at which viscous fingers are initiated and grow, and provides another aspect of the coreflood that cannot be simply taken as a direct indicator of reservoir performance.

Thus, for realistic testing of the effect of mobility control additives and procedures, the model should be large enough so that diffusion will not inordinately influence the initiation and growth of instability fingers. In too small a model, the growth of fingers would be severely limited, to the extent that the production or breakthrough curve would give a false picture of flood effectiveness. This constraint concerns the cross-section and length of the model. The model should be long enough so that when the instability fingers develop, they will have the opportunity to lengthen appreciably during the remainder of the flood. The size of the model is also related to the rates at which displacement runs should be performed in it. It is also important that the fluid velocities are high enough for the ratio of longitudinal to transverse dispersivities to be the same in the model as in the prototype.

In addition to the above considerations, a suitable model for this purpose should use real porous rock rather than a sand or bead pack. Actual reservoir samples would be preferred, but they are unavailable in large sizes. Further, the effectiveness of the mobility control additives should be tested in the presence of interstitial water (for "secondary" tests) and also with the higher water saturation to be expected after waterflooding. The model should also be operable at high pressure, so that dense CO<sub>2</sub> or compressed, light hydrocarbon gases can be used as displacing fluids. Because it is necessary to compare repeated runs, the system should be designed with the requirement in view that the sample can be cleaned and returned to the same initial state after each run. Similarly, it should be possible to use the same samples in the tests of CO<sub>2</sub>-foams and for tests of direct thickeners.

Finally, a less well-understood feature of any core flood is the fact that the core itself is not homogeneous, so that the Darcy streamlines are not really straight and evenly spaced. In these experiments, the results of the preliminary waterfloods are being carefully documented, so that the effect of stratification or other nonuniformities of the rock may be considered. It can also be seen that assessment of the utility of mobility control procedures for use in reservoirs is made more difficult because of the variability between the many parameters of oil reservoirs and because of the incompleteness of available information about them.

The design compromises adopted in meeting the constraints imposed by the previous considerations are discussed in the next section.

#### 4.6.3 Test System for Evaluation of Mobility Control

To satisfy the need to return repeatedly to the same oil and water saturations, it was decided not to use a natural crude oil system for these tests, but rather to use a refined, Soltrol®-based oil

that could be removed completely from the rock by displacement processes. For the aqueous fluid, brine with 0.5% NaCl and 0.5% CaCl<sub>2</sub> by weight was chosen.

As indicated, the major compromise concerned the shape of the model. The wide distribution of breakthrough times inherent in a five-spot system was sacrificed for the greater experimental convenience of a "linear" model in which all of the Darcy streamlines have the same velocity for the entire length of the flow system.

A currently operating system contains a dolomite rock sample of roughly 2.93-in.<sup>2</sup> (18.9-cm<sup>2</sup>) cross-sectional area (polygonal rather than circular) and 28.3-in. (71.9-cm) length. The pore volume of the sample is 256 cc. The rock is the so-called "Baker Dolomite," quarried by the J.E. Baker Co. of York, Pennsylvania. It is a fine-textured, vuggy carbonate rock, rather uniform in porosity and permeability. The ends of this rock sample have been joined at the edges to stainless steel "fluid spreaders" and coated with epoxy reinforced with glass tape. Because it was judged that this coating could tolerate only about 100 psi internal pressure without separating from the rock or bursting, the core system is operated inside a 4-inch-inside-diameter steel pressure vessel. The annulus is filled with an inert liquid (ethylene glycol) and controlled by a separate overburden pressure system.

A second system with a 2-inch diameter, 30-inch long Berea sandstone sample has also been partly constructed using a poured low-melting-point alloy around the sample inside a steel pipe. The sample is wrapped with Teflon<sup>®</sup> tape to prevent contact of brine with the overburden alloy, and the fluid spreaders have been machined from a heat-resistant plastic. Unfortunately, leaks along the sides of the metal have indicated the existence of a yet-unknown amount of void volume that may be connected to the pore space of the rock. In consequence, this second system cannot yet be used and is awaiting further diagnosis and repair.

#### 4.6.4 Flooding Experiments

The sample was first saturated with brine and then oil-flooded, removing 218.02 cc of brine and bringing the oil saturation to 85.16%. A second brine flood displaced 71.97 cc of oil, leaving the oil saturation at 57.05%. From this "tertiary" initial condition, a flood was carried out with unthickened liquid propane, producing 90.13 cc of oil and 50.72 cc of brine. The production histories of these displacement runs are shown in Figs. 4.38 and 4.39.

It can be seen that roughly the first half of the oil that was produced in the brine flood was water-free. Water breakthrough occurred at about 32.3 cc, after which the water fraction increased rapidly. After 64.3 cc injection, a total of only 1.3 more cc of oil was obtained in the remainder of the flood. The break at 32 cc might be interpreted to indicate the existence of a division of the flow system into two major channels in which the velocities of the fronts differ by about a factor of two. After the brine front in the slower channel reached the output face, little more oil remained mobile anywhere in the core, and the classic condition of residual oil saturation was gradually reached.

In contrast, the tertiary flood of the core, performed with unthickened propane after completion of the brine flood, showed quite different behavior. It can be seen in Fig. 4.39 that, as expected from the fact that the waterflood had reduced the oil saturation to its residual saturation, brine was the first fluid produced. Small amounts of Soltrol<sup>®</sup> were observed after only about 8 cc of propane injection, however. The oil fraction increased rapidly until at about 30 cc when there was a short period in which there was no brine in the effluent whatsoever.

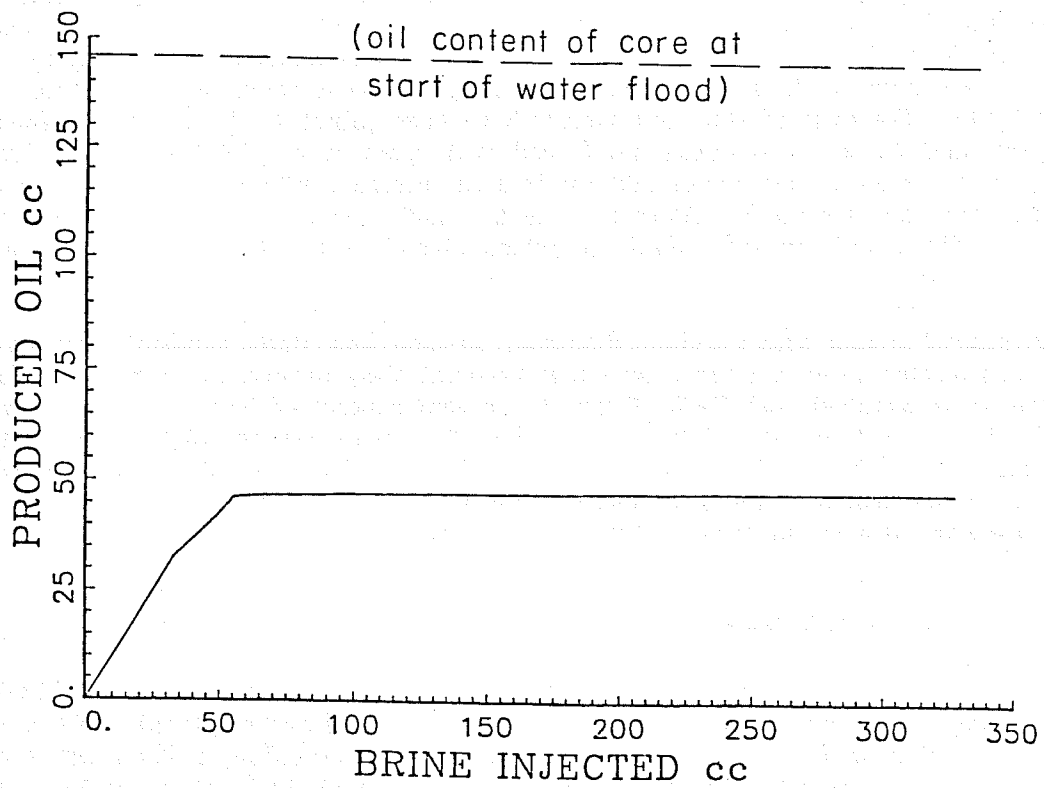


Figure 4.38. Waterflood of Baker Dolomite core.

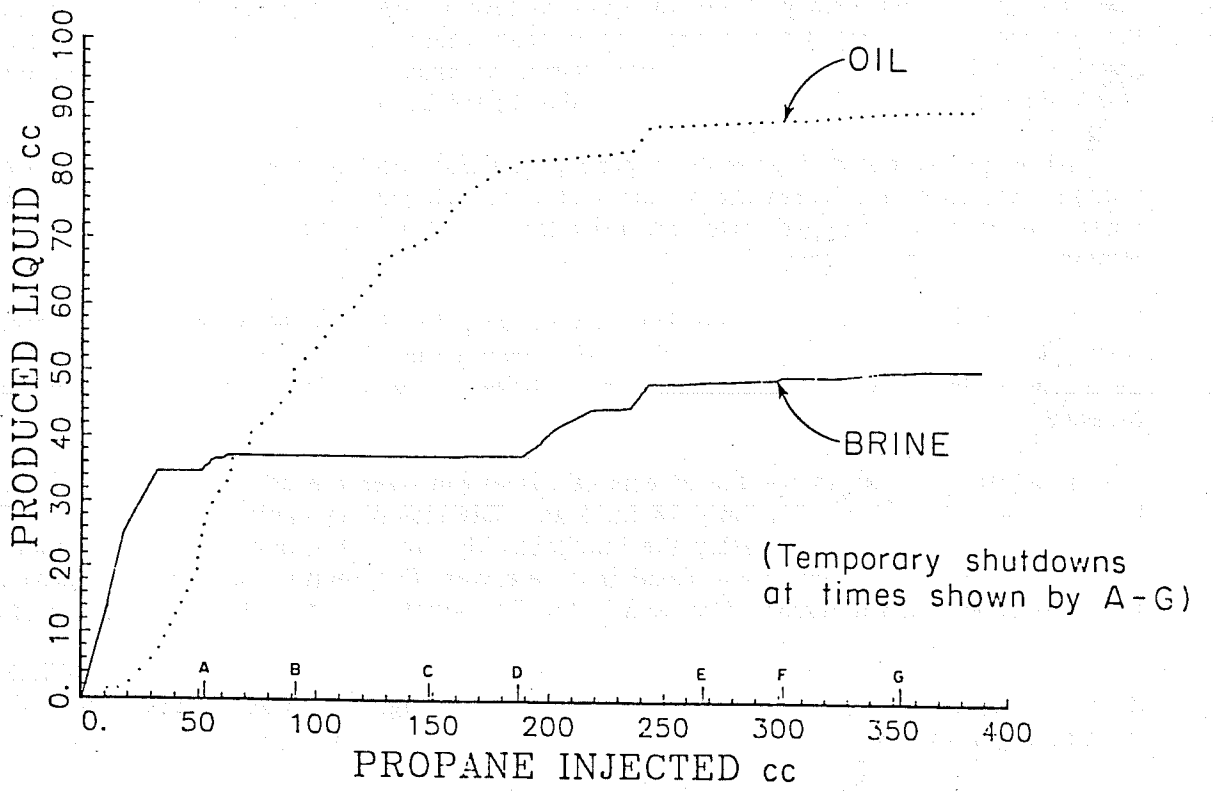


Figure 4.39. Unthickened propane flood of Baker Dolomite core.

After an overnight shutdown of the apparatus, a few more cc's of brine emerged, but this ceased again, and there was a long period (between 52 cc and 180 cc) in which only about 2 cc of brine were produced. This was again followed by a pair of short interludes during which brine was produced at a somewhat higher rate, after which brine was produced at less than about 0.025 of the rate of propane injection. Some, but definitely not all, of the shutdowns that occurred during the flood were associated with the "kicks" in brine production.

The production history of oil was quite different from that shown by the brine. Once started, the oil production rate did not drop lower than about 0.5 of the propane injection rate, until massive breakthrough of propane, which started at about 175 cc. During the last 140 cc of the flood, the oil production rate was as low as that of the brine.

Although, as noted, high-rate propane production did not begin until about 175 cc of liquid propane was injected, increasing amounts of produced gas were measured from the 58 cc mark. When the flood was stopped, after the injection of 388 cc of liquid propane, about 55.9 cc of oil remained in the core system.

The production history described above and by Fig. 4.39 is quite consistent with the conception of severe fingering (together with channelling due to the rock heterogeneity indicated by the waterflood) during the displacement of brine and waterflood residual oil by the unthickened propane.

It is also possible to see the effects of dispersion over the course of this experiment, which lasted several days, in a core only 28 in. long. Dispersion was able to mix enough of the liquid propane with the Soltrol<sup>®</sup> to delay the inevitable high rate of propane production until relatively late in the flood. In a large-scale flood in a reservoir, this feature could not be expected to have such a large effect, for reasons discussed in the "Introduction and Background" of this section.

Only a relatively small concentration of propane in the oil was, of course, sufficient to lower its viscosity, causing the displaced oil to finger through the water, rather than forming and maintaining a uniform "oilbank."

In the next experiment to be performed with this core system, the rock will be returned to the waterflood residual oil state, so that a directly thickened propane flood can be performed for direct comparison with the unthickened one described above.

## 4.7 Mobility Control of Actual CO<sub>2</sub> Floods

### 4.7.1 Field Application of CO<sub>2</sub> Mobility Control

Most operating CO<sub>2</sub> floods and most new designs use a water-alternating-with-gas (WAG) procedure in an attempt to improve areal coverage. The design of such a flood is usually based on one of two sets of calculation methods. These two methods can be traced to the original articles which appeared in the literature. The first method (Caudle & Dyes, 1958), claims its effect, a reduced mobility for the CO<sub>2</sub> displacing phase, through a reduction in the behind-the-front relative permeability of CO<sub>2</sub> by an increase in the water saturation in that region. The second method is based on a paper by Blackwell et al. (1960) in which partial vertical separation of the injected fluids by gravity is called upon to reduce that portion of the cross-sectional area of the reservoir behind the front that is available to CO<sub>2</sub>.

In their original forms, both papers suggested that the gas (or solvent, such as dense CO<sub>2</sub> or liquified petroleum gas (LPG)) should be injected simultaneously with the water. As a practical matter, however, simultaneous injection was changed to alternate injection. This change was helpful from an operational standpoint for two reasons. First is that the pumps used in the field do not meet the "constant rate" ideal with the near perfection of laboratory syringe pumps. Along the same lines it is to be noted that liquid CO<sub>2</sub> is about twenty times more compressible than water. As a consequence, the operation of the two separate pumps in simultaneous injection is a difficult control problem. It can give much more trouble than the alternate use of the same pumps to maintain the desired flow rates for each fluid separately for predetermined times.

A further operational reason for the alternation is the extremely corrosive nature of high-pressure mixtures of brine and CO<sub>2</sub>. Alternate injection simply minimizes the exposure of tubing and surface lines to this mixture and reduces maintenance and replacement costs.

In any case, WAG operations are subject to the same unresolved questions (regarding the growth of fingers during CO<sub>2</sub> injection) as are continuous solvent injection processes. Another uncertainty concerns the probable bypassing of residual oil in pores and assemblages of pores shielded by high-water saturation from the injected CO<sub>2</sub>.

The two major objectives of this research effort in CO<sub>2</sub> mobility control have been the development of additives to thicken the CO<sub>2</sub> so that frontal instabilities are reduced or suppressed, and the development of procedures to use these additives in the operation of CO<sub>2</sub> floods. Accomplishment of these two goals will enable the design and operation of CO<sub>2</sub> floods that directly incorporate mobility control, eliminating the uncertainty caused by the above unanswered questions. The improved sweep efficiency made possible by use of these additives for mobility control can also be expected to increase the overall reserves recoverable by CO<sub>2</sub> floods.

Two distinct kinds of additive, CO<sub>2</sub>-foams and direct thickeners, have different properties and problems and will consequently make different demands on the operator in their application. Whereas it seems unlikely that all of these demands can be anticipated at this time, the following paragraphs give information that is currently available.

#### 4.7.2 Reservoir Use of CO<sub>2</sub>-Foam

The principal characteristic of CO<sub>2</sub>-foam is that the mobility of this composite mixture of fluids does not depend on the microscopic features of the rock in the same way as that of ordinary fluids. The reason for the difference is that for "foam," the basic structural units, the lamellae, are the same size or larger than the pores, whereas ordinary fluids can be treated as continuous, since the molecular structure is on a much smaller scale than that of the porespace.

At least two major areas of uncertainty follow from this difference. First, although the mobility of ordinary fluids over a wide range of conditions can be calculated with assurance from standard measurements (of viscosity of the fluid and permeability of the rock), it is not yet possible to predict with assurance the mobility that will be attained with a given CO<sub>2</sub>-foam, without fairly specific high-pressure measurements in the same rock type as will be encountered in the reservoir, with the same volumetric flowing ratio of CO<sub>2</sub> and surfactant solution, and with the same concentration of surfactant. In addition, there are those uncertainties that stem from unknown, yet measurable, characteristics of particular surfactants in the reservoir environment. These consist of their ability to sustain foam lamellae between dense CO<sub>2</sub> and brine, their chemical stability, and the extent and speed of their adsorption on the rock. As has been discussed in the

CO<sub>2</sub>-Foam section, our research project is attacking all of these uncertainties, with the goal of enabling operators to use this method of mobility control with assurance in their CO<sub>2</sub> floods.

A second uncertainty is also caused by the difference between the microscopic flow behavior of "foam" and ordinary fluids. It is concerned with the manner of displacement. Because the lowered mobility of foam flow is associated with the distribution and motion of lamellae in the porespace, it is expected that the pattern of fluid displacement is altered and, in fact, made less uniform at the pore scale. But this condition is expected to be descriptive of the flow only in regions far back from that zone of the reservoir in which oil is being displaced. An intermediate transition zone must exist between the displacement front region (where the Hutchinson-Braun process enables CO<sub>2</sub> to displace the oil in a miscible fashion) and the foam flow region described above. The dimensions and dynamic behavior of this transition region introduce the second area of uncertainty into the foam displacement process.

It has often been noted that many crude oils are very destructive of the foam lamellae, and this has in fact been cited as a reason for doubt that any "foam displacement process" could be used effectively in an oil field. Actually, the contrary seems most reasonable; this chemical incompatibility will be most useful. Because of it, the foam lamellae will not be present in the Hutchinson-Braun region where CO<sub>2</sub> is displacing the oil and will not interfere with the uniformity of the contact and displacement. The crude-oil-induced breakage of foam lamellae will no doubt contribute to the generation of the needed transition region referred to earlier.

The uncertainties associated with this second point, however, cannot be satisfactorily disposed of by speculation. Further results are awaited from the ongoing large coreflooding experiments discussed in the previous section on Laboratory Procedures for Assessment of Mobility Control Additives.

Despite the need for further research, it is not premature to consider field application of CO<sub>2</sub>-foam flooding at this time. Our recent project results have supported the general design procedures that were described earlier by Heller (1984). That recommendation is that the CO<sub>2</sub>-foam should be introduced by simultaneous injection of CO<sub>2</sub> and surfactant solution. Depending on the measured adsorption parameters for the surfactant on the reservoir rock, a further suggestion is made. A preliminary quantity, or "surfactant pad" should be injected prior to the introduction of the CO<sub>2</sub>-foam. The pad should contain sufficient surfactant to satisfy the "irreversible adsorption" requirements of the volume of rock enclosed in the well pattern. This quantity can be calculated simply from the amount of such adsorption measured in the dynamic adsorption experiment described earlier in the CO<sub>2</sub>-Foam section of this report. Similarly the volume of brine, in which the pad surfactant should be dissolved, should be determined by the other parameter measured in that experiment, the chromatographic delay due to reversible adsorption.

The total volume of the CO<sub>2</sub>-foam slug is also discussed in an SPE/DOE paper (Heller, 1984). There should be a large enough quantity of CO<sub>2</sub>-foam injected prior to the chase water so that the displacement front will not be starved for CO<sub>2</sub> until the end of the flood, that is, until the front has contacted all of the reservoir volume that can be swept from the particular injection well. The requirement calls for a sizable volume of CO<sub>2</sub>-foam because, at the boundary where it is displaced by water, CO<sub>2</sub> will be left behind as a residual phase. The residual phase saturation of CO<sub>2</sub> was estimated in that paper to be equal to  $S_{rO}$ , the residual oil measured after waterflood. It might be advisable, in preparation for a flood to be designed along these lines, to obtain an actual experimental measurement of this quantity.

An attempt to operate a tertiary CO<sub>2</sub> flood in this manner was made in the Rock Creek field, in a joint project involving PENNZOIL, the U.S. Department of Energy and the New Mexico

Petroleum Recovery Research Center. A Final Report on that project was issued by the DOE (Heller, 1986). In addition, a different account of the same field experiment was presented at several meetings of the SPE (Heller et al., 1985).

The temperature of the Rock Creek field is only 75°F, and the reservoir rock is sandstone, so there was available a fairly wide choice of surfactants. Unfortunately, because of previous recovery operations, there was little oil remaining in the area available for the test. In addition, there were problems with the condition of the injection well that made necessary an extended interruption of the mobility control test. However, a clearly positive test result was attributed to the injection operations. It was proved possible to inject CO<sub>2</sub> and surfactant solution simultaneously, and the gradually declining injectivity (to be expected as a result of the spreading of the region containing foam lamellae) was observed.

Current laboratory experiments in this project are providing information and criteria by which more generally suitable surfactants might be recommended for this purpose. The planning of further field trials of the use of CO<sub>2</sub>-foam might then be justified. It would, of course, be desirable to have more favorable circumstances of residual oil distribution and well conditions.

This section cannot be concluded without repeating here an interesting possibility reported in the earlier section dealing with the measurement of the mobility of CO<sub>2</sub>-foam. This is the very exciting possibility that a new mechanism may exist by which CO<sub>2</sub>-foam can further improve displacement uniformity. This is based on the measured difference between the relative effectiveness of foam in high and in low permeability rock, and could only be expected to be effective in the proper ranges of operating parameters.

#### 4.7.3 Prospective Field Use of Direct Thickeners

Encouraging research results are reported in the earlier section on direct thickeners, and we are optimistic about further progress. Nevertheless, none of the materials that have been synthesized as of this date are suitable for use in dense CO<sub>2</sub>. However, we have found a large class of associative viscosifiers which are extremely effective in butane and propane. These trialkyltin fluorides exhibit a threshold concentration above which the solution viscosity increases rapidly, apparently because of a transient association between the tin and fluorine segments of adjoining molecules. With only small increments above a concentration threshold (which occurs in the range of 0.4 weight %), the viscosity rises into the tens or hundreds of centipoise. Whereas the quantities of these compounds that can be dissolved in the lighter alkanes (C<sub>3</sub> to C<sub>10</sub>) are adequate to display this effect, the solubilities in ethane and CO<sub>2</sub> of those of the compounds which have been synthesized are not high enough.

These trialkyltin fluorides could be used for LPG floods if the economics were favorable and if material could be obtained in sufficient quantity. As has been pointed out, one of the compounds is already commercially available (it is tributyltin fluoride, used in the manufacture of anti-fouling marine paints). The cost to thicken LPG or propane with this material would be about \$8 per barrel.

A second, and somewhat unrelated, possible oilfield use of these chemicals might be a water-free, thickened-butane frac. With only minor refrigeration, the vapor pressure of the butane could be kept low enough at the surface to permit normal blending operations to suspend the proppant in thickened butane. In contrast to the usual frac performed with water-based fluids, it might be expected that a thorough and rapid clean-up after completion of the frac job could be accomplished after only a slight reduction of surface pressure. This decrease would occur naturally during

recovery and re-storage of the butane, an operation that would be vital for safety as well as economic reasons.

In handling a direct thickener, the field engineer should consider carefully the operation by which the solution of polymer or associative chemical is put into solution in the CO<sub>2</sub> or other dense gas. It would probably be quite advantageous if the direct thickener could be supplied as a concentrated solution in a suitable solvent. This could then be mixed with the liquified displacing gas to form the needed solution. It should be possible to find many such co-solvents, in which the solubility of the chemical would be high enough so that such a handling procedure would be possible. Beyond this simple goal, in which the shipping solvent would play a helpful, but passive part, the procedure might be improved upon still further. It might be possible to find active co-solvents which would make a positive contribution, either to the solubility of the additive in the dense CO<sub>2</sub> or to the formation of longer molecular chains (and hence higher viscosity) in the polymeric solution.

It is necessary to add that we have no hint at this time of what such active solvents might be. None of our research efforts have been directed toward the discovery of such liquids, although the goal may soon become more urgent. It is apparent that research is needed on co-solvency effects from the common contaminant gases in CO<sub>2</sub> as well as other flooding gases. We expect to be most immediately concerned with the measurements of these effects.

A further consideration in the use of direct thickeners for CO<sub>2</sub> or LPG floods concerns the total quantity that will be economic to use. Even if all of the injected dense gas could be recovered after oil recovery declined to the point of abandonment, the cost of keeping such a large amount off the market and in the ground during the life of the flood would probably be excessive.

This question raises another that concerns one more advantage to be gained from the stabilization of the displacement front in a miscible flood. By using enough thickener to suppress the growth of viscous fingers, a principal cause of slug degradation would be eliminated.

Much of the modern history of EOR research concerns the development of the so-called slug processes, in which oil recovery is affected by the displacement through the reservoir of a sequence of fluids, starting with the crude in place, and ending with water, the least expensive fluid that can be pumped downhole and left there. As is well known, this simple ideal is made much more complicated by many technical as well as economic problems. Most of the former (and perhaps some of the latter) are concerned with the fact that the actual displacement in the reservoir is non-uniform, with the displacement heterogeneities ranging in scale from poresize upwards.

Most of the spatial variations of flow that occur at large scales--those that follow gross variations in rock type and stratification, and those that result from the pattern of well placement--are to be distinguished here from the generally smaller scale variations that display a shorter spatial wavelength. The former type of variation is relatively permanent and persists independently of the nature of the flowing fluid, in response to existing pressure gradients.

Much of the flow heterogeneity resulting from the viscosity difference between displaced and displacing fluids is prolific in the generation of new contact area between the fluids from long and short wavelength corrugations and fingers. Diffusive mixing that occurs at this added contact area is the principal mechanism by which slugs are degraded, and marks the locations where the slug of fluid ceases to be effective in keeping separate a pair of other fluids that are immiscible or otherwise incompatible with each other.

In a CO<sub>2</sub> flood, which depends on a Hutchinson-Braun process to generate a first-contact miscible zone, the fluids are crude oil and pure dense CO<sub>2</sub>. In this case, the incompatibility arises because a mixture of these two fluids separates into two or more phases that will not be swept completely from the reservoir rock. In the presence of severe frontal instability or viscous fingering, the natural slug of CO<sub>2</sub>-light hydrocarbon mixture (that is the Hutchinson-Braun zone) is continually pierced, and thus degraded, by diffusive mixing along the sides of the fingers. The Hutchinson-Braun zone must be continually regenerated, at the expense of increasing amounts of residual oil in a process that thus becomes less efficient in the field than in the laboratory.

If frontal instability is present, the degradation of fluid slugs that are purposely introduced into a flood is even more complete. This happens because no regeneration can occur once the injected slug material has been diffused away into the other fluids. It has been suggested that the recovery of crude oils which have abnormally low content of the lower hydrocarbons (and thus show a high MMP in slim tube tests) might be assisted by the use of a slug of the required gasoline-fraction hydrocarbons, injected before the CO<sub>2</sub>. The conclusion from the above discussion is that such a slug would not survive, because of the fingers that grow at the front between the relatively high viscosity crude oil and the CO<sub>2</sub>. No mechanism would be available in this case for the renewal of the artificially introduced Hutchinson-Braun zone.

But the situation would be fundamentally changed if the CO<sub>2</sub>, and perhaps the slug fluid, were to be thickened enough to suppress or greatly reduce the frontal instability. Effective direct thickeners would be very useful in this particular situation, where their major value would be in minimizing the volume of slug fluid required.

#### 4.7.4 Conclusions About Field Use of Mobility Control

It would indeed be visionary and unrealistic to expect that the procedures discussed or developed at an academic research institute like PRRC could serve as much more than a set of initial guidelines for an operating oil company. A different point of view is quite properly held by the oil company, in which the profitability of a particular oilfield is the primary consideration. At best, the work performed on these latter tasks of our project by PRRC personnel can be used by the operator's project engineers as starting points in the field situations they face. Even to make possible such use, special efforts in communication are required. In line with this goal, we have during the past year conducted seminars on or attended more detailed discussions on the principles and application of mobility control with engineers of the following companies:

Amoco Production Company  
Cities Service-Occidental Oil Company  
Imperial Chemical Industries  
Nalco Chemical Company  
Shell Chemical Company  
Sohio Production Research Laboratories

and on the development of special CO<sub>2</sub>-foam displacement simulators, with a group at the U.S. Department of Energy, Morgantown Energy Technology Center.

It is expected that such contacts will continue, to the end that the information and ideas presented in these reports can be more generally discussed. We trust that they can thus serve as useful bases for eventual incorporation into the activities and projects undertaken by the engineers and managers who are directly involved in field operations.

## REFERENCES

- Alston, R.B., Kokolis, G.P., and James, C.F. (1985) "CO<sub>2</sub> Minimum Miscibility Pressure: A Correlation for Impure CO<sub>2</sub> Streams and Live Oil Systems," Soc. Pet. Eng. J., (April) 268-274.
- Aronofsky, J.S. and Heller, J.P. (1957) "A Diffusion Model to Explain Mixing of Flowing Miscible Fluids in Porous Media," Trans., AIME 210, 345-349.
- Bahralolom, I.M. (1985) "Flow Visualization for CO<sub>2</sub>-Crude Oil Mixtures: Extraction Versus Solubility and the Effects of Pore Structure," M.S. Thesis, New Mexico Institute of Mining and Technology, Socorro, NM.
- Bahralolom, I.M. and Bretz, R.E. (1985) "Experimental Investigation of the Interaction of Phase Behavior with Microscopic Heterogeneity in a CO<sub>2</sub> Flood," paper SPE 14147 presented at the SPE Annual Technical Conference and Exhibition, Las Vegas, Sept. 22-25.
- Batycky, J.P., Mirkin, M.I., Jackson, C.H., and Besserer, G.J. (1980) "Miscible and Immiscible Displacement Studies on Carbonate Reservoir Cores," Petroleum Society of CIM, Preprint Paper No. 80-31-21 presented at 31st Annual Technical Meeting of the Petroleum Society of CIM, Calgary, May 25-28.
- Bernard, G.G., Holm, L.W., and Harvey, C.P. (1980) "Use of Surfactant to Reduce CO<sub>2</sub> Mobility in Oil Displacement," Soc. Pet. Eng. J., (Aug.) 20, 281-292.
- Blackwell, R.J., Rayne, J.R., and Terry, W.M. (1959) "Factors Influencing the Efficiency of Miscible Displacement," Trans., AIME 216, 1-8.
- Blackwell, R.J. et al. (1960) "Recovery of Oil by Displacement with Water-Solvent Mixtures," Trans., AIME 219, 293-300.
- Bretz, R.E., Specter, R.M., and Orr, F.M., Jr. (1986) "Mixing During Single-Phase Flow in Reservoir Rocks: Models, Effects of Pore Structure and Interpretation of Experiments," Reservoir Characterization, L.W. Lake and H.B. Carroll (eds.), Academic Press, Orlando, 585-642.
- Campbell, B.T. and Orr, F.M., Jr. (1985) "Flow Visualization for CO<sub>2</sub>/Crude-Oil Displacements," Soc. Pet. Eng. J., (Oct.) 665-678.
- Caudle, B.H. and Dyes, A.B. (1958) "Improving Miscible Displacement by Gas-Water Injection," Trans., AIME 213, 281-284.
- Charoensombut-amon, T. (1985) "Application of a Generalized Multiproperty Apparatus to the Measurement of Thermodynamic and Transport Properties to Measure Phase Equilibria and Vapor Phase Densities of Supercritical Carbon Dioxide in n-Hexadecane System," Ph.D. Dissertation, Rice University, Houston, TX.
- Clark, H.C., O'Brien, R.J., and Trotter, J. (1964) "Structure of Trimethyltin Fluoride," J. Chem. Soc., 2332.
- Coats, K.H. and Smith, B.D. (1964) "Dead End Pore Volume and Dispersion in Porous Media," Soc. Pet. Eng. J., (Mar.) 4, 73-84.

- Cronquist, C. (1978) "Carbon Dioxide Dynamic Miscibility with Light Reservoir Oils," Proc., Fourth Annual U.S. Department of Energy Symp., Tulsa, Aug. 28-30.
- Cullick, A.S. and Mathis, M.D. (1984) "Densities and Viscosities of Mixtures of Carbon Dioxide and n-Decane from 310 to 403 K and 7 to 30 MPa," J. Chem. Data, 29, 393-396.
- Dai, K.K. (1984) "Numerical Simulation of CO<sub>2</sub>-Crude Oil Displacement: Effects of High Water Saturations," M.S. Thesis, New Mexico Institute of Mining and Technology, Socorro, NM.
- Dandge, D.K., Heller, J.P., and Wilson, K.V. (1985) "Structure Solubility Correlations: Organic Compounds and Dense Carbon Dioxide Binary Systems," I. & E.C. Product Res. and Dev., 24, 162-166.
- Dandge, D.K., Heller, J.P., and Wilson, K.V. (1986) "Poly-1-hexene, Synthesis and Solubility in Dense CO<sub>2</sub>," J. Appl. Polym. Sci., 32, 3775-3781.
- Dandge, D.K. et al. (1986) "Kinetics of 1-Hexene Polymerization," J. Appl. Polym. Sci., 32, 5373-5384.
- Day, P. (1956) "Dispersion of a Moving Salt Water Boundary Advancing through a Saturated Sand," Trans., Am. Geophys. Union (Oct.) 37, 595.
- Deans, H.A. (1963) "A Mathematical Model for Dispersion in the Direction of Flow in Porous Media," Trans., AIME, 228, Part II, 49-52.
- Dunn, P. and Oldfield, D. (1970) "Tri-n-butyltin Fluoride: Novel Coordination Polymer in Solution," J. Macromol. Sci. Chem., A4, 1157-1168.
- Dymond, J.H., Young, K.J., and Isdale, J.D. (1980) "Transport Properties of Nonelectrolyte Liquid Mixtures: Viscosity Coefficients for the n-Hexane + n-Hexadecane System at Temperatures from 25 to 100°C at Pressures up to the Freezing Pressure or 500 MPa," Part II, Int. J. of Thermophysics, 1 (4), 345-373.
- Gardner, J.W. et al. (1981) "The Effect of Phase Behavior on a CO<sub>2</sub>-Flood Displacement Efficiency," JPT (Nov.) 2067-81.
- Gardner, J.W. and Ypma, J.G.J. (1984) "An Investigation of Phase-Behavior/Macroscopic-Bypassing Interaction in CO<sub>2</sub> Flooding," Soc. Pet. Eng. J., (Oct.) 508-520.
- Heller, J.P. (1963) "The Interpretation of Model Experiments for the Displacement of Fluids Through Porous Media," AICHE J., 9, 452-459.
- Heller, J.P. (1984) "Reservoir Application of Mobility Control Foams in CO<sub>2</sub> Floods," paper SPE/DOE 12644 presented at the Fourth (Tulsa) Symposium on EOR.
- Heller, J.P. (1986) "Mobility Control for CO<sub>2</sub> Injection," DOE/MC/16426-19, U.S. Department of Energy.
- Heller, J.P. and Taber, J.J. (1983) "Development of Mobility Control Methods to Improve Oil Recovery by CO<sub>2</sub>," final report to the U.S. Department of Energy, No. DOE/MC/10689-17, Nov.
- Heller, J.P. and Taber, J.J. (1986) "Improvement of CO<sub>2</sub> Flood Performance," annual report, U.S. Department of Energy, No. DOE/MC/21136-6 (DE 86000283), June.

- Heller, J.P., Kovarik, F.S., and Taber, J.J. (1987) "Improvement of CO<sub>2</sub> Flood Performance," annual report, U.S. Department of Energy, No. DOE/MC/21136-10 (DE 87001236), May.
- Heller, J.P., Boone, D.A., and Watts, R.J. (1985) "Testing CO<sub>2</sub>-Foam for Mobility Control at Rock Creek," paper SPE 14519 presented at the Eastern Regional Meeting, Morgantown, WV, Nov. 6-8.
- Heller, J.P. et al. (1985) "Direct Thickeners for Mobility Control of CO<sub>2</sub> Floods," Soc. Pet. Eng. J. (Oct. 1986) 679-686.
- Henry, R.L. and Metcalfe, R.S. (1983) "Multiple Phase Generation During Carbon Dioxide Flooding," Soc. Pet. Eng. J., (Aug.) 595-601.
- Hill, S. (1952) "Channelling in Packed Columns," Chem. Eng. Sci., 6, (1) 247-253.
- Holm, L.W. (1959) "Carbon Dioxide Solvent Flooding for Increased Oil Recovery," Trans., AIME 216, 225-231.
- Holm, L.W. (1963) "CO<sub>2</sub> Slug and Carbonated Water Oil Recovery Process," Prod. Monthly (Sept.) 6.
- Holm, L.W. and Josendal, V.A. (1974) "Mechanism of Oil Displacement by Carbon Dioxide," JPT (Dec.) 1427-1438; Trans., AIME, 257, 1427-1438.
- Huang, S.C. et al. (1978) "Relation of Liquid-Liquid Equilibrium at Low Temperature to Vapor-Liquid Equilibria Behavior at High Temperature and Elevated Pressure," Proc., 5th Annual GPA Convention, 7-12.
- Hutchinson, C.A. and Braun, P.H. (1961) "Phase Relations of Miscible Displacement in Porous Media," AIChE J. 7, 64-74.
- Johnson, C.E. and Sweeny, S.A. (1971) "Quantitative Measurement of Flow Heterogeneity in Laboratory Core Sample and Its Effect on Flow Characteristics," paper SPE 3610 presented at SPE 46th Annual Fall Meeting, New Orleans, October 3-6.
- Jossi, J., Stiel, L., and Thodos, G. (1962) "Viscosity of Pure Substances in the Dense Gaseous and the Liquid Phases," AIChE J. (March) 8 (1), 59-63.
- Kovarik, F.S. (1985) "A Minimum Miscibility Pressure Study Using Impure CO<sub>2</sub> and West Texas Oil Systems: Data Base, Correlations, and Compositional Simulation," paper SPE 14689 presented at the SPE Production Technology Symposium, Lubbock, Texas, November 11-12.
- Kovarik, F.S. (1986) "A Minimum Miscibility Pressure Study Using Impure CO<sub>2</sub> and West Texas Oil Systems: Data Base, Correlations, and Compositional Simulation," paper SPE 15004 presented at the SPE Permian Basin Oil and Gas Recovery Conference, Midland, Texas, March 13-14.
- Kovarik, F.S. and Taylor, M.A. (1987) "Viscosity Measurements of High Pressure CO<sub>2</sub>/Hydrocarbon Mixtures," presented at the 1987 AIChE Annual Meeting, New York City, November 15-20.
- Lansangan, R.M., Jangkamolkulchai, A., and Luks, K.D. (1987) "Binary Vapor-Liquid Equilibria Behavior in the Vicinity of Liquid-Liquid-Vapor Loci," Fluid Phase Equil., 36, 49-66.

- Lohrenz, J., Bray, B., and Clark, C. (1964) "Calculating Viscosities of Reservoir Fluids from Their Compositions," JPT (Oct.) 1171-1176.
- Metcalf, R.S. and Yarborough, L. (1979) "The Effect of Phase Equilibria on the CO<sub>2</sub> Displacement Mechanism," Soc. Pet. Eng. J., (Aug.) 242-252.
- Orr, F.M., Jr. (1980) "Simulation of One-Dimensional Convection of Four Phase, Four Component Mixture," Contract No. DE-AC21-78MC03260, U.S. DOE.
- Orr, F.M., Jr., Jensen, C.M., and Silva, M.K. (1981) "Effect of Solution Gas on the Phase Behavior of CO<sub>2</sub>-Crude Oil Mixtures," presented at the International Energy Agency Workshop on Enhanced Oil Recovery, Winfrith, U.K., Sept. 24.
- Orr, F.M., Jr., Silva, M.K., and Lien, C.L. (1983) "Equilibrium Phase Compositions of CO<sub>2</sub>/Crude Oil Mixtures - Part 2: Comparison of Continuous Multiple-Contact and Slim-Tube Displacement Tests," Soc. Pet. Eng. J., (April) 281-291.
- Orr, F.M., Jr., Yu, A.D., and Lien, C.L. (1981) "Phase Behavior of CO<sub>2</sub> and Crude Oil in Low Temperature Reservoirs," Soc. Pet. Eng. J., (Aug.) 480-492.
- Osipw, L.I. (1962) Surface Chemistry, Reinhold Corp., New York, N.Y., 144-225.
- Patel, P.D., Christman, P.G., and Gardner, J.W. (1985) "An Investigation of Unexpectedly Low Field-Observed Fluid Mobilities During Some Tertiary CO<sub>2</sub> Floods," paper SPE 14308 presented at the SPE Annual Fall Meeting, Las Vegas, Sept. 22-25.
- Peng, D.Y. and Robinson, D.B. (1976) "A New Two-Constant Equation of State," Ind. Eng. Chem. Fundam., 15, (1) 59-64.
- Perkins, T.K. and Johnston, O.C. (1963) "A Review of Diffusion and Dispersion in Porous Media," Soc. Pet. Eng. J. (March) 3, 70-84.
- Rathmell, J.J., Stalkup, F.I., and Hassinger, R.C. (1971) "A Laboratory Investigation of Miscible Displacement by Carbon Dioxide," paper SPE 3484 presented at the SPE Annual Conference and Exhibition, New Orleans, (Oct. 3-6).
- Rosen, M.J. (1972) "The Relationship of Structure to Properties in Surfactants," J. Am. Oil Chem. Soc., 49, 293.
- Schwartz, Pery, and Berch (1958) Surface Active Agents and Detergents, Vol. II, Interscience Inc., New York, N.Y.
- Sultan, A.J. (1987) "Simulation of Matched Viscosity Miscible Displacement in a Heterogeneous Porous Medium," M.S. Thesis, New Mexico Institute of Mining & Technology (July).
- Taylor, G.I. (1953) "Dispersion of Soluble Matter in Solvent Flowing Slowly Through a Tube," Proc. Roy. Soc., A219, 186-203.
- Taylor, M.A., Heller, J.P., and Hutter, C. (1987) "Design and Application of the Torsional Quartz Viscometer for the Continuous Phase Equilibrium Apparatus," Petroleum Recovery Research Center report No. 87-2.

Tiffin, D.L. and Kremesec, V.J. (1986) "A Mechanistic Study of Gravity-Assisted CO<sub>2</sub> Flooding," paper SPE/DOE 14895 presented at the 5th SPE/DOE Joint Symposium on Enhanced Oil Recovery, Tulsa, OK, April 20-23.

Turek, E.A., Metcalfe, R.S., and Fishback, R.E. (1984) "Phase Behavior of Several CO<sub>2</sub>-West Texas Reservoir Oil Systems," paper SPE 13117 presented at the SPE Annual Conference and Exhibition, Houston (Sept. 16-19).

van Meurs, P. and van der Poel, C. (1958) "A Theoretical Description of Water-Drive Processes Involving Viscous Fingering," Trans., AIME, 213, 103-112.

von Rosenberg, D.U. (1965) "Mechanics of Steady State Single Phase Fluid Displacement from Porous Media," AICHE J. (March) 2, 55.

S.Y. Wang et al. (1984) "Reconstruction of Oil Saturation Distribution Histories During Immiscible Liquid-Liquid Displacements by Computer-Assisted Tomography," AICHE J., 30, No. 4, 642-646.

Wellington & Vinegar (1987) "X-Ray Computerized Tomography," JPT., (August) 885-898.

Whorton, L.P., Brownscombe, E.R., and Dyes, A.B. (1952) "Method for Producing Oil by Means of Carbon Dioxide," U.S. Patent No. 2,623,596.

Yellig, W.F. (1982) "Carbon Dioxide Displacement of a West Texas Reservoir Oil," Soc. Pet. Eng. J., (Dec.) 805-815.

Yellig, W.F. and Metcalfe, R.S. (1980) "Determination and Prediction of CO<sub>2</sub> Minimum Miscibility Pressure," JPT (Jan.) 160-168.

**APPENDIX A**  
**SAMPLE CALCULATION FOR CRITICAL CO<sub>2</sub> FLOW RATE**

Sample Calculations for Critical CO<sub>2</sub> Flow Rate  
Run #9

Operating Conditions:

Pressure: 1206 psia  
Temperature: 93°F  
Oil Composition: 33.3 mol% nC<sub>10</sub>

Physical Properties of CO<sub>2</sub>:

Density = 0.6756 g/cc  
Viscosity = 0.0545 cp

Physical Properties of the nC<sub>10</sub>-nC<sub>16</sub> "Oil" Mixture:

Density = 0.7802 g/cc  
Viscosity = 1.9362 cp

Source: TRAPP Program

Physical Properties of Core 7:

Length = 14.94 cm  
Diameter = 3.79 cm  
Porosity = 0.19  
Pore Volume = 32 cc  
Permeability  
to air = 260 md  
Permeability  
to nC<sub>6</sub> = 216.5 md

$$\text{Critical Velocity, } v_c = \frac{2.741 \Delta \rho \sin \theta k}{\phi \Delta \mu} [=] \text{ ft/day}$$

where

$\Delta \rho$  = density difference (in-place minus solvent) [=] g/cc

k = core permeability [=] darcies

$\theta$  = dip angle

$\phi$  = core porosity

$\Delta \mu$  = viscosity difference (in-place minus solvent) [=] cp

$$v_c = \frac{2.741(0.7802 - 0.6756)(0.2165)}{0.19(1.9362 - 0.0545)}$$

$$= 0.1736 \text{ ft/day}$$

$$= 0.2205 \text{ cc/hr}$$

$$Q_c = 0.19(11.28)(0.2188)$$

$$= 0.4726 \text{ cc/hr}$$

APPENDIX B

EXPERIMENTAL DATA FOR THE CO<sub>2</sub> + n-C<sub>10</sub> + n-C<sub>16</sub>  
DISPLACEMENT RUNS

Table B.1. Experimental Data for CO<sub>2</sub> + n-C<sub>6</sub> Displacement Run  
(Run No. 1, page 10 of Lab Book)

Core:	B7
Pressure:	1013.5 psia
Temperature:	93°F
Oil Composition:	100 mol% n-C <sub>6</sub>
Critical Velocity:	12.9 cc/hr
Injection Velocity:	5.0 cc/hr
Q/Q <sub>c</sub> :	0.387

OIL PRODUCTION DATA:

PV CO <sub>2</sub> Injected	Oil Recovery (fract. OOIP)
0.052	0.028
0.104	0.053
0.156	0.079
0.208	0.104
0.260	0.123
0.312	0.143
0.365	0.163
0.417	0.191
0.469	0.211
0.521	0.232
0.573	0.253
0.625	0.270
0.677	0.286
0.724	0.308
0.781	0.332
0.833	0.353
0.885	0.371
0.938	0.385
0.990	0.399
1.040	0.420
1.090	0.443
1.150	0.470
1.200	0.491
1.250	0.507
1.300	0.526
1.350	0.550
1.410	0.573
1.460	0.595
1.510	0.616
1.560	0.636
1.620	0.658
1.670	0.679
1.720	0.699

Table B.1 continued...

1.770	0.720
1.820	0.741
1.880	0.760
1.930	0.772
1.980	0.786
2.030	0.801

Table B.2. Experimental Data for CO<sub>2</sub> + n-C<sub>6</sub> Displacement Run  
(Run No. 2, page 16 of Lab Book)

Core:	B7
Pressure:	1159.5 psia
Temperature:	93°F
Oil Composition:	100 mol% n-C <sub>6</sub>
Critical Velocity:	0.298 cc/hr
Injection Velocity:	4.0 cc/hr
Q/Q <sub>c</sub> :	13.4

OIL PRODUCTION DATA:

PV CO <sub>2</sub> Injected	Oil Recovery (fract. OOIP)
0.04	0.03
0.17	0.12
0.29	0.21
0.42	0.32
0.54	0.36
0.67	0.45
0.79	0.51
0.92	0.56
1.04	0.62
1.17	0.68
1.29	0.73
1.42	0.77
1.54	0.82
1.67	0.87
1.79	0.90
1.92	0.91
2.04	0.92

Table B.3. Experimental Data for CO<sub>2</sub> + n-C<sub>10</sub> + n-C<sub>16</sub>  
 Displacement Run  
 (Run No. 4, page 24 of Lab Book)

Core:	B7
Pressure:	1640 psia
Temperature:	93°F
Oil Composition:	33.3 mol% n-C <sub>10</sub>
Critical Velocity:	0.171 cc/hr
Injection Velocity:	4.0 cc/hr
Q/Q <sub>c</sub> :	23.4

OIL PRODUCTION DATA:

PV CO <sub>2</sub> Injected	Oil Recovery (fract. OOIP)
0.08	0.06
0.19	0.15
0.29	0.23
0.40	0.31
0.50	0.39
0.61	0.46
0.71	0.51
0.82	0.56
0.92	0.60
1.03	0.64
1.13	0.68
1.24	0.73
1.34	0.77
1.45	0.81
1.55	0.84
1.66	0.87
1.76	0.89
1.87	0.92
1.98	0.94
2.08	0.96

GAS PRODUCTION DATA:

PV CO <sub>2</sub> Injected	CO <sub>2</sub> Produced (cu. ft.)
0.667	0.0
0.949	0.0532
1.17	0.106
1.39	0.159
1.56	0.212
1.72	0.265

**Table B.3 continued...**

**1.86**  
**2.01**

**0.318**  
**0.371**

Table B.4. Experimental Data for CO<sub>2</sub> + n-C<sub>10</sub> + n-C<sub>16</sub>  
 Displacement Run  
 (Run No. 5, page 28 of Lab Book)

Core:	B7
Pressure:	1652 psia
Temperature:	93°F
Oil Composition:	33.3 mol% n-C <sub>10</sub>
Critical Velocity:	0.171 cc/hr
Injection Velocity:	1.456 cc/hr
Q/Q <sub>c</sub> :	8.54

OIL PRODUCTION DATA:

PV CO <sub>2</sub> Injected	Oil Recovery (fract. OOIP)
0.042	0.034
0.083	0.082
0.125	0.131
0.166	0.176
0.208	0.210
0.250	0.244
0.291	0.283
0.333	0.323
0.374	0.361
0.416	0.404
0.458	0.444
0.499	0.490
0.541	0.528
0.624	0.589
0.666	0.616
0.707	0.641
0.749	0.665
0.790	0.690
0.832	0.710
0.874	0.730
0.915	0.751
0.957	0.771
0.998	0.791
1.040	0.806
1.082	0.825
1.123	0.845
1.165	0.865
1.206	0.884
1.248	0.902
1.290	0.922
1.331	0.936
1.373	0.950
1.414	0.966

Table B.4 continued...

1.456	0.980
1.498	0.993

**GAS PRODUCTION DATA:**

PV CO <sub>2</sub> Injected	CO <sub>2</sub> Produced (cu. ft.)
-----------------------------	---------------------------------------

---

0.584	0.0
0.827	0.0328
0.992	0.0694
1.157	0.108
1.322	0.146
1.539	0.204

Table B.5. Experimental Data for CO<sub>2</sub> + n-C<sub>10</sub> + n-C<sub>16</sub>  
 Displacement Run  
 (Run No. 6, page 34 of Lab Book)

Core:	B7
Pressure:	1202 psia
Temperature:	93°F
Oil Composition:	33.3 mol% n-C <sub>10</sub>
Critical Velocity:	0.482 cc/hr
Injection Velocity:	1.095 cc/hr
Q/Q <sub>c</sub> :	2.28

OIL PRODUCTION DATA:

PV CO <sub>2</sub> Injected	Oil Recovery (fract. OOIP)
0.037	0.037
0.068	0.091
0.099	0.142
0.131	0.173
0.162	0.189
0.192	0.214
0.224	0.246
0.256	0.273
0.287	0.305
0.350	0.369
0.381	0.403
0.412	0.435
0.443	0.463
0.475	0.493
0.506	0.519
0.537	0.545
0.569	0.571
0.600	0.598
0.631	0.618
0.662	0.646
0.694	0.669
0.725	0.693
0.756	0.719
0.788	0.727
0.819	0.741
0.850	0.763
0.881	0.782
0.913	0.800
0.944	0.818
0.975	0.837
1.007	0.854
1.040	0.869
1.070	0.879

Table B.5 continued...

1.100	0.886
1.130	0.894
1.160	0.903
1.190	0.911
1.230	0.917

GAS PRODUCTION DATA:

PV CO <sub>2</sub> Injected	CO <sub>2</sub> Produced (cu. ft.)
0.578	0.0
0.720	0.0151
0.844	0.0332
0.968	0.0594
1.088	0.0972
1.155	0.134
1.231	0.166

Table B.6. Experimental Data for CO<sub>2</sub> + n-C<sub>10</sub> + n-C<sub>16</sub>  
 Displacement Run  
 (Run No. 7, page 38 of Lab Book)

Core:	B7
Pressure:	1089.5 psia
Temperature:	93°F
Oil Composition:	33.3 mol% n-C <sub>10</sub>
Critical Velocity:	2.160 cc/hr
Injection Velocity:	4.201 cc/hr
Q/Q <sub>c</sub> :	1.95

OIL PRODUCTION DATA:

PV CO <sub>2</sub> Injected	Oil Recovery (fract. OOIP)
0.096	0.006
0.216	0.093
0.336	0.148
0.456	0.195
0.576	0.237
0.696	0.280
0.816	0.345
0.936	0.405
1.056	0.439
1.176	0.482
1.296	0.525
1.416	0.573
1.536	0.613
1.656	0.653
1.776	0.689
1.896	0.727
2.016	0.755

GAS PRODUCTION DATA:

PV CO <sub>2</sub> Injected	CO <sub>2</sub> Produced (cu. ft.)
0.750	0.0
0.940	0.001
1.393	0.008
1.677	0.020
1.866	0.031
2.102	0.050

Table B.7. Experimental Data for CO<sub>2</sub> + n-C<sub>10</sub> + n-C<sub>16</sub>  
 Displacement Run  
 (Run No. 8, page 42 of Lab Book)

Core:	B7
Pressure:	1099.5 psia
Temperature:	93°F
Oil Composition:	33.3 mol% n-C <sub>10</sub>
Critical Velocity:	2.130 cc/hr
Injection Velocity:	2.787 cc/hr
Q/Q <sub>c</sub> :	1.31

OIL PRODUCTION DATA:

PV CO <sub>2</sub> Injected	Oil Recovery (fract. OOIP)
0.088	0.057
0.167	0.125
0.247	0.175
0.326	0.238
0.406	0.267
0.486	0.292
0.565	0.300
0.645	0.327
0.725	0.382
0.804	0.419
0.884	0.437
0.964	0.447
1.043	0.460
1.123	0.491
1.202	0.517
1.282	0.537
1.362	0.565
1.441	0.586
1.521	0.612
1.601	0.638
1.680	0.661
1.760	0.688
1.839	0.728
1.919	0.758
1.999	0.764

GAS PRODUCITON DATA:

PV CO <sub>2</sub> Injected	CO <sub>2</sub> Produced (cu. ft.)
0.779	0.0

Table B.7 continued...

1.192	0.004
1.521	0.013
1.750	0.023
1.849	0.034
2.038	0.044

Table B.8. Experimental Data for CO<sub>2</sub> + n-C<sub>10</sub> + n-C<sub>16</sub>  
 Displacement Run  
 (Run No. 9, page 44 of Lab Book)

Core:	B7
Pressure:	1206 psia
Temperature:	93°F
Oil Composition:	33.3 mol% n-C <sub>10</sub>
Critical Velocity:	0.473 cc/hr
Injection Velocity:	1.225 cc/hr
Q/Q <sub>c</sub> :	2.58

OIL PRODUCTION DATA:

PV CO <sub>2</sub> Injected	Oil Produced (fract. OOIP)
0.014	0.013
0.049	0.043
0.084	0.069
0.119	0.098
0.154	0.124
0.189	0.146
0.224	0.169
0.259	0.199
0.294	0.224
0.329	0.248
0.364	0.272
0.399	0.295
0.434	0.319
0.469	0.345
0.504	0.367
0.539	0.391
0.574	0.416
0.609	0.443
0.644	0.466
0.679	0.489
0.714	0.517
0.749	0.542
0.784	0.562
0.819	0.579
0.854	0.605
0.889	0.630
0.924	0.655
0.959	0.667
0.994	0.684
1.029	0.700
1.064	0.719
1.099	0.730
1.134	0.743

Table B.8 continued...

1.169	0.757
1.204	0.773
1.239	0.787
1.274	0.804
1.309	0.821
1.344	0.837

**GAS PRODUCTION DATA:**

PV CO<sub>2</sub> Injected

CO<sub>2</sub> Produced  
(cu. ft.)

0.575	0.0
0.852	0.003
1.014	0.010
1.171	0.021
1.280	0.032
1.342	0.039

Table B.9. Experimental Data for CO<sub>2</sub> + n-C<sub>10</sub> + n-C<sub>16</sub>  
 Displacement Run  
 (Run No. 10, page 48 of Lab Book)

Core:	B7
Pressure:	1212 psia
Temperature:	93°F
Oil Composition:	33.3 mol% n-C <sub>10</sub>
Critical Velocity:	0.458 cc/hr
Injection Velocity:	0.670 cc/hr
Q/Q <sub>c</sub> :	1.46

OIL PRODUCTION DATA:

PV CO <sub>2</sub> Injected	Oil Recovery (fract. OOIP)
0.010	0.005
0.029	0.017
0.048	0.051
0.086	0.107
0.144	0.158
0.182	0.197
0.220	0.240
0.259	0.273
0.297	0.318
0.335	0.348
0.373	0.373
0.412	0.404
0.450	0.436
0.488	0.466
0.527	0.494
0.565	0.521
0.603	0.545
0.641	0.568
0.680	0.590
0.718	0.616

GAS PRODUCTION DATA:

PV CO <sub>2</sub> Injected	CO <sub>2</sub> Produced (cu. ft.)
0.572	0.0
0.647	0.003
0.718	0.010

Table B.10. Experimental Data for CO<sub>2</sub> + n-C<sub>10</sub> + n-C<sub>16</sub>  
 Displacement Run  
 (Run No. 11, page 52 of Lab Book)

Core:	B7
Pressure:	1100 psia
Temperature:	93°F
Oil Composition:	33.3 mol% n-C <sub>10</sub>
Critical Velocity:	2.127 cc/hr
Injection Velocity:	2.460 cc/hr
Q/Q <sub>c</sub> :	1.16

OIL PRODUCTION DATA:

PV CO <sub>2</sub> Injected	Oil Recovery (fract. OOIP)
0.009	0.005
0.080	0.053
0.150	0.094
0.220	0.124
0.291	0.135
0.361	0.160
0.431	0.185
0.502	0.209
0.512	0.236
0.642	0.261
0.718	0.290
0.783	0.317
0.854	0.345
0.924	0.377
0.994	0.415
1.065	0.435
1.135	0.458
1.205	0.486
1.276	0.504
1.346	0.528
1.417	0.545
1.487	0.568
1.557	0.595
1.628	0.613
1.698	0.627
1.768	0.643
1.839	0.661
1.909	0.680
1.980	0.695
2.050	0.707
2.120	0.713
2.191	0.721
2.261	0.728

Table B.10 continued...

2.331	0.734
2.402	0.739
2.472	0.743
2.543	0.743

GAS PRODUCTION DATA:

PV CO <sub>2</sub> Injected	CO <sub>2</sub> Produced (cu. ft.)
-----------------------------	---------------------------------------

---

1.171	0.0
1.574	0.015
1.896	0.041
2.018	0.068
2.118	0.094
2.226	0.121
2.340	0.147
2.445	0.174
2.536	0.200
2.630	0.227

**APPENDIX C**

**CO<sub>2</sub> DENSITY PREDICTION**

Attached are the equations used and the method of solution implemented in TRAPP, the IUPAC equation of state, and the CMC LAB PROGRAM. The following is a brief description of the three different models.

The theoretical backbone of TRAPP is the corresponding states principle coupled with the conformal solution, one-fluid concept. The corresponding states principle simply stated suggests that values of the thermodynamic properties of different substances can be compared on the basis of their departures from their critical points. The theory of conformal solutions is a form of the perturbation theories of a mixture of spherical molecules. The theory states that the properties of a mixture of spherical molecules with conformal potential (i.e., molecules that interact with the same intermolecular potential) can be obtained as an expansion about those of a reference substance which may or may not be a component of the mixture. The choice of the reference fluid in TRAPP is methane. The choice was dictated by the abundance of reliable data correlated over a wide range of experimental conditions. This allowed for the development of an equation of state and the functional form of the transport properties for the reference fluid with accurate predictive power (a must if the properties of any given mixture is to be predicted with any degree of accuracy). The one-fluid concept is essentially an assumption that the configurational properties (i.e., the spatial orientation of molecules in a given volume of space) of a mixture can be approximated to be those of a hypothetical fluid whose properties are quadratic averages of those of the real mixture. This gives rise to the Van der Waals 1 (VdW1) mixing rules which allow for the prediction of the properties of mixtures. One final note: care must be taken when using TRAPP for mixtures containing C<sub>10</sub>+ because of the lack of conformality between methane and the heavier hydrocarbons due to increasing molecular dissimilarity.

The IUPAC equation of state was designed specifically for CO<sub>2</sub>. The equation has two parts, one is in the standard form

$$Pa = Z\rho RT$$

where

$$Z = Z(\rho_r, T_r, \{B_{ij}\})$$

The  $B_{ij}$ s are the parameters in the equation of state.

The second part is non-analytic and applies at the critical region. The pressure calculated from both parts of the equation of state is combined via switching function to yield the calculated system pressure which is then compared with the input pressure. The calcu-

lation proceeds until the calculated pressure is within the prescribed tolerance limit of the input pressure. Details of the procedure are described in the following pages.

The CMC LAB PROGRAM is essentially a program that linearly interpolates or extrapolates between the data points of Michels, Botzen, and Schuurman (1957).

## THE EXTENDED CORRESPONDING STATE THEORY AND CONFORMAL SOLUTION, ONE-FLUID CONCEPT

The theory used to predict the transport properties of natural gas and hydrocarbon mixtures is an extension of the corresponding-states principle coupled with the conformal solution, one-fluid concept. The latter assumes that the configurational properties of a single-phase mixture can be taken to be that of a hypothetical pure fluid. The properties of the hypothetical fluid are then evaluated via the corresponding-state theory with respect to a chosen reference fluid. The extended corresponding-states model introduces shape factors in the equivalent substance-reducing parameters which are functions of the acentric factor and the reduced temperature and volume.

In the formalism that follows, the viscosity of a mixture  $\eta_{mix}$  is given in terms of density and temperature. The choice of density rather than the laboratory variable pressure was dictated both by theoretical convenience and mathematical simplicity. The calculation of the density of the mixture given the temperature, pressure and composition is the task of the equation of state for the reference fluid. The calculation of density, therefore, is not the primary task of TRAPP but is done out of necessity.

### One-Fluid Model

Based on the one-fluid model, the viscosity of a fluid mixture can be approximated to be the viscosity of some hypothetical pure fluid  $x$ , that is,

$$\eta_{mix}(\rho, T, \{x_i\}) = \eta_x(\rho, T) \quad (C-1)$$

where

$\eta_x$  = viscosity of a hypothetical pure fluid

The viscosity of the hypothetical fluid  $x$  is then evaluated, via the theory of corresponding states, from that of some arbitrary reference fluid  $o$ ,

$$\eta_x(\rho, T) = \eta_o(\rho_o, T_o) F_\eta \quad (C-2)$$

where

- $\eta_0$  = corresponding viscosity of the reference fluid
- $\rho_0$  = corresponding density of the reference fluid
- $T_0$  = corresponding temperature of the reference fluid

$$F_\eta = \left(\frac{M_x}{M_0}\right)^{\frac{1}{2}} f_{x,0}^{\frac{1}{2}} h_{x,0}^{-\frac{2}{3}} \quad (\text{C-3})$$

$$T_0 = \frac{T}{f_{x,0}} \quad (\text{C-4})$$

$$\rho_0 = \rho h_{x,0} \quad (\text{C-5})$$

$M_x, M_0$  = molecular weight of the hypothetical and reference fluids, respectively

$f_{x,0}$  = equivalent substance temperature-reducing parameter

$h_{x,0}$  = equivalent substance volume-reducing parameter

In the special case of two pure fluids, the equivalent substance-reducing ratios become

$$f_{\alpha,0} = \frac{T_\alpha^c}{T_0^c} \quad (\text{C-6})$$

$$h_{\alpha,0} = \frac{V_\alpha^c}{V_0^c} \quad (\text{C-7})$$

### Extended Corresponding States Theory

Let  $\alpha$  = fluid of interest, thus Eqs. C-2 and C-3 become

$$\eta_\alpha(\rho, T) = \eta_0(\rho_0, T_0) F_\eta \quad (\text{C-8})$$

$$F_\eta = \left(\frac{M_\alpha}{M_0}\right)^{\frac{1}{2}} f_{\alpha,0}^{\frac{1}{2}} h_{\alpha,0}^{-\frac{2}{3}} \quad (\text{C-9})$$

where

$$f_{\alpha,0} = \left( \frac{T_{\alpha}^c}{T_0^c} \right) \Theta_{\alpha,0}(T_{\alpha}^*, V_{\alpha}^*, \omega_{\alpha}) \quad (\text{C-10})$$

and

$$h_{\alpha,0} = \left( \frac{V_{\alpha}^c}{V_0^c} \right) \Phi_{\alpha,0}(T_{\alpha}^*, V_{\alpha}^*, \omega_{\alpha}) \quad (\text{C-11})$$

$\Theta_{\alpha,0}$  and  $\Phi_{\alpha,0}$  are the shape factors introduced by the extended corresponding states theory. Notice that Eqs. C-10 and C-11 are essentially C-6 and C-7 except for the shape factors. For  $C_1$  to  $C_{15}$  with  $C_1$  as the reference fluid, the shape factors are given by

$$\Theta_{\alpha,0} = 1 + (\omega_{\alpha} - \omega_0)F(T_{\alpha}^*, V_{\alpha}^*) \quad (\text{C-12})$$

$$\Phi_{\alpha,0} = \{1 + (\omega_{\alpha} - \omega_0)G(T_{\alpha}^*, V_{\alpha}^*)\} \frac{Z_0^c}{Z_{\alpha}^c} \quad (\text{C-13})$$

where

$$F(T_{\alpha}^*, V_{\alpha}^*) = a_1 + b_1 \ln T_{\alpha}^+ + (c_1 + d_1/T_{\alpha}^+)(V_{\alpha}^+ - 0.5) \quad (\text{C-14})$$

$$G(T_{\alpha}^*, V_{\alpha}^*) = a_2(V_{\alpha}^+ + b_2) + c_2(V_{\alpha}^+ + d_2) \ln T_{\alpha}^+ \quad (\text{C-15})$$

$$T_{\alpha}^+ = \min \{2, \max [T_{\alpha}^*, 0.5]\} \quad (\text{C-16})$$

$$V_{\alpha}^+ = \min \{2, \max [V_{\alpha}^*, 0.5]\} \quad (\text{C-17})$$

$Z^c$  = compressibility factors for  $\alpha$  and the reference fluid at their critical points

$\omega$  = acentric factors for  $\alpha$  and the reference fluid

$a_i, b_i, c_i, d_i$  = constants

### Van der Waals 1 Mixing Rules

Let

$x = \text{mixture}$

$\alpha, \beta = \alpha^{\text{th}}$  and  $\beta^{\text{th}}$  components in an n-component mixture

The equivalent substance-reducing ratios defined in equations C-10 and C-11 then become

$$f_{x,0} = h_{x,0}^{-1} \sum_{\alpha} \sum_{\beta} x_{\alpha} x_{\beta} f_{\alpha\beta,0} h_{\alpha\beta,0} \quad (\text{C-18})$$

$$h_{x,0} = \sum_{\alpha} \sum_{\beta} x_{\alpha} x_{\beta} h_{\alpha\beta,0} \quad (\text{C-19})$$

where

$x_{\alpha}, x_{\beta} = \text{mole fraction of } \alpha^{\text{th}} \text{ and } \beta^{\text{th}} \text{ components}$

$$f_{\alpha\beta,0} = (f_{\alpha,0} f_{\beta,0})^{\frac{1}{2}} (1 - k_{\alpha\beta}) \quad (\text{C-20})$$

$$h_{\alpha\beta,0} = \frac{1}{2} (h_{\alpha,0}^{\frac{1}{3}} + h_{\beta,0}^{\frac{1}{3}})^3 (1 - l_{\alpha\beta}) \quad (\text{C-21})$$

$$M_{\alpha\beta} = \frac{2M_{\alpha}M_{\beta}}{M_{\alpha} + M_{\beta}} \quad (\text{C-22})$$

$k_{\alpha\beta}, l_{\alpha\beta} = \text{binary interaction parameters}$

Reference fluid: CH<sub>4</sub>

Input parameters:  $T_c, \rho_c, p_c, \omega, M$

Equation of state:

$$p_0 = \sum_{n=1}^9 a_n(T) \rho_0^n + \sum_{n=10}^{15} a_n(T) \rho_0^{2n-17} \exp(-\gamma \rho_0^2) \quad (\text{C-23})$$

Functional form of the viscosity:

$$\eta_0(\rho_0, T_0) = \eta_0(T_0) + \eta_1(T_0)\rho_0 + \Delta\eta(\rho_0, T_0) \quad (\text{C-24})$$

Component input parameters:

$$T_c^i, \rho_c^i, p_c^i, \omega^i, M^i$$

Experimental input variables:

$$p, T, \{x_i\}$$

Solution Algorithm: Given  $p, T$  and  $\{x_i\}$ , the following algorithm is performed to obtain the physical properties of the mixture.

1. For each component  $\alpha$  in the mixture, calculate  $f_{\alpha,0}$  and  $h_{\alpha,0}$  from Eqs. C-10 and C-11 setting the shape factors  $\Theta_{\alpha,0}$  and  $\Phi_{\alpha,0}$  equal to one.
2. Use the Van der Waals 1 mixing rules (Eqs. C-18–C-22) to obtain  $f_{x,0}$  and  $h_{x,0}$ .
3. Calculate  $p_0$  and  $T_0$  where

$$p_0 = p \frac{h_{x,0}}{f_{x,0}}$$

and  $T_0$  is given by Eq. C-4.

4. The equation of state for the reference fluid (Eq. C-23) is solved for  $\rho_0$ ; this then yields the initial estimate for  $\rho$  given by Eq. C-5.
5. With a value for the density  $\rho$ , calculate the shape factors from Eqs. C-10 and C-11; calculation then proceeds back to #2 and is repeated until the final value of  $\rho$  is obtained.
6. Having obtained the final values of  $\rho$ ,  $h_{x,0}$  and  $f_{x,0}$ , evaluate  $p_0$  and  $T_0$  which in turn yield  $\eta_0(\rho_0, T_0)$  via Eq. C-24.
7. Finally, evaluate  $F_\eta$  (Eq. C-3) to yield  $\eta_x(\rho, T)$ .

IUPAC EQUATION OF STATE FOR CO<sub>2</sub>:

Analytic Part

$$Pa = Z\rho RT \quad (C-25)$$

where

$$Z = 1 + \rho_r \sum_{i=1}^{10} \sum_{j=1}^7 B_{ij} (T_r^{-1} - 1)^{j-1} (\rho_r - 1)^{i-1} \quad (C-26)$$

$\rho_r$  = reduced density

$$= \rho / \rho_c$$

$\rho_c$  = critical molar volume of CO<sub>2</sub>

$$= 0.01063 \text{ gmol/cc}$$

$T_r$  = reduced temperature

$$= T / T_c$$

$T_c$  = critical temperature of CO<sub>2</sub>

$$= 304.21 \text{ K}$$

$B_{ij}$  = parameters ;  $i = 1, \dots, 10$ ,  $j = 1, \dots, 7$

$R$  = gas constant

$T$  = temperature (K)

Equation of State at the Critical Region

$$\Delta T = \frac{|T - T_c|}{T_c} \quad (C-27)$$

$$\Delta \rho = \frac{|\rho_r \rho_c - 0.01059|}{0.01059} \quad (C-28)$$

$$\delta = \Delta T + 0.647145(\Delta \rho)^2 \delta^{0.306} \quad (C-29)$$

$$\Theta = \frac{\Delta \rho}{1.4918 \delta^{0.347}} \quad (C-30)$$

$$\begin{aligned} \Delta P = & \delta^{1.935} \{ (36.98893 - 82.07936\Theta^2 + 56.66053\Theta^4) \\ & + C | 1 - 1.4402\Theta^2 |^{1.935} \} + 6.98\Delta T + 28.361\delta^{1.5879}\Theta(1 - \Theta^2) \end{aligned} \quad (C-31)$$

where

$$C = \begin{cases} 240.4358 & T > T_c \\ -58.38316 & T \leq T_c \end{cases}$$

if  $P > 73.825$  bars, then  $P_s = 73.825(1 + \Delta P)$ ;

if  $P_s < 0$  from above, then  $P_s = 73.825(1 - \Delta P)$ ;

if  $P \leq 73.825$  bars, then  $P_s = 73.825(1 - \Delta P)$ ;

if  $P_s < 0$  from above, then  $P_s = 73.825(1 + \Delta P)$ .

The pressure is then calculated from

$$P^{calc} = f(\delta)Pa + \{1 - f(\delta)P_s\} \quad (C-32)$$

where

$$f(\delta) = 1 - \left\{ 1 - \exp\left(\frac{-0.01}{\delta}\right)^{1.5} \right\} \left\{ 1 - \exp\left(\frac{-0.05}{\delta}\right)^3 \right\} \quad (C-33)$$

objective function:

$$q(P^{calc}) = \frac{P^{calc} - P}{P} \quad (C-34)$$

#### Solution Algorithm:

Given the pressure and the temperature, P and T, the following algorithm is performed iteratively to obtain the specific volume and Z factor for CO<sub>2</sub>.

1. The calculation is started by giving an initial estimate of the reduced density,  $\rho_r$ ; use

$$\rho_r = \begin{cases} 2.6 & \text{for the liquid phase} \\ 0.03 & \text{for the vapor phase} \end{cases}$$

2. With the values of  $\rho_r$  and T, calculate  $\delta$  and  $\Theta$  using the method of successive substitution.
3. Calculate  $Pa$ ,  $P_s$  and  $f(\delta)$  which in turn give the calculated pressure  $P^{calc}$ .

4. The Newton-Raphson method is then used to minimize the objective function within a prescribed tolerance limit, i.e., calculation is performed iteratively until

$$P^{calc} \simeq P$$

5. The specific volume is then calculated from

$$V = (44.011\rho_r\rho_c)^{-1}$$

where  $\rho_r$  = value of the reduced density at convergence.

